

Direction des bibliothèques

AVIS

Ce document a été numérisé par la Division de la gestion des documents et des archives de l'Université de Montréal.

L'auteur a autorisé l'Université de Montréal à reproduire et diffuser, en totalité ou en partie, par quelque moyen que ce soit et sur quelque support que ce soit, et exclusivement à des fins non lucratives d'enseignement et de recherche, des copies de ce mémoire ou de cette thèse.

L'auteur et les coauteurs le cas échéant conservent la propriété du droit d'auteur et des droits moraux qui protègent ce document. Ni la thèse ou le mémoire, ni des extraits substantiels de ce document, ne doivent être imprimés ou autrement reproduits sans l'autorisation de l'auteur.

Afin de se conformer à la Loi canadienne sur la protection des renseignements personnels, quelques formulaires secondaires, coordonnées ou signatures intégrées au texte ont pu être enlevés de ce document. Bien que cela ait pu affecter la pagination, il n'y a aucun contenu manquant.

NOTICE

This document was digitized by the Records Management & Archives Division of Université de Montréal.

The author of this thesis or dissertation has granted a nonexclusive license allowing Université de Montréal to reproduce and publish the document, in part or in whole, and in any format, solely for noncommercial educational and research purposes.

The author and co-authors if applicable retain copyright ownership and moral rights in this document. Neither the whole thesis or dissertation, nor substantial extracts from it, may be printed or otherwise reproduced without the author's permission.

In compliance with the Canadian Privacy Act some supporting forms, contact information or signatures may have been removed from the document. While this may affect the document page count, it does not represent any loss of content from the document.

Université de Montréal

**Role of nucleotides on lung epithelial cells :
mechanism of release and development of a side-view microscopic
chamber to study nucleotide-dependent airway surface liquid
height**

par
Sabina Tatur

Institut de génie biomédical
Faculté de médecine

Thèse présentée à la Faculté des études supérieures
en vue de l'obtention du grade de Doctor of Philosophy (Ph.D.)
en génie biomédical

Décembre 2007

© Sabina Tatur, 2007



Université de Montréal
Faculté des études supérieures

Cette thèse intitulée :

**Role of nucleotides on lung epithelial cells :
mechanism of release and development of a side-view microscopic
chamber to study nucleotide-dependent airway surface liquid
height**

présentée par
Sabina Tatur

a été évaluée par un jury composé des personnes suivantes :

Aimé Robert LeBlanc, Ph.D.

.....
président-rapporteur

Ryszard Grygorczyk, Ph.D.

.....
directeur de recherche

Yves Berthiaume, Ph.D.

.....
codirecteur

Jean-Louis Schwartz, Ph.D.

.....
membre du jury

John Hanrahan, Ph.D.

.....
examineur externe

Josette Noël, Ph.D.

.....
représentante du doyen de la FES

Résumé

La signalisation extracellulaire par les nucléotides régule d'importants processus physiologiques via les récepteurs purinergiques. Dans les poumons, les nucléotides extracellulaires sont impliqués dans la défense primaire en facilitant la clairance mucociliaire et en augmentant la sécrétion du surfactant. Cet ouvrage comprend deux parties : la première traite de l'étude du mécanisme de la libération des nucléotides, particulièrement de l'ATP, par les cellules A549 (une lignée utilisée comme système modèle des cellules alvéolaires) ; et la seconde partie est consacrée à une méthode d'imagerie que nous avons développée pour pouvoir éventuellement étudier l'implication des nucléotides extracellulaires dans le contrôle de la hauteur du liquide de surface (LS).

1. Pour la première partie, des cellules A549 ont été insérées dans une chambre à perfusion maintenue à 37 ° C et la sécrétion des nucléotides a été induite par un choc hypotonique de 50%. La concentration de l'ATP extracellulaire a été évaluée à l'aide d'un essai luciférine-luciférase. Nous avons testé des agents connus pour intervenir dans l'exocytose et dans les voies de signalisation calcique et purinergique. L'inhibition de l'exocytose a réduit significativement la sécrétion de l'ATP et ce résultat indique qu'une exocytose Ca^{2+} -dépendante est le principal mécanisme de sécrétion de l'ATP par les cellules A549. De plus, l'étude exhaustive du signal calcique a révélé que la sécrétion de l'ATP dépend entièrement de la mobilisation du Ca^{2+} des sources intracellulaires et qu'il provient essentiellement du reticulum endoplasmique, une source sensible à la thapsigargine. Toutefois, une petite fraction du signal calcique provient d'une source non identifiée, insensible à la thapsigargine et affectée par le pH intracellulaire. Les concentrations extracellulaires des divers nucléotides ont également été évaluées par HPLC. Nos données indiquent que les nucléotides sécrétés lors d'un choc hypotonique augmentent la sécrétion de l'ATP par un phénomène de feedback positif autocrine/paracrine.

2. Le montage expérimental conçu pour l'étude du LS comprend une chambre d'observation équipée d'un système de contrôle de la température et de l'humidité pour prévenir l'évaporation, et montée sur un microscope à épifluorescence. Les cellules sont cultivées sur filtre dans des conditions air-liquide et le filtre est ensuite inséré dans la chambre d'observation de façon à ce que la monocouche soit orientée perpendiculairement à l'objectif. Ce dispositif permet d'avoir une vue de profil du LS marqué avec une sonde fluorescente et de suivre avec une haute résolution temporelle les variations de sa hauteur.

Cette étude aura contribué à une meilleure compréhension des mécanismes physiologiques impliquées dans la défense primaire des poumons par les nucléotides extracellulaires et que cette connaissance pourra éventuellement servir au développement des nouvelles thérapies contre des maladies liées à des problèmes de clairance mucociliaire.

Mot clés :

signalisation purinergique, ATP extracellulaire, signalisation calcique, mécanisme de la sécrétion, exocytose, défense pulmonaire, liquide de surface pulmonaire, système optique, chambre à observation latéral, microscopie d'épifluorescence

Abstract

Extracellular nucleotides, acting via purinoreceptors, regulate important physiological processes in most body tissues. In the airways, extracellular nucleotides are implicated in the primary defence mechanism by potentiating mucociliary clearance and surfactant secretion. Two different approaches for studying extracellular nucleotides on the lung epithelium are presented and divide this thesis into two parts. The first part focuses on the physiological aspect of nucleotide release, especially ATP, from the alveolar type II cell line A549 and the second on the development of a side-viewing technique for the observation of ATP-dependent airway surface liquid (ASL) height variations:

1. While previous results showed that cell-swelling induced ATP secretion, and that this secretion was tightly correlated with an intracellular Ca^{2+} elevation, the present research was designed to establish the mechanism which is responsible for nucleotide release from A549 cells. Moreover, the source and the progress of the intracellular Ca^{2+} signal were thoroughly analyzed. In this study, nucleotide release from A549 cells was induced by a 50% hypotonic shock in a flow-through chamber at 37 °C. Agents, known to interfere with the exocytotic process, intracellular Ca^{2+} signalling and purinergic signalling, were applied, and the ATP concentration in the perfusate aliquots was determined with a luciferase-luciferin assay. The individual concentration of all nucleotides was determined by HPLC. The inhibition of the exocytotic process significantly reduced ATP secretion and indicated a Ca^{2+} -dependent exocytosis as the principal release mechanism. The study of the Ca^{2+} signal revealed that ATP release depended entirely on Ca^{2+} mobilization from intracellular stores, primarily from the thapsigargin-sensitive endoplasmic reticulum and to a lesser extent from an unidentified thapsigargin-insensitive source, which was, however, sensitive to intracellular pH alterations. Finally, cell-swelling

induced, Ca^{2+} -dependent ATP release from A549 cells was shown to be amplified by a positive autocrine/paracrine feedback of co-released nucleotides.

2. The side-viewing imaging technique was designed and constructed for a potential time-resolved study of ASL height alterations upon stimulation with extracellular ATP. A custom-designed side-viewing chamber was mounted on the microscope stage and was equipped with a temperature/humidity control system to keep an *in vitro* cell culture in a physiological environment and to prevent the ASL from insensible water loss. The chamber was comprised of a housing including a perforated knob, which accommodated a filter insert with an air/liquid grown cell monolayer and allowed perfusion of the basal side. The housing positioned the filter insert perpendicular to the microscope objective and enabled a direct observation of fluorescently labelled ASL through an epifluorescence microscope.

These two areas of study aim to contribute to a better understanding of the physiological mechanisms involved in the primary lung defence via extracellular nucleotides. This knowledge is the basis for the development of novel therapies especially against diseases of impaired mucociliary clearance.

Keywords:

purinergic signalling, extracellular ATP, Ca^{2+} -signalling, release mechanism, exocytosis, airway defence, airway surface liquid, optical system, side-viewing microscopy, epifluorescence microscopy

Contents

List of Tables	v
List of Figures	vi
List of Abbreviations	x
Acknowledgments	xvi
Introduction	1
I Mechanism of ATP release	5
1 Physiological background	6
1.1 Extracellular ATP	6
1.1.1 Introduction	6
1.1.2 Purinergic signalling in the lung epithelium	7
1.1.3 Release mechanisms of ATP	8
1.2 Intracellular calcium	11
1.2.1 Overview	11
1.2.2 Basics of calcium signalling	14
2 Theory of the experimental methods	24
2.1 Luminescence	24
2.1.1 Overview	24
2.1.2 Photoluminescence	26
2.1.3 Bioluminescence	28
2.2 ATP release chamber and ATP evaluation	30

2.2.1	Evaluation of ATP	30
2.2.2	Chamber for hypotonically induced ATP release	34
2.3	Ratiometric imaging	36
2.3.1	Basic principles	36
2.3.2	Calcium imaging	38
2.3.3	Intracellular pH	39
3	Articles: Mechanism of ATP release	40
3.1	ARTICLE 1: Ca ²⁺ -dependent Nucleotide Release	40
3.1.1	Preamble	40
3.1.2	Article	41
3.1.3	Further unpublished results	73
3.2	ARTICLE 2: Nucleotide Autocrine Signalling	81
3.2.1	Preamble	81
3.2.2	Article	81
3.2.3	Further unpublished results	134
II	Development of a side-viewing technique	141
4	Airway surface liquid	142
4.1	Characteristics of the ASL	142
4.2	Regulation of the ASL	143
5	Optical microscopy	146
5.1	Introduction	146
5.1.1	Development of the microscope	146
5.1.2	Components of a microscope	147
5.2	Some principles of optics	149
5.2.1	Refraction and reflection of light	149
5.2.2	Interference of light	151
5.2.3	Diffraction of light	152
5.3	Magnification and resolution	153
5.4	Lenses	157
5.4.1	Basic properties of lenses	157
5.4.2	Optical defects	161

5.4.3	Objectives	163
5.4.4	Eyepiece	167
5.4.5	Condenser	167
5.5	Light path in a compound microscope	168
5.6	Specialized methods	170
5.6.1	Brightfield	170
5.6.2	Phase contrast	171
5.6.3	Fluorescence microscopy	171
5.7	Photomicrography	173
5.7.1	Image formation on the sensor	173
5.7.2	Image resolution	174
5.7.3	Requirements for digital photography	175
6	Article 3: Side-viewing microscopy	178
6.1	Preamble	178
6.2	Article	178
7	Conclusions and future directions	212
	References	216
	APPENDICES	249
A	Materials	250
A.1	Cell lines	250
A.1.1	16HBE14o-	250
A.1.2	A549	253
A.2	Solutions	255
A.2.1	Growth media	255
A.2.2	Balanced salt solutions	257
A.2.3	Hypotonic solution	260
A.3	Chemicals and active agents	261
B	Microscope components	284

C	Technical drawings	287
C.1	Side-view microscopy set-up – Essential elements	287
C.2	Stage ring	290
C.3	Side-view chamber	292
	C.3.1 Assembly	292
	C.3.2 Chamber frame	294
	C.3.3 Filter holder	296
C.4	Cell culture filter inserts	298
	C.4.1 Modification of the Millicell [®] culture plate inserts . . .	298
	C.4.2 Preparation of the MCPI for cell culture	299
C.5	Incubator	301
	C.5.1 Assembly	301
	C.5.2 Main chamber	303
	C.5.3 Cover	305
C.6	Valve	307
	C.6.1 Assembly	307
	C.6.2 Main valve tube	309
	C.6.3 Valve tube accessories	311

List of Tables

I	Various types of luminescence	26
II	Peak and total release of ATP after interfering with the secretory pathway	75
III	Objective designations for common optical corrections	164
IV	Optical specifications and requirements for digital photography	176

List of Figures

1.1	Potential ATP release mechanisms	10
1.2	Sources of intracellular Ca^{2+} elevation	15
2.1	Jablonski diagram	25
2.2	Luciferase-luciferin bioluminescence	32
2.3	ATP release chamber	34
3.1	Selected steps of the secretory pathway	73
3.2	ATP Release after interfering with the secretory pathway . . .	77
3.3	Intracellular pH and Ca^{2+} alteration upon hypotonic shock . .	134
3.4	Intracellular pH and Ca^{2+} alteration induced by ionomycin . .	134
3.5	Intracellular pH and Ca^{2+} alterations induced by intracellular alkalization and acidification	135
4.1	Dual signalling system of ASL height control	144
5.1	Reflection and refraction of light	149
5.2	Dispersion of light by a glass prism	150
5.3	Two-wave interference	151
5.4	Diffraction of light	153
5.5	Rayleigh criterion for resolution	154
5.6	Numerical aperture	155
5.7	Common types of lenses	158
5.8	Image formed by a converging lens	159
5.9	Spherical aberration	162
5.10	Chromatic aberration	162
5.11	Geometrical optics of the light microscope	169

5.12 Schematic illustration of epifluorescence microscopy	172
5.13 Field of view – monitor versus eyepiece	174
7.1 Signalling pathway of Ca ²⁺ -dependent ATP release	213
A.1 Phase contrast picture of the cell line 16HBE14o-	250
A.2 Phase contrast picture of the cell line A549	253
A.3 ADP	261
A.4 A3P5PS	261
A.5 Alexa Fluor [®] 488	262
A.6 2-APB	262
A.7 ARL	264
A.8 ATP	264
A.9 Bafilomycin A1	265
A.10 BAPTA	265
A.11 BCECF, free acid	266
A.12 Brefeldin A	266
A.13 Caffeine	267
A.14 Cytochalasin D	267
A.15 Dapoxyl [®] sulfonic acid, sodium salt	268
A.16 DMSO	268
A.17 EGTA	269
A.18 Ethidium bromide	269
A.19 FCCP	270
A.20 Fura 2-AM	270
A.21 GPN	271
A.22 5-Hexadecanoylamino fluorescein	271
A.23 Ionomycin	272
A.24 Jasplakinolide	273
A.25 Latrunculin A	273
A.26 2-MeSADP	274
A.27 Monensin	274
A.28 NEM	275
A.29 Nigericin	275
A.30 Nocodazole	276

A.31 NPPB	276
A.32 Oligomycin A	277
A.33 Pluronic [®] F-127	277
A.34 PMA	278
A.35 PPADS	278
A.36 Probenecid	279
A.37 Ruthenium Red	279
A.38 Ryanodine	279
A.39 Suramin	280
A.40 Thapsigargin	281
A.41 UDP	281
A.42 UDP-glucose	282
A.43 UTP	282
A.44 Xestospongine C	283
B.1 Right-hand view of the microscope TE300	285
B.2 Left-hand view of the microscope TE300	286
C.1 Entire stage set-up – assembled	287
C.2 Entire stage set-up – cross-section	288
C.3 Entire stage set-up – exploded	289
C.4 Stage ring – 3D view	290
C.5 Stage ring – cross-section	290
C.6 Stage ring – 2D engineering drawing	291
C.7 Side-view chamber – assembled	292
C.8 Side-view chamber – cross-section	292
C.9 Side-view chamber – exploded	293
C.10 Chamber frame – 3D view	294
C.11 Chamber frame – cross-section	294
C.12 Chamber frame – 2D engineering drawing	295
C.13 Filter holder – 3D view	296
C.14 Filter holder – cross-section	296
C.15 Filter holder – 2D engineering drawing	297
C.16 Original MCPI	298
C.17 Modified MCPI	298

C.18 Dimensions of the modified MCPI	298
C.19 Design of the MCPI holding tube	299
C.20 Inserting the modified MCPI into the tube	299
C.21 3D view of modified MCPI in the tube	300
C.22 Incubator – assembled	301
C.23 Incubator – cross-section	301
C.24 Incubator – exploded	302
C.25 Main incubator chamber – 3D view	303
C.26 Main incubator chamber – cross-section	303
C.27 Main incubator chamber – 2D engineering drawing	304
C.28 Chamber cover – 3D view	305
C.29 Chamber cover – cross-section	305
C.30 Chamber cover – 2D engineering drawing	306
C.31 Valve – assembled	307
C.32 Valve – cross-Section	307
C.33 Valve – exploded	308
C.34 Main valve tube – 3D view	309
C.35 Main valve tube – cross-section	309
C.36 Main valve tube – 2D engineering drawing	310
C.37 Reducing tube – 3D view	311
C.38 Dimensions of the reducing tube	311
C.39 Valve shutter – 3D view	311
C.40 Dimensions of the valve shutter	311

List of Abbreviations

A

ADO	adenosine
ADP	adenosine 5'-diphosphate
2-APB	2-aminoethoxy-diphenylborate
AM	acetoxymethylester
AMP	adenosine 5'-monophosphate
ARL 67156	6- <i>N,N</i> -diethyl- β , γ -dibromomethylene-D-adenosine-5'-triphosphate
ASL	airway surface liquid
AT II	alveolar type II cells
ATP	adenosine 5'-triphosphate

B

BAPTA	1,2-bis(2-aminophenoxy)ethane- <i>N,N,N',N'</i> -tetraacetic acid
BAPTA-AM	1,2-bis(2-aminophenoxy)ethane- <i>N,N,N',N'</i> -tetraacetic acid tetrakis(acetoxymethyl ester)
BCECF	2',7'-bis-(2-carboxyethyl)-5,6-carboxyfluorescein
BFA	brefeldin A
BSS	balanced salt solution

C

cADPR	cyclic ADP-ribose
CaCC	Ca ²⁺ -activated Cl ⁻ -channel
CaM	calmodulin
cAMP	3'-5'-cyclic adenosine monophosphate

CCD	charge-coupled device
CF	cystic fibrosis
CFI	chromatic aberration-free infinity-corrected
CFTR	cystic fibrosis transmembrane conductance regulator
CICR	Ca ²⁺ -induced Ca ²⁺ release
ChS	CCD sensor chip size
CM	relay optics coupler magnification
CNT	concentrative nucleotide transporter
CR	correction collar
D	
DAG	diacyl glycerol
DMEM	Dulbecco's Modified Eagle Medium
DMSO	dimethylsulfoxide
E	
EDTA	ethylenediaminetetraacetic acid
EGTA	ethyleneglycol-bis(β -aminoethylether)- <i>N,N,N',N'</i> -tetraacetic acid
ELWD	extra long working distance
ENaC	epithelial sodium channel
EO	ethylene oxide
ER	endoplasmic reticulum
EtBr	ethidium bromide
EtOH	ethyl alcohol, ethanol
F	
FCCP	Carbonylcyanide-4-(trifluoromethoxy)phenylhydrazone
FN	field number
FoVS	field of view size on the monitor
F.W.	formula weight
G	
GPN	glycyl-L-phenylalanin- β -naphthylamide

H

HAF	5-hexadecanoylamino fluorescein
HEPES	<i>N</i> -(2-Hydroxyethyl)piperazine- <i>N'</i> -(2-ethanesulfonic acid)
HPLC-F	high performance liquid chromatography combined with fluorescence detection
HS	hypotonic solution

I

IICR	inositol-1,4,5-trisphosphate induced Ca^{2+} release
Im _{diag}	digital image diagonal dimension
INM	inner nuclear membrane
INO	inosine
IP ₃	inositol-1,4,5-trisphosphate
IP ₃ R	inositol-1,4,5-trisphosphate receptor
IS	isotonic solution

M

MALDI-MS	Matrix-assisted laser desorption/ionization mass spectrometer
MCPI	Millicell [®] Culture Plate Inserts
MEM	Minimum Essential Medium
MM	monitor magnification
M.W.	molecular weight

N

NA	numerical aperture
NAADP	nicotinic acid adenine dinucleotide phosphate
NaOAc	sodium acetate
NEM	<i>N</i> -ethylmaleimide
NPPB	5-nitro-2-(3-phenylpropylamino)benzoic acid
NSF	<i>N</i> -ethylmaleimide sensitive fusion protein

O

OM	objective magnification
ONM	outer nuclear membrane

P

PBS	phosphate buffered saline
PCL	periciliary liquid layer
pH _i	intracellular pH
pix _{max}	maximum pixel size
PIP ₂	phosphatidylinositol bisphosphate
PKC	protein kinase C
PMA	phorbol 12-myristate 13-acetate
PMCA	plasma membrane Ca ²⁺ ATPase
PO	propylene oxide
PPADS	pyridoxal phosphate-6-azo(benzene-2,4-disulfonic acid)
PS	physiological solution
PTP	permeability transition pore

R

ROS	reactive oxygen species
RS	ringer solution
RyR	ryanodine receptor

S

SERCA	sarco/endoplasmic reticulum Ca ²⁺ ATPase
SOC	store-operated Ca ²⁺ channel
SPCA	secretory pathway Ca ²⁺ ATPase

T

TG	thapsigargin
TEER	transepithelial electrical resistance
TM	total magnification

U

UDP	Uridine 5'-diphosphate
UDP-glc	Uridine 5'-diphosphoglucose
UTP	Uridine 5'-triphosphate

To my family

for the invaluable support and encouragement.

Acknowledgments

Being enrolled in a PhD program in a French university was as much an exciting experience as a formidable challenge. Thankfully, the late Dr. Ramesh Gulrajani, former Director of the "Institut de génie biomédical", enabled a smooth start for me through his steadfast support. In the course of the last four years, my director, Dr. Ryszard Grygorczyk, provided me with the opportunity to explore the world of surface lung physiology through microscopy – a field which opened for me new insights into interdisciplinary research. My co-director, Dr. Yves Berthiaume, with his in-depth knowledge of the workings of the "Université de Montréal" was of inestimable value to me during these four years. I could always count on his pertinent assistance for which I owe him many thanks.

I will always remember the warm welcome to the lab and the ambience of the "CHUM – centre de recherche" which made my work not only captivating but also engaging. It was a pleasure to work with Abdel, André, Camille, Cécile, Cedric, Chantal, Chloé, Emanuelle, Émilie, Florent, Francis, François-Xavier, Grégory, Jaques-Aurélien, Jean-Charles, Jędrzej, Johannes, Juanjo, Laura, Marie-Claude, Nicolas, Sergei, Stan, Thu Ngan, Vicky and Viviane. Especially, to Hélène Chabot, without whose assistance many times I would have felt lost in the labyrinth of our research centre as well as of the French language, I am profoundly grateful. It would have been a great loss for me to have missed our enriching discussions.

I have long depended on the financial support of the Canadian Cystic Fibrosis Foundation which made my studies at the "Université de Montréal" possible. And for that, I owe a special debt of gratitude to them. Blackwell

and Springer Publishing were kind enough to give me permission to reproduce my two published articles in this thesis. Furthermore, I would like to thank Dr. Christopher Hammond for his permission to reproduce an important figure.

There is no way to express how fortunate I am to have had Dr. Geneviève Patterson's generous encouragement, open ears and wise advice in times of need. I owe special debt to my teacher Dr. Ekkehard Seitz for his infectious enthusiasm for chemistry which instilled in me a love of science. Marcia Goldberg and Susan Kazenel, who painstakingly read through my script, offered meticulous attention to detail and incisive comments.

Finally, my family has accompanied me "through thick and thin" over the last four years. I am fortunate to have had the opportunity to have known my late Uncle Jerry, who – as he described himself – was indeed "A man of few words but many (wise) paragraphs." I count myself lucky to have shared the last years of my grandmother's life with her in Montréal. Her life-long thirst for knowledge until her very last years was inspirational. My father's enthusiasm for this country's natural beauty during his visit opened my eyes even more to the magnificence of this part of the world. I greatly treasure my Aunt Marie's hospitality, which went beyond sharing breakfast and dinner. She, above all, was generous with her time and thoughts. With Marco, I argued, debated and ended up usually following his advice – but most importantly, he made me laugh. My mother not only gave me the independence and freedom to implement my ideas and dreams but also participated and supported them in every possible way. To my family and my friends, my thanks and appreciation knows no bounds.

Introduction

In the lungs, on a surface of 140 m^2 , the blood is separated from the air by a tissue barrier of only $0.5 - 30 \text{ }\mu\text{m}$ [1]. This huge surface, which is almost directly exposed to the environment, risks being damaged resulting from contamination by bacteria, viruses and pollutants. To protect the lung from these harmful airborne insults, the respiratory tract has a range of powerful and effective defence mechanisms. Dysfunction of any of these mechanisms can result in respiratory diseases, among which cystic fibrosis (CF) is one of the most severe [2].

Sneezing and coughing are reflex defence mechanisms, providing the most instantaneous protection against airway irritants. The non-reflex mechanisms are independent units, and consist of the following processes:

- Physical defence:
 1. Air-conditioning is based on cooling, warming and humidification of the inhaled air through the evaporation of water from the airway surface liquid (ASL), which lines the air-conductive part of the respiratory tract [3].
 2. Air-filtration is based on the elimination and deposition of inhaled particles on the ASL-covered ciliated epithelium. Its efficiency is augmented by the anatomic structure of the lung with its bronchial tree [1].
- Chemical defence is based on the ability of the ASL to buffer and dilute inhaled toxic substances [4, 5].

- Cellular defence consists of the innate immunity response¹ to an invading microbe. The innate responses use phagocytic cells (neutrophils, monocytes, macrophages), cells that release inflammatory mediators (basophils, mast cells, and eosinophils), and natural killer cells [6, 7]. An important stage in cellular defence is the adhesion of the invading microbe to the airway fluids, i.e. the ASL in the air-conductive part and the alveolar fluid in the gas-exchange alveoli [8].
- Humoral defence is based on the secretion and effectivity of diverse biomolecules in the airway fluids. These biomolecules can be classified as: antimicrobial proteins, immunoglobulins, cytokines and inflammatory mediators, as well as antioxidants [9]. They can be released either continuously as a constant constituent of the airway fluids (e.g. antimicrobial surfactant proteins in the alveoli [10]) or temporary during an innate immunity response (e.g. cytokines, inflammatory mediators [9]).

In all of these non-reflex defence mechanisms, the airway fluids, which line the entire respiratory tract, play a crucial role in the successful maintenance of a sterile environment:

The ASL provides through its well-regulated periciliary fluid and mucus layer the best conditions for an effective mucociliary clearance. In this clearance process, particles bigger than $2 - 3 \mu\text{m}$ adhere on the mucus and are transported out of the airways by synchronous beats of cilia on epithelial cells.

The alveolar fluid contains surfactant proteins, among other bioactive molecules, that are synthesized and secreted by alveolar type II cells (AT II), one of the major cell types in the alveolar epithelium. Surfactant proteins, apart from their role in the reduction of surface tension in the lung, enhance phagocytosis by opsonizing² bacteria and other particles [10, 12].

¹The innate immune system consists of the immune defence that lacks immunologic memory [6].

²Opsonization is the process whereby particles become coated with molecules that allow them to bind to receptors on phagocytes [11].

Surfactant secretion from AT II cells [13], mucus secretion from goblet cells [14], and ciliary beat frequency on ciliated cells [15, 16] are all stimulated by extracellular ATP through purinergic receptors. Airway fluid homeostasis is likewise controlled by extracellular ATP through the regulation of transepithelial Cl^- transport [17].

This dissertation focuses on the significance of ATP and other nucleotides on the lung epithelium, which act as extracellular signalling molecules via purinergic receptors. Two different approaches for studying the involvement of extracellular nucleotides in lung defence are presented here, and therefore divide this Ph.D. thesis into two parts.

Part I, which comprises article 1 and article 2 (see sections 3.1 and 3.2, respectively), deals with the investigation of the mechanism of Ca^{2+} -dependent secretion of nucleotides and adenosine from A549 cells. A general introduction to extracellular ATP as a signalling molecule is given in section 1.1. Section 2.2 describes our set-up system for ATP release and the analytical method for its quantitative evaluation via bioluminescence. The A549 cell line is a model system for the study of AT II cell function and is briefly characterized in appendix A.1.2. Various types of mechanical stress, including membrane stretch and shear stress, provoke ATP-dependent surfactant secretion from AT II cells [18, 19, and references therein]. For the investigation of the associated ATP and nucleotide secretion, we chose hypotonic shock as an *in vitro* example of mechanical stress. This choice was motivated by the following reasons:

- Transient reorganization of actin cytoskeleton induced by hypotonic stress is quite similar to that induced by shear stress [19–21].
- Reported hypotonic stress-induced responses share some common characteristics with those that are shear stress-induced: both of these stresses induce ATP release in the endothelium [22, 23].
- Shear stress-activated chloride current is similar to hypotonic stress-activated volume-regulated anion channel (VRAC) current [24, 25].

The investigation of hypotonic stress-induced ATP-release provides, therefore, significant information about its mechano-sensitive release mechanism. In addition, hypotonic stress can be easily applied on liquid-covered cell-cultures (see appendix A.1), and does not require any sophisticated set-up, unlike mechanical stress. The magnitude of hypotonic stress can be easily controlled by the degree of solvent dilution.

As previously reported, a hypotonic shock induces a Ca^{2+} signal that is tightly involved in ATP [26] and surfactant release [27] from A549 cells. Section 1.2 offers a general physiological insight into Ca^{2+} signalling, whereas section 2.3 addresses ratiometric imaging as a measuring technique for intracellular Ca^{2+} alteration. For the extensive study of the ATP release mechanism and the Ca^{2+} signal, pharmacological agents were used to interfere with the exocytotic process, the Ca^{2+} signal and purinergic signalling. A complete list of these agents with their description is provided in appendix A.3.

Part II of this Ph.D. thesis concerns the design and construction of a side-viewing method based on epifluorescence microscopy. The aim of this method is to achieve a time-resolved (~ 100 ms) observation of ASL height on *in vitro* cell cultures, which will potentially provide a possibility to study ASL height variations upon stimulation of ATP secretion. The technique is described in article 3, chapter 6. Basic properties of the ASL and its regulation via extracellular ATP are described in chapter 4. The fundamentals of microscopy, which were necessary for the development of this technique, are explained in chapter 5. All technical drawings of the side-viewing system are reproduced in appendix C.

Every analytical method applied in the course of this Ph.D. project, i.e. bioluminescent ATP evaluation, fluorescent intracellular Ca^{2+} imaging and fluorescent ASL height measurement, is based on the principles of luminescence. Section 2.1 describes the principles responsible for the similarities and differences between these methods. The conclusions and the outlook for both parts of this thesis are given jointly at the end of part II in chapter 7.

Part I

Mechanism of ATP release

Chapter 1

Physiological background

1.1 Extracellular ATP

1.1.1 Introduction

In 1929 Drury and Szent-Györgyi were the first to describe potential actions of extracellular adenosine 5'-monophosphate (AMP) and adenosine on the mammalian heart muscle [28]. Fundamental studies of the effect of adenine nucleotides on cardiovascular physiology followed and were reviewed in a book by Green and Stoner in 1950 [29]. A few years later, adenosine 5'-triphosphate (ATP) was shown to be released from the adrenal medulla and sensory nerves following stimulation [30, 31]. In 1963, Robert M. Berne published a paper proposing a possible role for adenosine in the control of blood flow to the heart [32]. This work set the direction for the following years in the research field of extracellular signalling by adenosine. Ensuing studies on the transduction mechanisms triggered by extracellular adenosine were carried out by Sattin and Rall [33].

In 1972 Burnstock postulated that ATP was a neurotransmitter involved in non-adrenergic, non-cholinergic responses of smooth muscles in the gastrointestinal tract and the bladder, and introduced the term "purinergic" [34]. With his comment entitled "Do some nerves release more than one transmitter?" [35], he challenged the hitherto accepted *Dale's principle*, which stated that each neuron releases only one synaptic transmitter, and substantially

influenced the development of the concept of purinergic signalling. However, given the fact that ATP was initially recognized by Lipmann as the universal energy carrier of all living cells in the early 1940s [36], Burnstock's work experienced resistance to this new concept. Only in the early 1990s was ATP finally recognized as an important signalling molecule that mediates diverse biological effects via cell surface receptors – termed purinergic receptors [37]. To date, these receptors have been found in almost all organs, tissues and cells in the body [38].

In 1978 Burnstock provided a basis for distinguishing two types of purinergic receptor families, named P1 (adenosine) and P2 (ATP, ADP and UTP, UDP) [39]. Since then, four subtypes of P1 receptors have been cloned: A₁, A_{2A}, A_{2B} and A₃ [40]. All P1 adenosine receptors are typical G protein-coupled (*metabotropic*) receptors (see page 21).

The P2 receptors were further subdivided into a P2X family of ligand-gated ion channel (*ionotropic*) receptors and a P2Y family of metabotropic receptors. Currently, seven subtypes of the P2X family and eight subtypes for the P2Y family have been cloned and functionally characterized [38].

1.1.2 Purinergic signalling in the lung epithelium

P2 receptors are widely distributed throughout the lung. P2Y₂, P2Y₄, and P2Y₆ are the predominant and the most relevant receptor types in airway epithelial cells. Several P2X receptor subtypes have also been identified, primarily the P2X₄ receptor [38, 41].

A549 cells, an *in vitro* model of the alveolar type II (AT II) epithelium (see appendix A.1.2), express the P2Y₂ receptor, which responds equally to ATP and UTP, as well as the P2Y₆ receptor, whose agonist is UDP and to a much smaller extent UTP and ATP [38, 42]. Recently, they have been found to also express the UDP-glucose specific G_i protein-coupled P2Y₁₄ receptor [43].

16HBE14o- cells, a human bronchial epithelial cell line (see appendix A.1.1), express the P2X₄ and P2X₅ receptors, both activated through ATP, and the P2Y₄ receptor, which responds to UTP and ATP [44, 45].

Purinergic receptors transfer various signals and cause diverse effects in airway epithelial cells. In AT II cells, surfactant release is stimulated and regulated via P2Y receptors [46, 47]. The most potent endogenous stimulus for surfactant secretion is extracellular ATP. Several second messengers are activated in AT II cells following agonist binding: intracellular Ca^{2+} is mobilized, prostaglandin levels increase, and PKC is activated [13, 47].

ATP also exerts various effects on bronchial cells. Ciliated epithelial cells show an increase in ciliary activity in response to ATP enhancing mucociliary transport [48, 49]. Goblet cells are induced to synthesize and secrete mucins in response to extracellular ATP [50, 51]. Clara, serous and ciliated cells are stimulated by ATP and UTP to secrete Cl^- and HCO_3^- [52, 53]. All these effects are involved in the regulation of the airway surface liquid (ASL) volume. The ASL volume in turn is crucially involved in the efficient removal of noxious materials from the airway surfaces, and constitutes the lung's powerful primary defence mechanism (see chapter 4).

Airway epithelial cells release nucleotides under basal conditions and, in amplified form, after stimulation (e.g. shear stress, hypotonic stress, stretch) [54–56]. These released nucleotides are metabolized by surface-attached ectonucleotidases by sequential dephosphorylation (e.g. into ADP, AMP, and adenosine) [57]. This process terminates the large transient effects mediated by ATP and UTP and produces a sustained P2Y₆ receptor-mediated event [58, 59].

1.1.3 Release mechanisms of ATP

The cytoplasmic level of ATP under normal metabolic conditions is $5 - 10 \text{ mmol} \cdot \text{l}^{-1}$. This concentration is essential for maintaining the membrane potential and a low intracellular Ca^{2+} level, for assuring the synthesis of GTP and the activity of the G-proteins, for the signal transduction through various protein kinases, and for certain steps of exocytosis [60].

ATP and other nucleotides are also present in various types of organelles –

especially in the ER and Golgi, where ATP is required for the phosphorylation of transmembrane and secretory proteins and for other energy-requiring processes, such as the dissociation of complexes between chaperones and correctly folded and assembled proteins, disulfide formation and protein polymerization [61, 62]. Since ATP and other nucleotides are heavily charged molecules, they cannot pass the membranes by simple diffusion. Therefore, specific transporters are assumed to facilitate their uptake [61–64].

At first, it was assumed that the only source of extracellular ATP acting on purinoceptors was damaged or dying cells. But it is now recognized that ATP release following stimulation does not occur only through cell lysis but primarily through a well-controlled physiological mechanism [65]. There is an active debate, however, about the precise transport mechanism(s) involved. There are at least three general mechanisms by which ATP release may occur [65, 66] (see Fig. 1.1 on page 10):

Cytolysis during cell membrane damage or death – contributing to pathophysiological mechanisms.

Exocytosis of ATP-filled vesicles or granules.

Facilitated diffusion through ATP release channels or through ATP transporters (e.g. ABC proteins).

For a long time, exocytosis was considered as the common release mechanism of neurotransmitters [67]. As a neurotransmitter, ATP is also believed to be released through exocytosis; however, non-exocytotic release has not been dismissed yet [37, 60, 68]. The evidence of Ca^{2+} dependence in the process of ATP release is typically consistent with regulated exocytosis [69] (see also section 1.2.2).

For ATP release from non-neuronal cells, various transport mechanisms have been proposed, including ATP-binding cassette (ABC) transporters [70–72], connexin or pannexin hemichannels [73–75], plasmalemmal voltage-dependent anion channels (VDAC) [76], as well as vesicular exocytosis [26, 77, 78].

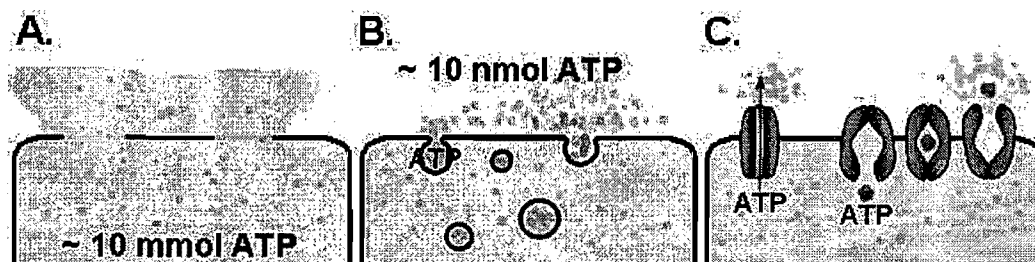


Figure 1.1: Potential ATP release mechanisms:

(A) cytolysis; (B) exocytosis; (C) facilitated diffusion - ATP channel, carrier protein (transporter)

The biggest controversy arose when the cystic fibrosis transmembrane conductance regulator (CFTR), one of the most common ABC proteins in eucariotic organisms, was suggested to conduct ATP [71]. Since then, various papers have described the observation of ATP transport by ABC proteins [79]. On the other hand, many other studies have convincingly determined the inability of ABC proteins to transport ATP [80–83]. Various efforts were made to explain earlier claims to the role of ABC proteins as ATP channels, such as differences in experimental set up or conditions [79].

Other possibilities for an implication of CFTR on ATP release were also proposed, such as the regulation of an associated ATP channel [84] or even the regulation of exocytosis [79].

To conclude, exocytosis appears to predominate as release mechanism, although some cell types may also release ATP by several parallel mechanisms, such as by exocytosis and through the activation of VDAC-like channels. Whichever way ATP and other nucleotides are released from the cells, their extracellular importance is finally well established.

1.2 Intracellular calcium

1.2.1 Overview

Ca^{2+} in the organism

Ca^{2+} is the most abundant metal ion in the body. An average adult body contains in total around 1 kg of calcium, 99% of which is a component of the skeleton in form of calcium phosphate and the remaining 1% is present in the extracellular fluid³ and the cellular protoplasm⁴ [85].

The free Ca^{2+} level in the extracellular fluid is held close to 1 mM, which allows the body to manipulate the precipitation of phosphates by slightly modifying phosphate and Ca^{2+} concentrations and, in this way, to build up bones and teeth. In the cytosol of eukaryotic cells, the resting level of free Ca^{2+} is closely controlled to around 100 nM. The large gradient from extracellular fluid to cytosol of about 10 000 is held up by actively pumping Ca^{2+} out of the cytosol, either into the extracellular space or into intracellular organelles, such as the endoplasmic reticulum (ER), which accumulates Ca^{2+} close to a concentration of 1 mM and serves as an intracellular Ca^{2+} store. The intracellular and extracellular Ca^{2+} level is further buffered by certain Ca^{2+} -binding proteins, such as parvalbumin, calmodulin and calbindin [86]. With the toolkit of intracellular Ca^{2+} stores, channels, pumps and Ca^{2+} -binding proteins of various binding affinity and kinetics, a cell is capable of precisely regulating alterations of the intracellular Ca^{2+} level both temporally and locally. Accordingly, specific triggers can increase the cytosolic Ca^{2+} level up to 500 - 1000 nM in different spatial and temporal domains by opening channels in the ER and/or plasma membrane. These Ca^{2+} signals, in turn, can control localized processes (e.g. exocytosis) and global responses (e.g. myocyte contraction) as well as responses of extremely wide time scale, from microseconds (e.g. activation of ion channels) to many hours, weeks, months or even years (e.g. synaptic plasticity, memory, long-term adapta-

³Extracellular fluid encompasses the blood plasma, the interstitial fluid and the lymph [11].

⁴The protoplasm is the substance within a cell enclosed by the cell membrane. It encompasses the cytosol and all organelles [11].

tion, neuronal ageing) [87]. Almost every cellular process – from fertilization to apoptosis – includes a Ca^{2+} -dependent step, making the Ca^{2+} ion the most versatile and universal signalling agent in advanced biological systems [88].

Properties of the Ca^{2+} ion

The following properties make the Ca^{2+} ion suitable for this unique role: Ca^{2+} is a large divalent cation with a radius of 0.95 Å. It is widely available since it is abundant in most natural waters in the presence of common anions such as Cl^- , HCO_3^- and NO_3^- [86]. The charge-to-size ratio distinguishes the Ca^{2+} ion from ions of similar size, such as Na^+ , and from ions of equal charge, such as Mg^{2+} and Zn^{2+} [86]. It also provides the Ca^{2+} ion with a particularity in structure and thermodynamic affinity for certain classes of ligands, as well as in reaction rates, which are summarized under the following three points:

- *Structure*

Ions with a radius $r \geq 0.75$ Å, such as Ca^{2+} , allow irregular coordination geometry, bond angle, bond distance, and high coordination numbers (7-10) in their complexes. This flexibility enables them to easily adjust to steric crowding⁵. Ca^{2+} differs in this respect strongly from Mg^{2+} ($r = 0.6$ Å) – an ion equally abundant in the body and essential for numerous biochemical processes – which is strictly octahedral in symmetry, and from Zn^{2+} ($r = 0.65$ Å) which is strictly tetrahedral in symmetry. Only conformational changes induced by binding to a Ca^{2+} ion will lead, therefore, to activation of Ca^{2+} -sensitive proteins. Based on the high coordination number, Ca^{2+} is, furthermore, an ideal cross-linking agent for proteins and biopolymers [86].

- *Kinetics*

Ca^{2+} has a much lower tendency to form complexes than Mg^{2+} , whose complexes with monodentate ligands, such as water, are relatively stable. Ca^{2+} , in contrast, exchanges water very rapidly, with a rate close

⁵Steric crowding occurs when a large number of functional groups belonging to one or several molecules accumulate inside a restricted area – usually around an ion. It very often results in steric hindrance of the individual groups.

to the collisional diffusion limit of 10^{10} s^{-1} . The activation speed of a protein through complexation of Ca^{2+} is, therefore, diffusion-limited, whereas the extent and duration of activation by a single Ca^{2+} ion is limited by the stability of the protein- Ca^{2+} complex [86].

- *Binding*

In contrast to monodentate ligands, multidentate ligands can form very stable chelation complexes with Ca^{2+} , whose stability constants exceed, in this case, those for Mg^{2+} . Within a multidentate ligand, Ca^{2+} is even able to interact with neutral oxygen donors such as carbonyls and ethers. This increase in stability and affinity can be attributed to steric factors, which favour the bigger ion to accommodate the donor atoms in a more convenient way [86].

Discovery of Ca^{2+} as signalling agent

The importance of Ca^{2+} for signal transduction was discovered by Sydney Ringer at the end of the 19th century. He showed that Ca^{2+} ions were indispensable for fish survival, development of fertilized eggs, muscle contraction, and cell adhesion [89–93]. Shortly after, Locke [94], and then Overton [95], found that Ca^{2+} is necessary for signal transmission between nerve and muscle. But only half a century later, a general theory of Ca^{2+} as a universal second messenger was promulgated by Lewis Victor Heilbrunn in his book *An Outline of General Physiology* [96]. There he wrote: "*The reaction of this calcium with the protoplasm inside the cell is the most basic of all protoplasmic reactions.*" This theory was ignored for another couple of decades, until the invention of the patch clamp technique and the synthesis of fluorescent Ca^{2+} indicators paved the way for the establishment of Ca^{2+} signalling as the most ubiquitous and pluripotent signalling system involved in almost all known cellular processes [97].

Nowadays, a vast number of research articles and reviews, dedicated to Ca^{2+} signalling, is being published every year. Many aspects of Ca^{2+} signalling (e.g. sources of Ca^{2+} , Ca^{2+} channels and pumps, local and global signalling, and trigger and responses) in physiology and pathophysiology of diverse cell

systems are being addressed and investigated.

The following two sections will introduce some of the principles of Ca^{2+} signalling by focusing this broad topic on the aspects that are relevant to this Ph.D. thesis, i.e. the variety of intracellular Ca^{2+} stores, the types of Ca^{2+} events, the variety of stimuli that can trigger Ca^{2+} signalling, and, finally, exocytosis as an example for Ca^{2+} -regulated processes.

1.2.2 Basics of calcium signalling

Intracellular calcium stores

As mentioned above, the concentration of free Ca^{2+} -ions in the cytosol is precisely regulated, and can rapidly increase in response to various types of stimuli. A rise in the cytosolic Ca^{2+} concentration can be caused by the opening of Ca^{2+} channels in the plasma membrane and/or by the release of Ca^{2+} from internal stores. The major intracellular pool of Ca^{2+} is the ER with two subsets of Ca^{2+} release channels: the Ca^{2+} -gated Ca^{2+} release channel, generally known as ryanodine receptor (RyR), and the IP_3 -gated Ca^{2+} release channel, referred to as IP_3 -receptor (IP_3R) [98]. Almost all other organelles of an eukaryotic cell, such as the mitochondria, the nucleus, the Golgi apparatus, lysosomes and acidic secretory granules were also found to play a significant role in the shaping of cytosolic Ca^{2+} signalling in various cells [99–102]. All of these organelles have both specific Ca^{2+} release channels and Ca^{2+} uptake mechanisms. A more recent concept of Ca^{2+} signalling involves even the cytoskeleton of the cell. Ca^{2+} storage at high-affinity binding sites of F-actin subunits were shown to be involved in the store-operated Ca^{2+} influx pathway, in Ca^{2+} spiking and oscillations, as well as in Ca^{2+} induced Ca^{2+} release (CICR) [103]. Figure 1.2 on page 15 illustrates the potential Ca^{2+} stores within a cell with the major transport pathways responsible for Ca^{2+} movement. Each of these stores will be briefly characterized in the following descriptions.

The *Endoplasmic Reticulum* (ER) is an organelle found in all eukaryotic cells.

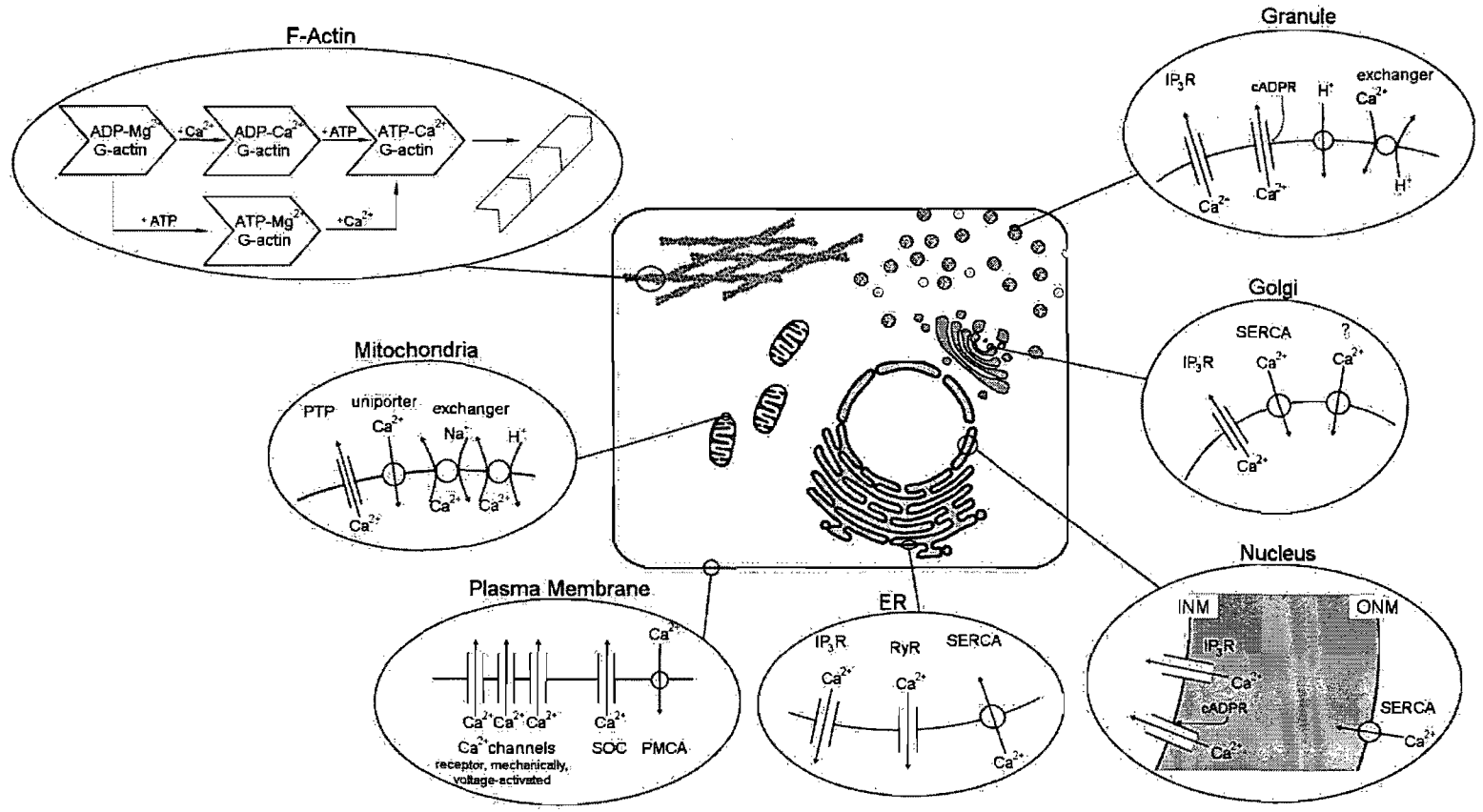


Figure 1.2: Schematic drawing of a cell showing parts of its structure responsible for controlled intracellular Ca^{2+} movement.

PTP, permeability transition pore; SOC, store-operated Ca^{2+} channel; PMCA, plasma membrane Ca^{2+} ATPase; ER, endoplasmic reticulum; IP_3R , inositol-1,4,5-triphosphate receptor; RyR, ryanodine receptor; SERCA, sarco/endoplasmic reticulum Ca^{2+} ATPase; INM, inner nuclear membrane; ONM, outer nuclear membrane; cADPR, cyclic ADP-ribose

It forms a complex continuous network system of endomembranes which can be structurally divided into rough ER, smooth ER and nuclear membrane. The entire ER controls a wide range of cellular processes such as synthesis and storage of transmembrane and secretory proteins, lipids, steroids and other biomolecules [11]. Mainly the smooth ER also plays a central role in signalling processes by producing local or global Ca^{2+} fluctuations. It releases Ca^{2+} into the cytosol through RyR Ca^{2+} channels via CICR and cyclic ADP-ribose (cADPR) activation [87], or through IP_3R Ca^{2+} channels via IP_3 -induced Ca^{2+} release (IICR) [104]. The role of the ER as an internal Ca^{2+} store and signalling organelle is supported by several families of proteins localized in the endomembrane as well as within the ER lumen: especially by the Ca^{2+} pumps, which belong to the sarco/endoplasmic reticulum Ca^{2+} ATPase (SERCA) type, three types of IP_3R and three types of RyR Ca^{2+} release channels, as well as intraluminal Ca^{2+} -binding proteins most of which also serve as Ca^{2+} -regulated enzymes. It is, furthermore, supported by the high degree of organization with specialized regions that are localized close to areas where they can generate specific Ca^{2+} signals [104]. Since the ER has a finite capacity, its signalling function depends on the abundance of Ca^{2+} in its lumen. To prevent Ca^{2+} store depletion, the cell employs a store-operated entry mechanism to ensure a sufficient replenishment of the ER with Ca^{2+} . The entry of Ca^{2+} takes place through store-operated Ca^{2+} channels (SOC) in the plasma membrane after their stimulation by an empty ER. The nature of the signal emanating from the ER and the identity of the SOCs were a matter of debate for 20 years. Only recently were two major players in the signalling and permeation mechanism discovered: an ER Ca^{2+} -sensor, called STIM1⁶, was found to be involved in the activation of SOCs by triggering Orai proteins, which constitute subunits of SOCs, to form a pore [105, 106].

The *Mitochondria* are functionally closely connected with the Ca^{2+} signalling function of the ER. They cooperate in generating Ca^{2+} signals of precise shape, the ER releasing Ca^{2+} and the mitochondria assisting in the recovery

⁶STIM1 is a single spanning membrane protein with an unpaired Ca^{2+} binding EF-hand.

phase by rapidly sequestering it. After the recovery phase, the mitochondria return the sequestered Ca^{2+} back to the ER [107]. At equilibrium, most of the Ca^{2+} resides within the lumen of the ER. During a Ca^{2+} signal, Ca^{2+} moves from the ER lumen into the mitochondria, where it induces the generation of reactive oxygen species (ROS) [107]. ROS can feedback to the ER and sensitize its Ca^{2+} release channels. This ROS-dependent sensitization of the Ca^{2+} release channels is particularly important when the cell has to generate repetitive Ca^{2+} spikes [104, 108]. A prolonged shift of Ca^{2+} from the ER to the mitochondria induces a number of stress signals (including ROS) which triggers the onset of apoptosis by activating the formation of a permeability transition pore (PTP) [108].

The *Nucleus* is surrounded by a double membrane, the nuclear envelope, that separates it from the cytoplasm. Both of the membranes have characteristics of the ER, the outer nuclear membrane (ONM) containing a SERCA and the inner nuclear membrane (INM) containing IP_3R and RyR Ca^{2+} channels [102]. The nuclear envelope contains large nuclear pores with a large ion conductance which is drastically reduced either after accumulation of Ca^{2+} inside the nuclear envelope or by transport of macromolecules through nuclear pore complexes [102]. Upon stimulation, many cells exhibit Ca^{2+} signals both in the cytosol and the nucleus. The following ways of nuclear Ca^{2+} signal generation exist: • Ca^{2+} may reach the nucleus directly from the cytosol through the nuclear pores [102]. • Nuclear Ca^{2+} signals can be triggered independently of cytosolic Ca^{2+} signals by direct release of Ca^{2+} from the nuclear envelope. IP_3 , cADPR and nicotinic acid adenine dinucleotide phosphate (NAADP) were observed to induce such a release [102]. • Ca^{2+} could be released to the nucleoplasm from Ca^{2+} containing microvesicles which reside in the nucleoplasm [102]. In contrast to the mitochondria and the ER, the nucleus does not act as a Ca^{2+} sink. Rather, the nuclear envelope is destined to slow down the cytosolic Ca^{2+} wave to the nucleus since a rise in nuclear Ca^{2+} controls specific nuclear processes such as gene transcription, development, protein transport into the nucleus and cell growth [109].

The *Golgi Apparatus* primarily processes, sorts and packs macromolecules synthesized by the cell for secretion (exocytosis) or for use within the cell. Changes in Ca^{2+} concentration either within the Golgi lumen or in the adjacent cytosol regulate Golgi function. In addition, the Golgi apparatus contains a release and sequestration apparatus for Ca^{2+} which accumulates it to a concentration of around $300 \mu\text{M}$ [110]. The generation of IP_3 stimulates Ca^{2+} release from the Golgi through the IP_3R release channel which is the only Ca^{2+} release channel found in the Golgi membrane. The Golgi apparatus contains, furthermore, two types of Ca^{2+} ATPases, one of which is a thapsigargin-sensitive SERCA and the other a thapsigargin-insensitive secretory pathway Ca^{2+} ATPase (SPCA) [110]. The Golgi collaborates with the ER – with different kinetics – in elevating cytosolic Ca^{2+} in response to IP_3 stimulation and modulates the duration and pattern of cytosolic Ca^{2+} signals [110].

Lysosomes and *Acidic Secretory Granules* were found to be responsible for nicotinic acid adenine dinucleotide phosphate (NAADP) induced Ca^{2+} release [111]. NAADP-sensitive Ca^{2+} channels are located on lysosome-related acidic organelles. These organelles are thapsigargin-insensitive and are loaded with Ca^{2+} by a $\text{H}^+/\text{Ca}^{2+}$ exchanger [111]. There has been a considerable amount of controversy regarding the ability of secretory granules to actively participate in the regulation of Ca^{2+} concentration in their environment. Since, however, exocytosis requires high local Ca^{2+} concentrations, it strongly suggests that Ca^{2+} release from secretory granules is an appropriate signal [99].

The theory of *F-Actin*⁷-dependent Ca^{2+} signalling is based on the *in vitro* observation that F-actin is able to store and release Ca^{2+} within the physiological concentration range of $20 - 1000 \text{ nM}$ Ca^{2+} [103]. Ca^{2+} is bound to a high-affinity binding site of G-actin⁸ in a reversible manner. In the polymerized F-actin form, the Ca^{2+} binding site is inaccessibly hidden within the

⁷F-actin or filamentous actin is a polymer of G-actin subunits [11].

⁸G-actin or globular actin is the actin monomer which polymerizes above a critical concentration to F-actin [11].

filament structure [103]. The Ca^{2+} -storing actin system has the following characteristics: • Monomeric ATP-G-actin is the high-affinity Ca^{2+} -binding species of the store exhibiting a pH-dependent $K_d^{\text{Ca}^{2+}} = 2 - 8 \text{ nM}$ [103]. • Monomeric ADP-G-actin is the low-affinity Ca^{2+} -binding species of the store with a 100-fold lower affinity for Ca^{2+} ($K_d^{\text{Ca}^{2+}} = 400 \text{ nM}$) compared to the high-affinity monomeric ATP-G-actin [103]. • Ca^{2+} bound to the high-affinity Ca^{2+} -binding site of F-actin can only be released upon depolymerization to G-actin monomers. The $\text{Ca}^{2+}/\text{Mg}^{2+}$ exchange rate, $k_{\text{ex}}^{\text{Ca}^{2+}}$, on F-actin is about 4 000-fold lower than on G-actin [103].

Spatiotemporal modulation of Ca^{2+} signals

Since intracellular Ca^{2+} controls a large number of different processes in the same cell, the spatial and temporal organization of cytosolic Ca^{2+} signals is of crucial importance. Stimulation of cells can evoke Ca^{2+} signals that are either local or global, depending on the agonist concentration and the length of the stimulation period [112]. Moreover, the following features of the Ca^{2+} signalling machinery control the localization of high- Ca^{2+} concentration:

- Although the Ca^{2+} ion is very mobile in water, it diffuses only slowly in the cytosol due to the many high-affinity binding sites on relatively immobile proteins, such as actin. The combination of the rapidly diffusible messenger IP_3 with the slowly diffusible Ca^{2+} in succession enables the restriction of Ca^{2+} signalling events to a local area [86].
- Many effects of Ca^{2+} are initiated through binding to calmodulin (CaM). In these cases, the final response to the Ca^{2+} signal depends on both the local Ca^{2+} and CaM concentrations [113].
- Upon activation, elementary Ca^{2+} -releasing events are produced by the brief opening of a single or a small group of Ca^{2+} channels located in either the plasma membrane or in intracellular Ca^{2+} -storing organelles. These elementary events appear as localized plumes of Ca^{2+} around the channels and have been labelled with different names depending on the channel responsible for their formation: 1) A *sparklet* is formed as a

result of the brief opening of voltage-operated channels. 2) A *spark* is formed by the opening of RyR Ca^{2+} channels. 3) A *puff* results from the release of Ca^{2+} from IP_3R Ca^{2+} channels [114].

- Of particular significance with regard to the spatiotemporal aspects of Ca^{2+} signalling is the process of CICR from both types of intracellular receptor channels, the IP_3R and RyR. This Ca^{2+} sensitivity enables the Ca^{2+} released from one receptor to stimulate Ca^{2+} release from its neighbours, thereby causing a regenerative wave of Ca^{2+} release throughout the entire cytosol. Especially, puffs are the building blocks of intracellular Ca^{2+} waves in cells and are likely to be responsible for global Ca^{2+} signals [112].
- A close juxtaposition of mitochondria with a cluster of release channels can form a rapid and transient high- Ca^{2+} microdomain in the perimitochondrial space (see page 16).
- Intracellular pH is known to modulate IP_3 -induced Ca^{2+} release by altering binding of IP_3 and Ca^{2+} to the receptor site [115, 116]. In addition, the activity of several membrane proteins, including channels, exchangers and pumps are pH sensitive. A change in intracellular pH may control, therefore, intracellular Ca^{2+} homeostasis [117–119].

As a result of the different Ca^{2+} influx pathways (see page 14) and the feature of the Ca^{2+} signalling machinery, the cell is able to precisely manipulate the location, size, shape and duration of intracellular Ca^{2+} elevation, enhancing greatly the versatility, accuracy and efficiency of Ca^{2+} signalling.

Stimuli provoking calcium signalling

Inside the cell, the Ca^{2+} ion acts as a secondary messenger, relaying signals received on the outer cell surface into the cell interior and amplifying their strength.

The main stimuli that can trigger intracellular Ca^{2+} elevation are:

- Biomolecules, which can be functionally classified as:

1. Hormones – chemical messengers, usually peptides or steroids, produced and released into the bloodstream by one tissue and affecting another [120].
 2. Neurotransmitters – chemical messengers, such as acetylcholine, dopamine, etc., that transmit nerve impulses across a synapse [120].
 3. Extracellular matrix components – including fibronectin, laminin, collagen, etc., that are involved in the transmission of mechanical stimuli via membrane-attached integrins [121].
 4. Cytokines – regulatory proteins and peptides, e.g. interleukines and interferon, produced by cells of the immune system [122].
 5. Extracellular nucleotides and adenosine – messengers involved in purinergic signalling (see chapter 1.1).
- Environmental stimuli, such as:
 1. Physical stimuli (e.g. light [123], change in electrical potential difference [124], shear stress [125], osmotic stress [26, 126]).
 2. Chemical stimuli (e.g. extracellular oxidative stress [123], taste [123], odour [127]).

All molecular messengers bind to receptors on the outer side of the plasma membrane, which can be classified as:

- Ionotropic receptors, which are ligand-gated ion channels that open or close in response to agonist binding [128].
- Metabotropic receptors, which are G-protein⁹ coupled receptors that dissociate into G_{α} and $G_{\beta\gamma}$ subunits upon agonist binding and then interact with effectors [129]:

G_{α} can be subdivided into four main families:

G_{α_s} stimulates adenylyl cyclase and increases the level of cAMP.

⁹ *Guanine nucleotide-binding* protein

G_{α_q} stimulates phospholipase C and generates the second messengers IP_3 and diacylglycerol (DAG).

G_{α_i} inhibits adenylyl cyclase and lowers the level of cAMP.

G_{α_t} increases cGMP Phosphodiesterase and lowers the level of cGMP.

$G_{\beta\gamma}$ directly regulates many proteins, including enzymes and channels.

Ca^{2+} influx across the plasma membrane can, furthermore, occur via mechanically and voltage-activated Ca^{2+} channels.

The primary trigger employed in the experiments conducted for this Ph.D. project was osmotic stress induced by a 50% hypotonic solution. It caused cell-swelling induced, Ca^{2+} -dependent ATP release. The justification for this choice of stimulus is stated in the introduction. The source and progress of the Ca^{2+} signal were studied extensively in the course of this Ph.D. project. The results are presented in section 3.2.

Calcium signalling in regulated exocytosis

Regulated exocytosis requires an elevation of intracellular Ca^{2+} concentration over the basal level of ~ 100 nM. The extent of the fusion process is controlled by the magnitude and duration of local intracellular Ca^{2+} increase. Either full fusion of the vesicle or "kiss-and-run" fusion – where the vesicle's integrity is maintained and only transient release is achieved – is possible [130]. The required Ca^{2+} elevation may originate either from Ca^{2+} entry across the plasma membrane or from Ca^{2+} mobilization from internal stores, or from both. Non-excitabile cells rely on Ca^{2+} entry through ionotropic receptors as well as metabotropic receptor-activated second-messenger-induced mobilization of Ca^{2+} from intracellular stores [131].

Ca^{2+} regulation of exocytosis is achieved via the interaction with a number of distinct molecular targets located at or near the site of membrane fusion. Various proteins with Ca^{2+} -binding domains and Ca^{2+} -activated protein kinases are involved in the regulation of exocytosis, including SNARE proteins, synaptotagmin, munc18, syntaxin, calmodulin, CaMKII, PKC and others.

Since a further description of these proteins and their function goes beyond the scope of this Ph.D. thesis, the interested reader is referred to the many detailed review articles which have been written on this topic [130, 132–138].

Chapter 2

Theory of the experimental methods

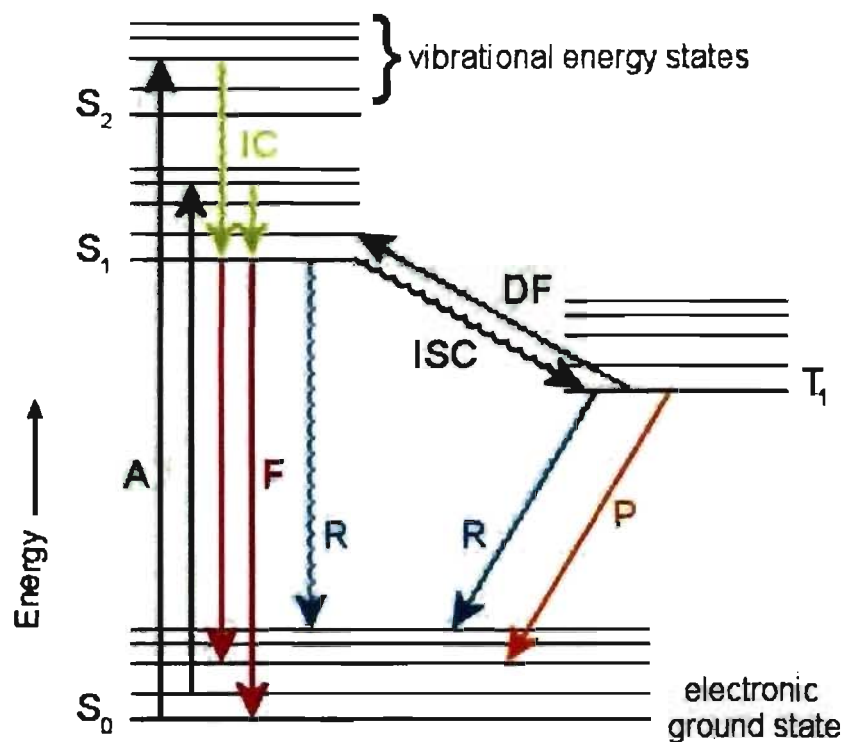
2.1 Luminescence

2.1.1 Overview

Luminescence is a general term for any process in which photons are emitted from a system that was shifted to an excited electronic state by some form of energy [139]. Fig. 2.1 on page 25 presents a schematic depiction¹⁰ of vibrational and electronic transitions.

Multiple mechanisms exist by which a system can be excited [139]. Table I on page 26 lists the most important types of luminescence according to the excitation mechanism. *Photoluminescence* occurs after excitation with light (i.e. radiation within the optical range – UV to IR), whereas *chemiluminescence* appears as a result of a chemical reaction. *Bioluminescence* is a special form of chemiluminescence in presence of an enzyme. Photoluminescence and bioluminescence will be discussed more in depth as part of the techniques used in the course of this Ph.D. work. Special attention will be given to the phenomenon of fluorescence as a pathway for deactivation of photoluminescence.

¹⁰called Jablonski Diagram after the Polish photophysicist Aleksander Jabłoński

Figure 2.1: Jablonski diagram¹¹

S	Singlet state
T	Triplet state
A	Absorption (10^{-15} s)
F	Fluorescence ($10^{-9} - 10^{-7}$ s)
P	Phosphorescence ($10^{-3} - 10^2$ s)
R	Non-radiative relaxation (e.g. quenching)
IC	Internal conversion ($10^{-14} - 10^{-11}$ s)
ISC	Intersystem crossing ($10^{-6} - 10^{-5}$ s)
DF	Delayed fluorescence

¹¹The distances between electronic states and vibrational states are not to scale.

Table I: Various types of luminescence

Term	Excitation mechanism
Photoluminescence	Light
Chemiluminescence Bioluminescence	Chemical reaction
Cathodoluminescence	Electrons
Thermoluminescence	Heating
Radioluminescence	X-rays, α -, β - or γ -rays
Electroluminescence	Electric field or current
Triboluminescence	Mechanical energy
Sonoluminescence	Sound waves in liquids

2.1.2 Photoluminescence

Photoluminescence is the emission of light subsequent to the absorption of light. The absorbance A of light by a substance follows the law of Lambert-Beer:

$$\lg \frac{I_t}{I_0} = -\varepsilon Cl = -A \quad (2.1)$$

I_0 intensity of incident light [lx]

I_t intensity of transmitted light [lx]

ε molar absorptivity [$\text{m}^2 \cdot \text{mol}^{-1}$]

C concentration of absorbing molecules [$\text{mol} \cdot \text{l}^{-1}$]

l depth of the sample [m]

The molar absorptivity coefficient (also *molar extinction coefficient*) is an intrinsic measure of absorption strength of a substance at a specific wavelength. The absorbance A is higher, the higher the ε . The energy of absorbed

light is given by Planck's relation:

$$E = Nh\nu = Nh\frac{c}{\lambda} \quad (2.2)$$

- E energy [J]
 N Avogadro's number
 h Planck's constant [$6.626 \cdot 10^{-34}$ J · s]
 ν light frequency [s^{-1}]
 c velocity of light [$2.998 \cdot 10^8$ m · s^{-1}]
 λ light wavelength [nm]

Electronic excitation of a substance occurs only if E corresponds to the difference in energy between its ground electronic state (S_0 in Fig. 2.1, page 25) and the electronically excited state (S_1 or S_2 in Fig. 2.1, page 25).

Fluorescence is the radiative transition between excited state and ground state of the same spin multiplicity which occurs in a time frame of 10^{-9} – 10^{-7} s after excitation (called fluorescent life time τ_f) [140]. Several processes, such as quenching and intersystem crossing (see Fig. 2.1, page 25), compete with fluorescence for the deactivation of the vibrationally lowest excited state. Hence, the intensity of fluorescence I_f can be determined by following equation [140]:

$$I_f = I_a \Phi_f \quad (2.3)$$

- I_f intensity of fluorescence [lx]
 I_a intensity of absorbed light ($I_0 - I_t$) [lx]
 Φ_f fraction of excited molecules that fluoresce ($\frac{\text{number of events}}{\text{number of photons absorbed}}$)

Since every electronic state of a molecule has several associated vibrational levels, excitation and emission do not occur at one single wavelength, but over a range of wavelengths, called a spectrum. Before electrons return from the excited state to the ground state, they lose vibrational energy as

part of internal conversion. As a result, the emission spectrum is shifted to longer wavelengths than the excitation spectrum, which is known as *Stokes shift*¹² [140]. The greater the Stokes shift, the less excitation and emission spectra overlap. As a result, it is easier to eliminate excitation light by appropriate selection of excitation and emission filters for a better detection of the weaker fluorescence light.

2.1.3 Bioluminescence

Bioluminescence is the process of light production through oxidation of a compound catalyzed by an enzyme. The light production results from the generation of a product molecule in an excited state. In order to discard the excess of energy, the molecule either fluoresces or transfers its energy to a fluorescent acceptor (sensitized bioluminescence) [141]. Each chemiluminescent compound or group can produce no more than one photon of light. The quantum yield of bioluminescence is, therefore, the ratio of the total number of photons produced to the total number of substrate molecules utilized. It can be expressed as the product of several terms [141]:

$$\Phi_b = \Phi_c \cdot \Phi_f \cdot \Phi_{ex} \quad (2.4)$$

Φ_b	$\frac{\text{total number of photons produced}}{\text{total number of substrate molecules utilized}}$
Φ_c	chemical yield of product; in general, $\Phi_c = 1$
Φ_f	fraction of excited molecules that fluoresce
Φ_{ex}	fraction of product molecules produced in an electronically excited state

Numerous examples of bioluminescence exist in nature, most notably the light emitted by the male firefly. Other examples include glow worms, certain mushrooms and various marine organisms [142]. In these organisms, a compound called luciferin reacts with an ATP-complex of the enzyme luciferase to form an excited oxidized molecule that subsequently emits light.

¹²after the Irish mathematician and physicist Sir George Gabriel Stokes

It is important to note that the names luciferin and luciferase are generic terms for the active agent in bioluminescent organisms, and that their actual molecular structures differ significantly from organism to organism [142, 143].

2.2 ATP release chamber and ATP evaluation

2.2.1 Evaluation of ATP

General considerations

Two methods are mainly used for the evaluation of ATP: the luciferase-luciferin assay [144] and high-performance liquid chromatography combined with fluorescence detection (HPLC-F) of derivatized nucleotides [145]. Both techniques are very sensitive and allow the detection of ATP down to ~ 0.5 pmol [144, 145]. The luciferase-luciferin assay is very simple and does not require any additional handling of the sample. However, it allows solely the detection of ATP. On the other hand, HPLC-F enables a simultaneous detection of all nucleotides and nucleosides from one sample, but involves a derivatization step between collection and measurement.

Radiolabelled ATP has also been used in the detection of ATP release. However, the incorporation of the radioactive label does not necessarily follow the uptake and release of endogenous ATP, and the released radioactive label is a mixture of ATP and other purines liberated from the cell. Consequently, it does not provide a clear evaluation of the amount of released endogenous ATP [146].

Both methods, the luciferase-luciferin assay and HPLC-F, were applied in the scope of this Ph.D. work to evaluate ATP released from A549 cells upon hypotonic shock (see section 3.1 and 3.2). However, HPLC-F was performed elsewhere (by Dr. Silvia Kreda, University of North Carolina at Chapel Hill, Cystic Fibrosis/Pulmonary Research Treatment Center) and therefore will not be described here in detail. The luciferase-luciferin assay is elaborated in the following subsection.

Luciferase-luciferin assay

Fig. 2.2 on page 32 delineates the particular reaction steps of the formation of oxyluciferin and light in the presence of the enzyme luciferase. The first reaction catalyzed by luciferase is the formation of adenylyl-D (-)-luciferin (an active form of luciferin) from D (-)-luciferin and ATP-Mg. The oxidation

of the acyl adenylate by oxygen leads to the formation of an enzyme-bound product molecule in the excited state. The complex decays to free luciferase and the ground-state oxyluciferin with the emission of light [147]. The luminescence intensity is proportional to the ATP concentration if firefly reagents are present in excess [148].

At low ATP concentrations, luminescence rises to a maximum value and remains constant for a minute or longer. As the ATP level increases, there is a rapid rise to peak luminescence intensity followed by a rapid decay due to product inhibition [149, 150].

The high specificity of the light reaction for ATP is the basis for the utilization of this reaction for the evaluation of ATP. Other nucleoside triphosphates are inactive in light production and, importantly, only negligibly inhibit the reaction with ATP [151]. Some nucleoside triphosphates even support photon production due to the promotion of the dissociation of the oxyluciferin-luciferase complex [152], or in the presence of transphosphorylases, due to the coupling of nucleoside triphosphates to ATP production [153].

The performance of the luciferase-luciferin assay has been enhanced by modifications of the luciferase enzyme, which increases its chemical and physical stability [144]. Furthermore, different reaction conditions, including the presence of particular cations or anions, and the type of solvent influence the activity of firefly luciferase, the kinetics of light emission, as well as the emission spectra and quantum yield of firefly bioluminescence. They have to be known or adequately chosen to correctly evaluate quantitative ATP measurements, and are therefore presented in the following paragraphs.

EFFECT OF METAL IONS

The bioluminescent luciferase-luciferin reaction requires a divalent cation. The actual substrate for the reaction is the ATP-Mg complex, while uncomplexed ATP competitively inhibits the reaction. Some divalent metal-ions can replace Mg^{2+} , such as Mn^{2+} and Ca^{2+} , which both enhance the bioluminescent reaction. On the other hand, cations such as Sr^{2+} , Zn^{2+} , Cd^{2+} , Ni^{2+} , Ba^{2+} , Cu^{2+} , Sn^{2+} , Co^{2+} , Ca^{2+} , Hg^{2+} , as well as the lanthanide Gd^{3+} ,

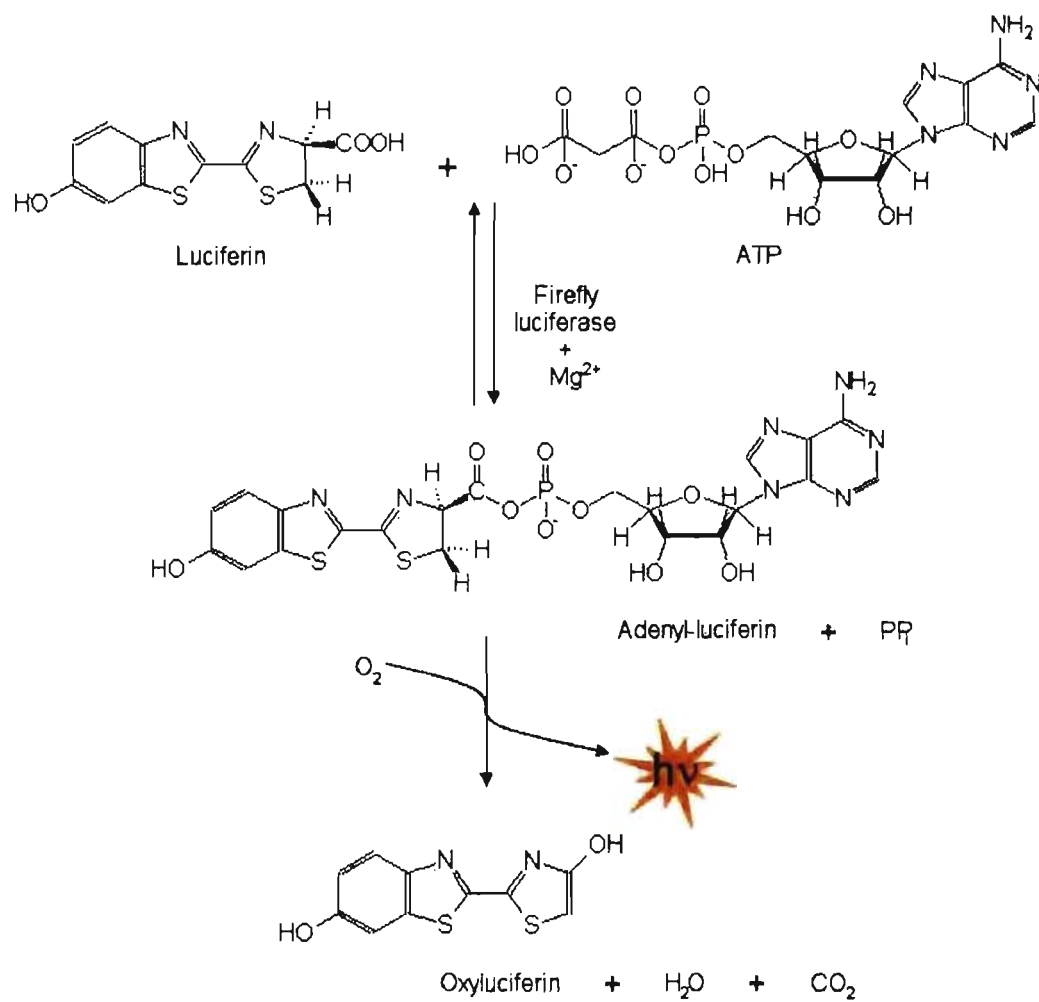


Figure 2.2: Luciferase-luciferin bioluminescence

inhibit the reaction to various degrees [154, 155]. Millimolar and higher concentrations of all cations except Mg^{2+} , Ca^{2+} and Mn^{2+} inhibit luminescence strongly. The addition of monovalent metal salts always leads to the inhibition of luciferase. The degree of inhibition varies depending on the anion part of the salt (see next paragraph) [155].

EFFECT OF ANIONS

The activity of firefly luciferase was shown to be very sensitive to the presence of anions, and the amount of inhibition at a particular ionic strength was strongly dependent on the nature of the anion. The inhibitory effect of anions increases in the following order: $\text{Cl}^- < \text{CO}_3^{2-} \sim \text{SO}_3^{2-} \sim \text{Br}^- < \text{SO}_4^{2-} \sim \text{PO}_4^{3-} < \text{NO}_3^- < \text{I}^- \ll \text{Cr}_2\text{O}_7^{2-} \ll \text{Fe}(\text{CN})_6^{3-}$ [155, 156]. The inhibition by these anions is non-competitive with respect to luciferin [155]. Arsenate AsO_4^{3-} and other anions were used to reduce background light, which interfered with the detection of low levels of ATP. They are also used to inhibit peak fluorescence preventing the rapid decay in fluorescence intensity at high ATP levels [150]. Na^+ , K^+ , and NH_4^+ cations have been found to have no influence on the extent of the inhibition of their anions [156].

EFFECT OF SOLVENTS

At neutral and alkaline pH the colour of light emitted is yellow-green, whereas at acid pH a red emission is observed using luciferase from *Photinus pyralis* [157]. The quantum yield for the bioluminescent reaction at alkaline pH is close to unity, indicating the formation of an excited product-luciferase-complex that is protected from solvent quenching [157].

Various solvents, such as polyvinylpyrrolidone, polyethylene glycols and non-ionic detergents, stimulate the activity of firefly luciferase. The solvents affect the oxidative reaction and enhance both peak light and total light emission [158].

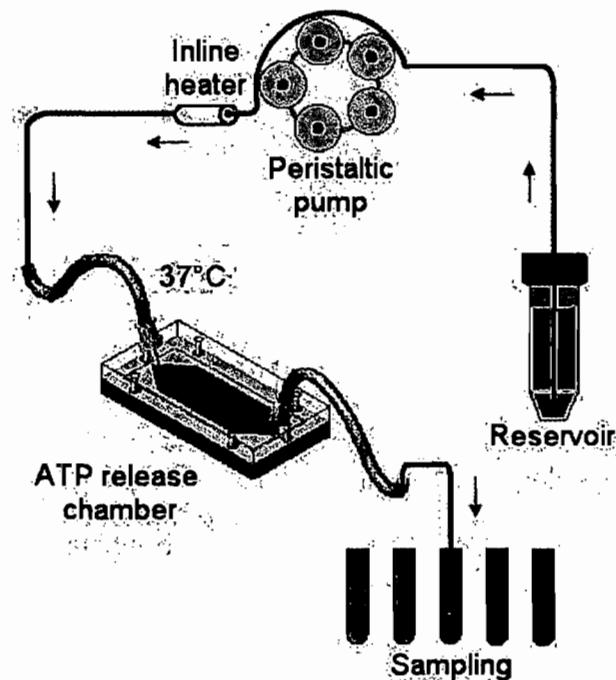


Figure 2.3: Chamber for hypotonicly induced ATP release

2.2.2 Chamber for hypotonicly induced ATP release

A low-volume, flow-through chamber was previously designed to collect ATP secreted during hypotonic challenge [26]. Fig. 2.3 on page 34 illustrates the experimental set-up:

A 24 mm x 60 mm cover-glass slip with an adherent cell monolayer is placed between two 6 mm-thick polycarbonate plates, one of them bearing a 0.5 mm-thick silicon gasket (cut out of a medical grade silicon rubber sheet). The cut-out area of the silicon sheet is $\sim 600 \text{ mm}^2$.

The physiological or hypotonic solution are pumped from a reservoir through an in-line heater and enter the ATP release chamber at a temperature of 37°C. After the perfusion of the chamber with the cell monolayer, the solution is collected into fractions of 30 s to 1 min, respectively. Their ATP content is measured by the luciferase-luciferin assay.

The time course of ATP release during the experiment can be evaluated by the following equation:

$$[\text{ATP}]_{\text{rel}} = (Lu - Bk) \cdot \left[\frac{1}{Tn \cdot (Lu_{\text{ini}} - De \cdot sn)} \right] \cdot ps \cdot \left[\frac{10^6}{qc} \right] \quad (2.5)$$

$[\text{ATP}]_{\text{rel}}$	amount of ATP released
Lu	acquired luminescence [rLU] ¹³
Bk	background fluorescence [rLU]
Tn	tonicity (e.g. 1 for isotonic; 0.7 for 30% hypotonic)
Lu_{ini}	initial calibration with 100 nM ATP [(100 nM ATP) ⁻¹]
De	decrease in luminescence [rLU]
sn	sample number
ps	perfusion speed [ml · min ⁻¹]
qc	quantity of cells (~ 500 cells mm ⁻² for A549) [confluent cells]

Consequently, the unit for $[\text{ATP}]_{\text{rel}}$ is:

$$\left[\frac{100 \text{ pmoles ATP}}{\text{min} \cdot 10^6 \text{ confluent cells}} \right]$$

¹³relative light unit

2.3 Ratiometric imaging

Ratiometric imaging is a fluorescence microscopic technique that takes advantage of the spectral shifts exhibited when fluorescent dyes bind to their target ions. Since intracellular ion measurements with ratiometric indicators are relatively independent of uneven dye loading, cell thickness, photobleaching effects and dye leakage, this method is generally given preference over non-ratiometric imaging [159]. Various types of ratiometric imaging have been developed, including Fura-2 imaging of intracellular calcium and BCECF imaging of intracellular pH.

2.3.1 Basic principles

Requirements for the fluorescent indicator

Fluorescent dyes used for ratiometric imaging are designed to have high selectivity, but low affinity for the specific ion in question. High selectivity assures an accurate and specific measurement of ion concentration, whereas low affinity is necessary to avoid non-genuine alteration of intracellular ion concentrations as a result of ion binding to the dye [160]. Fast kinetics in ion binding is required for kinetic studies of intracellular ion alterations [159]. Large absorbance and large fluorescence changes resulting from ion binding are also essential attributes for an effective performance of the dye [161].

Experimental set-up

Ratiometric imaging by means of microscopy requires an epifluorescence microscope (see page 171) equipped with a CCD or other type of detector, and a computer for system control and image processing. A multi-filter wheel with two different excitation filters are controlled by the computer and placed in the path of excitation light. Fluorescent images are recorded with the detector, digitized and stored. A subsequent image analysis and processing enable quantification of spatial and temporal distribution of ion concentration within the cell [159]. To avoid photobleaching and phototoxicity, low

levels of excitation energy, short exposition time and high sensitivity detectors should be used.

Loading of the cells

Most fluorescent indicators are membrane-impermeable. Various dye-loading procedures were developed, of which some are considerably invasive to the cell [159]. In contrast, derivatization of the indicators to acetoxymethyl (AM) esters renders them cell-permeable, and enables them to passively diffuse across the intact cell membrane. Inside the cell, ubiquitous intracellular esterases hydrolyze the AM group and release the ion-sensitive polyanionic, cell-impermeable indicator. The final intracellular concentration and the degree of hydrolyzation of the indicator, which can reach up to several millimolar [161], depends on various factors, including type of indicator, cell type, loading concentration of indicator, number of cells, loading time, loading temperature and potential pre- and post-treatment of cells [159]. The loading medium should not contain any amino acids or amines because they may cleave the AM esters and prevent loading. The nonionic and nondenaturing detergent Pluronic[®] F-127 (see page 277) is frequently added to help disperse the indicator in the loading medium, especially at low loading temperatures. Some problems during the cell loading process have been encountered [162, 163]:

1. Indicators may be sequestered in non-cytoplasmic compartments (i.e. cytoplasmic organelles) either due to incomplete hydrolysis of the AM ester or mediated by organic anion transport systems;
2. Loaded cells may actively and passively lose dye, either due to incomplete hydrolysis of the AM ester or mediated by organic anion transport systems.

The following solutions have been found:

1. Sequestration of the fluorescent indicator can be avoided through low loading temperatures (15–33 °C) or through pre-chilling at 4 °C before loading the cells [162].

2. Ratiometric measurements help to minimize the impact of indicator leakage on experimental data (see above). However, active extrusion of anionic indicators from cells by organic ion transporters should be reduced by performing experiments at lower than physiologic temperatures (15 – 33 °C) or by applying inhibitors such as probenecid (see page 279) or sulfinpyrazone [163].

2.3.2 Calcium imaging

Calcium indicators shift their absorption spectrum and change their emitted fluorescence intensity in response to $[Ca^{2+}]_i$ alterations in the range between $0.3 \cdot K_d$ and $10 \cdot K_d$ [159]. A description of the ratiometric Ca^{2+} chelator Fura-2 is given on page 270. To estimate $[Ca^{2+}]_i$, fluorescent intensities ($\lambda_{em} = 520$ nm) are acquired for $\lambda_{ex1} = 340$ nm and $\lambda_{ex2} = 380$ nm and entered into the following equation [164]:

$$[Ca^{2+}] = K_d \left(\frac{R - R_{min}}{R_{min} - R} \right) \left(\frac{F_{380_0}}{F_{380_s}} \right) \quad (2.6)$$

K_d	equilibrium dissociation constant for Ca^{2+} and Fura-2, according to [164]: ~ 224 nM at 37 °C
R	Ratio (F_{340}/F_{380}) of measured fluorescence intensity
R_{min}	ratio (F_{340}/F_{380}) of fluorescence intensity, formed at minimum Ca^{2+} concentration
R_{max}	ratio (F_{340}/F_{380}) of fluorescence intensity, formed at maximum Ca^{2+} concentration
F_{380_0}	fluorescence intensity for $\lambda_{ex2} = 380$ nm at minimum Ca^{2+} concentration
F_{380_s}	fluorescence intensity for $\lambda_{ex2} = 380$ nm at maximum Ca^{2+} concentration

For *in situ* calibration of Fura-2, ionomycin (see page 272) is used as ionophore to equilibrate the controlled external ion concentration with the ion concentration within the cell [165]. The calibration procedure is complex and rather

imprecise and is, therefore, avoided if a qualitative analysis is sufficient.

2.3.3 Intracellular pH

The pH indicator BCECF is characterized on page 266. Intracellular pH measurements with BCECF are accomplished by measuring the pH-dependent fluorescence intensity ($\lambda_{em} = 535$ nm) for $\lambda_{ex_1} = 490$ nm and for its isosbestic point¹⁴ of $\lambda_{ex_2} = 440$ nm. They are entered into the following equation [166]:

$$\text{pH} = \text{pK} + \log \frac{(R - R_{max})}{(R_{max} - R)} \quad (2.7)$$

- pK pK value for BCECF under experimental conditions ($\text{pK}_a = 6.98$)
 R ratio (F_{495}/F_{440}) of measured fluorescence intensity
 R_{max} ratio (F_{495}/F_{440}) of fluorescence intensity at maximum calibrated

BCECF is commonly calibrated *in situ* using the K^+/H^+ ionophore nigericin in the presence of 100 – 150 mM K^+ to equilibrate internal and external pH [167].

¹⁴At the isosbestic point, the fluorescence spectrum of an indicator is independent of the ion concentration.

Chapter 3

Articles: Mechanism of ATP release

3.1 ARTICLE 1: Calcium-dependent release of adenosine and uridine nucleotides from A549 cells

3.1.1 Preamble

Previous results from this group showed that hypotonic shock-induced ATP release from A549 cells was tightly correlated with an intracellular Ca^{2+} signal. This finding suggested that ATP release from these cells is triggered by an intracellular Ca^{2+} elevation and pointed toward a Ca^{2+} -dependent exocytotic release mechanism [26].

The objective of this research was to reassess and to strengthen the assumption of a Ca^{2+} -dependent exocytotic ATP release mechanism from A549 cells and to further analyze the potential co-release of other nucleotides, i.e. ADP, AMP, adenosine, UTP and UDP.

3.1.2 Article

Tatur, S.; Kreda, S.; Lazarowski, E.; Grygorczyk, R.

Calcium-dependent release of adenosine and uridine nucleotides from A549 cells. *Purinergic Signalling*, Epub 25 July 2007.

Reproduced on pp. 42–72 with permission.

Running title: Nucleotide release and Ca^{2+}
Original Research Article

Calcium-dependent release of adenosine and uridine nucleotides from A549 cells

Sabina Tatur¹, Silvia Kreda², Eduardo Lazarowski² and Ryszard
Grygorczyk¹

¹ Research Centre, Centre hospitalier de l'Université de Montréal (CHUM) – Hôtel-
Dieu, and Department of Medicine, Université de Montréal, Montréal, Québec,
Canada

² Departments of Pharmacology and Medicine and the Cystic Fibrosis Center,
University of North Carolina, Chapel Hill, North Carolina


Address for correspondence:

Ryszard Grygorczyk

CHUM - Hôtel-Dieu

3850 rue Saint-Urbain, Montréal, Québec, Canada, H2W 1T7

Tel: (514) 890-8000 ext. 15089 Fax: (514) 412-7204


e-mail: 

or

Eduardo Lazarowski

University of North Carolina, 7017 Thurston-Bowles Bldg., CB 7248,

Chapel Hill, NC 27599-7248, U.S.A.

e-mail: 

Abstract

Extracellular nucleotides play an important role in lung defense, but the release mechanism and relative abundance of different nucleotide species secreted by lung epithelia are not well defined. In this study, to minimize cell surface hydrolysis, we used a low-volume, flow-through chamber and examined adenosine and uridine nucleotide concentrations in perfusate aliquots of human lung A549 cells challenged by 50% hypotonic shock. ATP, ADP, AMP, and Ado were quantified in HPLC analysis of fluorescent etheno derivatives, and UTP and UDP were measured using HPLC-coupled radioenzymatic assays. After the onset of hypotonic shock, ATP, ADP, UTP, and UDP in the perfusates increased markedly and peaked at approximately 2.5 min, followed by a gradual decay in the next 15-20 min; peak changes in Ado and AMP were relatively minor. The peak concentrations and fold increment (in brackets) were: 34 ± 13 nM ATP (5.6), 11 ± 5 nM ADP (3.7), 3.3 ± 1.2 nM AMP (1.4), 23 ± 7 nM Ado (2.1), 21 nM UTP (>7), and 11 nM UDP (27). Nucleotide release was almost completely abolished from cells loaded with the calcium chelator BAPTA. Under isotonic conditions, elevation of intracellular calcium with the calcium ionophore ionomycin (5 μ M, 3 min) also released nucleotides with kinetics and relative abundance as above, albeit less robust. ADP:ATP (1:3) and UDP:UTP (1:2) ratios in perfusates from stimulated cells were markedly higher than the cytosolic ratios of these species, suggesting that an NDP-rich compartment, e.g., the secretory pathway, contributed to nucleotide release. Laser confocal microscopy

experiments illustrated increased FM1-43 uptake into the plasma membrane upon hypotonic shock or ionomycin treatment, consistent with enhanced vesicular exocytosis under these conditions. In summary, our results strongly suggest that calcium-dependent exocytosis is responsible, at least in most part, for adenosine and uridine nucleotide release from A549 cells.

Keywords: Ca^{2+} dependence, exocytosis, hypotonic shock, lung epithelial cells, nucleotide secretion

Introduction

Extracellular nucleotides control a diverse range of physiological processes by interacting with a large group of cell surface P2Y and P2X receptor families [1-3]. In the lungs, extracellular nucleotides regulate airway surface liquid homeostasis and mucociliary clearance by modulating epithelial ion and fluid transport as well as ciliary beating [4]. In alveoli, ATP is a potent secretagogue that stimulates type II cell surfactant secretion. Nucleotide levels on airway surfaces, measured *in vitro* and *ex vivo*, show dynamic changes due to the combination of basal and stimulated release and their rapid metabolism by several groups of membrane-associated and secreted soluble ecto-enzymes. These ecto-enzymes extend the signaling potential of ATP by converting it to Ado, a ligand of the A₁₋₃ family of G protein-coupled receptors [1,4-7].

Nucleotide release is stimulated by cell mechanical perturbations, such as shear stress, membrane stretch, medium change, hyposmotic swelling and hypoxia [1,8]. It is now recognized that mechano-sensitive ATP release occurs from healthy cells via physiological processes, which do not involve cell damage. Numerous reports have suggested that the cystic fibrosis transmembrane conductance regulator (CFTR) and other members of the superfamily of ATP-binding cassette transport proteins serve as a conductive pathway for ATP release, or regulate an associated ATP channel. However, other groups using patch-clamp, lipid-bilayer and

luminometry techniques, have not found any detectable CFTR-mediated or CFTR-regulated ATP release (reviewed in [1]). Volume-regulated anion channels (VRAC) and voltage-dependent anion channels (VDAC, porins or maxi Cl⁻ channels) are known to have considerable permeability to cations and large organic anions, and several laboratories have implicated these channels in cell swelling-induced ATP release and the autocrine regulation of cell volume. However, recent studies have demonstrated that conductive pathways, including VRAC, VDAC and stretch-activated channels, are not involved in cell swelling-induced ATP release from A549 cells [1,9,10]. Finally, connexin hemichannels also have been proposed to mediate ATP release, but their role in this process in a physiological setting is not always clear [1].

While conductive release mechanisms are still being debated, exocytotic ATP release is well established in excitatory cells, blood platelets and chromaffin cells. Furthermore, there is growing experimental evidence supporting such a release mechanism also by epithelial and other non-excitatory cells. In particular, we have recently demonstrated that cell swelling-induced ATP release from A549 and 16HBE14o⁻ epithelial cells and NIH 3T3 fibroblasts is tightly correlated with intracellular Ca²⁺ elevations; it is abolished in cells loaded with the Ca²⁺ chelator BAPTA or by low temperature, strongly suggesting the involvement of Ca²⁺-dependent exocytosis [10]. Whether release of other nucleotides from epithelial cells

also involves Ca^{2+} -dependent exocytosis remains incompletely explored. Such studies, however, are complicated by nucleotide hydrolysis at the airway surface, which makes it difficult to assess the magnitude and relative abundance of different nucleotide species released. Therefore, we used a flow-through chamber to minimize cell surface hydrolysis.

We found that hypotonic shock markedly increased ATP, ADP, UTP, and UDP concentrations in perfusates, which peaked at approximately 2.5 min. Nucleotide release was almost completely abolished from cells loaded with the calcium chelator BAPTA and, under isotonic conditions, could be evoked by elevation of intracellular calcium with the calcium ionophore ionomycin. High nucleotide diphosphates (NDPs) concentrations in perfusates of stimulated cells suggested that an NDP-rich compartment, e.g., the secretory pathway, contributed to this release. Together with real-time FM1-43 fluorescence experiments, our results strongly indicate that calcium-dependent exocytosis is a major mechanism of adenosine and uridine nucleotide release from A549 cells.

Materials and Methods

Cells

Human lung carcinoma A549 cells were grown in DMEM supplemented with 10% FBS, 2 mM L-glutamine, 56 U/mL penicillin-G and 56 µg/mL streptomycin sulfate. All constituents of the culture media were from GIBCO-BRL (Burlington, ON). ATP efflux was measured from cell monolayers grown to confluency on 24x60-mm glass coverslips. Fura-2 calcium imaging and FM1-43 microscopy experiments were performed on cells grown on circular 15-mm diameter no. 1 glass coverslips.

Nucleotide efflux assay

To measure nucleotide efflux during hypotonic challenge with high temporal resolution, we used a custom-designed low-volume (300 µL), flow-through chamber, as described previously [10]. Briefly, 24x60-mm glass coverslips with confluent cell monolayers of ~500 cells/mm² were mounted in the chamber and perfused with warm (37°C/in-line heater - Warner Instrument Co., Hamden, CT) Ringer solution at the rate of 1.3 mL/min. The Ringer solution contained (in mM): 110.5 NaCl, 24 NaHCO₃, 1.3 KCl, 1 MgCl₂, 1 CaCl₂, 2.5 Na₂HPO₄, 2.5 KH₂PO₄, 1.2 K₂HPO₄, 10 glucose; pH 7.4 was maintained by bubbling with 5% CO₂. After an equilibration period in isotonic solution (5-15 min), a 50% hypotonic solution was applied, and the perfusate was continuously collected for 30-s intervals during the initial burst of ATP

secretion (0-5 min) and during 1 min elsewhere. Nucleotide concentrations in the samples were evaluated by high-performance liquid chromatography (HPLC) analysis, as described below. For studies in absence of extracellular calcium, CaCl_2 was omitted and the solutions were supplemented with 0.1 mM EGTA. The 50% hypotonic solution was prepared by appropriate reduction of salt concentration while divalent cation concentrations were kept constant.

HPLC quantification of adenine and uridine nucleotides

UTP concentrations were quantified by UDP-glucose pyrophosphorylase-based reaction [11]. Briefly, 100- μl samples were incubated in the presence of 0.5 U/mL UDPglucose pyrophosphorylase, 0.5 U/mL inorganic pyrophosphatase, 1.6 mM CaCl_2 , 2 mM MgCl_2 , 25 mM HEPES (pH 7.4), and $\sim 100,000$ cpm 1 μM [^{14}C]glucose-1P. Incubations lasted 1 h at 30°C. Reactions were terminated by heating the samples at 95°C for 2 min. Conversion of [^{14}C]glucose-1P to [^{14}C]UTP was determined by HPLC (Shimadzu) via a Nova Pack C18 column and ion pairing mobile phase. Radioactivity was measured on-line with a Packard Flo-One detector. Assay sensitivity was 1 pmol (3 nM in 100- μl samples)

UDP was quantitatively phosphorylated in the presence of [$\gamma^{32}\text{P}$]ATP, using nucleoside diphosphokinase (NDPK). Briefly, 100- μl samples containing 0.1 U/ml NDPK, 0.1 μCi 60 nM [$\gamma^{32}\text{P}$]ATP, 1.6 mM CaCl_2 , 2 mM MgCl_2 , and 25 mM HEPES (pH 7.4) were incubated for 5 min at 30°C. Reactions were terminated by heating the

samples at 95°C for 2 min. The resulting conversion of [$\gamma^{32}\text{P}$]ATP to [$\gamma^{32}\text{P}$]UTP was monitored by HPLC [12]. A calibration curve employing known amounts of UDP was chartered in parallel during each assay. This assay allows UDP quantification with sensitivity of 20 fmol (0.2 nM in 100- μl samples).

Etheno derivatization. Samples (200 μl) were derivatized for 30 min at 72°C in the presence of 1.0 M chloroacetaldehyde and 25 mM Na_2HPO_4 (pH 4.0). The resulting fluorescent 1,N6-ethenoadenine derivatives were analyzed by HLPC (Waters), in a Hamilton PRP-X100 anion exchange column, as described previously [4]. Etheno (ϵ)-ATP, ϵ ADP, ϵ -AMP, and e-adenosine were quantified with a sensitivity of 200 fmol (1 nM in 200- μl samples).

FM1-43 studies

Bulk exocytosis was quantified in A549 cells as changes in the fluorescence intensity of FM1-43 incorporated into the plasma membrane [13,14], and recorded by real-time confocal microscopy. Cells were washed with Hank's Balanced Salt Solution + 20 mM HEPES + 2 mM MgCl_2 and 1.6 mM CaCl_2 (HBSSH) or with HBSSH devoid of calcium (HBSSH 0 Ca). They were mounted onto the stage of a Leica SP2 AOBS confocal microscope equipped with HCX Apo L63x NA 0.9 immersion Leica lens and a 488 nm Argon laser. Experiments were initiated by incubation of the cells with 3 μM FM1-43. Cells were incubated for at least 10 min, and hypotonic shock was applied by decreasing salt concentration 33% while maintaining calcium, magnesium

and FM1-43 concentrations constant. Alternatively, cells incubated with FM1-43 in HBSSH or HBSSH 0 Ca were stimulated with 5-10 μ M ionomycin. Real-time recording was performed by laser scanning in the xz axes with a galvostage, initially every 10 and then every 30 s for the time periods indicated in the figures. Overall fluorescence intensity changes associated with the plasma membrane were estimated by measuring the intensity value associated with each pixel through time. The entire apical membrane compartment displayed in a confocal plane and 5 random regions of basolateral and sub-apical domains were analyzed, normalized to basal values (time=0) and averaged for each region. Cell swelling was estimated as a change of cell height in the xz plane at different time points, normalized to basal values, and averaged.

Fura-2 calcium measurements

To load Fura-2, cells were incubated (1 h, 37°C, 5% CO₂) in physiological solution containing 25 μ M Fura-2-AM + 0.02% Pluronic[®] F127 and 2.5 mM probenecid. This was followed by 30 min de-esterification period in physiological solution containing probenecid. The physiological saline solution was comprised (in mM) of: 140 NaCl, 5 KCl, 1 MgCl₂, 1 CaCl₂, 10 glucose and 10 HEPES, pH 7.4, adjusted with NaOH. 50% hypotonic medium was prepared by reducing the salt concentration while keeping divalent cation concentration constant. For calcium imaging, coverslips with Fura-2-loaded cells were mounted in the imaging/perfusion chamber attached to the

heated platform (Warner Instruments Co.) on the stage of an inverted microscope (Nikon TE300). The cells were exposed to alternate (200 ms) illumination at 340 and 380 nm with a high-pressure mercury lamp (100 W) via interference filters (Chroma Technology, Brattleboro, VT) mounted on a filter wheel (Sutter Lambda 10-C, Sutter Instrument Co., Novato, CA) and a dichroic mirror (510/540 nm, Chroma Technology). Fluorescence images were recorded at 15- to 60-s intervals with the digital camera and stored for later analysis.

Chemicals

For calcium imaging experiments, Fura-2-AM was obtained from Molecular Probes, Invitrogen Corp. (Burlington, ON). Probenicid, Pluronic[®] F127 and all other reagents were from Sigma Aldrich (Oakville, ON).

Results

Kinetics of nucleotide release

Figure 1 shows an example of the time-course of nucleotide release induced by 50% hypotonic shock. For clarity, the release of adenine and uridine nucleotides appears on separate graphs: A and B, respectively. The kinetics of release were remarkably similar for all nucleotides; after the onset of hypotonic shock nucleotide concentration increased rapidly, peaking at ~2.5 min, followed by a gradual decay in the next 10-15 min. The average peak values from several separate experiments are shown in Figure 1C. Interestingly, ATP was the major species at the peak of stimulated release, whereas for basal release, Ado was the predominant species. The rank order of nucleotide abundance at the peak was: $ATP > Ado \geq UTP > ADP \approx UDP > AMP$. Relative increases of nucleotide concentrations at the peak were also the highest for NTPs and NDPs (ATP 5.6-fold, ADP 3.7-fold, UTP >7-fold, UDP 27-fold), whereas the increase was smaller for AMP and Ado (1.4-fold and 2.1-fold, respectively).

Role of $[Ca^{+2}]_i$

To investigate the role of $[Ca^{+2}]_i$ in adenine nucleotide release, we tested the effect of the Ca^{2+} ionophore ionomycin. In the absence of hypotonic shock, exposure to 5 μ M ionomycin for 3 min induced transient nucleotide release from A549 cells: Figure 2A. This release reached a peak at approximately 1.5 min, i.e. slightly earlier and at

somewhat lesser absolute peak amplitude compared to that induced by 50% hypotonic shock. Otherwise, the kinetics and relative nucleotide abundance were similar for both stimuli. Almost complete inhibition of swelling-induced adenine nucleotide release was observed for A549 cells loaded with the Ca^{2+} chelator BAPTA, compared to control untreated cells of the same batch tested in parallel experiments: Figure 2B and C, respectively. Fura-2 fluorescence $[\text{Ca}^{+2}]_i$ measurements confirmed a dramatic reduction of the $[\text{Ca}^{+2}]_i$ response to 50% hypotonic shock in BAPTA-loaded cells: Figure 2D. These experiments demonstrate that elevation of $[\text{Ca}^{+2}]_i$ was required to trigger adenine nucleotide release from A549 epithelial cells.

FM1-43 fluorescence changes implicate vesicular exocytosis

Strong calcium dependence of nucleotide release may indicate the involvement of vesicular exocytosis. To further explore this possibility, bulk exocytosis was examined by real time confocal microscopy in cells bathed in FM1-43. Fluorescence intensity associated with the plasma membrane increased rapidly by incorporation of the soluble probe into the membrane and remained almost constant after 5 min in non-stimulated cells. Plasma membrane-associated fluorescence intensity rose rapidly (~20 s) with hypotonic shock stimulation. This change was accompanied by increased cell volume seen as increment of cell height: Figure 3A and B. Cell volume peaked at about 3 min, followed by a regulatory volume decrease in the next 10-15 min (data

not shown). A similar plasma membrane associated FM1-43 fluorescence intensity increase was observed in the absence of hypotonic shock, when the cells were stimulated with ionomycin, in the presence but not in the absence of calcium in the bathing solution: Figure 4. These data indicate that both hypotonic shock and ionomycin stimulated bulk exocytosis in A549 cells.

Discussion

In this study, we used the flow-through chamber and an etheno derivatization measurement technique to examine the kinetics of nucleotide release from A549 lung epithelial cells induced by hypotonic shock. We demonstrated that ATP, ADP, AMP, Ado, UTP and UDP appeared in the perfusates with the same kinetics, peaking at ~2.5 min (Figure 1), which coincided with the peak of $[Ca^{+2}]_i$ elevation evoked by hypotonic shock: Figure 2D. Similar tight temporal correlation between the $[Ca^{+2}]_i$ signal and ATP release, measured by luciferase-luciferin luminescence assay, was reported previously for A549, 16HBE14o⁻ epithelial cells and NIH-3T3 fibroblasts [10]. Such a close temporal association suggests that hypotonic shock-induced elevation of $[Ca^{+2}]_i$ is a trigger for the release of nucleotides. This was supported by the strong inhibitory effect of the intracellular Ca^{2+} chelator BAPTA-AM and the induction of nucleotide release in the absence of hypotonic shock solely by the rise of $[Ca^{+2}]_i$ with ionomycin. These data demonstrate tight Ca^{2+} -dependence of nucleotide release, and point to a Ca^{2+} -dependent exocytotic mechanism. It should be noted, that the bulk $[Ca^{+2}]_i$ changes shown in Figure 2D, likely represent superposition of spatially separated, distinct $[Ca^{+2}]_i$ responses, one evoked directly by hypotonic shock and the other due to autocrine/paracrine actions of the released nucleotides on P2Y receptors. The latter effects might be minimized, at least partially, by continuous perfusion, which reduced nucleotide concentration in the bulk of the chamber far

below the IC_{50} of P2Y receptor activation, however, this possibility requires further study.

Consistent with a Ca^{2+} -dependent exocytotic mechanism, FM1-43 fluorescence studies revealed enhanced incorporation of the probe into the plasma membrane induced by hypotonic shock or ionomycin treatment. Increased plasma membrane-associated FM1-43 fluorescence intensity was a measure of the cumulative amount of membrane added by exocytosis [13]. FM1-43 fluorescence increased rapidly during the first 20 s of hypotonic shock: Figure 3. Interestingly, the initial fluorescence increment exceeded the cell surface increase estimated from xz confocal scans. In our previous study using a dual-image 3D cell reconstruction technique [15], we observed only a 11% to 30% surface increase of single substrate-attached A549 cells swollen in 50% hypotonic solution [10]. This difference could be attributed, in part, to different method of cell height and surface evaluation in that study as well as differences in swelling responses of single isolated cells compared to confluent cell monolayer. However, a similar discrepancy between FM1-43 fluorescence, cell surface and membrane electrical capacitance has been also reported by others, e.g. with pituitary lactotrophs, where the dense granules docked into the plasma membrane, were intensely stained by FM1-43, in addition to the membrane added to the cell surface [16]. Therefore, the divergence of fluorescence and the cell surface changes seen in our study with A549 cells may be also result in part, from FM1-43

staining of the lipophilic content of fused vesicles, in addition to the staining of fused vesicular membranes. The FM1-43 dye is often employed to fluorescently mark surfactant-containing lamellar bodies in alveolar type II (ATII) cells [17,18], and A549 cells, a model of ATII cells, also contain granules enriched in surface active phospholipids [19]. However, the exact contribution of such granules to increased FM1-43 fluorescence in stimulated A549 cells was out of the scope of the present investigation and will require future direct study.

Vesicle exocytosis may be mechanistically associated with nucleotide release in 2 ways: nucleotides can be delivered to the extracellular medium as cargo molecules within exocytotic vesicles, or, alternatively, secreted from the cytosol via vesicle-associated nucleotide-conducting channels or transporters, transiently expressed at the plasma membrane as a consequence of vesicle-plasma membrane fusion. Analysis of the relative abundance of different nucleotide species that appear in the extracellular medium may help to distinguish between these 2 mechanisms. ATP and UDP-sugars accumulate in the lumen of the secretory pathway up to 20-50 fold above their cytosolic concentrations, and luminal utilization of these molecules generates ADP and UDP. UDP is the major uridine nucleotide detected in ER/Golgi fractions [20] and, eventually, a UDP-selective apyrase (UDPase) converts UDP to UMP [21]. ER/Golgi ADP and UMP are exchanged for cytosolic ATP and UDP-glucose via specific transporters [22-25]. Since intraluminal nucleotides are not subject to the mechanisms that retrieve resident ER/Golgi proteins, they are predicted

to remain within trafficking vesicles, and to be released to the extracellular space from the secretory pathway. Our results suggest that this mechanism likely accounted for UDP release from A549 cells. Figure 1C illustrates that hypotonic stimulation promoted a sharp increase in UDP levels, with a UTP:UDP concentration ratio of 2:1. Since the cytosolic UTP:UDP ratio is >10:1 [26], our results suggest, at least in part, a vesicular rather than a cytosolic source of UDP and, as a corollary, of ATP and ADP.

In summary, our results provide strong evidence for Ca^{2+} -dependent vesicular exocytosis as a major mechanism of adenosine and uridine nucleotide release from A549 epithelial cells induced by hypotonic stress. Part of this release involves vesicles of the protein secretory pathway. Further investigations are needed to clarify the origin and contribution of other vesicular pools as well as the mechanisms and sources of intracellular Ca^{2+} elevations that evoke nucleotide secretion.

Acknowledgements

This study was supported in part by the Canadian Institutes of Health Research and the Canadian Cystic Fibrosis Foundation (CCFF) (to R.G.), and by NIH R01 HL076303 (to E.L.). S.T. was the recipient of a CCFF studentship. The authors acknowledge the editorial assistance of Ovid Da Silva, Research Support office, Research Centre, CHUM.

Figure legends**Figure 1. Transient nucleotide release from A549 cells induced by 50% hypotonic shock.**

Time-course of adenosine (A) and uridine (B) nucleotide release observed in response to 50% hypotonic shock. A representative experiment is shown, out of 4 performed under the same conditions. Hypotonic shock was applied at $t=0$ min and was preceded by 15-min equilibration in isotonic solution. C, Basal ($t=0$ min) and peak ($t=2.5$ min) nucleotide concentrations detected in perfusates. Average values (\pm S.D.) are from 3-4 experiments, such as in A and B, except for UTP and UDP, which are from a single experiment. * due to the limited sensitivity of UTP evaluations (≈ 3 nM), the basal level of UTP was found to be below the detection limit and was not shown.

Figure 2. Effect of intracellular Ca^{2+} modulators on nucleotide release.

(A) In the absence of hypotonic shock, application of 5 μM ionomycin resulted in transient nucleotide release with kinetics similar to that induced by hypotonic shock. An example, out of $n=2$ similar experiments, is shown. Loading A549 cells with the Ca^{2+} chelator BAPTA almost completely inhibited hypotonic stress-induced nucleotide release compared to controls that were run in parallel: B and C respectively ($n=2$). Effect of BAPTA on the $[\text{Ca}^{2+}]_i$ response is shown in D. The 2 traces represent changes of the Fura-2 fluorescence ratio at 2 excitation wavelengths,

$\lambda_{340}/\lambda_{380}$, in response to 50% hypotonic shock, applied at $t=0$ min, in control and BAPTA-loaded cells. Note that the rapid peak of the $[Ca^{2+}]_i$ response was abolished in BAPTA-loaded cells. Similar responses were observed in $n=4$ experiments.

Figure 3. Effect of hypotonic shock on FM1-43 surface membrane staining.

A. Confocal FM1-43 fluorescence images of confluent A549 cells after 20 min of dye loading in isotonic solution, followed by 50% hypotonic shock stimulation. The images depict the xz scans of the cell monolayer at different time points. Note the increase in cell size and fluorescence intensity consistent with hypotonic shock-induced cell swelling and heightened bulk exocytosis.

B. Time-course of FM1-43 plasma membrane fluorescence and cell height changes during hypotonic shock.

Figure 4. Effect of ionomycin on FM1-43 surface membrane staining.

A. Confocal FM1-43 fluorescence images of confluent A549 cells prior to and after 4-min exposure to 5 μ M ionomycin in the presence of extracellular calcium. The images show the the xz scans of the cell monolayer at different time points. Note the increase in fluorescence intensity after ionomycin stimulation, indicating enhanced exocytosis.

B. Time-course of FM1-43 plasma membrane fluorescence changes of unstimulated cells (Δ CON), and cells during ionomycin treatment in the presence (\blacksquare ION) or absence (\bullet ION 0 Ca) of extracellular calcium.

REFERENCE LIST

1. Lazarowski E R, Boucher R C, Harden T K. Mechanisms of release of nucleotides and integration of their action as P2X- and P2Y-receptor activating molecules. *Mol. Pharmacol.* 2003; **64**: 785-795.
2. Burnstock G. Historical review: ATP as a neurotransmitter. *Trends Pharmacol Sci* 2006; **27**: 166-176.
3. Burnstock G. Purinergic signalling. *Br J Pharmacol* 2006; **147 Suppl 1**: S172-S181.
4. Lazarowski E R, Tarran R, Grubb B R, Van Heusden C A, Okada S, Boucher R C. Nucleotide release provides a mechanism for airway surface liquid homeostasis. *Journal of Biological Chemistry* 2004.
5. Zimmermann H. Extracellular metabolism of ATP and other nucleotides. *Naunyn Schmiedebergs Arch. Pharmacol* 2000; **362**: 299-309.

6. Donaldson S H, Lazarowski E R, Picher M, Knowles M R, Stutts M J, Boucher R C. Basal nucleotide levels, release, and metabolism in normal and cystic fibrosis airways. *Mol.Med.* 2000; **6**: 969-982.
7. Boucher R C. Regulation of airway surface liquid volume by human airway epithelia. *Pflugers Arch.* 2003; **445**: 495-498.
8. Grygorczyk R, Hanrahan J W. CFTR-independent ATP release from epithelial cells triggered by mechanical stimuli. *Am.J.Physiol* 1997; **272**: C1058-C1066.
9. Boudreault F, Grygorczyk R. Cell swelling-induced ATP release and gadolinium-sensitive channels. *Am.J.Physiol Cell Physiol* 2002; **282**: C219-C226.
10. Boudreault F, Grygorczyk R. Cell swelling-induced ATP release is tightly dependent on intracellular calcium elevations. *J Physiol* 2004; **561**: 499-513.
11. Lazarowski E R, Harden T K. Quantitation of extracellular UTP using a sensitive enzymatic assay. *Br J Pharmacol* 1999; **127**: 1272-1278.
12. Lazarowski E R, Boucher R C, Harden T K. Constitutive release of ATP and evidence for major contribution of ecto- nucleotide pyrophosphatase and nucleoside diphosphokinase to extracellular nucleotide concentrations. *J Biol.Chem.* 2000; **275**: 31061-31068.

13. Smith C B, Betz W J. Simultaneous independent measurement of endocytosis and exocytosis. *Nature* 1996; **380**: 531-534.
14. Cochilla A J, Angleson J K, Betz W J. Monitoring secretory membrane with FM1-43 fluorescence. *Annu.Rev Neurosci.* 1999; **22**: 1-10.
15. Boudreault F, Grygorczyk R. Evaluation of rapid volume changes of substrate-adherent cells by conventional microscopy 3D imaging. *J.Microsc.* 2004; **215**: 302-312.
16. Brumback A C, Lieber J L, Angleson J K, Betz W J. Using FM1-43 to study neuropeptide granule dynamics and exocytosis. *Methods* 2004; **33**: 287-294.
17. Ashino Y, Ying X, Dobbs L G, Bhattacharya J. $[Ca^{2+}]_i$ oscillations regulate type II cell exocytosis in the pulmonary alveolus. *Am.J.Physiol Lung Cell Mol.Physiol* 2000; **279**: L5-13.
18. Mair N, Haller T, Dietl P. Exocytosis in alveolar type II cells revealed by cell capacitance and fluorescence measurements [In Process Citation]. *Am J Physiol* 1999; **276**: L376-L382.
19. Shapiro D L, Nardone L L, Rooney S A, Motoyama E K, Munoz J L. Phospholipid biosynthesis and secretion by a cell line (A549) which resembles type II alveolar epithelial cells. *Biochim.Biophys.Acta* 1978; **530**: 197-207.

20. Fleischer B. The nucleotide content of rat liver Golgi vesicles. *Arch.Biochem.Biophys.* 1981; **212**: 602-610.
21. Wang T F, Guidotti G. Golgi localization and functional expression of human uridine diphosphatase. *J.Biol.Chem.* 1998; **273**: 11392-11399.
22. Wang T F, Guidotti G. Golgi localization and functional expression of human uridine diphosphatase. *J Biol Chem.* 1998; **273**: 11392-11399.
23. Hirschberg C B, Robbins P W, Abeijon C. Transporters of nucleotide sugars, ATP, and nucleotide sulfate in the endoplasmic reticulum and Golgi apparatus. *Annu.Rev Biochem.* 1998; **67**: 49-69.
24. Waldman B C, Rudnick G. UDP-GlcNAc transport across the Golgi membrane: electroneutral exchange for dianionic UMP. *Biochemistry* 1990; **29**: 44-52.
25. Ishida N, Kawakita M. Molecular physiology and pathology of the nucleotide sugar transporter family (SLC35). *Pflugers Arch.* 2004; **447**: 768-775.
26. Kochanowski N, Blanchard F, Cacan R, Chirat F, Guedon E, Marc A, Goergen J L. Intracellular nucleotide and nucleotide sugar contents of cultured CHO cells determined by a fast, sensitive, and high-resolution ion-pair RP-HPLC. *Anal.Biochem.* 2006; **348**: 243-251.

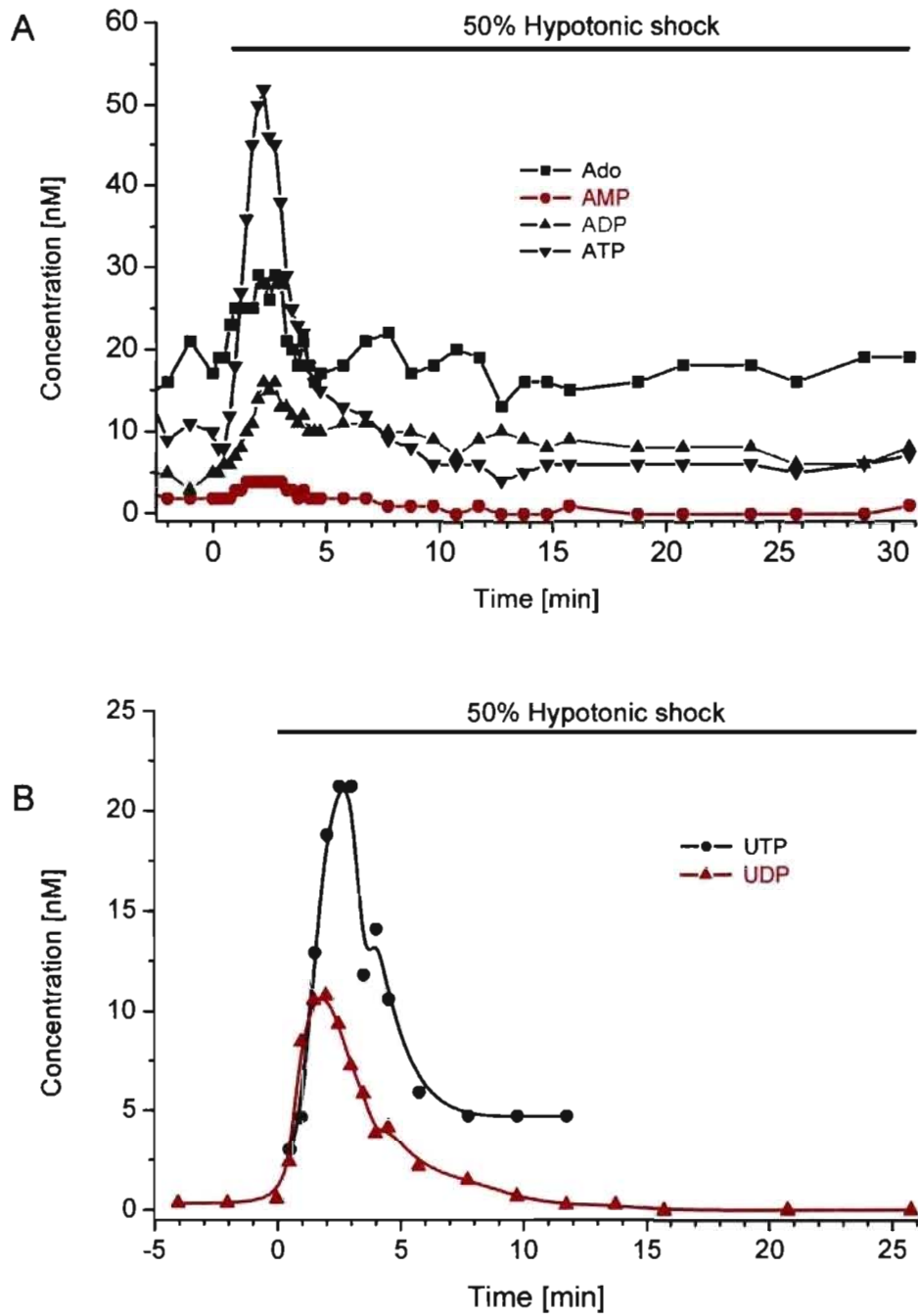


Figure 1 A,B

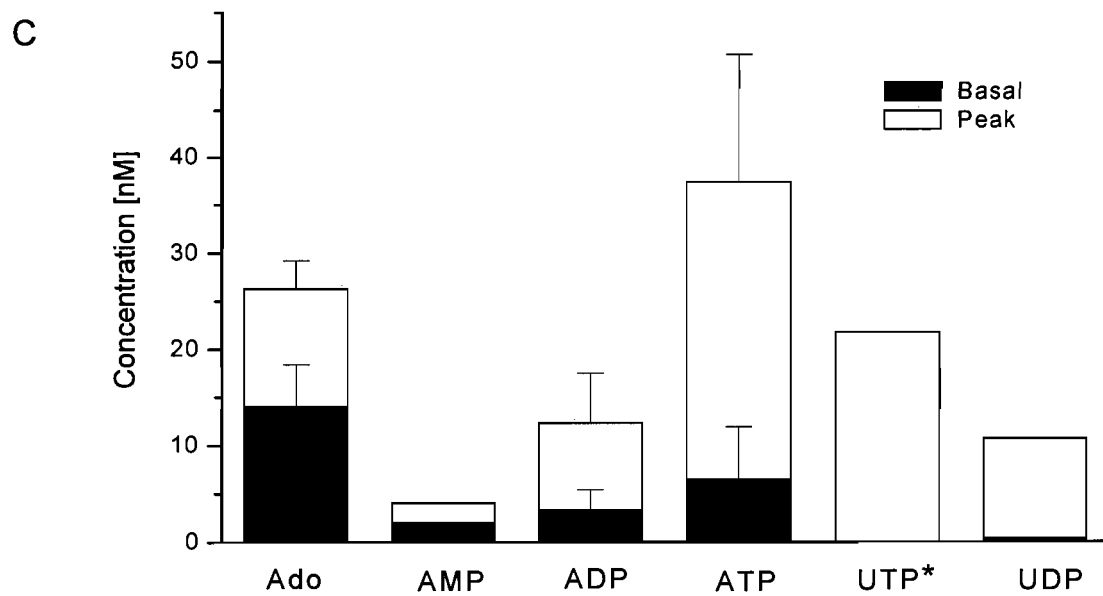


Figure 1 C

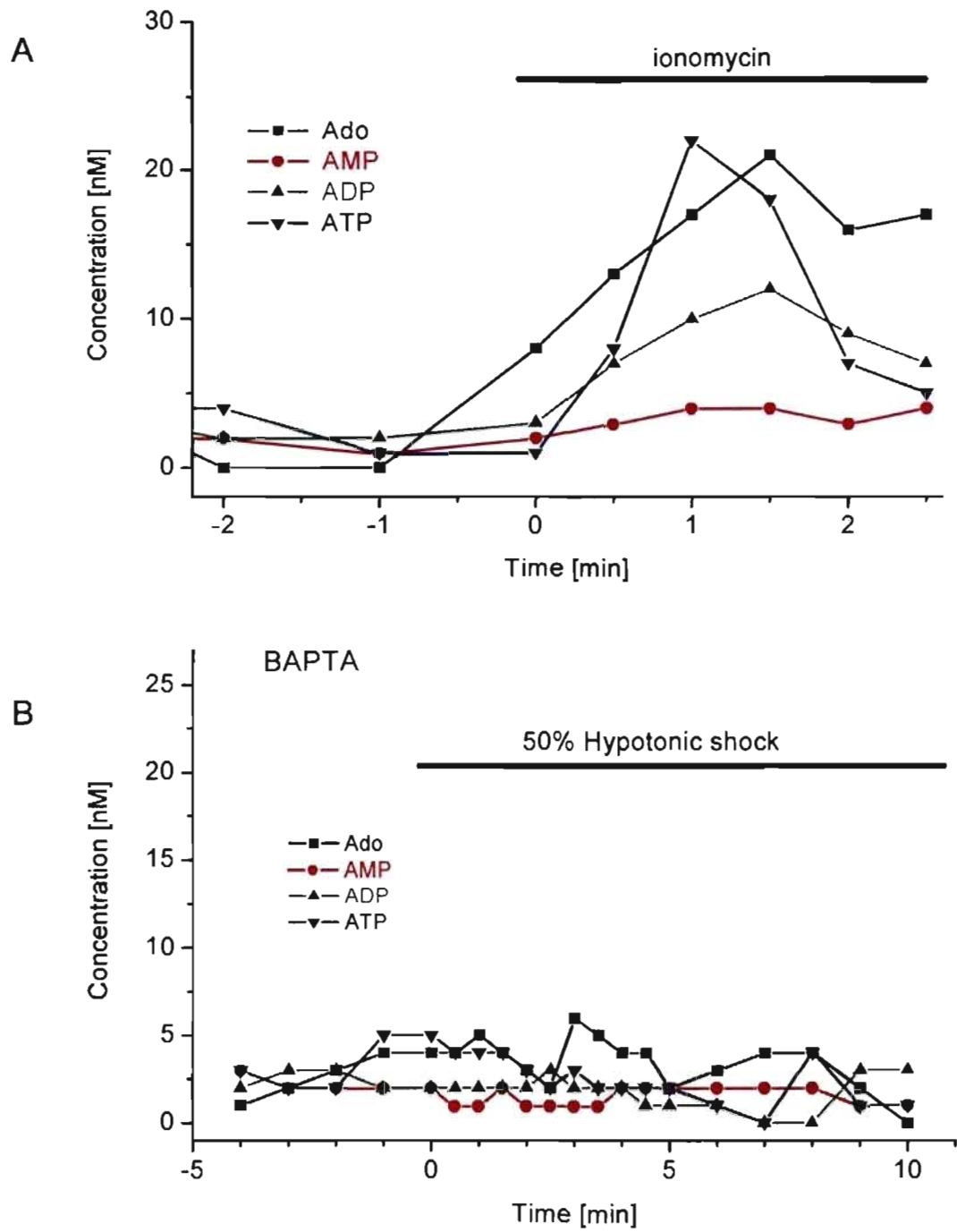


Figure 2 A, B

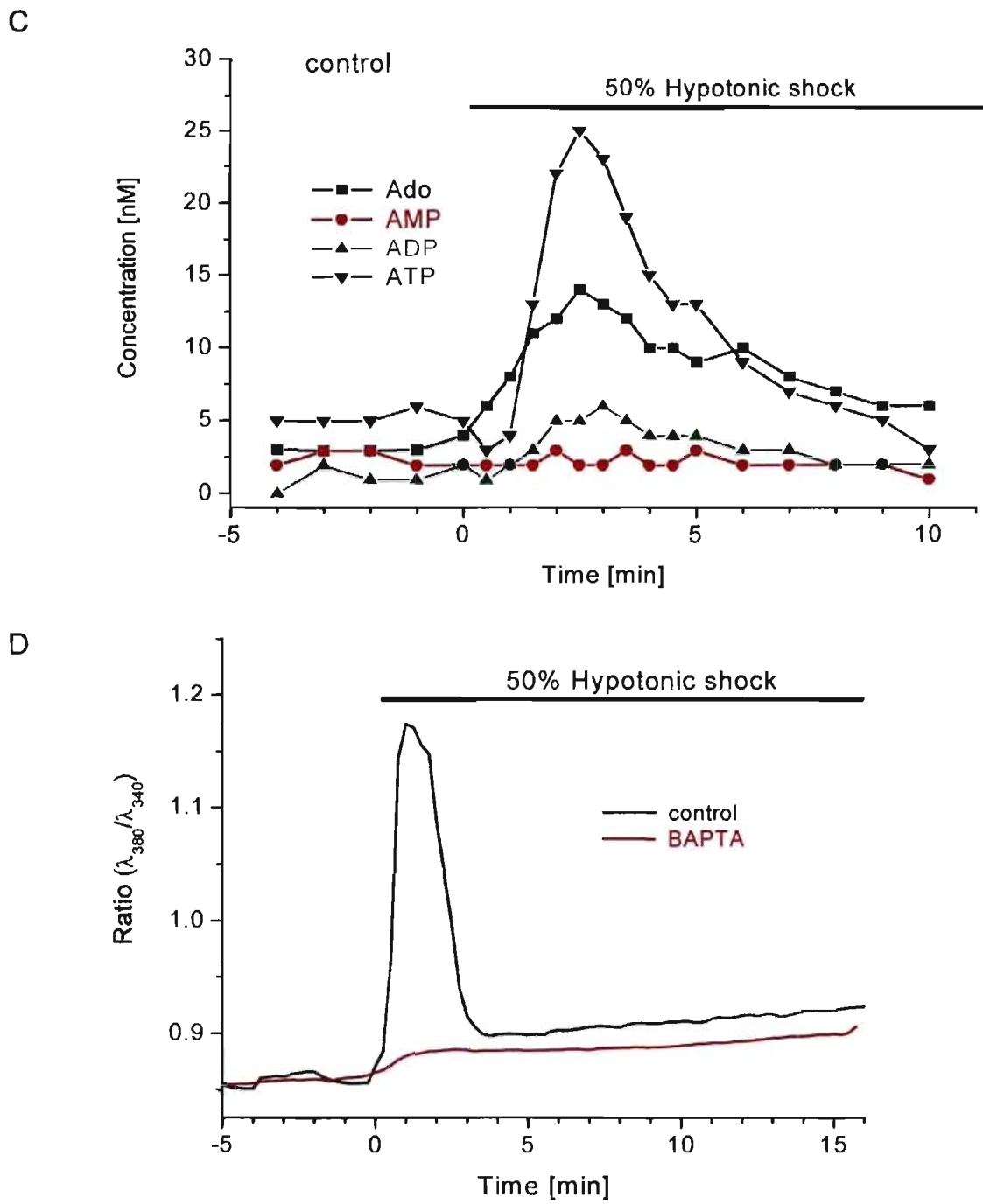


Figure 2 C, D

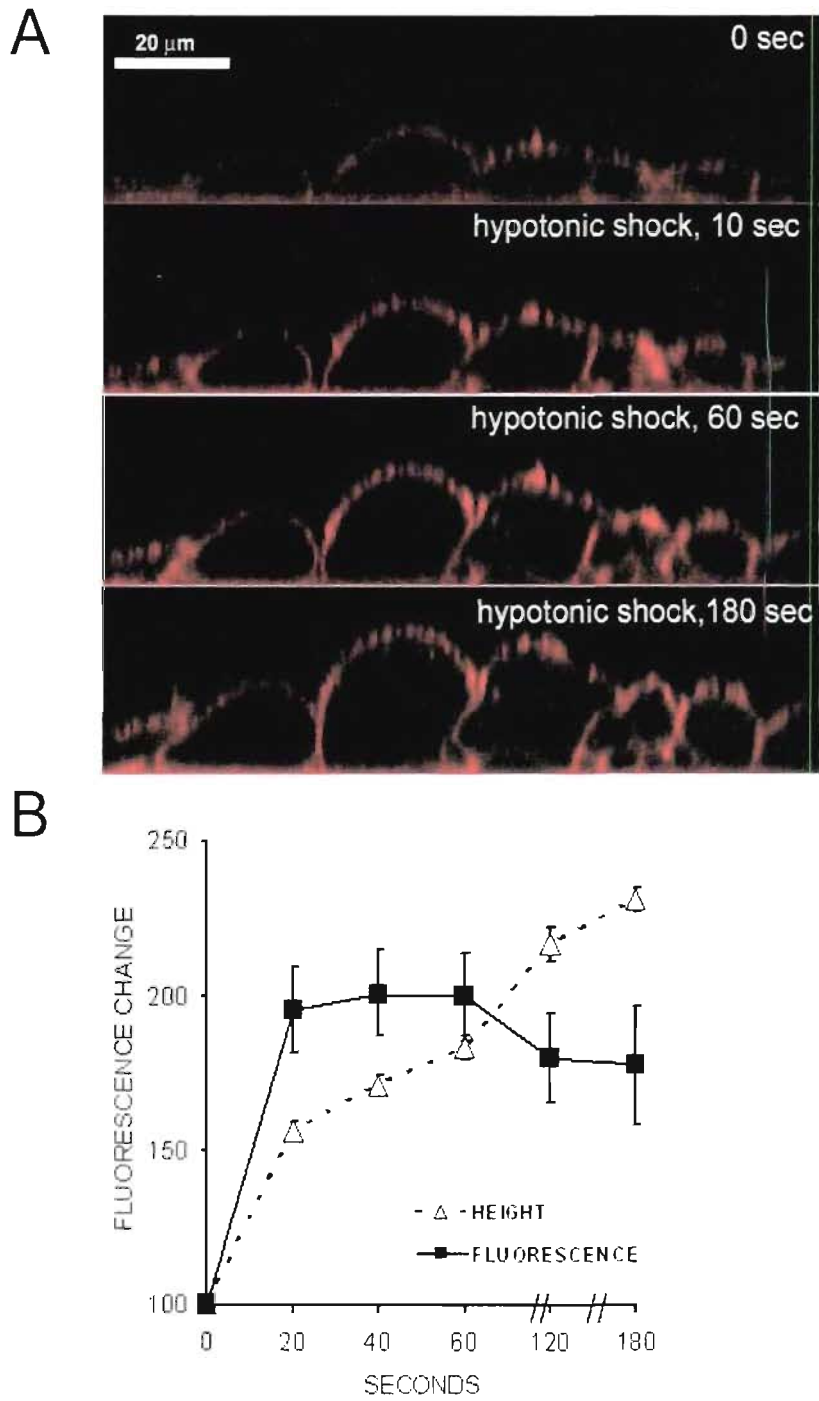


Figure 3

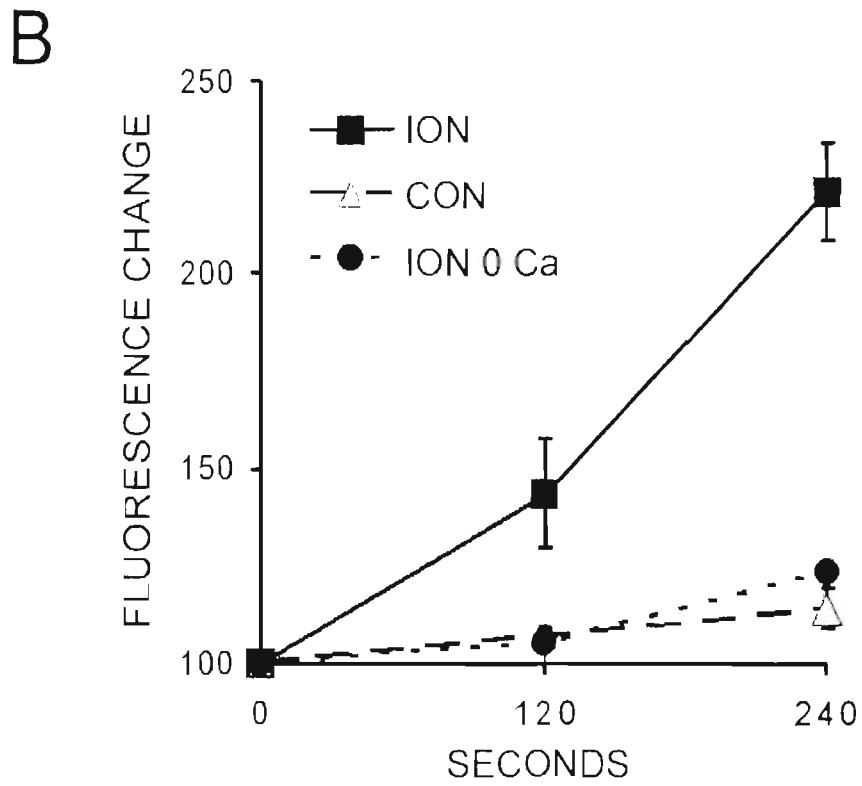
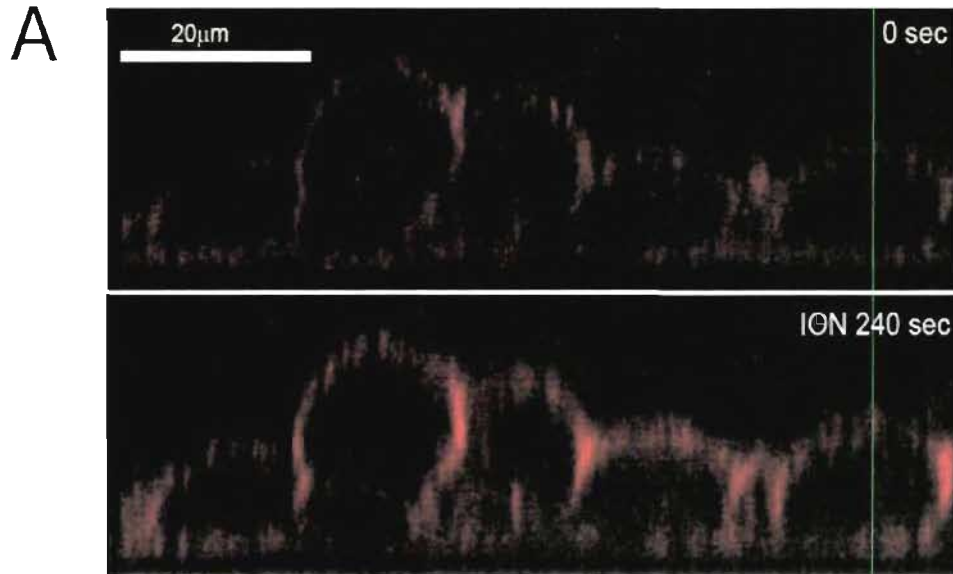


Figure 4

3.1.3 Further unpublished results

The A549 cell line has characteristics of alveolar type II (AT II) cells (see page 253) whose primary function is to synthesize and secrete surface-active material. AT II cells contain typical organelles such as mitochondria, ER, microperoxisomes, various filaments and microtubules, as well as unique organelles referred to as lamellar bodies (LB), which contain layers of surfactant [168]. Pulmonary surfactant forms a thin monolayer at the air-water interface of the alveolar epithelium and reduces surface tension in the alveoli. In addition, it also plays a role in the protection against infection (see page 2). Structurally, surfactant is a homogenous material consisting of $\sim 80\%$ saturated and unsaturated glycerophospholipids (mainly phosphatidylcholine (PC)), $\sim 12\%$ neutral lipids (predominantly cholesterol) and $\sim 8\%$ proteins (predominantly surfactant proteins SP-A, SP-B, SP-C, SP-D, but also enzymes and other proteins) [169]. Whereas the secretion of phospholipids was shown to be mediated solely by the exocytosis of LBs [170], the secretion of

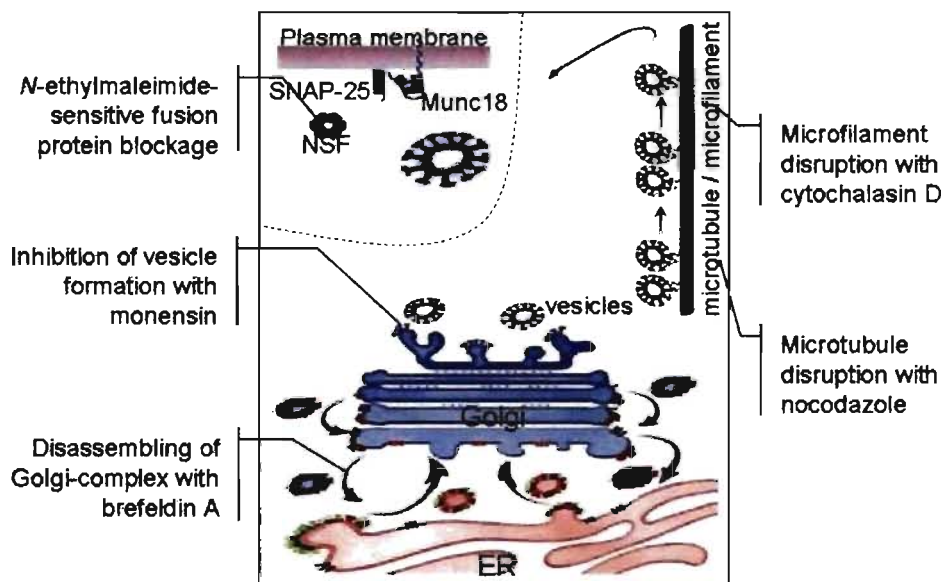


Figure 3.1: Selected steps of the secretory pathway and their inhibitors

Munc18, mammalian homologue of unc-18; NSF, *N*-ethylmaleimide-sensitive factor; SNAP-25, synapto-somal-associated protein of 25 kDa

proteins seems to be more complex. While the small hydrophobic polypeptides SP-B and SP-C are localized inside the LBs and co-secreted with the LB contents, the large hydrophilic proteins SP-A and SP-D are secreted in a LB-independent manner [171, 172].

Since the principal release mechanism of ATP from A549 cells upon hypotonic shock was shown to be vesicular (see section 3.1.2), the question arises if ATP might be released as a by-product from LBs or rather by a LB-independent pathway. In order to be able to discuss this question, the different steps of the secretory pathway will first be outlined in general terms. The experiments examining the secretory steps leading to ATP release will then be analysed in comparison with the biogenesis of LBs and the release of surfactants.

Fig. 3.1 on page 73 depicts selected steps and proteins of a typical secretory pathway: the smooth ER, rich in a wide variety of enzymes, is involved in the synthesis of lipids, triglycerides, and steroids, whereas the rough ER is the site of the synthesis of (secretory) proteins. Some secretory products are then transported to the Golgi apparatus (GA) where they are modified (e.g. by glycosylation, phosphorylation) and sorted [173]. ATP and other nucleotide derivatives, which are required as energy source or as substrates for protein modification, are transported into both of these organelles, the ER and the GA, through specific transporters in exchange for the analogous monophosphate [174]. The vesicles destined for secretion are transported and stored close to the plasma membrane, ready to be released upon an appropriate signal [173]. The fusion of the vesicles with the plasma membrane involves many different proteins (see section 1.2.2, page 22) of which only three are presented in the figure (SNAP-25, Munc18, NSF).

The significance of the particular steps in the secretion process depends on the cell type and varies between the different secretory products. In order to compare cell-swelling induced ATP release from A549 cells with the LB-dependent secretory pathway in AT II cells, various inhibitors, such as brefeldin A (BFA), monensin, nocodazole, cytochalasin D and *N*-ethylmaleimide (NEM), which interfere with the secretory pathway, were used. Their targets and functions are indicated in fig. 3.1 on page 73.

Table II: Peak and total release of ATP after interfering with the secretory pathway

Agent	Peak ATP release ^a	Total ATP release ^a	<i>n</i> ^b
Brefeldin A	59 ± 7 ^c	81 ± 3 ^c	3
Monensin	19 ± 8 ^c	45 ± 15 ^c	3
Nocodazole	42 ± 22 ^c	56 ± 20 ^c	3
Cytochalasin D	33 ± 6 ^c	56 ± 5 ^c	4
<i>N</i> -ethylmaleimide	6 ± 4 ^c	8 ± 6 ^c	4

^aData are mean ± S.D. as percentage of control.

^bnumber of experiments

^c*P* < 0.05

BFA was previously used by Osanai et al. [175, 176] to study the involvement of the GA in protein and lipid trafficking to the LBs in cultured AT II cells. The disruption of the GA by BFA (2.5 – 10 μg/ml for 15 min) completely blocked protein secretion but did not alter PC secretion. It was, furthermore, demonstrated that PC was transported to the LB via a Golgi-independent and SP-B via the Golgi-dependent pathway. It appears, therefore, that surfactant components take different pathways to reside in the LBs.

Fig. 3.2a on page 77 shows the time course of cell-swelling induced ATP release from A549 cells after the incubation with BFA (10 μg/ml for 2.5 h). The peak was reduced to 59 ± 7% and the total amount to 81 ± 3% (cf. table II). This result indicates that the major part of released ATP originates from a source that by-passes the GA, suggesting an at least partly LB-dependent pathway.

Monensin alters, on the one hand, protein transport in association with ultrastructural changes in the GA. In this regard, treatment of AT II cells from rat lung with monensin (1 μM for 1 h) was found to inhibit the rate of sialylation and secretion of SP-A [177]. On the other hand, the effect of monensin seems to be also related to its function as H⁺ ionophore by collapsing H⁺ gradients

of acidic compartments (see 274). For instance, a normal posttranslational proteolysis of proSP-C occurs in acidic intracellular compartments, including LBs, and is inhibited by monensin ($2 \mu\text{M}$ for 1 h) [178]. Chander et al. reported that LBs maintain an acidic interior (pH 6.1 or lower) which is generated by an energy dependent process [179].

The pretreatment of A549 cells with monensin ($10 \mu\text{M}$ for 18 h) strongly reduced ATP peak secretion upon 50% hypotonic shock to $19 \pm 8\%$ and the total amount to $45 \pm 15\%$ (cf. table II, page 75 and fig. 3.2b, page 77). Considering that the majority of ATP release occurs on a GA-independent pathway (see BFA), it seems unlikely that the strong effect of monensin is only caused by the inhibition of the trans GA function. The reduction could have been, moreover, caused by ATP depletion from the LBs due to the attempt to counteract the uncoupled H^+ flux and to maintain the pH gradient. Should this be, indeed, the case, the strong inhibition of ATP release by monensin would speak in favour of a LB-dependent ATP release pathway. Further experiments with agents that induce an elevation of vacuolar pH could clarify this point. Since a reduction of cytosolic ATP could also affect the amount of mechanism-independent ATP secretion, monensin and all other agents were tested for a potential influence on the intracellular ATP level. For this purpose, the treated cells were washed twice with cold PBS and lysed in a 0.1 M NaOH/0.5 mM EDTA mixture. The cell lysates were incubated at 60°C for 20 min and frozen at -20°C . The ATP levels were measured by the standard luciferin/luciferase assay. None of the agents was found to influence the intracellular ATP level of A549 cells under the experimental conditions (data not shown).

The cytoskeletal elements (microfilaments and microtubules) have two opposite roles in respect to vesicle secretion: one advancing secretory vesicles toward the plasma membrane and the other impeding vesicle fusion with the plasma membrane by forming a physical barrier. In AT II cells, a microtubule-based mechanism delivers LBs to the plasma membrane [180] and a subplasmalemmal actin filament system forms a mechanical hindrance that has to be transiently depolymerized to allow LB membrane fusion and

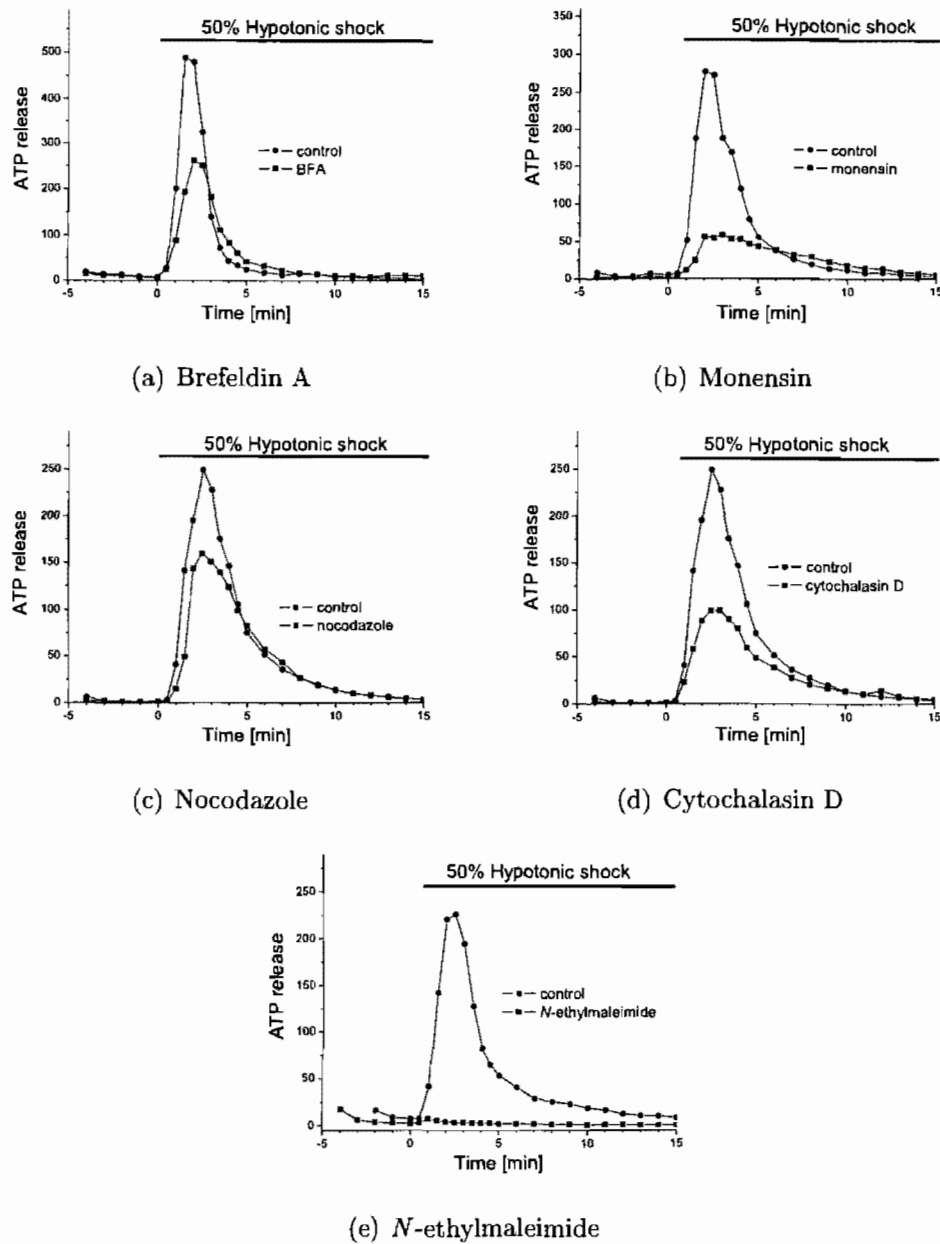


Figure 3.2: Time-course of ATP release after interfering with the secretory pathway

ATP release unit: $[\text{pMoles} / (\text{min} \cdot 10^6 \text{ confl. cells})]$, (see section 2.2.2)

exocytosis [181].

The exposure of A549 cells to nocodazole (20 μM for 18 h), which disassembles microtubules, led to a reduction of peak ATP release to $42 \pm 22\%$ and of total ATP release to $56 \pm 20\%$ (cf. table II, page 75 and fig. 3.2c, page 77). These data indicate the involvement of microtubules in the translocation of ATP containing vesicles to the site of exocytosis and support the hypothesis that hypotonically released ATP might be a co-secretagogue of surfactant from LBs.

The role of actin filaments in the process of surfactant secretion from AT II cells was previously examined among others by the application of cytochalasins. These studies gave, however, controversial results since both a reduction as well as an increase in the release of surfactant was measured [182, 183]. This inconsistency may be explained with the limited specificity of cytochalasins binding to different cellular target sites. The complex interaction with the microfilament network might result rather in a redistribution of actin than in its disassembling [184, 185]. In A549 cells, the exposure to cytochalasin D (2 μM for 18 h) inhibited the peak of ATP release to $33 \pm 6\%$ and the total amount of ATP release to $56 \pm 5\%$ (cf. table II, page 75 and fig. 3.2d, page 77) indicating an involvement of microfilaments in cell-swelling induced ATP release.

The two results indicate that ATP release upon 50% hypotonic shock from A549 cells depends on an intact microtubular system as well as on functional microfilaments for a well-controlled exocytotic process. ATP is, thus, mediated by the microtubule-microfilament system, similar to surfactant release.

Little is known about the molecular machinery that regulates the exocytosis of lamellar bodies [172]. Only recently, components of the vesicle fusion machinery of AT II cells have been identified. These include SNARE proteins synaptobrevin-2, syntaxin-1, soluble NSF attachment proteins SNAP-23 and SNAP-25 [186], as well as the *N*-ethylmaleimide sensitive fusion protein (NSF) and α -SNAP proteins, which disassemble SNARE complexes [187]. NEM has been, furthermore, found to interfere with the transport of proteins from the ER on account of a NEM-sensitive component distinct from

the NSF [188, 189] and to have stimulatory and inhibitory effects on various ion channels [190].

The incubation of A549 cells with the thiol-alkylating agent NEM (1 mM for 15 min) almost completely blocked cell-swelling induced ATP release, only leaving $6 \pm 4\%$ of its peak and $8 \pm 6\%$ of its total amount (cf. table II, page 75 and fig. 3.2e, page 77) demonstrating the substantial contribution of exocytosis to the ATP release mechanism. NEM-inhibited ATP release might, however, not only be a result of a direct interference with the fusion process on the plasma membrane, but also of an interference with some intracellular processes and/or with potentially other release pathways.

In conclusion, these experiments give an interesting insight into the exocytotic pathway responsible for cell-swelling induced ATP release from A549 cells. It seems that ATP is released in big part as a co-secretagogue of surfactant in a LB-dependent pathway. The partial inhibition of ATP release with BFA suggests that both a GA-dependent pathway, accountable for SP-B transport to the LBs, and a GA-independent pathway, accountable for PC transport to the LBs, contribute to cell-swelling induced ATP secretion. The strong inhibitory effect of monensin on ATP release might only be partially a result of GA disruption. It could be, moreover, explained by a direct action on the acidic LBs as a H^+ ionophore, leading to ATP depletion over the effort to maintain the pH gradient. Finally, the cytoskeleton was shown to play an important, however, not yet defined role in ATP-release. So far, no conclusions can be drawn as to the implication of a LB-independent pathway. More experiments are necessary to confirm and to further analyse the proposed pathways and some of them are suggested in the following points:

- All specified inhibitors were applied in the above discussed experiments in a relatively high concentration and for a rather long period of time. It could be, therefore, interesting to repeat the experiments with concentrations and incubation times similar to the ones used for the studies of surfactant secretion. This would make it easier to compare the two sets of data.

- Information about the co-released products upon hypotonic shock could clarify the relative contribution of LB-dependent and LB-independent pathway of ATP release. For this purpose, the perfusate aliquots could be analysed for their content of surfactant components by HPLC combined with a matrix-assisted laser desorption/ionization mass spectrometer (HPLC-MALDI-MS), in addition to the ATP concentration by the luciferin/luciferase assay.
- To verify the suggested hypothesis for the inhibitory effect of monensin on ATP release, the intralamellar pH could be increased by acidotropic agents (e.g. NH_4Cl , methylamine, chloroquine, amantadine) followed by a stimulation of ATP release. The incubation time should be relatively long to allow a potential intralamellar ATP depletion (see incubation time of monensin) without affecting cell viability.
- To further examine the role of the cytoskeleton in cell-swelling induced ATP release, various other agents, which have a well-defined effect on the cytoskeleton (e.g. jasplakinolide, latrunculin A), could be tested for their impact on ATP release.

3.2 ARTICLE 2: Ca^{2+} -dependent ATP release from A549 cells involves synergistic autocrine stimulation by co-released uridine nucleotides

3.2.1 Preamble

Section 3.1 deals with the analysis of nucleotide co-release from A549 cells upon hypotonic shock and confirms a Ca^{2+} -dependent exocytotic release mechanism.

The objective of this research was to specify the origin(s) of the intracellular Ca^{2+} elevation and to further analyze the components of the Ca^{2+} signal leading to the exocytosis of ATP.

3.2.2 Article

Tatur, S.; Groulx, N.; Orlov, S.N.; Grygorczyk, R.

Ca^{2+} -dependent ATP release from A549 cells involves synergistic autocrine stimulation by co-released uridine nucleotides. *Journal of Physiology – London*, 584(2):419-435, October 2007.

Reproduced on pp. 82–133 with permission.

Ca²⁺-dependent ATP release from A549 cells involves synergistic autocrine stimulation by co-released uridine nucleotides

Sabina Tatur, Nicolas Groulx, Sergei N. Orlov and Ryszard Grygorczyk

Research Centre, Centre hospitalier de l'Université de Montréal (CHUM) – Hôtel-Dieu, and Department of Medicine, Université de Montréal, Montréal, Québec, Canada

Running title: Nucleotide autocrine signaling promotes ATP release

Total number of words: 7,040


Address for correspondence:

Ryszard Grygorczyk

CHUM - Hôtel-Dieu

3850 Saint-Urbain, Montréal, Québec, Canada H2W 1T7

Tel: (514) 890-8000 ext. 15089 Fax: (514) 412-7204

e-mail: 

Keywords: ATP release, autocrine signaling, Ca²⁺ stores, exocytosis, hypotonic shock

SUMMARY

Extracellular ATP is a potent surfactant secretagogue but its origin in the alveolus, its mechanism(s) of release and regulatory pathways remain unknown. Previously, we showed that hypotonic swelling of alveolar A549 cells induces Ca^{2+} -dependent secretion of several adenosine and uridine nucleotides, implicating regulated exocytosis. In this study, we examined sources of intracellular Ca^{2+} ($[\text{Ca}^{2+}]_i$) elevation evoked by acute 50% hypotonic stress and the role of autocrine purinergic signaling in Ca^{2+} -dependent ATP release. We found that ATP release does not directly involve Ca^{2+} influx from extracellular spaces, but depends entirely on Ca^{2+} mobilization from intracellular stores. The $[\text{Ca}^{2+}]_i$ response consisted of slowly-rising elevation, representing mobilization from thapsigargin (TG)-insensitive stores and a superimposed rapid spike due to Ca^{2+} release from TG-sensitive endoplasmic reticulum (ER) Ca^{2+} stores. The latter could be abolished by hydrolysis of extracellular triphospho- and diphosphonucleotides with apyrase; blocking $\text{P2Y}_2/\text{P2Y}_6$ receptors of A549 cells with suramin; blocking UDP receptors (P2Y_6) with PPADS; emptying TG-sensitive stores downstream with TG or caffeine in Ca^{2+} -free extracellular solution; or blocking the Ca^{2+} -release inositol 1,4,5-triphosphate receptor channel of the ER with 2-aminoethyl diphenylborinate. These data demonstrate that the rapid $[\text{Ca}^{2+}]_i$ spike results from the autocrine stimulation of $\text{IP}_3/\text{Ca}^{2+}$ -coupled P2Y , predominantly P2Y_6 , receptors, accounting for ~70% of total Ca^{2+} -dependent ATP release evoked by hypotonic shock. Our study reveals a novel paradigm in which stress-induced ATP release from alveolar cells is amplified by the synergistic autocrine/paracrine action of co-released uridine and adenosine nucleotides. We suggest that a similar mechanism of purinergic signal propagation operates in other cell types.

INTRODUCTION

Extracellular nucleotides, such as ATP and UTP, are important autocrine-paracrine mediators in most tissues. In the distal lung, ATP is a potent secretagogue that stimulates type II cell surfactant secretion (Rooney, 2001). In the airways, through interactions with purinergic receptors, ATP, UTP, UDP, and adenosine control the volume of airway surface liquid by regulating transepithelial ion transport rates (Lazarowski *et al.*, 2004), activating cilia beating (Geary *et al.*, 1995) and mucin secretion (Lethem *et al.*, 1993) and thereby mobilizing the mucociliary clearance process that removes noxious materials from the airways. Despite the physiological relevance of responses triggered by extracellular nucleotides in the lungs, little is known about their origin on the epithelial surface and the release pathways. Increasing evidence suggests that extracellular ATP functions as a stress-responsive molecule, and mechanically-induced ATP release is a cell-regulated process that does not involve cell lysis. In particular, mechanical stresses, such as stretch, shear, media change or osmotic stress, have been shown to evoke ATP release from many cell types. Except in freshwater drowning, lung epithelia are seldom exposed to hypotonic shock. It represents, however, an experimentally-convenient and frequently-used surrogate of mechanical stress, with which it shares many common characteristics, including induction of ATP release, transient cytoskeleton reorganization, intracellular Ca^{2+} ($[\text{Ca}^{2+}]_i$) elevation and stimulation of other signaling pathways (Koyama *et al.*, 2001). We have shown recently that swelling-induced ATP release from lung alveolar A549 cells, bronchial epithelial 16HBE14o⁻ cells and NIH 3T3 fibroblasts tightly correlates with $[\text{Ca}^{2+}]_i$ elevation, indicating the involvement of Ca^{2+} -dependent exocytosis (Boudreault & Grygorczyk, 2004a). We also demonstrated that besides ATP, significant amounts of ADP, UTP and UDP are co-released from A549 cells by hypotonic shock (Tatur *et al.*, 2007). Mechanical stresses and hypotonic cell swelling are known to induce elevations of $[\text{Ca}^{2+}]_i$, which may involve Ca^{2+} influx from extracellular spaces and/or mobilization from intracellular

stores. Furthermore, once released, extracellular nucleotides could have paracrine-autocrine effects on metabotropic P2Y receptors expressed on the surface of airway epithelia. Because stimulation of P2Y receptors is coupled to elevation of $[Ca^{2+}]_i$, it may lead to nucleotide-induced enhancement of ATP release. Indeed, ATP-induced ATP release from astrocytes, could play a role in Ca^{2+} wave propagation (Anderson *et al.*, 2004).

In this study, we investigated hypotonic stress-induced ATP release from A549 cells and examined the role of Ca^{2+} influx and mobilization from intracellular stores. We also examined the contribution of the autocrine effects of released nucleotides on $[Ca^{2+}]_i$ signaling and ATP release.

METHODS

Cells

Human lung carcinoma A549 cells were grown in Dulbecco's Modified Eagle Medium supplemented with 10% fetal bovine serum, 2 mM L-glutamine, 56 U/mL penicillin-G and 56 µg/mL streptomycin sulfate. All culture media constituents were from GIBCO-BRL (Burlington, ON). ATP efflux was measured from cell monolayers grown to confluence (~ 500 cells*mm⁻²) on 24x60 mm glass coverslips. Cell volume was quantified from cells plated at low density on 22x22 mm glass coverslips, while Fura-2 calcium imaging experiments were performed with cells grown on circular 15-mm diameter glass coverslips.

Solutions and chemicals

Physiological isotonic solution (IS) contained (in mM): 140 NaCl, 5 KCl, 1 MgCl₂, 1 CaCl₂, 10 glucose and 10 TES, pH 7.4, adjusted with NaOH. 50% hypotonic saline (HS) was prepared by reducing NaCl concentration to 70 mM while keeping divalent cation concentration constant. In some control experiments, solutions with the same reduced NaCl content were used, while iso-osmolarity was maintained by adding 140 mM mannitol. Osmolarity of the solutions was checked with a freezing point osmometer (Micro Osmometer 3300, Advanced Instruments Inc., Norwood, MA) and was 316 mOsm for IS, 161 mOsm for HS and 316 mOsm for HS with added mannitol. For studies in the absence of extracellular calcium ([Ca²⁺]_o), CaCl₂ was omitted and the solutions were supplemented with 0.1 mM ethylene glycol-bis(β-aminoethyl ether)-*N,N,N',N'*-tetraacetic acid (EGTA) to chelate trace Ca²⁺. All reagents, including Pluronic[®] F127 and probenecid, were obtained from Sigma-Aldrich Canada, Ltd., Oakville, ON. For calcium imaging, Fura-2-AM was procured from Invitrogen-Molecular Probes, Kingston, ON. Apyrase (2 U/ml), bafilomycin (1 µM), glycyl-L-phenyl-β-naphthylamid (GPN, 100 µM),

carbonylcyanide p-trifluoromethoxyphenylhydrazone (FCCP, 10 μM), suramin (100 μM) as well as modulators of $[\text{Ca}^{2+}]_i$, 2-aminoethyl diphenylborinate (2-APB, 75 μM), caffeine (10 mM), ruthenium red (100 μM) and thapsigargin (TG, 1 μM), were purchased from Sigma-Aldrich Canada, Ltd. 6-*N,N*-Diethyl- β,γ -dibromomethylene-D-adenosine-5'-triphosphate (ARL 67156) was bought from Calbiochem (San Diego, CA). In general, the cells were pre-treated for 30 min in IS with the indicated concentration of the test compound. The experiments were then conducted in the absence of the inhibitor in case of bafilomycin, GPN and TG. By contrast, 2-APB, caffeine, ruthenium red, and suramin were also present during ATP efflux experiments by including them in the perfusate solutions. Thus, they were also present in perfusate aliquots used to evaluate ATP content by luciferase bioluminescence. Therefore, all these compounds were tested for their ability to directly interfere with luciferase bioluminescence (see below).

ATP efflux assay

ATP efflux during hypotonic challenge was measured with high temporal resolution using a custom-designed, low-volume (325 μL), flow-through chamber, as described previously (Boudreault & Grygorczyk, 2004a). Briefly, a 24x60 mm coverslip with confluent cell monolayer was mounted in the chamber and perfused with a warm (37°C/in-line SF-28 heater, Warner Instrument Co., Hamden, CT) solution at 1.3 mL/min. After an equilibration period in IS (5-15 min), 50% hypotonic shock was applied by HS perfusion ($t=0$), and the perfusate was collected continuously at 30-s intervals during the initial burst of ATP secretion (0-5 min) and every 1 min thereafter. ATP in the samples was quantified by a luciferase-luciferin-based assay, using ATP Assay Mix and ATP Assay Mix Dilution Buffer supplied by Sigma-Aldrich Canada, Ltd. ATP release rates were expressed in $\text{pmol}/(\text{min}\cdot 10^6 \text{ cells})$. Total ATP release was calculated by summing all ATP values collected,

starting from the application of hypotonic shock until the release rate returned to baseline, typically after about 15 min.

All test compounds that were added to the extracellular solution during the ATP efflux experiments were also examined for their ability to directly interfere with luciferase bioluminescence. We found strong inhibition of bioluminescence by suramin (see inset in Figure 5A), moderate by caffeine, and weak by 2-APB. The color of ruthenium red-containing solution also interfered with bioluminescence detection and contributed to inaccuracies in ATP evaluation. To correct for these inhibitory effects, calibration of luciferase-luciferin luminescence versus ATP standards was always performed in the presence of these reagents.

Statistical significance was determined by paired *t*-test, and $P < 0.05$ was considered significant.

[Ca²⁺]_i measurements

For [Ca²⁺]_i measurements, cells were loaded (1 h, room temperature) with 10 μM Fura-2-AM in physiological solution containing 0.02% Pluronic[®] F127 and 2.5 mM probenecid, followed by a 30-min de-esterification period in IS containing probenecid and the desired inhibitor (see below). For fluorescent imaging, a coverslip with Fura-2-loaded cells was mounted in an imaging/perfusion chamber (RC-20, volume 48 μl) attached to a heated platform (P-5, Warner Instrument Co.) on the stage of an inverted microscope (Nikon TE300). The imaging chamber was perfused continuously with a warm solution (37°C) via an in-line heater (SF-28, Warner Instrument Co.) at ~0.5 ml/min. The cells were illuminated for 100 ms with alternate light wavelengths of 340 and 380 nm, using a high-pressure mercury lamp (100 W) via interference filters (Chroma Technology, Brattleboro, VT) mounted on a filter wheel (Sutter Lambda 10-C, Sutter Instrument Co., Novato, CA) and a dichroic mirror (510/540 nm, Chroma Technology Corp., Brattleboro, VT). Fluorescence

images were recorded at 15-s intervals with the digital camera and stored for later analysis. Fura-2 measurements are presented as the fluorescence F_{340}/F_{380} ratio. In some experiments, to chelate intracellular Ca^{2+} , cells were loaded with BAPTA-AM (25 μM) for 30 min at room temperature in physiological solution.

All test compounds that were added to the extracellular solution during Ca^{2+} -imaging experiments were examined for their potential interference with Fura-2 fluorescence. To do so, control cell-free experiments were performed with Fura-2 solution in the cuvette, and fluorescence was measured in the presence and absence of the test compound at 340 nm and 380 nm excitation wavelengths with a SPEX FluoroMax spectrofluorimeter (Edison, NJ, USA). Only ruthenium red affected fluorescence noticeably and was, therefore, not used in $[\text{Ca}^{2+}]_i$ imaging experiments.

Cell volume evaluation

To evaluate the volume changes of substrate-attached cells, we deployed an upgraded version of the 3D imaging technique described in our previous work (Boudreault & Grygorczyk, 2004b; Groulx *et al.*, 2006). Briefly, the method involves 3D reconstruction of cell shape based on cell images acquired in two perpendicular directions. Side-view and top-view cell images were acquired at 10- to 60-s intervals prior to hypotonic challenge and at 5- to 30-s intervals during the challenge, to closely follow rapid cell volume changes. The 3D topography of the cell surface was reconstructed by a dual image surface reconstruction technique (Boudreault & Grygorczyk, 2004b). This technique generates a set of topographical curves of the cell surface from its digitized profile and base outline. Cell volume, surface and height were calculated from such a reconstructed cell topographical model. All calculations were carried out entirely with MatLab (MathWorks, Inc., Natick, MA).

RESULTS

We previously showed that hypotonic stress-induced ATP release from A549 cells was triggered by $[Ca^{2+}]_i$ elevation, but the sources and mechanism of Ca^{2+} mobilization were not determined. In this study, we examined the contribution of different intracellular Ca^{2+} stores to hypotonic stress-evoked $[Ca^{2+}]_i$ responses and their role in triggering ATP release from A549 cells. We also investigated the involvement of $[Ca^{2+}]_i$ signals resulting from autocrine purinoreceptor stimulation by secreted nucleotides. Throughout this study, the kinetics of ATP release, $[Ca^{2+}]_i$ responses and cell volume changes evoked by acute 50% hypotonic stress were measured in parallel experiments.

Role of extracellular Ca^{2+}

We first examined the role of Ca^{2+} influx from the extracellular spaces in hypotonic shock-evoked ATP release and $[Ca^{2+}]_i$ responses. Under control conditions, with 1 mM $CaCl_2$ in the extracellular solution, 50% hypotonic shock rapidly increased the ATP release rate, reaching a peak at approximately 2 min and followed by decay that lasted approximately 15 min, before returning to baseline (Figure 1A). To abolish calcium influx from the extracellular spaces, experiments were carried out with nominally Ca^{2+} -free extracellular solutions containing 0.1 mM EGTA to chelate any trace of Ca^{2+} . When the cells were perfused with a Ca^{2+} -free IS for up to 10 min, the kinetics and amount of released ATP, induced by subsequent application of a Ca^{2+} -free HS, were indistinguishable from those observed in parallel control experiments performed in the presence of Ca^{2+} (Figure 1A). Longer, up to 40 min, pre-incubation in Ca^{2+} -free IS slightly altered the time course of hypotonic shock-evoked ATP release, reducing the peak and total amount of secreted ATP, but the changes remained statistically insignificant. These experiments demonstrated that hypotonic shock-induced ATP release does not directly require Ca^{2+} influx from the

extracellular spaces, but depends entirely on Ca^{2+} mobilization from intracellular stores.

Figure 1B shows the typical $[\text{Ca}^{2+}]_i$ response of A549 cells to 50% hypotonic shock with Ca^{2+} present in extracellular solution. The response, represented by the Fura-2 fluorescence F_{340}/F_{380} ratio, consisted of a slow, pre-spike elevation initiated at the onset of hypotonic shock ($t = 0$), lasting approximately 0.5 min (see inset in Figure 1B), and followed by a rapid spike at about 1.5 min. After the peak, $[\text{Ca}^{2+}]_i$ decayed to a level that was significantly above baseline. This sustained $[\text{Ca}^{2+}]_i$ elevation lasted as long as the cells remained in HS (at least 20 min) and returned to baseline only after re-perfusion with IS. Thus, kinetically, it appears that the $[\text{Ca}^{2+}]_i$ response to hypotonic shock consists of two superimposed components, a slowly-rising response that includes the pre-spike and post-spike sustained elevation, and a rapid spike (see also Figures 2B and 3 below). Figure 1C examines the impact of extracellular Ca^{2+} removal on basal $[\text{Ca}^{2+}]_i$ under isotonic conditions and its response to 50% hypotonic shock. During short (3-5 min) incubation in Ca^{2+} -free IS, basal $[\text{Ca}^{2+}]_i$ decreased slowly, consistent with a steady Ca^{2+} leak from the extracellular spaces, but the subsequent response to Ca^{2+} -free HS remained unaffected (data not shown). However, longer (>10 min) incubation in Ca^{2+} -free IS gradually reduced the peak $[\text{Ca}^{2+}]_i$ response to HS, and after 30-40 min incubation, it was significantly but not completely diminished (Figure 1C). Interestingly, the pre-spike and sustained post-spike $[\text{Ca}^{2+}]_i$ elevation remained almost unaffected in these experiments. The results suggest that the rapid $[\text{Ca}^{2+}]_i$ spike induced by hypotonic shock is due to Ca^{2+} mobilization from intracellular stores, which are gradually depleted during cell incubation in Ca^{2+} -free solution. In contrast, the slow component of the $[\text{Ca}^{2+}]_i$ response remained unchanged even after prolonged Ca^{2+} -free incubation and, thus, likely represents Ca^{2+} mobilization from different intracellular source(s).

The fact that prolonged Ca^{2+} -free incubation significantly reduced the rapid $[\text{Ca}^{2+}]_i$ spike but had no effect on ATP release suggests that part of the ATP response

is Ca^{2+} -independent, or that the remaining $[\text{Ca}^{2+}]_i$ signal is sufficient to trigger a full ATP response. Indeed, the latter seems to be the case, because BAPTA chelation of intracellular Ca^{2+} almost completely abolished both $[\text{Ca}^{2+}]_i$ elevation and ATP release induced by 50% hypotonic shock (Figure 1D). This experiment confirms the conclusion of our previous study that hypotonic shock-induced ATP release from A549 cells depends entirely on $[\text{Ca}^{2+}]_i$ signaling (Boudreault & Grygorczyk, 2004a). Interestingly, we noticed that residual $[\text{Ca}^{2+}]_i$ and ATP responses to hypotonic shock varied between individual experiments, likely reflecting the variable efficiency of BAPTA loading and/or the spatiotemporal dependence of intracellular Ca^{2+} buffering by BAPTA in A549 cells.

In our experiments, we applied hypotonic shock by perfusing cells with a HS made by reducing NaCl content. When the cells were presented with a solution of the same reduced NaCl content but with iso-osmolarity kept constant with added mannitol, no responses were observed (Figure 1E). This result demonstrates that $[\text{Ca}^{2+}]_i$ and ATP release responses evoked by HS are caused by reduced osmolarity and not by changes in ionic strength. During 50% hypotonic shock, cell swelling reached a peak at 2-3 min; this was followed by a regulatory volume decrease (RVD) (Figure 1F). Removal of extracellular Ca^{2+} may change the kinetics of cell swelling or RVD, and could thus contribute to altered $[\text{Ca}^{2+}]_i$ responses. To verify this, cell volume changes evoked by 50% hypotonic shock were investigated in Ca^{2+} -containing and Ca^{2+} -free solutions. As Figure 1F shows, the kinetics, extent of hypotonic swelling and subsequent RVD in A549 cells were not different in the presence or absence of extracellular Ca^{2+} .

Role of TG-sensitive Ca^{2+} stores

To examine, in more detail, the nature of the intracellular Ca^{2+} stores contributing to the complex $[\text{Ca}^{2+}]_i$ response induced by hypotonic shock, we applied pharmacological tools acting on specific stores or release mechanisms. The

endoplasmic reticulum (ER), the most eminent and active Ca^{2+} store in most cells (Brini & Carafoli, 2000), was the first target of our investigation. In Ca^{2+} -containing IS, acute addition of TG (1 μM), a specific, irreversible inhibitor of the sarco-ER Ca^{2+} pump (SERCA) (Thastrup *et al.*, 1990), produced significant Ca^{2+} mobilization. However, despite large $[\text{Ca}^{2+}]_i$ responses, it induced only negligible ATP release (Figure 2A). When the cells were pre-treated with TG (1 μM) for 30 min in Ca^{2+} -free IS to empty the intracellular Ca^{2+} stores, and then challenged by Ca^{2+} -free HS, the rapid $[\text{Ca}^{2+}]_i$ spike was completely abolished, while the slow component of the $[\text{Ca}^{2+}]_i$ response remained unaffected (Figure 2B, top panel). Thus, it confirms that the rapid spike and the slow component of the hypotonic shock-induced $[\text{Ca}^{2+}]_i$ response represent Ca^{2+} mobilization from two different stores, one of which is TG-sensitive and the other TG-insensitive. The peak rate of hypotonic shock-induced ATP release from TG-treated cells was significantly reduced to $42 \pm 8\%$ of that observed with control, untreated cells ($n = 6$; Figure 2B, lower panel). As a result, total ATP release was also reduced but to a lesser degree ($62 \pm 3\%$ of control, Table 1). These data also indicate that both Ca^{2+} stores contributed to ATP release; the rapid $[\text{Ca}^{2+}]_i$ spike involving TG-sensitive stores was closely correlated with the rapid peak of ATP release. However, with cells having their TG-sensitive stores depleted, hypotonic shock induced only a slowly-rising $[\text{Ca}^{2+}]_i$ response, representing Ca^{2+} mobilization from TG-insensitive stores, and a significantly slower rate of ATP release was observed (Figure 2B, lower panel).

Using 3D cell imaging, we also verified that swelling and the RVD of TG-treated cells were similar to those seen with untreated cells ($n = 4$, data not shown). Therefore, the effects of TG treatment on ATP release could be entirely attributed to a specific action of TG on Ca^{2+} signaling.

Two major types of Ca^{2+} -release receptor channels, ryanodine (RyR) and inositol 1,4,5-trisphosphate (IP_3R), may be involved in Ca^{2+} mobilization from TG-sensitive stores such as the ER (Galione & Churchill, 2002). Cell pre-treatment (30

min, 37°C) with caffeine (10 mM), or 2-APB (75 μ M), modulators of RyR and IP₃R respectively, had a similar effect on $[Ca^{2+}]_i$ responses to Ca²⁺-free hypotonic shock as TG, i.e., they completely abolished the rapid Ca²⁺ mobilization spike, while the slowly-rising component remained unaffected (Figure 3, top panel). These two compounds also diminished the peak rate of ATP release to $56 \pm 4\%$ and $58 \pm 6\%$ of control values, respectively (Figure 3, bottom panel). Table 1 summarizes the effects of several RyR and IP₃R modulators on ATP secretion induced by 50% hypotonic shock in Ca²⁺-containing and Ca²⁺-free solutions. It confirms that both RyR and IP₃R play a role in this process. From Table 1, it is also apparent that simultaneous application of TG, caffeine and 2-APB did not completely abolish ATP secretion. The residual ~30% of total ATP release was therefore due to Ca²⁺ mobilization from TG-insensitive Ca²⁺ stores. When the ER-Ca²⁺ store modulators (TG, 2-APB, caffeine, ruthenium red) were tested in the presence of extracellular Ca²⁺, the time-course of cell swelling-induced ATP release displayed larger variability, with a slightly higher peak and a shallower decline, compared to experiments performed in the absence of extracellular Ca²⁺ (data not shown). This could be attributed to Ca²⁺ entry via store-operated plasma membrane Ca²⁺ channels (SOC), such as Trp1 and Trp6, which are expressed in A549 cells (Brough *et al.*, 2001; Xue *et al.*, 2000). However, the difference in total ATP released remained statistically insignificant (see Table 1). It should be remembered, however, that most of the pharmacological modulators in our study have limited specificity, e.g. 2-APB likely has many targets affecting not only IP₃R-mediated Ca²⁺ release but also Ca²⁺ influx via SOC, phospholipase C (PLC) activity and IP₃ production (Padar *et al.*, 2005).

Role of extracellular ATP degradation and autocrine effects of secreted nucleotides

To minimize the hydrolysis of secreted ATP by ecto-nucleotidases, our ATP release experiments were carried out in a custom-made flow-through chamber (internal volume = 325 μ l), which was continuously perfused at the rate of 1.3

ml/min, providing complete solution replacement in the experimental chamber every ~15 s. This allowed us to maintain the bulk ATP concentration in the chamber below 100 nM, even at the peak of ATP secretion (Boudreault & Grygorczyk, 2004a). This approach, however, may not completely prevent ATP degradation or the autocrine effects of secreted nucleotides. If ecto-nucleotidases are located in close proximity to ATP release sites, a significant fraction of extracellular ATP could be hydrolyzed before it is washed away from the cellular surface. Furthermore, the local cell surface concentration of ATP and other co-released nucleotides may go much higher than in the bulk perfusate, and may thus be sufficient to activate P2Y receptors. To assess the extent of ATP degradation at the cell surface in our experiments, release was studied in the presence of 100 μ M ARL 67156, an ATP analog and selective inhibitor of ecto-ATPases, which shows 300-fold greater selectivity for ecto-ATPase versus P2Y receptors (Drakulich *et al.*, 2004; Berra-Romani *et al.*, 2004). As Figure 4 demonstrates, ARL 67156 significantly enhanced ATP content in perfusate aliquots and, at the peak, the rate of ATP release observed in the presence of ARL reached $146 \pm 5\%$ of control values ($n=4$, Table 2). Thus, in the absence of ARL 67156, despite continuous perfusion, a significant fraction of secreted ATP was hydrolyzed by cell surface ecto-ATPases. However, we did not notice the contribution of secreted nucleotidases to ATP degradation in our experiments, because ATP concentration in perfusate aliquots remained stable at room temperature for at least 1-2 h after collection.

We have previously reported that upon hypoosmotic challenge, several other nucleotides besides ATP are secreted from A549 cells, in particular, significant amounts of UTP and UDP have been detected (Tatur *et al.*, 2007). These nucleotides may have autocrine/paracrine effects by acting on P2Y and P2X receptors. However, the contribution of ionotropic Na^+ - and Ca^{2+} -permeable P2X receptors to the autocrine effects is unlikely, because the responses were independent of Ca^{2+} influx from the extracellular spaces, as demonstrated in Figure 1 above. Therefore we

focused on P2Y₂ and P2Y₆ receptors that were found on the A549 cell surface (Schafer *et al.*, 2003; White & Burnstock, 2006; Xue *et al.*, 2000). Activation of these IP₃/Ca²⁺-coupled receptors could provide a positive feedback loop, where nucleotide-induced [Ca²⁺]_i elevation could further enhance Ca²⁺-dependent nucleotide release, a mechanism similar to ATP-induced ATP release reported in astrocytes (Anderson *et al.*, 2004). To investigate this possibility, [Ca²⁺]_i responses and ATP release induced by hypotonic shock were examined in the presence of 100 μM suramin, a nonspecific P2Y receptor antagonist. Figure 5A (top panel) shows that the peak [Ca²⁺]_i response, representing release from TG-sensitive stores, was drastically reduced in the presence of suramin. The peak rate and cumulative ATP release were also significantly reduced to 10 ± 1% and 32 ± 21% respectively of control values (Figure 5A, bottom panel and Table 2). The reduction of ATP release could not be attributed to the strong inhibitory effect of suramin on luciferase bioluminescence reaction, because this was corrected by using suramin-containing ATP standards (see inset in Figure 5A). Thus, the above experiments strongly suggest that the autocrine stimulation of P2Y receptors and the IP₃/Ca²⁺ signaling pathway contribute significantly (~70%) to ATP secretion evoked by hypotonic shock. This was further confirmed in experiments performed in the presence of apyrase (2 U/ml; 30°C), an enzyme which hydrolyzes the triphospho- and diphosphonucleotides (Figure 5B, *left panel*). The rapid [Ca²⁺]_i spike, which represents Ca²⁺ mobilization from TG-sensitive stores, was almost completely abolished, demonstrating that it was, in fact, evoked by the autocrine effects of rapidly-secreted extracellular tri- and diphosphate nucleotides acting on P2Y receptors. These experiments also showed that secreted nucleotides are susceptible to hydrolysis by exogenously-added apyrase. When similar experiments were performed with hexokinase (10 to 20 U/ml; 30°C), which, in the presence of 10 mM glucose, effectively converts nucleotide triphosphates (ATP, UTP) into diphosphates (ADP, UDP) (Lazarowski *et al.*, 1997), no effect on the peak [Ca²⁺]_i response was observed (Figure 5B, *right panel*). If hexokinase was indeed effective in

removing nucleotide triphosphates in these experiments, the result may suggest that autocrine stimulation of the peak $[Ca^{2+}]_i$ response could be attributed mainly to UDP, acting on the P2Y₆ receptor, and/or ADP, acting on the P2Y₁ receptor, while UTP, ATP acting on the P2Y₂ receptor seems to play a less prominent role. We addressed this point further in the experiments presented below.

Because of the wide and nonspecific effects of suramin (Zhang *et al.*, 1998), to examine the involvement of P2Y₁, P2Y₂ and P2Y₆ receptors more explicitly, we tested their known antagonist and agonists. Figure 5C shows that PPADS, a more specific P2Y₆ receptor antagonist, abolished the hypotonic shock-induced peak $[Ca^{2+}]_i$ response and strongly inhibited peak ATP release (by ~76%), effects that were similar to that of suramin and consistent with the prominent role of P2Y₆ receptors. In the absence of hypotonic shock, direct bulk addition of 10 μ M UDP, a selective P2Y₆ receptor agonist, or 100 μ M UTP, a selective P2Y₂ receptor agonist, induced a significant $[Ca^{2+}]_i$ response but small ATP release, which at the peak amounted only to ~1% to 6 % respectively, compared to that induced by 50% hypotonic shock (Figure 5D and E). We also verified that contaminating ATP levels in 100- μ M UTP and 10- μ M UDP samples were negligible (<0.1 nM), assuring that ATP detected in the perfusate indeed originated from UTP- or UDP-induced cellular ATP release. Exogenous ATP, which is equipotent with UTP at P2Y₂ receptors, also induced a significant $[Ca^{2+}]_i$ response (Figure 5F, *left panel*). These results confirm that both P2Y₂ and P2Y₆ receptors are functionally expressed in A549 cells. Recently, the presence of UDP-glucose (UDP-glc)-specific P2Y₁₄ receptors was reported in A549 cells (Muller *et al.*, 2005). In our hands, however, 10 μ M UDP-glc did not evoke any detectable $[Ca^{2+}]_i$ responses in A549 cells (Figure 5F, *left panel*), suggesting that P2Y₁₄ receptor expression may vary between different laboratories, e.g., due to different number of cell passages or culture conditions. Interestingly, 10 μ M ADP or 2-MeSADP, a P2Y₁ receptor agonist, evoked a strong, although transient, short-lasting (<1 min) $[Ca^{2+}]_i$ spike (Figure 5F, *right panel*). Such a transient response is

consistent with the reported fast desensitization of P2Y₁ receptors observed in other cell types (Palmer et al., 1998). To determine if the P2Y₁ receptor significantly contributes to autocrine [Ca²⁺]_i responses during hypotonic shock, hexokinase experiments, such as those in the Figure 5B (*right panel*), were repeated in the presence of the P2Y₁ receptor antagonist A3P5PS (1 μM). We found no effect of the antagonist on the hypotonic shock-induced [Ca²⁺]_i response in these experiments (not shown), demonstrating that P2Y₁ receptors do not contribute significantly to the autocrine effects noted in our study.

Collectively, the above results confirm that A549 cells express functional P2Y₂ and P2Y₆ receptors and, in addition, suggest the functional expression of P2Y₁ receptors. Although all three receptors are functionally present, only P2Y₆ seems to play a prominent role in autocrine [Ca²⁺]_i signaling during hypotonic shock-evoked nucleotide release.

Role of TG-insensitive Ca²⁺ stores

The above experiments demonstrated an important role of purinoreceptor-mediated Ca²⁺ mobilization from TG-sensitive Ca²⁺ stores in hypotonic shock-induced ATP release. Here, we investigated the role of the TG-insensitive part of the [Ca²⁺]_i response, which is seen as a slowly-rising, sustained component during hypotonic shock (see e.g., Figures 2B and 3). Acidic compartments, such as lysosomes, are being recognized as a part of TG-insensitive Ca²⁺ stores (Galione & Churchill, 2002); therefore, we examined the effect of bafilomycin, an inhibitor of the lysosomal H⁺-Ca²⁺ exchanger, and GPN, which disrupts lysosomal organelles. Both of these agents did not affect the peak rate or total ATP released from A549 cells induced by hypotonic shock (Table 1), demonstrating that TG-insensitive Ca²⁺ mobilization in A549 cells involves stores other than acidic-lysosomal compartments. Next, we examined the modulators of mitochondrial function: FCCP, a proton ionophore which depolarizes the inner mitochondrial membrane and reduces the

electrochemical driving force for Ca^{2+} uptake, and oligomycin, inhibitor of F1/F0 ATP synthase. Figure 6A shows that both modulators were without effect, suggesting that mitochondria also do not contribute to the TG-insensitive Ca^{2+} response evoked by hypotonic shock.

The actin cytoskeleton is known to regulate diverse cellular processes, including secretion and Ca^{2+} signaling. Some studies even suggest that the actin cytoskeleton itself may be part of intracellular Ca^{2+} stores (Janmey *et al.*, 1998; Lange & Brandt, 1996; Lange, 1999). We, therefore, explored the possibility that in our experiments the actin cytoskeleton may function as a TG-insensitive Ca^{2+} store. To perform such studies in isolation from TG-sensitive stores, the contribution of the latter was eliminated by pre-treating cells with TG in Ca^{2+} -free solution for 30 min to completely empty them. We found that disruption of actin filaments with latrunculin had no effect on hypotonic shock-induced, TG-insensitive Ca^{2+} responses or on corresponding ATP release (Figure 6B). Disruption of actin filaments with cytocholasin D was also without effect (data not shown). Similarly, induction of actin polymerization with jasplakinolide had no effect on the Ca^{2+} response, while ATP release showed only slightly slower kinetics, with the peak rate and total ATP release not being affected significantly (Figure 6B and Table 1). In contrast, in control cells not treated with TG, cytocholasin D had a significant (~70%) inhibitory effect on ATP release (Table 1). Thus, the intact cytoskeleton has an important role in modulating ATP release from cells with functional TG-sensitive stores. However, it has no direct role in Ca^{2+} storage and mobilization from TG-insensitive stores and corresponding ATP release.

DISCUSSION

The present study examined different sources of $[Ca^{2+}]_i$ elevations induced by acute hypotonic stress in A549 cells and their role in stimulating Ca^{2+} -dependent ATP release. We found that ATP release depends entirely on Ca^{2+} mobilization from intracellular stores. Both TG-sensitive and TG-insensitive stores are involved, contributing approximately 70% and 30% respectively to total ATP released by hypotonic shock. Importantly, we also found that despite rapid perfusion of the experimental chamber, autocrine stimulation of P2Y receptors by co-released uridine and adenosine nucleotides plays a major role in amplifying the initial hypotonic stress-induced $[Ca^{2+}]_i$ response and further promoting ATP release.

Two components of the $[Ca^{2+}]_i$ response to acute hypotonic stress

The $[Ca^{2+}]_i$ response induced by acute 50% hypotonic shock in A549 cells consisted of two superimposed, kinetically-different components. Both were due to Ca^{2+} mobilization from intracellular stores, while Ca^{2+} influx from extracellular spaces was not directly involved. The rapid $[Ca^{2+}]_i$ spike originated from Ca^{2+} mobilization from TG-sensitive stores, such as the sarco- endoplasmic reticulum, and was abolished when the stores were depleted by blocking SERCA with TG, or by activating RyR Ca^{2+} release channels with caffeine, under Ca^{2+} -free conditions to prevent refilling the stores. Antagonists of IP₃R (2-APB) and RyR (ruthenium red) also inhibited the $[Ca^{2+}]_i$ spike and ATP release (Table 1), indicating that Ca^{2+} mobilization via both channels plays a role in triggering ATP secretion. RyR may contribute to the propagation of $[Ca^{2+}]_i$ signaling via cyclic ADP-ribose and Ca^{2+} -induced Ca^{2+} release mechanism (Galione & Churchill, 2002). Interestingly, full inhibition of the rapid $[Ca^{2+}]_i$ peak by 2-APB, a non-competitive IP₃R Ca^{2+} release channel antagonist (Figure 3), suggests that this component of the hypotonic shock-induced $[Ca^{2+}]_i$ response results from activation of plasma membrane receptor(s) that

couple with the IP_3/Ca^{2+} signaling pathway. Indeed, autocrine activation of P2Y purinoreceptors was confirmed in a further study, and is discussed below.

The absence of the rapid spike after pre-treatment with TG revealed the slowly-rising $[Ca^{2+}]_i$ component originating from a TG-insensitive intracellular source. Beside the ER, the mitochondria and the nucleus appear to be crucial for the generation of Ca^{2+} signals of high spatiotemporal complexity (Brini & Carafoli, 2000). However, both organelles are implicated in the buffering and uptake of cytosolic Ca^{2+} rather than initiating and extending Ca^{2+} signaling (Brini & Carafoli, 2000). Hence, they are unlikely to be responsible for the TG-insensitive part of the hypotonic shock-induced Ca^{2+} signal. Indeed, the modulators of mitochondrial function, FCCP and oligomycin, were without effect on the TG-insensitive Ca^{2+} response to hypotonic shock. Furthermore, experiments with bafilomycin and GPN, which interfere with the Ca^{2+} -storage capability of acidic compartments, showed that they are not involved in triggering ATP release, suggesting the involvement of Ca^{2+} stores different from acidic lysosomal compartments. Interestingly, even prolonged ~40-min absence of extracellular Ca^{2+} had no effect on the slow $[Ca^{2+}]_i$ component, indicating that TG-insensitive stores may not be of an organellar nature and prompting us to examine the hypothesis that actin may act as a non-organellar Ca^{2+} store (Lange & Brandt, 1996; Lange, 1999). However, our experiments with agents that promote either actin polymerization or depolymerization were without significant effect on hypotonic shock-induced Ca^{2+} mobilization from TG-insensitive stores and corresponding ATP release. Thus, the nature of this slow $[Ca^{2+}]_i$ response component remains incompletely understood.

Earlier reports with other cell types showed that $[Ca^{2+}]_i$ elevations caused by hypotonic shock could either result from Ca^{2+} influx across the plasma membrane and/or from Ca^{2+} release from internal stores (McCarty & O'Neil, 1992; Sanchez *et al.*, 2003; Tinel *et al.*, 2000; Wu *et al.*, 2001; Wu *et al.*, 1997). In our experiments, Ca^{2+}

influx did not play a direct role in either the slow or rapid peak of the $[Ca^{2+}]_i$ response to acute hypotonic shock, although the prolonged absence of extracellular Ca^{2+} , led to partial depletion of TG-sensitive stores and reduction of the rapid $[Ca^{2+}]_i$ peak. These differences may be due to the different cell types studied and experimental conditions. Our experiments were performed with substrate-attached cells at 37°C, while some other studies utilized cells in suspension or at room temperature. Because the rapid peak of $[Ca^{2+}]_i$ responses results from the autocrine/paracrine purinergic loop in A549 cells, other factors may include the differential expression of P2Y receptors, differences in nucleotide release and the expression of different plasma membrane Ca^{2+} -permeable channels.

Ca^{2+} and ATP release.

Our previous study demonstrated a tight correlation between $[Ca^{2+}]_i$ elevations and ATP release in A549, 16HBE14o and NIH-3T3 fibroblasts during the initial ~5 min of hypotonic stress (Boudreault & Grygorczyk, 2004a). The present work shows correspondingly that maneuvers which eliminated the rapid $[Ca^{2+}]_i$ spike also significantly reduced the rate of ATP release. Complete emptying of TG-sensitive stores by pharmacological maneuvers reduced, by up ~70%, the total ATP release evoked by subsequent 50% hypotonic shock (Table 1). The remaining ~30% of ATP release could be attributed to the slow $[Ca^{2+}]_i$ signal originating from TG-insensitive stores. Interestingly, TG on its own provoked quite significant $[Ca^{2+}]_i$ elevation, but in contrast to hypotonic shock, induced only minor ATP release. We previously observed that the strong $[Ca^{2+}]_i$ signal generated by application of the Ca^{2+} -ionophore ionomycin produced relatively minor ATP release (Boudreault & Grygorczyk, 2004a). Both experiments imply that other factor(s) besides global $[Ca^{2+}]_i$ elevation modulate ATP release from A549 cells. For example, the spatiotemporal dependence of $[Ca^{2+}]_i$ signaling is now a widely recognized feature of this universal second messenger, which restricts the Ca^{2+} action to specific

intracellular microdomains, allowing the fine control of cell function (Oheim *et al.*, 2006; Spat, 2006). Thus, relatively minor ATP release might indicate that ATP release sites are distant from TG-induced Ca^{2+} mobilization sites. Moreover, besides Ca^{2+} , other signaling pathways not investigated in this study have been implicated in the regulation of ATP release, including tyrosine kinase, Rho/Rho kinase and PI3-kinase (Grygorczyk & Guyot, 2001; Koyama *et al.*, 2001).

Some studies found that only a fraction of hypotonic shock-induced ATP release could be inhibited by loading cells with intracellular Ca^{2+} chelator BAPTA-AM, which suggests a Ca^{2+} -independent release mechanism (Okada *et al.*, 2006). Mobile Ca^{2+} buffers, such as BAPTA, provide an efficient mechanism to spatially restrict the $[\text{Ca}^{2+}]_i$ increase (Oheim *et al.*, 2006), but its efficiency in preventing Ca^{2+} -triggered vesicular exocytosis will critically depend on the distance between Ca^{2+} release sites and secretory vesicles. Ca^{2+} transients might be highly localized, reaching as high as 5 μM to 30 μM at submembrane microdomains (reviewed in (Oheim *et al.*, 2006). Thus, despite a high Ca^{2+} -binding rate, BAPTA may not completely prevent localized $[\text{Ca}^{2+}]_i$ increases. This may be especially the case for highly-differentiated primary epithelial cells, where secretory vesicles may co-localize with submembrane Ca^{2+} stores. Further studies are required to explore the effectiveness of BAPTA in preventing hypotonic shock-induced submembrane $[\text{Ca}^{2+}]_i$ transients and ATP release from such cells.

Role of the autocrine/paracrine loop in ATP release

Our data demonstrate that the rapid $[\text{Ca}^{2+}]_i$ peak induced by hypotonic shock results entirely from the autocrine/paracrine effects of released nucleotides acting on $\text{IP}_3/\text{Ca}^{2+}$ signaling pathway-coupled P2Y receptors. This conclusion is supported by the following experimental evidence. The rapid $[\text{Ca}^{2+}]_i$ peak could be almost completely abolished by: (i) the hydrolysis of extracellular triphospho- and

diphosphonucleotides with apyrase, but not hexokinase; (ii) blocking P2Y receptors with the non specific P2Y receptor antagonist suramin; (iii) blocking the P2Y₆ receptor with its more specific antagonist PPADS, but not the P2Y₁ receptor antagonist A3P5PS; (iv) blocking the ER Ca²⁺-release IP₃R channel with its antagonist 2-APB downstream of the P2Y receptor; or (v) completely emptying ER stores with TG or caffeine.

We have recently reported that several adenine and uridine nucleotides are transiently released from A549 cells in response to hypotonic shock (Tatur *et al.*, 2007). Importantly, apart from ATP, significant amounts of UTP, UDP and ADP could be detected in cell perfusates (ATP > UTP > UDP > ADP). Therefore, released nucleotides, by interacting with their specific receptors, could contribute to autocrine/paracrine signaling in A549 cells. In this study, by investigating [Ca²⁺]_i responses to the bulk addition of UTP, ATP, or UDP, we confirmed the functional expression of P2Y₂ and P2Y₆ receptors respectively (Clunes & Kemp, 1996; Zhao *et al.*, 2000), but not UDP-glc-specific P2Y₁₄ receptors (Muller *et al.*, 2005) in A549 cells. Interestingly, we also found evidence for the functional expression of the ADP receptor P2Y₁. Based on their functional presence, we conclude that, in principle, the three P2Y receptor subtypes may contribute to the autocrine effects of released nucleotides. In particular, the involvement of P2Y₆ receptor was further confirmed by using its more specific antagonist PPADS, which almost completely abolished the hypotonic shock-induced rapid [Ca²⁺]_i peak and significantly diminished ATP release, while the P2Y₁ receptor antagonist A3P5PS had no detectable effect on the rapid [Ca²⁺]_i response. This suggests an important role for P2Y₆ receptor in the autocrine/paracrine loop. The relative contribution of P2Y₂ receptors could not be independently determined in complementary experiments because selective P2Y₂ receptors antagonists are not available commercially. However, complementary support that P2Y₆ but not P2Y₂ receptors are the main players in the autocrine [Ca²⁺]_i response was provided by experiments with apyrase and hexokinase. Apyrase, by

hydrolyzing nucleotide tri- and diphosphates, eliminates the agonists of both P2Y₂ and P2Y₆ receptors, completely abolishing the peak $[Ca^{2+}]_i$ response. However, hexokinase, which eliminates only agonists of P2Y₂ receptors by converting UTP and ATP into UDP and ADP (Lazarowski *et al.*, 1997), had no noticeable effect.

Based on our data, we propose the following mechanism of hypotonic shock-induced ATP release. Upon hypotonic shock, initial Ca^{2+} mobilization likely occurs from TG-insensitive stores, seen as the slowly-rising pre-spike in Figure 1B. This initial $[Ca^{2+}]_i$ elevation triggers the vesicular exocytosis of adenosine and uridine nucleotides which, via autocrine/paracrine activation of G_q protein-coupled P2Y receptors, stimulates the PLC/IP₃ signaling pathway, leading to subsequent activation of IP₃R Ca^{2+} release channels of the ER. At this point, Ca^{2+} -induced Ca^{2+} release via RyR will also contribute to $[Ca^{2+}]_i$ signal propagation. The enhanced $[Ca^{2+}]_i$ signal, seen as the rapid $[Ca^{2+}]_i$ spike in Figure 1B will, in turn, further promote Ca^{2+} -dependent ATP release. Such nucleotide-promoted nucleotide release likely leads to almost full depletion of exocytosis-available vesicular pools in A549 cells, since after ~5 min, the rate of ATP release does not tightly correlate with the $[Ca^{2+}]_i$ signal any longer. As a result, after the initial peak, the rate of ATP release decays towards background, despite significantly elevated $[Ca^{2+}]_i$ (Boudreault & Grygorczyk, 2004a; Grygorczyk & Boudreault, 2005).

The proposed mechanism might be a general scheme of hypotonic or mechanical stress-induced ATP release from other cell types, although the specific players of the autocrine loop may vary, depending on the type of P2Y receptor expressed by a given cell and its ability to release different adenosine and uridine nucleotides. In the particular case of A549 cells, UDP acting on P2Y₆ receptors seems to have a prominent role. As exemplified by the effect of the ecto-ATPase inhibitor ARL in our experiments, extracellular nucleotide metabolism, and possibly their interconversion, may also have an important role in regulating nucleotide release and autocrine signaling and requires future investigation. Our findings may have

interesting implications for the regulation of surfactant secretion by alveolar type II cells. Although the stimulatory effect of stretch and involvement of P2Y₂ receptors in surfactant secretion are well-established (Dietl & Haller, 2005;Rooney, 2001), the contribution of other P2Y receptors remains unclear. Our study suggests an important role of P2Y₆ receptors in synergistic autocrine/paracrine stimulation of the IP₃/Ca²⁺ signaling pathway after stress-induced nucleotide release from A549 cells, a model of type II pneumocytes. The resulting amplification and spatiotemporal extension of the [Ca²⁺]_i signal may influence several steps of surfactant secretion, including lamellar body fusion, pore-opening and surfactant dispersion (Dietl & Haller, 2005).

In summary, our study demonstrates an important role of autocrine purinergic signaling in hypotonic stress-induced ATP release. The autocrine loop amplifies the initial stress-evoked Ca²⁺ response, accounting for the majority (~70 %) of released ATP. Our study also provides a novel paradigm in which stress-induced ATP release from alveolar A549 cells is amplified predominantly by the autocrine/paracrine action of co-released UDP acting on P2Y₆ receptors. We propose that such synergistic effects of co-released nucleotides may be a general mechanism of purinergic signal propagation and amplification in other cell types.

REFERENCES

Anderson, C. M., Bergher, J. P., & Swanson, R. A. (2004). ATP-induced ATP release from astrocytes. *J.Neurochem.* **88**, 246-256.

Berra-Romani, R., Rinaldi, C., Raqeeb, A., Castelli, L., Magistretti, J., Taglietti, V., & Tanzi, F. (2004). The duration and amplitude of the plateau phase of ATP- and ADP-evoked Ca(2+) signals are modulated by ectonucleotidases in in situ endothelial cells of rat aorta. *J Vasc.Res* **41**, 166-173.

Boudreault, F. & Grygorczyk, R. (2004a). Cell swelling-induced ATP release is tightly dependent on intracellular calcium elevations. *J.Physiol.*

Boudreault, F. & Grygorczyk, R. (2004b). Evaluation of rapid volume changes of substrate-adherent cells by conventional microscopy 3D imaging. *J.Microsc.* **215**, 302-312.

Brini, M. & Carafoli, E. (2000). Calcium signalling: a historical account, recent developments and future perspectives. *Cell Mol.Life Sci.* **57**, 354-370.

Brough, G. H., Wu, S., Cioffi, D., Moore, T. M., Li, M., Dean, N., & Stevens, T. (2001). Contribution of endogenously expressed Trp1 to a Ca2+-selective, store-operated Ca2+ entry pathway. *The FASEB Journal* **15**, 1727-1738.

Clunes, M. T. & Kemp, P. J. (1996). P2u purinoceptor modulation of intracellular Ca²⁺ in a human lung adenocarcinoma cell line: down-regulation of Ca²⁺ influx by protein kinase C. *Cell Calcium* **20**, 339-346.

Dietl, P. & Haller, T. (2005). Exocytosis of lung surfactant: from the secretory vesicle to the air-liquid interface. *Annu.Rev Physiol* **67**, 595-621.

Drakulich, D. A., Spellmon, C., & Hexum, T. D. (2004). Effect of the ecto-ATPase inhibitor, ARL 67156, on the bovine chromaffin cell response to ATP. *Eur.J Pharmacol* **485**, 137-140.

- Galione, A. & Churchill, G. C. (2002). Interactions between calcium release pathways: multiple messengers and multiple stores. *Cell Calcium* **32**, 343-354.
- Geary, C. A., Davis, C. W., Paradiso, A. M., & Boucher, R. C. (1995). Role of CNP in human airways: cGMP-mediated stimulation of ciliary beat frequency. *Am J Physiol* **268**, L1021-L1028.
- Groulx, N., Boudreault, F., Orlov, S. N., & Grygorczyk, R. (2006). Membrane reserves and hypotonic cell swelling. *J Membr. Biol* **214**, 43-56.
- Grygorczyk, R. & Boudreault, F. (2005). The emerging role of calcium-dependent exocytosis in ATP release from nonexcitable cells. *Physiology News* **60**, 21-22.
- Grygorczyk, R. & Guyot, A. (2001). Osmotic swelling-induced ATP release: a new role for tyrosine and Rho-kinases? *J. Physiol* **532**, 582.
- Janmey, P. A., Kas, J., Shah, J. V., Allen, P. G., & Tang, J. X. (1998). Cytoskeletal networks and filament bundles: regulation by proteins and polycations. *Biol Bull.* **194**, 334-335.
- Koyama, T., Oike, M., & Ito, Y. (2001). Involvement of Rho-kinase and tyrosine kinase in hypotonic stress-induced ATP release in bovine aortic endothelial cells. *J Physiol* **532**, 759-769.
- Lange, K. (1999). Microvillar Ca⁺⁺ signaling: a new view of an old problem. *J Cell Physiol* **180**, 19-34.
- Lange, K. & Brandt, U. (1996). Calcium storage and release properties of F-actin: evidence for the involvement of F-actin in cellular calcium signaling. *FEBS Lett.* **395**, 137-142.
- Lazarowski, E. R., Paradiso, A. M., Watt, W. C., Harden, T. K., & Boucher, R. C. (1997). UDP activates a mucosal-restricted receptor on human nasal epithelial cells that is distinct from the P2Y2 receptor. *Proc Natl Acad Sci U.S.A* **94**, 2599-2603.

Lazarowski, E. R., Tarran, R., Grubb, B. R., Van Heusden, C. A., Okada, S., & Boucher, R. C. (2004). Nucleotide release provides a mechanism for airway surface liquid homeostasis. *J Biol Chem.* **279**, 36855-36864.

Lethem, M. I., Dowell, M. L., Van Scott, M., Yankaskas, J. R., Egan, T., Boucher, R. C., & Davis, C. W. (1993). Nucleotide regulation of goblet cells in human airway epithelial explants: normal exocytosis in cystic fibrosis. *Am J Respir. Cell Mol. Biol* **9**, 315-322.

McCarty, N. A. & O'Neil, R. G. (1992). Calcium signaling in cell volume regulation. *Physiol Rev.* **72**, 1037-1061.

Muller, T., Bayer, H., Myrtek, D., Ferrari, D., Sorichter, S., Ziegenhagen, M. W., Zissel, G., Virchow, J. C., Jr., Luttmann, W., Norgauer, J., Di Virgilio, F., & Idzko, M. (2005). The P2Y₁₄ Receptor of Airway Epithelial Cells: Coupling to Intracellular Ca²⁺ and IL-8 Secretion. *American Journal of Respiratory Cell and Molecular Biology* **33**, 601-609.

Oheim, M., Kirchhoff, F., & Stuhmer, W. (2006). Calcium microdomains in regulated exocytosis. *Cell Calcium* **40**, 423-439.

Okada, S. F., Nicholas, R. A., Kreda, S. M., Lazarowski, E. R., & Boucher, R. C. (2006). Physiological regulation of ATP release at the apical surface of human airway epithelia. *J Biol Chem.* **281**, 22992-23002.

Padar, S., Bose, D. D., Livesey, J. C., & Thomas, D. W. (2005). 2-Aminoethoxydiphenyl borate perturbs hormone-sensitive calcium stores and blocks store-operated calcium influx pathways independent of cytoskeletal disruption in human A549 lung cancer cells. *Biochem. Pharmacol.* **69**, 1177-1186.

Palmer, R. K., Boyer, J. L., Schachter, J. B., Nicholas, R. A., & Harden, T. K. (1998). Agonist action of adenosine triphosphates at the human P2Y₁ receptor. *Mol. Pharmacol* **54**, 1118-1123.

Rooney, S. A. (2001). Regulation of surfactant secretion. *Comparative Biochemistry and Physiology - Part A: Molecular & Integrative Physiology* **129**, 233-243.

Sanchez, J. C., Danks, T. A., & Wilkins, R. J. (2003). Mechanisms involved in the increase in intracellular calcium following hypotonic shock in bovine articular chondrocytes. *Gen. Physiol Biophys.* **22**, 487-500.

Schafer, R., Sedehizade, F., Welte, T., & Reiser, G. (2003). ATP- and UTP-activated P2Y receptors differently regulate proliferation of human lung epithelial tumor cells. *AJP - Lung Cellular and Molecular Physiology* **285**, L376-L385.

Spat, A. (2006). Calcium microdomains and the fine control of cell function--An introduction. *Cell Calcium* **40**, 403-404.

Tatur, S., Kreda, S. M., Lazarowski, E. R., & Grygorczyk, R. Calcium-dependent release of adenosine and uridine nucleotides from A549 cells. *Purinergic Signalling* . 2007.

Ref Type: In Press

Thastrup, O., Cullen, P. J., Drobak, B. K., Hanley, M. R., & Dawson, A. P. (1990). Thapsigargin, a tumor promoter, discharges intracellular Ca²⁺ stores by specific inhibition of the endoplasmic reticulum Ca²⁺(+)-ATPase. *Proc Natl Acad Sci U S A* **87**, 2466-2470.

Tinel, H., Kinne-Saffran, E., & Kinne, R. K. (2000). Calcium signalling during RVD of kidney cells. *Cell Physiol Biochem.* **10**, 297-302.

White, N. & Burnstock, G. (2006). P2 receptors and cancer. *Trends Pharmacol.Sci* **27**, 211-217.

Wu, M. M., Grabe, M., Adams, S., Tsien, R. Y., Moore, H. P., & Machen, T. E. (2001). Mechanisms of pH regulation in the regulated secretory pathway. *Journal of Biological Chemistry* **276**, 33027-33035.

Wu, X., Yang, H., Iserovich, P., Fischbarg, J., & Reinach, P. S. (1997). Regulatory volume decrease by SV40-transformed rabbit corneal epithelial cells requires ryanodine-sensitive Ca²⁺-induced Ca²⁺ release. *J Membr. Biol* **158**, 127-136.

Xue, H. H., Zhao, D. M., Suda, T., Uchida, C., Oda, T., Chida, K., Ichiyama, A., & Nakamura, H. (2000). Store depletion by caffeine/ryanodine activates capacitative Ca(2+) entry in nonexcitable A549 cells. *J.Biochem.(Tokyo)* **128**, 329-336.

Zhang, Y. L., Keng, Y. F., Zhao, Y., Wu, L., & Zhang, Z. Y. (1998). Suramin is an active site-directed, reversible, and tight-binding inhibitor of protein-tyrosine phosphatases. *J Biol Chem.* **273**, 12281-12287.

Zhao, D. M., Xue, H. H., Chida, K., Suda, T., Oki, Y., Kanai, M., Uchida, C., Ichiyama, A., & Nakamura, H. (2000). Effect of erythromycin on ATP-induced intracellular calcium response in A549 cells. *Am.J.Physiol Lung Cell Mol.Physiol* **278**, L726-L736.

ACKNOWLEDGEMENTS

This study was supported in part by the Canadian Institutes of Health Research and the Canadian Cystic Fibrosis Foundation (CCFF). S.T. was the recipient of a CCFF studentship. The authors acknowledge the technical work of H el ene Chabot, Cedric Mawle and Laura De Benedetti, and the editorial assistance of Ovid Da Silva, Research Support Office, Research Centre, CHUM. Thanks are due to Dr. Eduardo Lazarowski for his comments on the manuscript.

Table 1.

		Peak ATP release						Total ATP release					
Agent		[Ca ²⁺] _o			Absence of [Ca ²⁺] _o			[Ca ²⁺] _o			Absence of [Ca ²⁺] _o		
	Action	% of control ± SD	n	P	% of control ± SD	n	P	% of control ± SD	n	P	% of control ± SD	n	P
2-APB	IP ₃ R inhibition	70 ± 2	3	< 0.05	58 ± 6	3	< 0.05	108 ± 1	3	< 0.05	69 ± 10	3	< 0.05
Caffeine	RyR stimulation	65 ± 12	6	< 0.05	56 ± 4	3	< 0.05	60 ± 15	6	< 0.05	42 ± 8	3	< 0.05
Ruthenium Red	RyR inhibition	51 ± 4	3	< 0.05	73 ± 5	3	< 0.05	72 ± 5	3	< 0.05	75 ± 12	3	> 0.05
Thapsigargin (TG)	ER-Ca ²⁺ -pump inhibition	44 ± 14	7	< 0.001	42 ± 8	6	< 0.001	94 ± 31	6	> 0.05	62 ± 3	6	< 0.001
2-APB + caffeine + TG					31 ± 9	3	< 0.05				30 ± 6	3	< 0.05
Bafilomycin	Ca ²⁺ -H ⁺ exchanger inhibition	104 ± 9	3	> 0.05				98 ± 3	3	> 0.05			
GPN	lysosome disruption	105 ± 28	3	> 0.05				108 ± 13	3	> 0.05			
BAPTA	[Ca ²⁺] _i chelating agent	10 ± 2	3	< 0.05				11 ± 2	3	< 0.05			
Cytochalasin D	inhibition of actin polymerization	33 ± 6	3	< 0.05				56 ± 5	3	< 0.05			
					% of TG ± SD						% of TG ± SD		
Jasplakinolide + TG	induction of actin polymerization				97 ± 15	3	> 0.05				135 ± 10	3	> 0.05
Latrunculin A + TG	disruption of microfila- ment-mediated processes				88 ± 9	3	> 0.05				121 ± 9	3	> 0.05

Table 2.

		Peak ATP release			Total ATP release		
Agent		[Ca ²⁺] _o			[Ca ²⁺] _o		
	Action	% of control ± SD	n	P	% of control ± SD	n	P
ARL	Ecto-nucleotidase inhibition	146 ± 5	4	< 0.05			
Suramin	P2X, P2Y receptor inhibition	10 ± 1	3	< 0.001	32 ± 21	3	< 0.05
PPADS	P2Y ₆ receptor inhibition	24 ± 2	3	< 0.001	35 ± 10	3	< 0.05

Table 1.

Effect of Ca^{2+} signaling and cytoskeleton modulators on 50% hypotonic shock-induced ATP release from A549 cells.

Table 2.

Modulation of hypotonic shock-induced ATP release by selected inhibitors of ectonucleotidases and P2Y receptors.

FIGURE LEGENDS**Figure 1. Role of extracellular Ca^{2+} in hypotonic shock-induced ATP release, $[\text{Ca}^{2+}]_i$ and cell volume responses.**

- A.** Time-course of ATP release induced by 50% hypotonic shock ($t = 0$) from confluent A549 cell monolayers. The data points shown as (●) represent ATP efflux observed with 1 mM Ca^{2+} present in the perfusate throughout the experiment ($n = 4$). The data points shown as (■) and (▼) represent ATP efflux observed in the absence of extracellular Ca^{2+} when it was removed 10 min and 40 min before hypotonic shock, respectively ($n = 3$ and $n = 4$ respectively). Peak and total ATP releases were not significantly different between the three experimental groups.
- B.** Time-course of the hypotonic shock-induced $[\text{Ca}^{2+}]_i$ response in A549 cells in Ca^{2+} -containing HS. The response consisted of a slow pre-spike elevation initiated at the onset of hypotonic shock ($t = 0$), a rapid spike at about 1.5 min, and a sustained after-spike $[\text{Ca}^{2+}]_i$ elevation, which returned to baseline after the cells were re-perfused with physiological IS. The inset shows the initial $[\text{Ca}^{2+}]_i$ response acquired with higher temporal resolution, clearly demonstrating the existence of a pre-spike.
- C.** Effect of extracellular Ca^{2+} removal on the hypotonic shock-induced $[\text{Ca}^{2+}]_i$ response. The three representative traces (out of $n = 3$ to 4 independent experiments) show the Fura-2 fluorescence F_{340}/F_{380} ratio response to hypotonic shock recorded with Ca^{2+} present throughout the experiment (●), or after removal of extracellular Ca^{2+} for 17 min (■) or 40 min (▼) before Ca^{2+} -free 50% HS was applied. Note the significant reduction of the peak $[\text{Ca}^{2+}]_i$ response in cells incubated for 40 min in Ca^{2+} -free extracellular solution.
- D.** The $[\text{Ca}^{2+}]_i$ and ATP responses to hypotonic shock are abolished in BAPTA-loaded (25 μM , 30 min) cells; representative of $n = 3$ independent experiments.

- E. The $[Ca^{2+}]_i$ and ATP responses, *upper* and *lower panels*, respectively, are evoked by reduced osmolarity, not ionic strength. The control traces (●) refer to responses triggered by HS that had 50% reduced NaCl content. When the cells were perfused with HS complemented with mannitol to maintain iso-osmolarity (see Methods), no responses were observed (■); representative of $n = 3$ independent experiments.
- F. 50% hypotonic shock-induced volume responses of single, substrate-attached A549 cells in Ca^{2+} -containing (*left panel*) and Ca^{2+} -free (*right panel*) solutions. *Thin lines* represent data from individual single-cell experiments, and *solid lines* represent a fit to the average data (\pm S.D.; $n = 3$ to 4). Cell swelling and RVD were similar for both experimental conditions.

Figure 2. Modulation of the cell swelling-induced $[Ca^{2+}]_i$ response and ATP release by TG.

- A. Time course of $[Ca^{2+}]_i$ changes (*top panel*) and ATP release (*bottom panel*) in response to the acute addition of 1 μ M TG in Ca^{2+} -free IS. Each trace is representative of 3 independent experiments.
- B. *Top panel*: Hypotonic shock-induced $[Ca^{2+}]_i$ response in TG-treated cells, representative of 4 independent experiments. *Bottom panel*: Hypotonic shock-induced ATP release from TG-treated cells, representative of 6 independent experiments. (●) refers to control cells incubated for 30 min in Ca^{2+} -free solution prior to the experiment, and (▼) refers to cells incubated for 30 min in Ca^{2+} -free solution containing 1 μ M TG.

Figure 3. Role of RyR and IP₃R in the cell swelling-induced $[Ca^{2+}]_i$ response and ATP release.

Hypotonic shock-induced $[Ca^{2+}]_i$ response (*top panel*) and ATP release (*bottom panel*) in caffeine (▼) and 2-APB (■) pre-treated cells. Representative traces are

shown out of $n = 3$ independent experiments; control (●) refers to the $[Ca^{2+}]_i$ response in untreated cells. All experiments were performed in Ca^{2+} -free solutions.

Figure 4. Blocking ecto-ATPases enhances peak ATP release.

Effect of the ecto-ATPase inhibitor ARL 67156 (100 μ M) on hypotonic shock-induced ATP release. Control experiments (●) were performed in the presence of $[Ca^{2+}]_o$ without the addition of inhibitor; (■) represents the time course of ATP release in the presence of $[Ca^{2+}]_o$ and ARL. Representative traces out of $n = 4$ are shown.

Figure 5. Role of autocrine/paracrine purinergic signaling.

- A. Effect of hypotonic shock on $[Ca^{2+}]_i$ (*top panel*) and ATP release (*bottom panel*) after blocking purinergic receptors with suramin (▼); (●) refers to the control response in the absence of suramin. Representative traces out of $n = 3$ independent experiments are shown. *Inset in bottom panel*: Calibration curve of luciferase-luciferin luminescence (in relative light units, RLU) versus standard ATP concentrations: (●) refers to ATP standards in IS; (■) refers to ATP standards in IS containing 100 μ M suramin. Similar effect of suramin on luciferase-luciferin luminescence was observed in HS.
- B. Effect of apyrase (▼, *left panel*), or hexokinase (▼, *right panel*) on the hypotonic shock-induced $[Ca^{2+}]_i$ response. Apyrase (or hexokinase) was added 3 min prior to and throughout hypotonic shock. On each panel, a representative trace out of $n = 3$ independent experiments is shown. Control (●) refers to untreated cells. All experiments were performed in the presence of 1 mM extracellular Ca^{2+} and at 30°C, not as usually at 37°C, in accordance with the optimal temperature of the enzyme activity. Therefore, the extent of peak reduction by apyrase at 37°C might be slightly different.

- C. Effect of the P2Y₆ receptor antagonist PPADS on hypotonic shock-induced ATP release and the [Ca²⁺]_i response. 100 μM PPADS was added to cells 30 min before the application of hypotonic shock and was present throughout the experiment were performed in Ca²⁺-containing solutions. For each condition, a representative experiment out of n = 3 is shown. (●) refers to untreated cells, and (■) refers to PPADS-treated cells.
- D. Effect of 10 μM UDP, a P2Y₆ agonist, on the [Ca²⁺]_i response (representative of n = 3) and ATP release (average ± S.D. of n = 3), *top* and *bottom panels*, respectively.
- E. Effect of 100 μM UTP, a P2Y₂ agonist, on the [Ca²⁺]_i response (representative of n = 3) and ATP release (average ± S.D. of n = 3), *top* and *bottom panels*, respectively.
- F. *Left panel*: Effect of 10 μM ATP (●), a P2Y₂ agonist, and 10 μM UDP-glc (■), a P2Y₁₄ agonist, added at t = 0, on the [Ca²⁺]_i response. Note that UDP-glc had no effect, although the cells did respond robustly to the subsequent addition of UTP (■). *Right panel*: 10 μM ADP or 2-MeSADP, agonists of P2Y₁ receptors, evoked short-lasting [Ca²⁺]_i responses that were kinetically different from those observed for other nucleotides, shown in D and E. For these experiments, ADP was pre-treated with 10 U/ml of hexokinase in the presence of 10 mM glucose for 1 h at room temperature to remove any contaminating ATP and UTP. For each condition, a representative experiment out of n = 3 is shown.

Figure 6. Role of mitochondria and actin in the TG-insensitive [Ca²⁺]_i response to hypotonic shock.

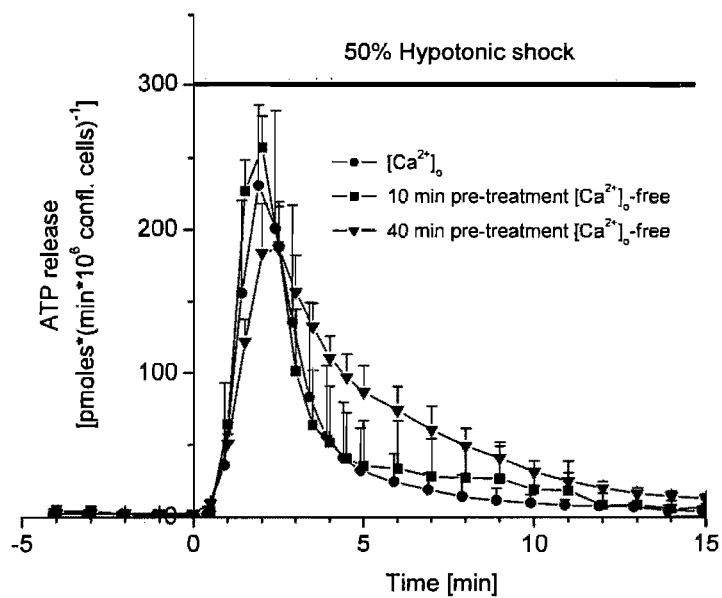
- A. Effect of FCCP and oligomycin (OM), on the hypotonic shock-induced [Ca²⁺]_i response. Cells were pre-treated for 30 min with 10 μM FCCP + 1 μM TG, or 10 μM OM + 1 μM TG, in Ca²⁺-free IS for 30 min prior to the experiment. Experiments were performed in the absence of extracellular Ca²⁺. (●) refers to

TG-treated cells, (■) refers to FCCP + TG-treated cells, and (▼) refers to OM + TG-treated cells. For each condition, a representative experiment out of $n = 3$ is shown.

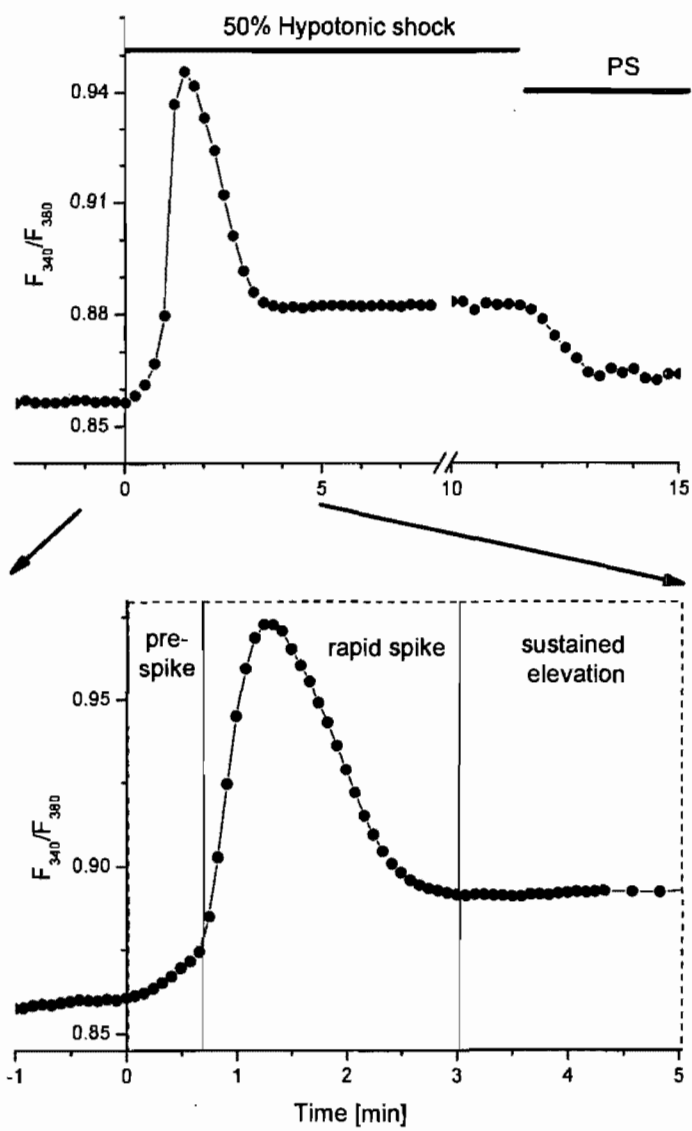
- B.** Effect of jasplakinolide (JASP), an inducer of actin polymerization, and latrunculin A (LA), a microfilament-disrupting agent, on the hypotonic shock-induced $[Ca^{2+}]_i$ response (*top panel*) and ATP release (*bottom panel*). The cells were pre-treated for 2 h with 1 μ M JASP, or 1 h with 1 μ M LA, and with 1 μ M TG for 30 min in Ca^{2+} -free IS prior to the experiment. Experiments were performed in the absence of extracellular Ca^{2+} . (●) refers to TG-treated cells, (■) refers to LA + TG-treated cells, and (▼) refers to JASP + TG-treated cells. For each condition, a representative experiment out of $n = 3$ is shown.

Figure 1

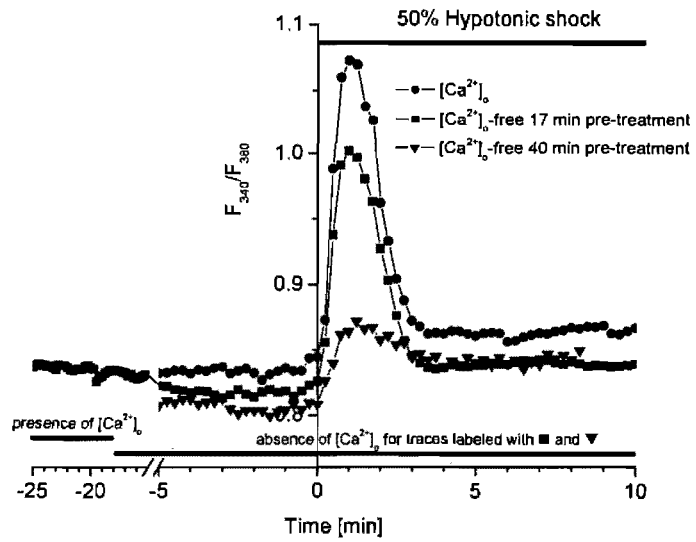
A.



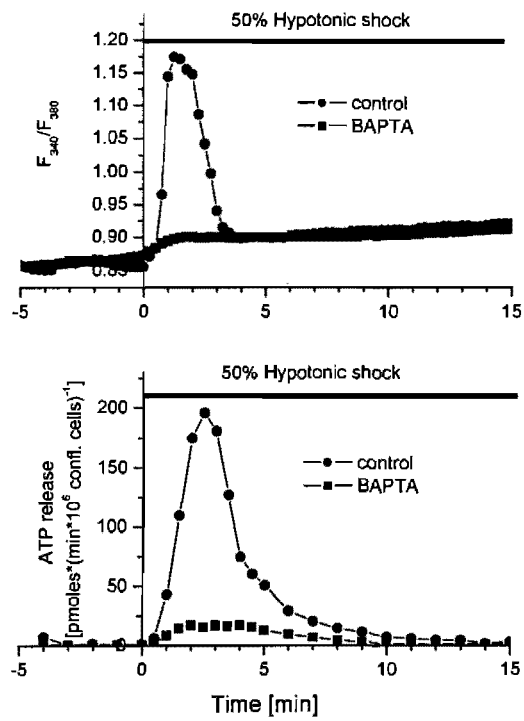
B.



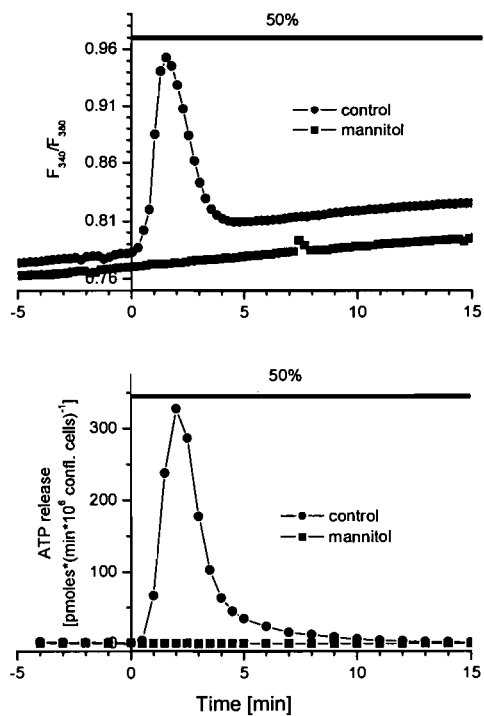
C.



D.



E.



F.

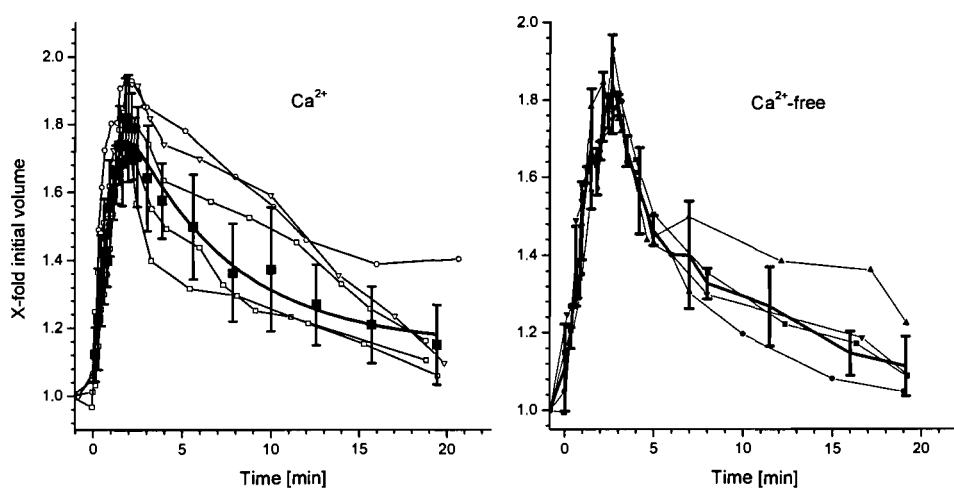
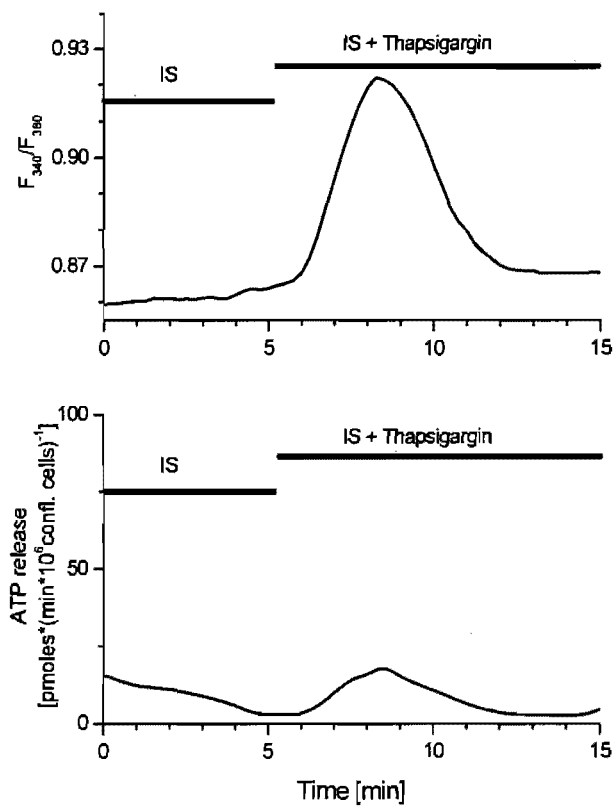


Figure 2

A.



B.

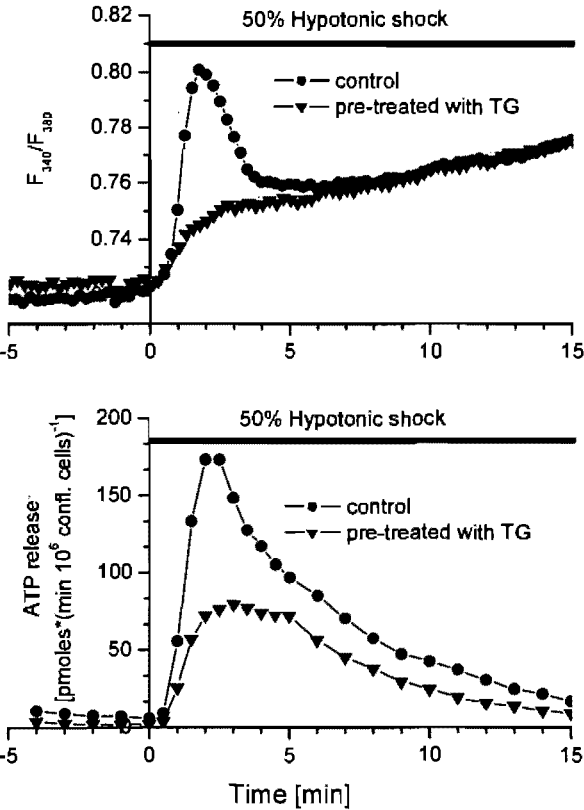


Figure 3

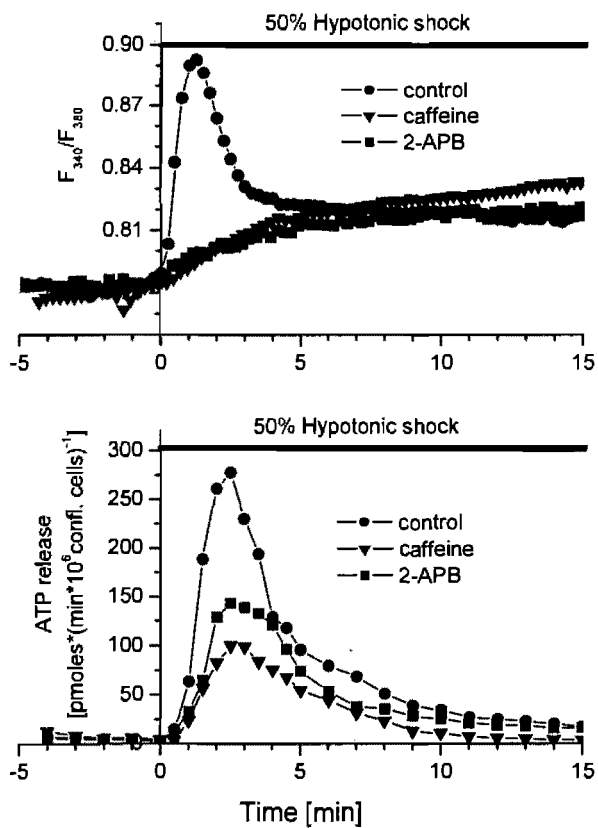


Figure 4

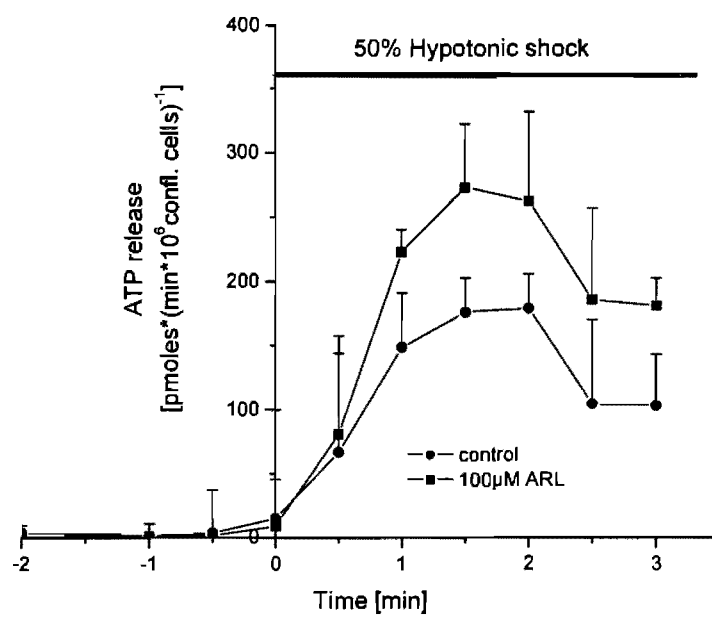
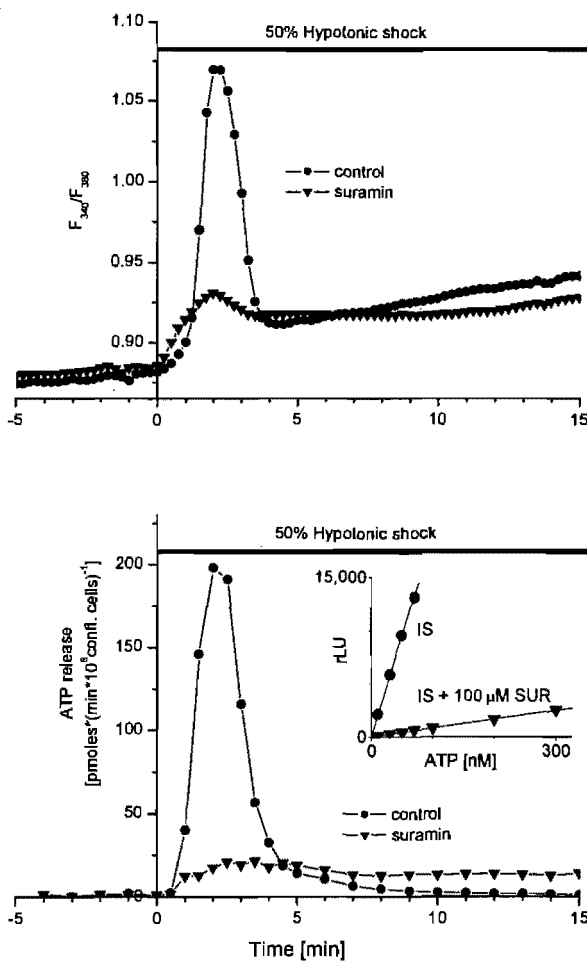
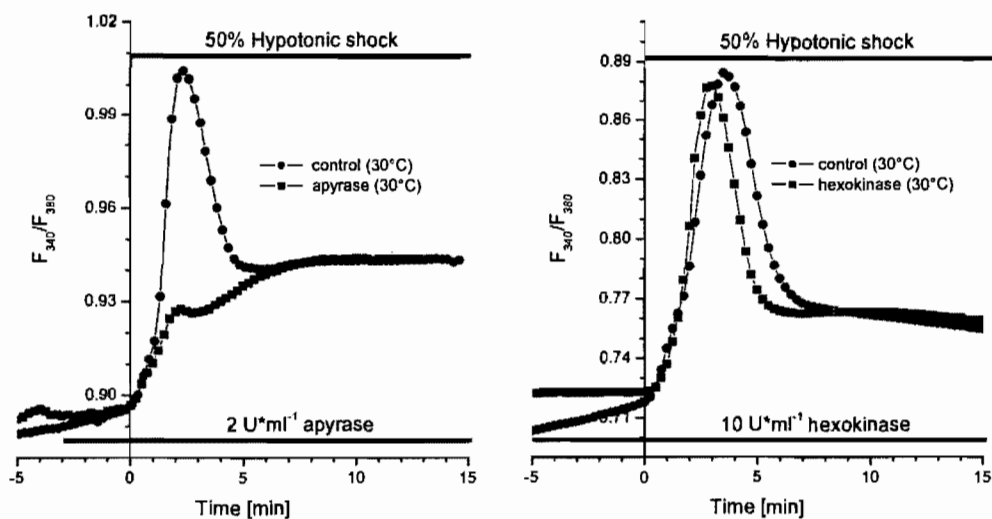


Figure 5

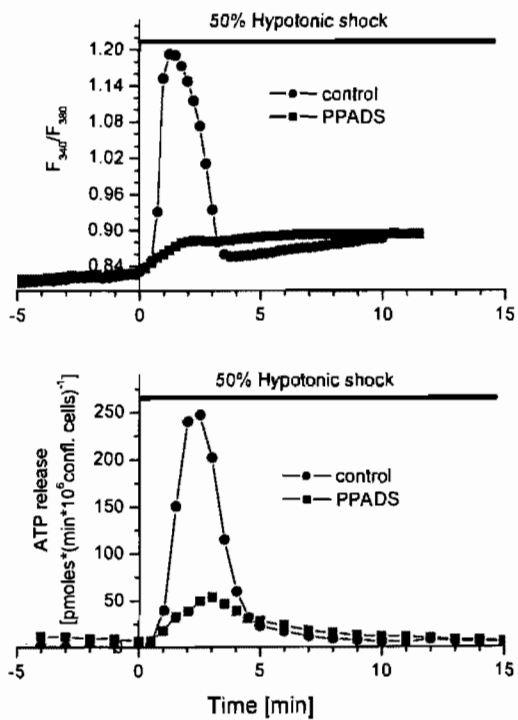
A.



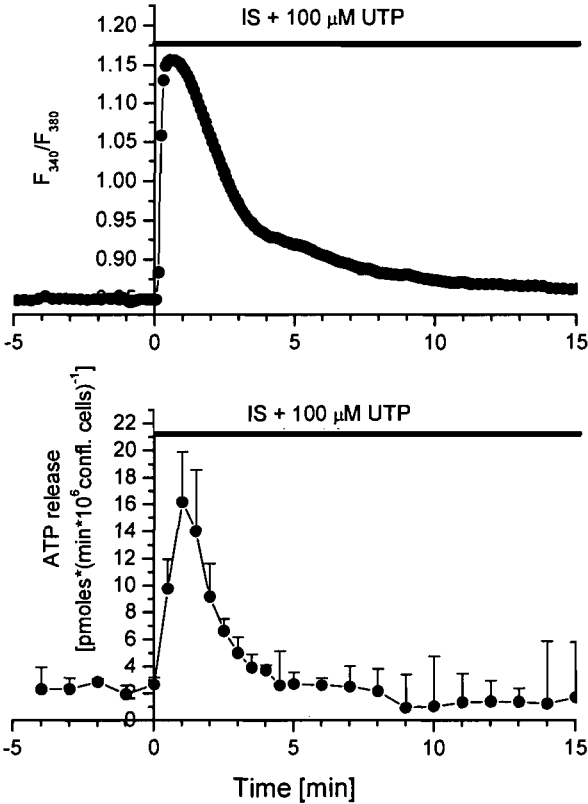
B.



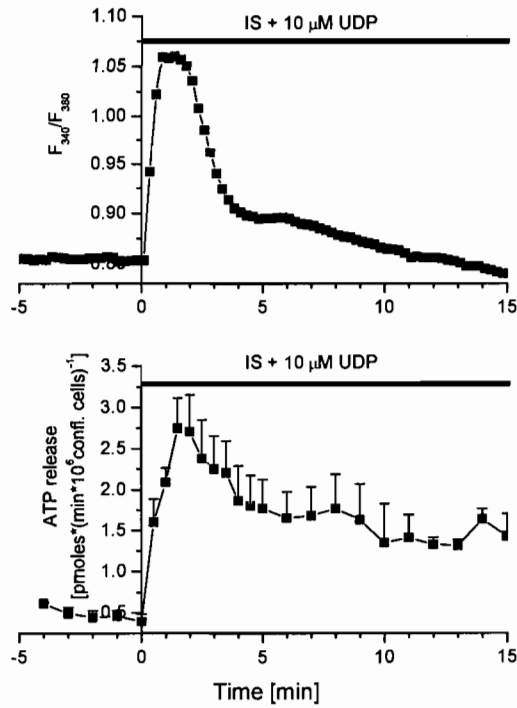
C.



D.



E.



F.

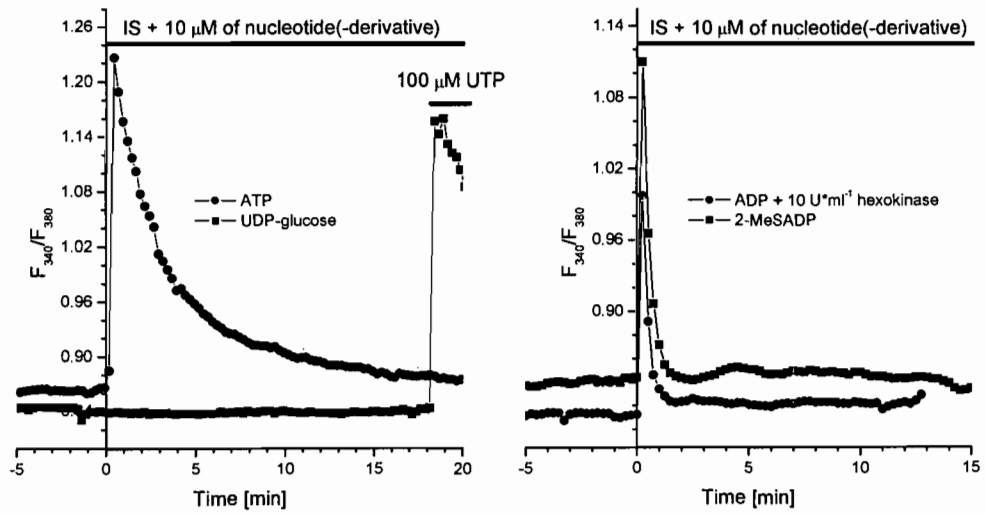
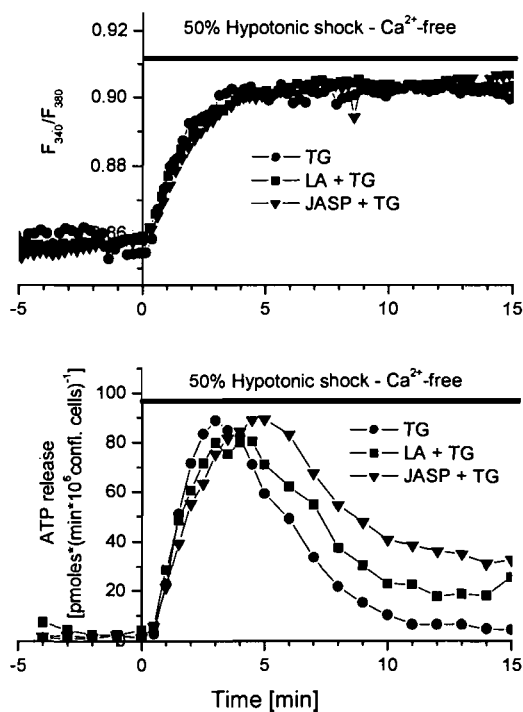
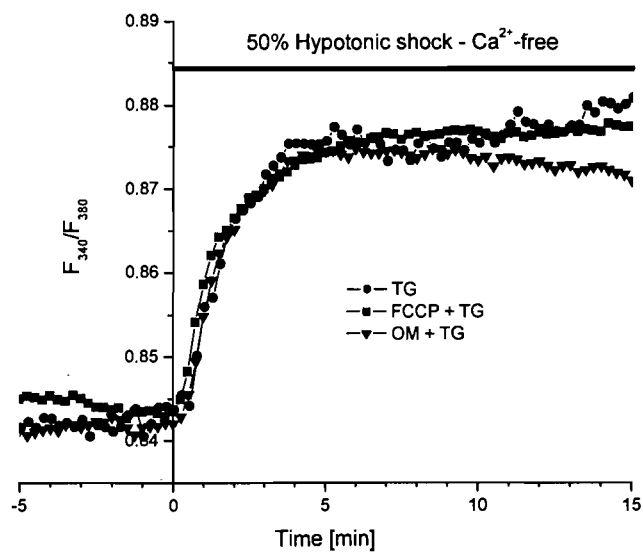


Figure 6

A.



B.



3.2.3 Further unpublished results

The origin of the thapsigargin (TG)-insensitive Ca^{2+} -elevation was further analyzed in the context of some publications reporting that various cell types responded to osmotic challenge with changes in intracellular pH (pH_i) and that these changes were associated with alterations in intracellular Ca^{2+} [191, 192].

When A549 cells were exposed to a 50% hypotonic solution, they responded with a short rise and a subsequent slow decrease in pH_i to about pH 6.9. As soon as the cells were reperfused with isotonic solution (IS), the pH_i returned to its initial value of about pH 7.1 (see Fig. 3.3, page 134). The cells were next exposed to 1 μM ionomycin and to isotonic solutions containing 40 mM sodium acetate (NaOAc) or 20 mM NH_4Cl (in exchange to NaCl), and intracellular Ca^{2+} as well as pH_i alterations were measured by ratiometric imaging (see section 2.3).

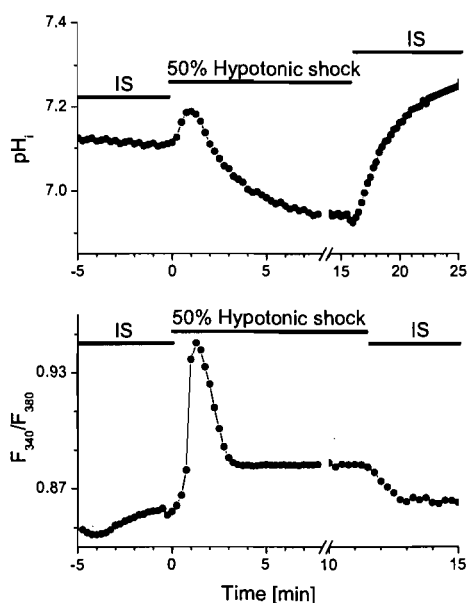


Figure 3.3: Time-course of intracellular pH and Ca^{2+} upon application of a 50% hypotonic shock; representatives of $n = 3$ independent experiments each

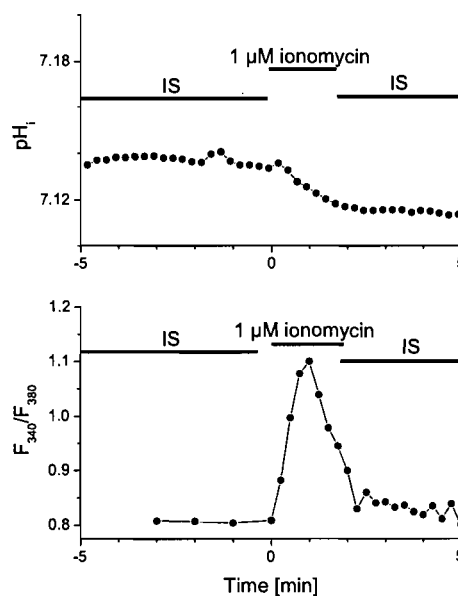


Figure 3.4: Alteration of intracellular pH and Ca^{2+} upon application of 1 μM ; representatives of $n = 2$ independent experiments each

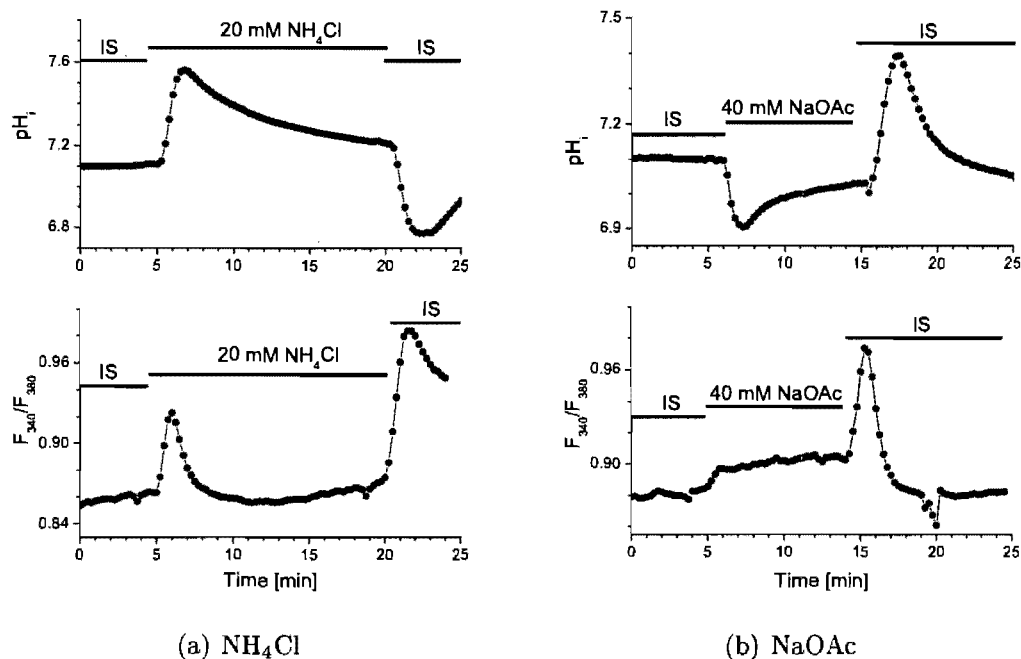


Figure 3.5: Alteration of intracellular pH_i and Ca^{2+} upon intracellular alkalization and acidification with 20 mM NH_4Cl ($n = 3$) and 40 mM NaOAc ($n = 3$), respectively

Although the intracellular Ca^{2+} level increased very strongly upon treatment with ionomycin, a Ca^{2+} -ionophore (see page 272), the corresponding pH_i alteration was very small and rather negligible (see Fig. 3.4, page 134). In contrast, intracellular alkalization as well as acidification with NH_4Cl and NaOAc also evoked intracellular Ca^{2+} alterations (see Fig. 3.5, page 135). It has to be considered that the observed alterations in the intracellular Ca^{2+} level associated with the pH_i changes might be an artifact of a pH-dependence of the Ca^{2+} -affinity to Fura-2, even though the fluorochrome has been considered relatively insensitive to pH changes [164]. However, an acidification would protonate Fura-2, decrease thereby its Ca^{2+} -binding ability and diminish the magnitude of Ca^{2+} -bound fluorescence as well as the associated fluorescence ratio – an effect opposite to that which was actually observed. To be able to interpret the observed responses of A549 cells to NH_4Cl and

to NaOAc, the physiological role of these molecules will be briefly reviewed in the following two paragraphs:

The *Ammonium Cation*, NH_4^+ , is produced in the body during amino acid catabolism [193]. It is a weak acid ($\text{NH}_4^+ + \text{H}_2\text{O} \rightleftharpoons \text{NH}_3 + \text{H}_3\text{O}^+$; $\text{pK}_a = 9.25$ at 25°C , $\text{pK}_a = 9.15$ at 37°C [194]) and appears, therefore, mainly in the protonated form as ammonium cation NH_4^+ at the physiologic pH range of $7.1 - 7.4$ ¹⁵. The major metabolic pathway responsible for the removal of NH_4^+ is the synthesis of nontoxic urea in the liver via the ornithine cycle [193].

During the exposure of cells to ammonium salts, the lipophilic free base NH_3 can passively penetrate cell membranes. In the cell, NH_3 protonates again ($\text{NH}_3 + \text{H}_2\text{O} \rightleftharpoons \text{NH}_4^+ + \text{OH}^-$; $\text{pK}_b = 4.75$ at 25°C [194]) leading thereby to an intracellular alkalization. Different cell types show diverse responses following the uptake of $\text{NH}_3/\text{NH}_4^+$. In addition to the effect of NH_4^+ on metabolism and diverse cellular processes (for further information see [195–199]), NH_4^+ was shown to induce an intracellular Ca^{2+} rise in a variety of cell types either from internal Ca^{2+} stores or through Ca^{2+} influx. The increase in intracellular Ca^{2+} was mainly a result of the ammonia-induced intracellular alkalization [200–202]. However, also pH-independent pathways were reported, where $\text{NH}_3/\text{NH}_4^+$ seem to directly affect proteins involved in the Ca^{2+} signalling pathway [203, 204].

The *Acetate Anion*, AcO^- , is found in the blood plasma in a concentration of < 0.2 mM [205, 206]. After the intake of ethanol, the concentration can rise by as much as 20-fold [207]. Cells take up AcO^- from the blood plasma and use it either as a source of energy [208, 209] or they transform it to acetyl coenzymeA (acetyl-CoA), an activated form of AcO^- [210].

Free acetate is a weak base ($\text{AcO}^- + \text{H}_2\text{O} \rightleftharpoons \text{AcOH} + \text{OH}^-$; $\text{pK}_b = 9.25$ at 25°C [194]) and its conjugate acid readily permeates the cell membrane. Inside the cell, acetic acid deprotonates again and causes thereby an intracellular acidification. In addition to the intracellular acidification, AcO^- was shown to also induce in some cases an intracellular Ca^{2+} increase. Similarly to

¹⁵Only 1 – 2% exists in the deprotonated form NH_3 .

NH_4^+ , acetate-induced intracellular Ca^{2+} rise was shown to be triggered either through a pH-dependent or through an unknown pH-independent pathway [211–213].

Obviously, both ions are endogenous substances to whose exposure cells may react in various ways. Most important in regard to the present study is the observation that both ions evoke *in vitro* a pH_i alteration and a concomitant intracellular Ca^{2+} elevation, which, however, do not necessarily have to be interrelated.

The experiment, in which the intracellular Ca^{2+} in A549 cells was increased with the aid of ionomycin (see Fig. 3.4, page 134), reveals that an intracellular Ca^{2+} increase only insignificantly altered the pH_i . This result indicates that – in case of an existing correlation between the pH_i alteration and the intracellular Ca^{2+} signal – the pH_i should affect the intracellular Ca^{2+} level and not vice versa.

The exposure of A549 cells to NH_4^+ as well as the removal of extracellular AcO^- (see Fig. 3.5, page 135), led to an intracellular alkalization as well as to a transient increase in intracellular Ca^{2+} with a relatively fast return to the initial baseline after around 3 min. In contrast, the exposure to AcO^- as well as the removal of extracellular NH_4^+ led to an intracellular acidification and to an increase in intracellular Ca^{2+} , which declines slower than during alkalization (removal of NH_4^+) or stays on an elevated level (exposure to AcO^-). Interestingly, the A549 cells responded to the first stimulus, the exposure to NH_4^+ (alkalization) or to AcO^- (acidification), with a smaller Ca^{2+} signal than to the second stimulus, the removal of NH_4^+ (acidification) or AcO^- (alkalization). The differences in the size of the Ca^{2+} signals in response to the alkalization upon the exposure to NH_4^+ and the removal of AcO^- , respectively, may emanate from the fact that in one case the alkalization was induced on resting cells and in the other case on already stimulated cells; the same explanation may apply to the differences in the magnitude of the Ca^{2+} signals following intracellular acidification in response to the exposure to AcO^- and the removal of NH_4^+ .

The described observations indicate a potential pH-dependence of the Ca^{2+}

signal since it seems unlikely that NH_4^+ and AcO^- , two ions of completely different chemical properties, evoke Ca^{2+} signals whose patterns are of similar shape during intracellular alkalization (transient increase) and acidification (slow decrease or sustained elevation). Furthermore, the hypothesis that NH_4^+ and AcO^- were responsible for a pH-independent Ca^{2+} elevation would rather imply that only the exposure to these ions induces a Ca^{2+} increase and not their removal.

In conclusion, the discussed experiments show that a 50% hypotonic shock induces a pH_i alteration in A549 cells, which is not evoked by the intracellular Ca^{2+} signal. Although there is evidence that the pH_i alterations may, in turn, induce an intracellular Ca^{2+} signal in A549 cells, further experiments are essential to clarify the possibility of a pH_i -induced thapsigargin-insensitive Ca^{2+} -increase. The following experiments could give additional information about the interrelation of pH_i and the intracellular Ca^{2+} level:

1. pH_i alterations of different magnitude:

- The exposure of A549 cells to NH_4^+ and AcO^- concentrations (5 – 40 mM), which induce similar pH_i changes, could reveal a possible correlation between the magnitudes of the pH_i alterations and the concomitant Ca^{2+} signals.
- The application of different ammonium salts (e.g. $\text{NH}_4^+ \text{Cl}^-$, $\text{NH}_4^+ \text{AcO}^-$, $\text{NH}_4^+ \text{SO}_4^{2-}$, $(\text{NH}_4^+)_2 \text{CO}_3^{2-}$) would induce pH_i alterations of different magnitudes while keeping the NH_4^+ concentration constant. A resulting Ca^{2+} signal of equal magnitude in all cases (except for $\text{NH}_4^+ \text{AcO}^-$) would imply its ammonium-dependence and pH-independence.

2. NH_4^+ - and AcO^- -independent pH_i alterations:

- An intracellular alkalization can be induced with alkylated ammonium derivatives (e.g. tetramethylammonium). If the ammonium-induced Ca^{2+} signal was pH-independent, tetraalkylammonium-

induced alkalization should not trigger any intracellular Ca^{2+} signal.

- The modification of the extracellular pH results, usually, in a parallel pH_i alteration. A correspondent intracellular Ca^{2+} signal would prove the potentiality of pH-dependent Ca^{2+} signalling in A549 cells.
- The inhibition of the Na^+/H^+ exchanger in the A549 plasma membrane with 5-(*N,N*-dimethyl)-amiloride (DMA) leads to an intracellular acidification [214]. Also in this case, a correspondent intracellular Ca^{2+} signal would prove the potentiality of pH-dependent Ca^{2+} signalling in A549 cells.

To examine the thapsigargin-sensitivity of the potentially pH-dependent Ca^{2+} signal, the above mentioned experiments should be carried out on thapsigargin-pretreated cells. To ensure, furthermore, that the pH_i alterations do not induce any Ca^{2+} influx from the extracellular fluid, Ca^{2+} -free solutions should be used during the experiments.

Proof of a pH-dependence of the thapsigargin-sensitive Ca^{2+} -signal would rise the two following questions:

1. What is the origin of hypotonic shock-induced acidification?
2. How does the intracellular pH affect the intracellular Ca^{2+} level?

Several potential sources of intracellular acidification are known:

- Mitochondria: uncoupled mitochondria were reported to cause intracellular acidification as well as intracellular Ca^{2+} increase [215].
- Na^+/H^+ -exchanger (NHE): NHE is known to be a major carrier involved in the regulation of both cytosolic pH_i and cell volume [216].
- H^+ -carriers other than NHE: the $\text{Cl}^-/\text{HCO}_3^-$ -exchanger or $\text{Na}^+-\text{HCO}_3^-$ cotransporter, as well as other ion channels were also involved in intracellular acidification [217–219].

Various mechanisms of intracellular Ca^{2+} elevation due to pH_i changes have been described as follows:

- Ca^{2+} was released from intracellular storages, such as acidic compartments [220].
- Ca^{2+} was released from TG-sensitive compartments, i.e. the ER [221, 222].
- Ca^{2+} -influx was observed through pH_i -sensitive Ca^{2+} -permeable, non-selective cation channels [223].
- A decrease in pH reduced the Ca^{2+} -binding affinity of EF-hand proteins [224] and may thereby increase the cytosolic Ca^{2+} homeostasis.

According to section 3.2.2, mitochondria do not play a role in the TG-insensitive Ca^{2+} elevation. Moreover, acidic compartments and Ca^{2+} -influx from the extracellular space were also excluded from participating in the Ca^{2+} signal. Hence, further experiments are necessary to investigate the other potential origins of pH_i decrease and the associated intracellular TG-insensitive Ca^{2+} increase.

Part II

Development of a side-viewing technique

Chapter 4

Airway surface liquid – Physiological background

4.1 Characteristics of the ASL

The conducting airways (trachea, bronchi, bronchioli) are lined by a thin layer of airway surface liquid (ASL), which plays an important role in the self-cleaning mechanism of the lung – the airway mucus clearance. The efficiency of airway mucus clearance depends in large part on the height and the properties of both of the ASL components, the mucus layer and the underlying periciliary liquid layer (PCL). The mucus layer is an adhesive, viscoelastic gel generated by secreted high-molecular weight mucins (MUC5AC, MUC5B). The viscoelastic properties, and hence the transportability, of this layer are determined by the entanglement of the polymeric mucins with "sticker" proteins and, importantly, by the hydration of this layer. This layer entraps airborne particles and bacteria, inhibits bacterial growth and biofilm¹⁶ formation and protects the airways from fluid loss [226]. At its inner surface, the mucus layer interfaces with the PCL layer, which has been reported to vary from 7 to 70 μm in height and was recently suggested to be comprised of grafted mucins and other molecules such as cell surface glycolipids [227]. This design likely accounts for the important interdependence of the hydra-

¹⁶A biofilm is a complex aggregation of microorganisms highly resistant to antimicrobial agents [225].

tion status of the mucus layer and PLC. In the form of grafted brushes, it provides, furthermore, very low friction, enabling efficient ciliary beating [227, 228].

For a long time, ciliary activity and mucin secretion were thought to be the principal determinants of airways mucus clearance. While both are very important, it is now believed that airway surface hydration is the most important variable in controlling the efficiency of mucus clearance [229]. The dehydration of the ASL and the associated reduction in ASL height causes the following impairments:

- a highly viscoelastic, adhesive mucus layer; and
- collapse of the PCL, and loss of its lubricant properties that separate the mucus layer from the cell surface.

The combined loss of the PCL lubrication and the increased adhesiveness of the mucus layer results in the adhesion of mucus to the airway surfaces [229].

4.2 Regulation of the ASL

The significance of accurate ASL regulation becomes apparent in the genetic disease cystic fibrosis (CF) which is characterized by ASL depletion followed by mucus stasis and chronic infection [229]. The regulation of ASL height is extremely complex, and it is still not completely understood. In normal airway epithelia, ASL height is under the control of a finely tuned balance of Na^+ absorption through the apical membrane epithelial Na^+ channel (ENaC), and Cl^- secretion, mediated by two apical membrane Cl^- channels, the cystic fibrosis transmembrane conductance regulator (CFTR) Cl^- channel and the Ca^{2+} -activated Cl^- channel (CaCC). The tuning of these channels occurs through release and metabolism of ATP via a dual purinergic signalling system (see section 1.1.2), which is illustrated in Fig. 4.1 on page 144 [227].

Under static conditions, airway epithelial cells continuously release a low basal level of ATP ($\sim 300 \text{ fM} \cdot \text{cm}^{-2} \cdot \text{min}^{-1}$ [230]) to the airway lumen that is mostly converted into adenosine by surface ecto-nucleotidases. This basal concentration of adenosine ($\sim 100 \text{ nM}$ [230]) on airway surfaces is sufficient to

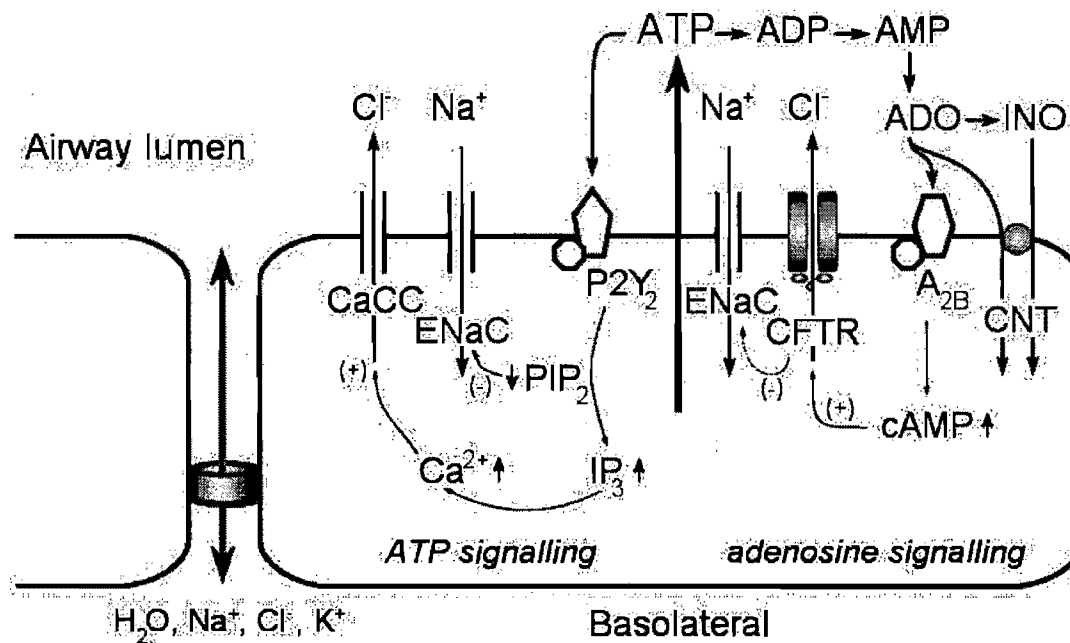


Figure 4.1: Dual purinergic signalling pathway for ion transport across the apical membrane of airway epithelial cells – both pathways control ASL height in normal Lung Epithelia.

CFTR, cystic fibrosis transmembrane conductance regulator; ENaC, epithelial sodium channel; CaCC, Ca²⁺-activated Cl⁻-channel; CNT, concentrative nucleotide transporter; ATP, adenosine 5'-triphosphate; ADP, adenosine 5'-diphosphate; AMP, adenosine 5'-monophosphate; cAMP, 3'-5'-cyclic adenosine monophosphate; ADO, adenosine; INO, inosine; PIP₂, phosphatidylinositol bisphosphate; IP₃, inositol-1,4,5-trisphosphate

activate the A_{2B} purinoceptor which generates an intracellular raise of cAMP. cAMP, in turn, activates CFTR, which regulates Cl^- secretion and ENaC activity to maintain the homeostatic ASL height on airway surfaces [229].

Under stress conditions, such as shear stress and compression, the rate of ATP release is greatly increased, raising ATP concentrations in the ASL to 30–50 nM [229]. This concentration of ATP activates additionally the $P2Y_2$ receptor-dependent signalling pathway inhibiting Na^+ absorption and stimulating CaCC-mediated Cl^- secretion [229].

In CF airway epithelia, ASL height regulation depends solely on the ATP-signalling system which, under static conditions, causes ASL to be absorbed to the degree that the cilia collapse onto the airway surface [229].

The ability of the airway epithelia to determine ASL height is still an area of active investigation and discussion. While for a long time it was thought that cilia were somehow involved in sensing ASL height, it is now suggested that the concentrations of soluble mediators in the ASL, such as ATP, adenosine, and channel-activating proteins are the crucial factors in this process [230].

To further study how ASL height is regulated, especially by extracellular ATP, a microscopic technique was developed in the course of this Ph.D. work that enables a direct observation of the fluorescently labelled ASL. This technique is described in chapter 6.

Chapter 5

Optical microscopy

5.1 Introduction

5.1.1 Development of the microscope

Historians credit the invention of the compound microscope to the Dutch lenscrafters, Zacharias and Hans Janssen, around the year 1590 [231]. The compound microscope uses two converging lens systems and light to produce an enlarged image of an object that is too minute to be viewed by the naked eye. In the early 17th century, Galileo Galilei, the father of modern astronomy and physics, heard of this invention, and developed, first, his own telescope and, later, a tripod microscope [231]. In 1664, Robert Hooke published "Micrographia" [232], a fascinating work on optical microscopy. Hooke's work describes and illustrates observations he made with a compound microscope on a wide variety of organisms including insects, plants and bird feathers. Anton van Leeuwenhoek (1632-1723), a Dutch tradesman, developed his own microscopes which consisted of one single magnifying glass. With his handcrafted simple microscopes, which reached a magnification up to 250x, he was the first one to observe and describe microorganisms, such as bacteria and yeast [231].

During the 18th century, the main focus of instrument makers was on the development of the microscope's design to facilitate focusing and to meet the needs of the user [231]. In the 19th century, optical improvements increased

magnification and resolving power. In 1830, Joseph Jackson Lister reduced the problem of spherical and chromatic aberration by developing the first apochromat. Carl Zeiss and Ernst Abbe were the first to design lenses of – for their time – the technically highest possible quality based on optical theory and the laws of physics [231].

The 20th century was marked by the advancement of the traditional optical compound microscope and by the development of new microscopic techniques, such as the ultramicroscope (Richard Adolf Zsigmondy, Nobel Prize 1925), the phase-contrast microscope (Frits Zernike, Nobel Prize 1932), the electron microscope (Ernst Ruska, Nobel Prize 1938), and the scanning tunneling microscope (Gerd Binnig and Heinrich Rohrer, Nobel Prize 1981) [233].

The development of optical microscopes and their applications has proceeded rapidly over the last several decades. This is due both to the improvement in the manufacture of optical lenses and to the improvement in the design of optical systems. The development of new fluorescent labels has also accelerated the expansion of fluorescent microscopy in research.

5.1.2 Components of a microscope

The performance of a good compound microscope depends on good mechanical parts (stability and rigidity of the microscope, the precise holding frame for objectives and eyepieces, flexibility for focusing and moving a specimen) and excellent lenses (magnification and resolution). The components of a Nikon Inverted Microscope ECLIPSE TE300, which was used in the course of this Ph.D. project, are depicted in Fig. B.1 on page 285 and Fig. B.2 on page 286.

During illumination with transmitted light, the rays first pass through the collector lens and some filters and then through the condenser, microscope slide (if available), specimen, cover glass (if available), objective and ocular. Finally, it enters the observer's eyes. Additional filters, prisms and a tube lens (for *infinity corrected* optical systems) might also be necessary to complete the optical setup of a compound microscope [234].

There are at least nine methods to illuminate a specimen:

1. Transmitted light with brightfield;
2. Transmitted light with darkfield;
3. Transmitted light with polarization;
4. Incident light with brightfield;
5. Incident light with darkfield;
6. Transmitted light with phase contrast;
7. Transmitted light with interference contrast;
8. Incident light with fluorescent specimen (e.g. epifluorescence microscopy);
9. Incident light with polarization.

Essentially, there are two main principles of illumination in microscopy. One was devised by Edward Nelson, which is generally called *critical illumination*, and the other by August Köhler, which is named after its inventor, *Köhler illumination*. At the present time, critical illumination is preferred for use in simple microscopes, whereas the modern research microscopes have a built-in illuminator based on the *Köhler principle of illumination*.

The physical principles of optical microscopy include interference, diffraction and coherence of light, which operate constructively or destructively in the microscope. A geometrical approach to microscopical imaging is based on refraction and reflection of rays, represented in the ability of lenses and mirrors to focus and change the convergence and divergence of light beams. The diffraction theory of image formation, first formulated by Ernst Abbe in 1873, explains some fundamental problems related to resolution and contrast [234]. All these principles and further fundamentals of microscopy are described in the following sections in order to give every reader of this thesis the necessary background for the understanding of chapter 6.

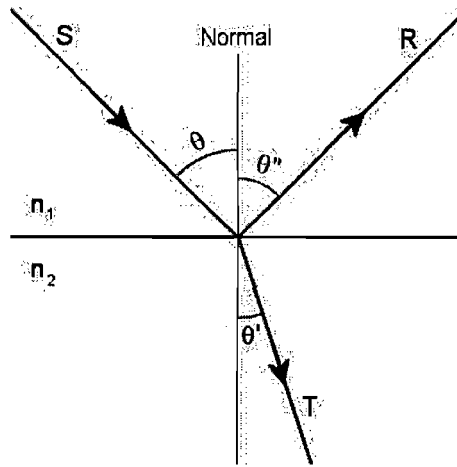


Figure 5.1: Reflection and refraction at an interface between two media:

S = incident ray, R = reflected ray, T = transmitted/refracted ray
 θ = angle of incidence, θ' = angle of refraction, θ'' = angle of reflection

5.2 Some principles of optics

5.2.1 Refraction and reflection of light

Geometric optics, employing the theory of refraction and reflection of light rays, is along with *wave optics* one of the two approaches that describe the ability of a microscope to both magnify and resolve.

Refraction occurs when light passes from one medium of one optical density to another one with a different optical density (see Fig. 5.1, page 149). The measure of optical density is the refractive index n ¹⁷. The exact refractive index for a medium varies with the wavelength of light. This physical phenomenon causes dispersion, which is the separation of white light into its spectral components (see Fig. 5.2, page 150). Dispersion in lenses produces the undesired effect of chromatic aberration, which is described in detail on page 161.

While only part of the travelling light is transmitted (refracted) through the second medium, the remainder reflects at the interface. The proportion

¹⁷The refractive index n equals the speed of light in a vacuum divided by its speed in a material.

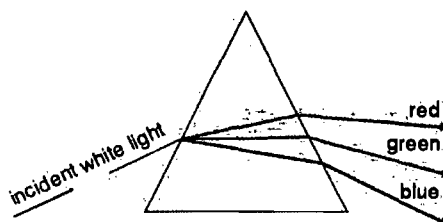


Figure 5.2: Dispersion of light by a glass prism

of refraction to reflection depends on the refractive indices of both media, the direction of light travelling, the light polarization and the angle of incidence [235].

The angle of reflection θ'' is equal to the angle of incidence θ with opposite sign [235]:

$$\theta = -\theta''$$

The degree of refraction depends on the refractive indices of the two media and is described by *Snell's law*:

$$\frac{\sin \theta}{\sin \theta'} = \frac{n_2}{n_1} = n_{21} \quad (5.1)$$

θ, θ' angle of incidence, angle of refraction

n_1, n_2 refractive index of first medium, refractive index of second medium

n_{21} relative index of refraction

If the first medium is optically less dense than the second one ($n_1 < n_2$, e.g. air \rightarrow glass), the angle of incidence θ is greater than the angle of refraction θ' . For $\theta = 90^\circ$, θ' reaches its maximum and is called *critical angle of refraction* θ'_{cr} [235]:

$$\theta'_{cr} = \arcsin \frac{n_1}{n_2} \quad (5.2)$$

If the second medium is optically less dense than the first one $n_1 > n_2$, e.g. glass \rightarrow air), the angle of refraction θ' is greater than the angle of

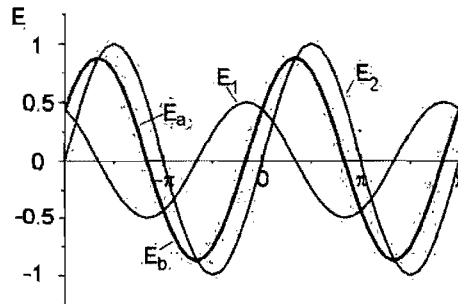


Figure 5.3: Two-wave interference

$$E_1 = a_1 \sin(x - \psi_1)$$

$$E_2 = a_2 \sin(x - \psi_2)$$

$$E = a_1 \sin(x - \psi_1) + a_2 \sin(x - \psi_2)$$

E_a : destructive for multiples of $x \in (\pi + \psi_1, \pi + \psi_2)$

E_b : constructive for multiples of $x \in (\pi + \psi_2, \pi + \psi_1)$

incidence θ . If $\theta > \theta_{cr}$, in which θ_{cr} is related to $\theta' = 90^\circ$, the phenomenon of *total internal reflection* occurs. In the case of $\theta < \theta_{cr}$, the incident ray (S) is only refracted (T); in the case of $\theta > \theta_{cr}$, it is exclusively reflected (R), and for $\theta = \theta_{cr}$, the refracted ray (T) propagates along the interface [235].

In accordance with the *reversibility theorem* of optical rays the critical angle of incidence θ_{cr} is equal to the critical angle of refraction θ'_{cr} .

5.2.2 Interference of light

In *wave optics*, which employs the theory of interference and diffraction, light is considered as a wave. The phenomenon of interference is the basis of most microscopic techniques, such as interference, phase contrast, and brightfield microscopy [234].

Two coherent¹⁸ monochromatic waves propagating in an isotropic medium in the same direction with amplitudes a_1 and a_2 , and phases ψ_1 and ψ_2 , respectively, (see Fig. 5.3, page 151) can be represented by:

$$E_1 = a_1 \sin(x + \psi_1), \quad E_2 = a_2 \sin(x + \psi_2) \quad (5.3)$$

¹⁸Only coherent waves, which have similar optical properties (wavelength, direction, phase – either the same phase or a fixed phase difference), are capable of interfering [235].

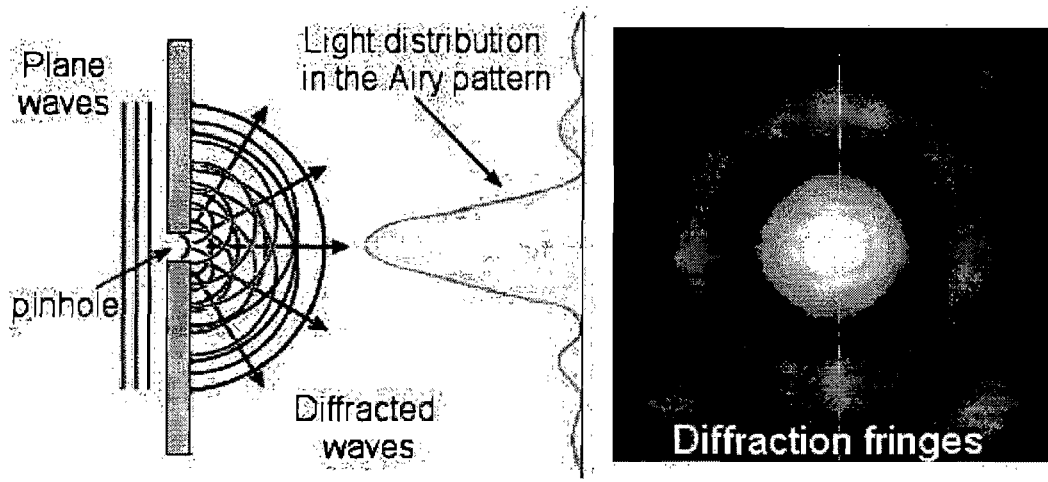


Figure 5.4: Diffraction of light through a pinhole

principle which states that each point of an advancing wave front can be considered as the centre of a source of a new wave. Fig.5.4 on page 153 shows how a narrow pinhole can be considered as a source of spherical waves whose superposition generates a new wavefront with a non-uniform intensity distribution (I) around the geometric shadow limit (*interference or diffraction fringes*) [235].

In microscopy, diffraction fringes form the smallest unit of an image. This unit is called Airy disc, and together with a whole series of concentric rings *Airy pattern*²⁰, which determines the limits of optical resolution.

In conclusion, it should be noted that diffraction interacts with interference in the case of coherent waves, as can be best observed in the form of diffraction fringes (see Fig. 5.4, page 153).

5.3 Magnification and resolution

The principle function of a microscope is to enhance resolution. Resolution can be measured as the smallest distance between two points, which the human eye is capable of seeing as distinct [236]. The microscope enlarges the

²⁰after the British Astronomer Royal Sir George Biddell Airy

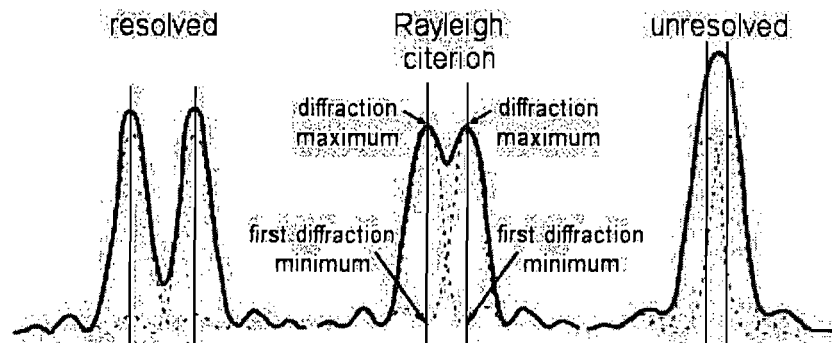


Figure 5.5: Rayleigh criterion for resolution

view of an object so that details of this object can be observed which otherwise cannot be resolved by the human eye [236]. If image formation was solely based on geometric optics then magnification would increase along with resolution without limit. However, other factors, based on diffraction and interference, limit useful magnification. Additional magnification that does not yield higher resolution and more detail is called *empty magnification*.

The limit for the microscope's resolution is set by the diffraction at the aperture of the objective. For a point source, the resulting image is an Airy pattern (see Fig. 5.4, page 153). The Rayleigh criterion for resolution of two point sources in a diffraction-limited system²¹ is given when the first diffraction minimum of the Airy pattern of one source point coincides with the maximum of another (see Fig. 5.5, page 154). Hence, the smaller the Airy discs are, the less likely they overlap and the better the resolution. The Airy disc projected by an objective is all the smaller the higher the numerical aperture (NA) of the objective is.

The NA is a crucial value that indicates the light acceptance angle, which in turn determines the light gathering power, the resolving power, and the

²¹If all parts of an imaging system are perfect, then the resolution of any imaging process will be limited by diffraction.

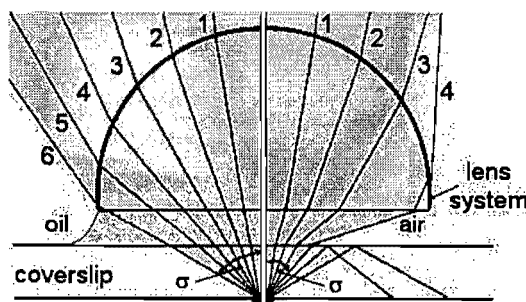


Figure 5.6: Numerical aperture of oil immersion and dry objective

depth of field (axial resolving power) of the objective. It is given by:

$$NA = n \cdot \sin \sigma \quad (5.6)$$

n refractive index of medium between the coverslip and the lens system

σ half of the entrance angle of the light cone (see Fig. 5.6, page 155)

Since the half aperture angle σ cannot exceed 90° , the maximum possible NA is equal to the refractive index n of the immersion medium. Hence, for dry systems (immersion medium: air, $n = 1$) the theoretically maximum NA is 1. In practice, the maximum NA of dry systems cannot exceed 0.95, and greater values may be obtained only with immersion systems [235, 234].

Light-gathering power is a measure of the illumination and image brightness provided. The illumination brightness as well as the image brightness are determined by the square of the condenser NA and objective NA, respectively. The image brightness (B_{im}) is additionally inversely proportional to the square of magnification M [235]:

$$B_{im} \propto \left(\frac{NA}{M} \right)^2 \quad (5.7)$$

Resolving power has been defined as the ability of a microscope to form separate images of two points lying close together [234]. The resolving power

of a microscope can be determined by the following equations:

$$r = \frac{1.22 \cdot \lambda}{NA_{\text{obj}} + NA_{\text{cond}}} \quad (\text{self-luminous objects; acc. to Rayleigh}) \quad (5.8)$$

$$r = \frac{\lambda}{NA_{\text{obj}} + NA_{\text{cond}}} \quad (\text{non-luminous objects; acc. to Abbe}) \quad (5.9)$$

r	minimal space between two adjacent particles while still allowing the particles to be perceived as separate [nm]
λ	wavelength of illumination [nm]
NA_{obj}	numerical aperture of the objective
NA_{cond}	numerical aperture of the condenser

NA is associated with both the condenser and the objective. For the sharpest images in brightfield and phase contrast microscopy (see page 171), the NA value of the condenser should be matched by the NA value of the specific objective; equation (5.9) on page 156 for non-luminous objects applies. For epifluorescence microscopy (see page 171) only the NA of the objective determines the degree of resolution; equation (5.8) on page 156 for self-luminous objects applies.

The axial resolving power of an objective, which is measured parallel to the optical axis, is referred to as *depth of field*²². High magnification and high NA objectives are also accompanied by a shallow depth of field. It can be calculated by the following equation [237, page 255]:

$$d = \frac{\lambda \sqrt{n^2 - NA^2}}{NA^2} \quad (5.10)$$

²²Not to be confused with *focal depth*, which is the placement of the image plane in relation to the lens.

d	depth of field [nm]
λ	wavelength of illumination [nm]
n	refractive index of medium between coverslip and objective's front lens
NA	numerical aperture of the objective

5.4 Lenses

5.4.1 Basic properties of lenses

Lenses can be classified by two main types: the *convex* lenses with a thickness greater at the optical centre of the lens than at the edges and the *concave* lenses with a thickness greater at the edges of the lens than at the optical centre (see Fig. 5.7, page 158). If the optical density of the lens is higher than its surrounding medium (e.g. air), a convex lens converges parallel light rays and is also called *positive* lens; a concave lens, in contrast, diverges parallel light rays and is called *negative* lens [235, 234].

The most important parameter of a lens is its focal length f [235, 234]. The object-side (front) focal length is denoted by f , and the image-side (back) focal length by f' (see Fig. 5.8, page 159). The focal lengths f and f' are always opposite in sign and:

$$\frac{f}{f'} = -\frac{n}{n'} \quad (5.11)$$

n refractive index of the medium in front of the lens

n' refractive index of the medium behind the lens

If these media are identical, i.e. $n = n'$, the front and back focal lengths are the same:

$$f = -f'$$

The value

$$K = \frac{n'}{f'} = -\frac{n}{f} \quad (5.12)$$

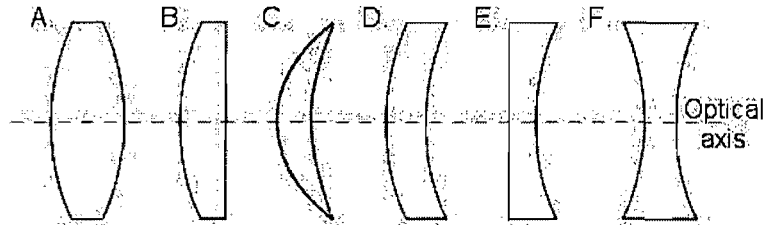


Figure 5.7: Common types of lenses:

Positive lenses: (A) biconvex; (B) plano-convex; (C) convergent meniscus

Negative lenses: (D) biconcave; (E) plano-concave; (F) divergent meniscus

is known as optical power (in air: $1/f$) and is expressed in m^{-1} or in diopters.

For thin lenses²³ the focal length of a lens surrounded by air can be roughly calculated according to the *lensmaker equation*:

$$\frac{1}{f} \approx (n - 1) \left[\frac{1}{r_{l1}} - \frac{1}{r_{l2}} \right] \quad (5.13)$$

f focal length of the lens
 n refractive index of the lens material
 r_{l1} and r_{l2} radii of curvature of the lens surfaces

Two planes or points are said to be conjugate if one is the image of the other. Their related distances can be calculated by the *Cartesian lens equation* (applicable only for thin lenses):

$$\frac{1}{S_1} + \frac{1}{S_2} = \frac{1}{f} \quad (5.14)$$

²³Lenses whose axial thickness t can be dismissed: $t \ll r_{l1}, r_{l2}$.

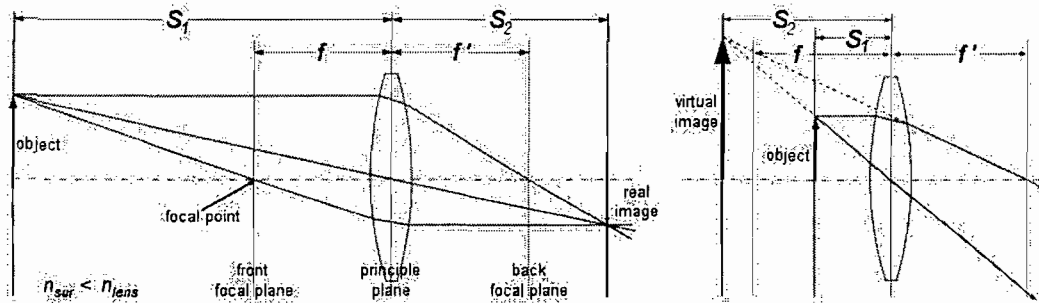


Figure 5.8: Image formed by a converging lens

Real images are inverted, virtual images are upright. The following relations hold:

$$\begin{array}{ll}
 S_1 > 2 \cdot f \Rightarrow |M| < 1, \text{ real} & 2 \cdot f > S_1 > f \Rightarrow |M| > 1, \text{ real} \\
 S_1 = 2 \cdot f \Rightarrow |M| = 1, \text{ real} & f > S_1 > 0 \Rightarrow |M| > 1, \text{ virtual}
 \end{array}$$

- S_1 distance from an object to the principle plane of the lens
- S_2 distance from the principle plane of the lens to the image
- f focal length

The magnification factor of a lens specifies the power of increasing or reducing an object's apparent size on its image. It is defined as:

$$M = -\frac{S_2}{S_1} \tag{5.15}$$

- M magnification factor
- S_1 distance from an object to the principle plane of the lens
- S_2 distance from the principle plane of the lens to the image

The image is larger than the object if $|M| > 1$, and smaller if $|M| < 1$. M is negative for real images and positive for virtual images (see Fig. 5.8, page 159).

Lenses may be combined to make more complex systems, such as in objectives. If thin lenses with focal lengths f_1 and f_2 , respectively, are separated

by a distance d , the combined focal length f can be calculated according to:

$$\frac{1}{f} = -\frac{f_2(d - f_1)}{d - (f_1 + f_2)} \quad (5.16)$$

The simplest case is when lenses are placed in contact:

$$\frac{1}{f} = \frac{1}{f_1} + \frac{1}{f_2}, \text{ for } d \rightarrow 0$$

The combined magnification factor M_c for multi-lens systems is given by:

$$M_c = M_{c1}M_{c2} \cdots M_{cm} = \prod_{k=1}^m M_{ck} \quad (5.17)$$

Equations for multi-lens systems can be extended limitlessly because all combined lenses can be treated as a single system to which an additional lens is added.

A compound microscope has two systems of lenses for magnification:

1. The *objective* (also called *object lens* or *object glass*) (see section 5.4.3) is the lens closest to the observed specimen. Usually, a microscope accommodates four to six parfocal objectives²⁴, which typically consist of 10x, 20x, 40x and 60x magnification factors.
2. The *eyepiece* (also called *ocular*) (see section 5.4.4) is the lens closest to the eye. It additionally magnifies the primary image and projects it onto the retina of the eye.

Three other systems of lenses are necessary for Köhler illumination:

1. The *collector lens* projects the image of the lamp filament onto the condenser aperture.

²⁴Objectives with identical parfocal distances can be interchanged while remaining in focus.

2. The *field lens* focuses the image of the lamp filament at the plane of the substage condenser aperture diaphragm.
3. The *condenser lens* system (see section 5.4.5) gathers and focuses the light onto the specimen. It provides an illumination of uniform intensity over the entire viewfield.

5.4.2 Optical defects

Lenses are subject to some optical defects (also called *aberrations*) which cause non-ideal images to be formed. This topic is large and complex, therefore only the two most important aberrations will be discussed in the following paragraphs.

Spherical aberration

Spherical aberration is an optical defect caused by spherical lens shape. Fig. 5.9 on page 162 illustrates that the focal length of the rays entering the lens is dependent on the distance of the ray from the optical axis, e.g. the marginal rays are focused closer to the lens than the central ones (negative spherical aberration). A spherically aberrated lens has, therefore, no well-defined focus [238].

The *lateral* (or *transverse*) *spherical aberration* is defined by the radius ρ of the *circle of confusion* in the paraxial image planes. As a result of the circle of confusion, the image of a point formed by a spherically aberrated lens is a dot surrounded by a halo of light [234].

In general, positive lenses exhibit negative spherical aberration, whereas negative lenses exhibit positive spherical aberration. Thus, spherical aberration of optical systems is corrected by combining positive and negative lenses [234, 238].

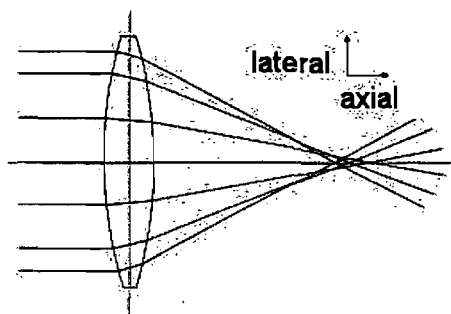


Figure 5.9: Spherical aberration

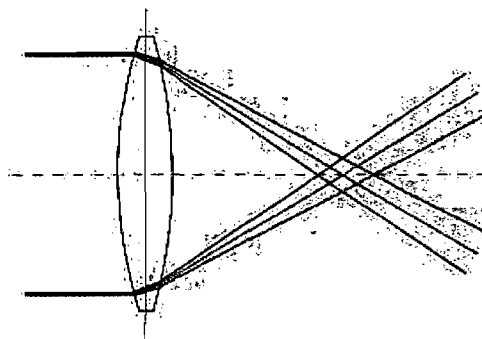


Figure 5.10: Chromatic aberration

Chromatic aberration

Spherical aberration has been discussed on the assumption of the presence of monochromatic light. All aberrations are, however, wavelength dependent, which is known as chromatic aberration (see Fig. 5.10, page 162).

Chromatic aberration is caused by the dispersion of light (see page 150) through the lens, whose refractive index n varies with the wavelength of light. Equation 5.13 on page 158 demonstrates that f is dependent on n , which is the reason that different wavelengths of light will have different focal lengths. The result is a halo of colours around the image that is seen through the lens [234, 238].

Chromatic aberration can be reduced using an *achromat*, which is a lens system of two combined lenses with different dispersion characteristics. They usually correct chromatically for two wavelengths (red and blue), and spherically for green.

The next higher level of correction can be achieved with *fluorites*. Fluorites contain natural or synthetic fluorite and have lower dispersion than normal glass. These lens systems correct chromatically for two wavelengths (red and blue), and also spherically for two wavelengths (blue and green).

An *apochromat* uses a three-lens system to correct chromatic aberration for three wavelengths (red, green and blue). The lenses are made of special low-dispersion glass. An apochromatic objective can minimize chromatic aberration to the degree that coloured halos are not seen around a point. It

also spherically corrects for two wavelengths (blue and green) [234, 238].

The achromat and apochromat correct chromatic aberration in the axial direction (axial chromatic aberration).

Since off-axis rays are also dispersed, images of different sizes are formed depending on the wavelength of the ray. This optical defect is known as *lateral chromatic aberration* or *chromatic difference of magnification*. Newer objectives and oculars with *chromatic-aberration-free* optics are independently corrected for both longitudinal chromatic aberration and chromatic difference of magnification [234, 239].

Other kinds of aberration include astigmatism, barrel, coma, field curvature and pincushion distortion (for further details see [234, 235]).

5.4.3 Objectives

The most important component of an optical compound microscope is the objective. It is responsible for primary image formation and plays, therefore, a crucial role in the quality of the final image, i.e. magnification, resolution and correction for lens aberrations. Lenses in modern objectives are made of high-quality glass of specific optical properties and precise design [240].

Essential specifications are inscribed on the barrel of each objective and will be briefly discussed in the following.

Magnification

Magnifying power is, together with the resolving power (see section 5.3), the most important optical parameter in microscopy. The magnifying power from available objectives ranges from 0.5x (low power) to 250x (high power) [239].

Numerical aperture

The numerical aperture (NA) determines primarily the resolving power of the objective and is usually inscribed on the barrel next to the magnification (see section 5.3).

The NA of an objective depends, to a certain degree, on the amount of

Table III: Objective designations for common optical corrections [239]

Abbreviation	Type
Achro, Achromat	Achromatic aberration correction
Fluor, Fl, Fluar, Neofluar, Fluotar	Fluorite aberration correction
Apo	Apochromatic aberration correction
Plan, Pl, Achroplan, Plano	Flat Field optical correction
Plan Apo	Apochromatic and Flat Field correction
CF, CFI	Chrome-Free, Chrome-Free Infinity-Corrected

correction for optical aberration. Objectives with a high degree of optical correction have larger numerical apertures for the respective magnification than for uncorrected ones [239]. Some objectives are designed for special immersion media between front lens and cover glass (see *Working Distance* on page 166), to attain even higher working numerical apertures.

Optical corrections

The correction for optical aberrations is crucial for good performance of an objective. Table III on page 164 lists the objective designations of the most common optical corrections.

Mechanical tube length

The mechanical tube length is defined as the distance from the nosepiece opening, where the objective is mounted, to the top edge of the observation tubes, where the oculars are inserted.

Until the 1980s, objectives were designed for finite tube lengths ranging from 160-210 mm, depending on the manufacturer and the application. This system requires that a specimen is placed between f_{obj} and $2f_{obj}$. The objective

focuses the magnified image of the specimen (primary image) at the level of the diaphragm of the eyepiece (see section 5.5). Objectives designed for a fixed tube length bear the inscription of the length of mechanical tube: e.g. 160 [239]. The drawback of these objectives is the alteration of the optical tube length (optical path between objective and eyepiece) whenever an accessory, such as a prism or a fluorescence illuminator, is placed in the lightpath between objective and eyepiece. To compensate for this alteration, the specimen has to be moved, which can be regarded as defocusing. This procedure introduces spherical aberration into a microscope system corrected for a standard mechanical tube length [234].

Nowadays, microscopes are designed for use with infinity corrected objectives (inscription: ∞). Their principle is described on page 170. Infinity-corrected systems are easier to design than finite systems. Moreover, they allow insertion of accessories in the parallel light path between objective back focal plane and the tube lens without introducing aberrations [234].

Cover glass thickness

Most objectives intended for use with a coverslip are corrected for a cover glass thickness $t = 0.17$ mm. A deviation of this conventional thickness causes poor image quality due to optical aberration. The larger the NA_{obj} , the smaller is the tolerable deviation Δt . For this reason, some high-power objectives have a correction collar adjustment of the internal lens elements to compensate for this variation [234]. In addition to the presence of a correction collar, these objectives are labelled as Corr, w/Corr, or CR [239].

Working distance

The working distance d_{obj} is the free distance between the front lens of the objective and the coverslip or the object plane for no-cover-glass objectives. In general, the distance d_{obj} decreases as the NA_{obj} increases. Objectives with short d_{obj} , such as immersion objectives, have a spring-loaded front lens which will retract if driven onto a surface. This feature protects the lens from being damaged [234].

In general, it is useful to have dry objectives with working distances as long as possible. Specially designed CFI objectives can achieve working distances that are several times longer than working distances of typical objectives with comparable NAs [241]. Common abbreviations are: LWD (long working distance), ELWD (extra-long working distance), SLWD (super-long working distance), and ULWD (ultra-long working distance) [239].

Immersion medium

Objectives requiring a liquid instead of air between the front lens and the coverslip are called *immersion systems*. Accordingly, systems having an air gap between the front lens and coverslip are called *dry systems*. The basic function of the immersion liquid is to increase the NA_{obj} (see Fig. 5.6, page 155). Common immersion liquids are special immersion oil ($n = 1.51$, abbrev. oil or oel), water ($n = 1.33$, abbrev. W), and glycerol ($n = 1.47$, abbrev. Gly) [234].

Specialized objectives

Some specialized microscopic techniques require specific objectives that house additional devices. For instance, objectives for phase contrast (see page 171) are fitted with a phase plate close to the back focal plane of the objective. They are designated with a Ph [239].

Epifluorescence applications (see page 171) require high-NA objectives in order to capture the highest possible amount of light emitted by fluorescing specimen. Fluorescence objectives are made of quartz and special glass that have high transmission from the UV (down to 340 nm) to the IR, and are extremely low in auto-fluorescence [239].

Coatings

An uncoated air-glass interface reflects 4-5 % of light striking normal to its surface. Since there are many such air-glass interfaces within a microscope, the initial light intensity, the contrast and the overall quality of the microscopic image tend to be greatly reduced. To counteract this phenomenon,

optical elements are coated with *antireflecting films*, which interferentially decrease the reflections of light at air-glass interfaces [234]. A typical antireflective coating is magnesium fluoride [240].

5.4.4 Eyepiece

The eyepiece (or ocular) is a lens system that magnifies the primary image and projects it either as a real image on a camera system or a virtual image on the human eye, depending on the location of the internal fixed eyepiece field diaphragm [234].

The diameter of the fixed eyepiece diaphragm opening determines the field size observed by the microscopist. It is inscribed on the eyepiece as a field number (FN) and varies from 18-26 mm. Another designation present on the eyepiece barrel is the magnification, which ranges from $\sim 6x$ to 25x [241].

Eyepiece/objective combinations should be chosen appropriate to the correction and type of objective to ensure optimal magnification of specimen detail without adding unnecessary artifacts. The range of useful magnification for an eyepiece/objective combination is defined by the numerical aperture of the system (see section 5.3). Therefore, the most common eyepieces are in the range of 10x to 20x.

5.4.5 Condenser

The basic function of a condenser is to gather the light coming from the light source and to concentrate it into a cone of light that illuminates the specimen with uniform intensity over the entire viewfield. Conventional microscopes have a substage condenser that is fitted below the stage of the microscope; whereas inverted microscopes comprise system condensers above the stage (ELWD or LWD) and a turret with components for phase contrast, differential interference or darkfield microscopy [241].

Condensers are available according to different levels of correction. The simplest substage condenser is the Abbe condenser which can reach a NA_{cond} up to 1.25. However, it is not well-corrected chromatically nor spherically. The best level of correction is achieved in aplanatic-achromatic condensers.

They are well-corrected for spherical and chromatic aberration, and are the condensers of choice for colour observation and recording in white light [234]. The size of condenser aperture (NA_{cond}) and the proper focusing of the condenser are crucial for an optimal performance of the objective. The NA_{cond} should be equal or higher than NA_{obj} to receive the highest resolution possible (see section 5.3).

5.5 Light path in a compound microscope

Fig. 5.11 on page 169 depicts a ray diagram of light microscopy under the condition of Köhler illumination in which the illuminating and image-forming light paths are merged into one diagram. In both of the light paths (illuminating and image-forming), there are four separate conjugate planes, which are simultaneously in focus.

The conjugate planes in the illuminating light pathway, in which the lamp filament is in focus, are [242]:

1. The lamp filament $a_0b_0c_0$ from which light is radiating out.
2. The aperture diaphragm in the front focal plane of the condenser lens $a_1b_1c_1$.
3. The back focal plane of the objective lens $a_2b_2c_2$.
4. The eyepoint (or Ramsden disc) in the back focal plane of the eyepiece $a_3b_3c_3$ where the pupil of the microscopist's eye should be placed.

The conjugate planes in the image-forming light pathway, in which the specimen is in focus, are [242]:

1. The field diaphragm in the back focal plane of the collector lens $1_02_03_0$.
2. The object plane on the back focal plane of the condenser lens $1_12_13_1$.
3. The primary (or intermediate) image plane on the front focal plane of the eyepiece $1_22_23_2$. The magnification of the primary image is given

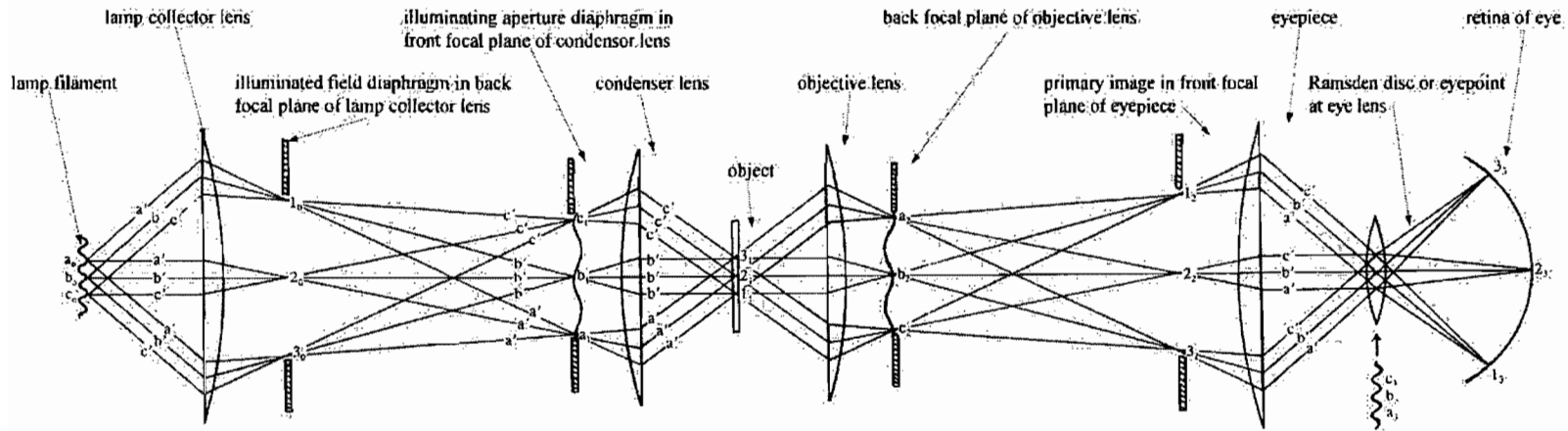


Figure 5.11: Symmetrical ray diagram of the light microscope; taken with permission from source [242]

The rays $a'a'a'$, $b'b'b'$ and $c'c'c'$ arising from the separate points $a_0b_0c_0$ in the lamp filament illuminate the whole area of the object as a series of parallel bundles of rays and are focused in the illuminating aperture series of conjugate planes $a_1b_1c_1$ (illuminating aperture diaphragm), $a_2b_2c_2$ (back focal plane of objective) and $a_3b_3c_3$ (Ramsden disc).

The parallel bundle of rays $a'b'c'$ arising from the whole area of the filament are focused in the illuminated field series of conjugate planes $1_02_03_0$ (illuminated field diaphragm), $1_12_13_1$ (object) and $1_22_23_2$ (primary or intermediate image). The pupil of the eye, focused at infinity, is situated at or near the Ramsden disc ($a_3b_3c_3$) and produces the secondary image $1_22_23_2$ on the retina of the eye.

by the ratio of the image distance and the specimen distance to the principle plane of the objective lens system (see equation 5.15).

4. The microscopist's retina of the eye.

In infinity-corrected systems, the specimen is placed at the front focal plane of the objective. Hence, the rays from the object plane $1_1 2_1 3_1$ proceed parallel through the objective and its back focal plane, theoretically forming an image at infinity. An additional *tube lens* in the mechanical tube forms the primary image by focusing the parallel rays at the front focal plane of the eyepiece $1_2 2_2 3_2$ [242]. The magnification of the primary image in an infinity-corrected system is given by the ratio of the focal length of the tube lens and the focal length of the objective.

5.6 Specialized methods

A wide spectrum of microscopic techniques has been developed to enhance contrast and to provide better observation, such as phase contrast, darkfield, modulation contrast, differential interference contrast, polarized light and fluorescence microscopy – to mention only a few. A qualitative description will be given in the following as to the techniques used in connection with this dissertation, i.e. brightfield, phase contrast and fluorescence microscopy.

5.6.1 Brightfield

Standard transmission of light through the specimen is called brightfield microscopy. Specimen which are coloured or thick enough to absorb a significant amount of light can be easily observed using this technique. However, unstained thin specimen do not offer much contrast and are very difficult to see. In this case, a fixed²⁵ specimen can be stained to provide contrast against the background [243].

²⁵Fixation refers to the technique of preserving a deceased specimen for microscopic study in an intact and stable state.

5.6.2 Phase contrast

Phase contrast microscopy is a contrast-enhancing optical technique which produces high-contrast images of colourless, transparent specimen without the exigence of staining. Invented by Frits Zernike [244] in the 1930s, it employs an optical mechanism to translate minute variations in phase into corresponding changes in amplitude that can be observed as differences in brightness.

Upon application of Köhler illumination (see section 5.5), light is focused by a collector lens on a specialized annulus (*phase plate*) positioned on the front focal plane of the condenser lens (plane $a_1b_1c_1$ in Fig. 5.11, page 169). Light rays passing successively through the annulus and the condenser illuminate the specimen as partially coherent light bundles. The rays pass through the specimen either undeviated or diffracted and retarded in phase due to a variation in refractive indices. On the back focal plane of the objective (plane $a_2b_2c_2$ in Fig. 5.11, page 169), which is a conjugate plane to the condenser's front focal plane, a second phase plate is positioned in a way whereby it is precisely aligned with the condenser phase plate. Undeviated and diffracted light emitted from the specimen and collected by the objective is segregated by this second phase plate and focused to a primary phase contrast image that can be observed through the eyepiece [234].

5.6.3 Fluorescence microscopy

Fluorescence microscopy is a specialized technique for the study of fluorescent substances. The principles of fluorescence are described in detail in section 2.1.2.

The first fluorescence microscope was developed by Otto Heimstädt and Heinrich Lehmann in 1911. It was originally employed to observe specimen with strong inherent (*primary*) fluorescence [234]. In 1933, Max Haitinger used for the first time secondary fluorescence to overcome the limitation of weak primary fluorescence of most cells and tissues [234]. Since then, myriad fluorescence labels have been developed for diverse applications (e.g. see section 2.3).

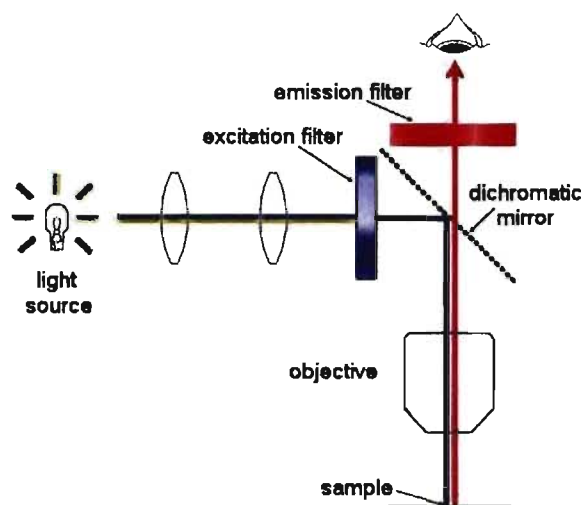


Figure 5.12: Schematic illustration of epifluorescence microscopy

Fig. 5.12 on page 172 schematically illustrates the principle of epifluorescence microscopy, which uses the objective to illuminate the sample (in contrast to trans-fluorescence, where the sample is illuminated from the opposite side). As a light source, typically a mercury or a Xenon lamp is coupled in to the back of the inverted microscope. The wavelength required for fluorescence excitation is selected by an excitation filter, which transmits only exciting radiation (e.g. blue light). A dichromatic mirror²⁶ (also called a dichroic mirror) totally reflects the exciting light, which impinges on the sample. Part of the exciting radiation is absorbed by the sample and re-emitted at longer wavelengths as fluorescence light (e.g. red light). The fluorescence light passes first through the dichromatic mirror and subsequently through an emission filter that absorbs the residual reflected excitation light. A coloured image can be observed against a dark background [234].

²⁶A dichromatic mirror selectively passes light comprising a range of wavelengths while reflecting other wavelengths.

5.7 Photomicrography

Photomicrography is photography through a compound microscope. The quality of a photomicrograph depends on the quality of the microscope. It is essential that the microscope uses Köhler illumination, that the field and condenser diaphragms are adjusted correctly and the condenser height is optimized. When properly adjusted, the microscope will yield images that have even illumination over the entire field of view and display the best compromise of contrast and resolution.

Today, digital cameras replace the traditional sensitized film with a CCD (charge-coupled device) photon detector, which consists of a thin silicon wafer divided into a geometrically regular array of small, light-sensitive regions – called pixels. These pixels capture and store image information in the form of localized electrical charges that vary with incident light intensity and exposure time. The electronic signal associated with each pixel of the detector is read out very rapidly as an intensity value for the corresponding image location. The following digitization of the values enables a computer to reconstruct the image and to display it on a monitor virtually instantaneously [245]. For photomicrography with a digital camera, it is important that the sensor size, relay magnification and pixel dimensions are selected appropriately [246, 247].

5.7.1 Image formation on the sensor

The objective of a compound microscope forms a circular primary image (see section 5.5) of the object at the aperture of the eyepiece. The diameter of this image, which is directed through the eyepiece to the eye, is specified by the FN (see page 167). In photomicrography, the primary image is projected onto the surface of a camera sensor by using relay optics or simply a coupler. If the diagonal size of the sensor matches the FN of the eyepiece, the size of the directly recorded image (1x magnification) will correspond roughly to the image size seen through the eyepiece (see Fig. 5.13, page 174). If the diagonal size of the sensor is smaller than the FN of the eyepiece, the

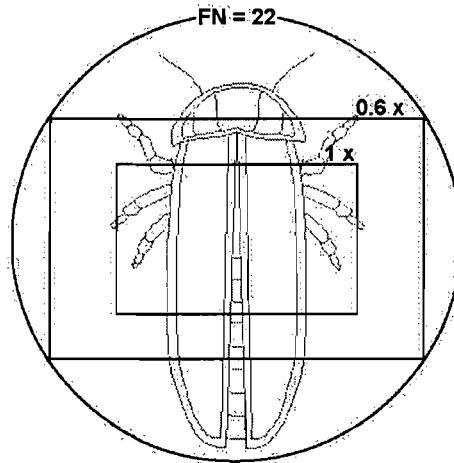


Figure 5.13: Field of view – monitor versus eyepiece (example: firefly)

primary image has to be reduced in size with the relay optics (magnification value < 1) in order to record what is seen through the eyepiece. With a $1x$ magnification, only the centre section of the eyepiece view will be recorded (see Fig. 5.13, page 174). *The field of view size (FoVS)*, which is the portion of the object that is visible on the monitor, varies with changes in:

1. Size of the CCD sensor chip – height, width or diagonal (ChS [mm])
2. Objective magnification (OM)
3. Relay optics coupler magnification (CM).

FoVS is determined by the following formula:

$$FoVS = \frac{ChS}{OM \cdot CM} \quad (5.18)$$

5.7.2 Image resolution

The resolution limit of a microscope (optical resolution) is determined by the NAs of condenser and objective, as well as the wavelength of light (see equation 5.9, page 156). The size of the smallest resolvable distance r between two points appears enlarged at the primary image, and further enlarged or

reduced by the relay optics at the sensor surface. The size of the resolution limit at the sensor (r_{sen}) can be determined by:

$$r_{sen} = r \cdot OM \cdot CM \quad (5.19)$$

- r_{sen} resolution limit at the sensor
- r smallest resolvable distance
- OM objective magnification
- CM relay optics coupler magnification

The largest physical pixel size of the sensor, which allows us to record the smallest resolvable distance, is further constrained by the *Nyquist-Shannon sampling theorem*. It states that the exact reconstruction of a signal from its sample is possible if the sampling frequency is greater than twice the signal frequency.

The required maximum pixel size (pix_{max}) on the sensor is, therefore, determined by the optics, which form the image, and the *Nyquist-Shannon theorem*:

$$pix_{max} \leq \frac{1}{2} \cdot r_{sen} \quad (5.20)$$

- r_{sen} resolution limit at the sensor

If the pixels on the sensor are larger than the maximum allowable, the sensor is not suitable for recording the finest detail with the optics as configured. In this case, the magnification of the relay optics should be increased.

5.7.3 Requirements for digital photography

The optical specifications of our available objectives and relay optics coupler, resulting magnifications, field of view size, and pixel requirements for digital photography are listed in table IV on page 176. A description of total mag-

Table IV: Optical specifications and requirements for digital photography

<i>OM</i>	(NA)	<i>CM</i>	<i>TM</i> ^a eq. 5.21	<i>FoVS</i> ^a [mm] eq. 5.18	<i>r</i> ^b [μm] eq. 5.8	<i>r_{sen}</i> ^b [μm] eq. 5.19	<i>pix_{max}</i> [μm] eq. 5.20
10x	(0.3)	0.6x	70	1.58	1.01	6.04	3.02
10x	(0.3)	1x	116	0.95	1.01	10.07	5.03
10x	(0.3)	4x	464	0.24	1.01	40.26	20.13
20x	(0.4)	0.6x	139	0.79	0.75	9.06	4.53
20x	(0.4)	1x	232	0.47	0.75	15.1	7.55
20x	(0.4)	4x	929 ^c	0.12	0.75	60.39	30.2
40x	(0.6)	0.6x	278	0.39	0.50	12.08	6.04
40x	(0.6)	1x	464	0.24	0.50	20.13	10.07
40x	(0.6)	4x	1857 ^c	0.06	0.50	80.52	40.26
40x	(0.75)	0.6x	279	0.39	0.40	9.66	4.83
40x	(0.75)	1x	464	0.23	0.40	16.10	8.05
40x	(0.75)	4x	1857 ^c	0.06	0.40	64.42	32.21
60x	(1.4)	0.6x	418	0.26	0.22	7.76	3.88
60x	(1.4)	1x	697	0.16	0.22	12.94	6.47
60x	(1.4)	4x	2786 ^c	0.04	0.22	51.76	25.88

^acalculated with a monitor magnification ($MM = 10x$), a square CCD format ($ChS_{diag} = 9.5$ mm) and a digital image diagonal dimension of $Im_{diag} = 110$ mm

^bcalculated for $\lambda = 495$ nm, regarding only NA_{obj}

^c $TM \gg TM_{max}$; for more details see page 177

nification and field of view size is briefly outlined below.

The total magnification (TM) depends on:

1. Objective magnification (OM)
2. Relay optics coupler magnification (CM)
3. CCD chip diagonal dimension (ChS_{diag} ; [mm])
4. Digital image diagonal dimension (Im_{diag} ; [mm])

TM can be calculated by the following formula:

$$TM = OM \cdot CM \cdot MM \quad (5.21)$$

with the monitor magnification $MM = \frac{Im_{diag}}{ChS_{diag}}$.

The range of useful total magnification for an objective/relay optics (objective/eyepiece, resp.) combination is defined by the NA of the system (see section 5.3). The minimum magnification, which is necessary for the resolution of a detail present in an image, is arbitrarily set at $TM_{min} = 500 \times NA$ [234]. The maximum useful magnification of an image is set at $TM_{max} = 1000 \times NA$. Magnifications higher than this value will usually lead to empty magnification, whereby increasing magnification through the relay optics lens (or eyepiece) only causes the image to become more magnified, with no corresponding increase in detail resolution.

Chapter 6

Article 3: Side-viewing microscopy

6.1 Preamble

Extracellular ATP is the major factor controlling ASL height in the conductive airways (see section 4). It is thus interesting to study the effects of released ATP on the properties of ASL. This study required the development of a novel system that allowed a continuous observation of the ASL. This approach would extend the methodological technique available in the group and could potentially provide a complementary aspect to the subject of extracellular ATP in lung epithelia.

The objective of this research was to design and set up a side-viewing system based on epifluorescent microscopy that would allow time-resolved observation of ASL height alterations on *in vitro* air-liquid cultured cell monolayers.

6.2 Article

Tatur, S.; Chabot, H.; Grygorczyk, R.

Method for Measuring Surface Liquid Height of *in vitro* Airway Epithelial Cell Cultures with Epifluorescence Microscopy. To be submitted to the *Journal of Microscopy*.

Manuscript included on pp. 180-211.

All technical drawings are reproduce in appendix C.

**Method for Measuring Surface Liquid Height of *in vitro* Airway
Epithelial Cell Cultures with Epifluorescence Microscopy**

Sabina Tatur^{1,2}, H  l  ne Chabot² and Ryszard Grygorczyk^{1,2}

¹Institut de g  nie biom  dical, Universit   de Montr  al, Montr  al, Qu  bec, Canada

²Centre de recherche, Centre Hospitalier de l'Universit   de Montr  al (CHUM) –
H  tel-Dieu, Montr  al, Qu  bec, Canada

Running title: ASL Imaging with Epifluorescence Microscopy

Address for correspondence:

Sabina Tatur and Ryszard Grygorczyk

Centre Hospitalier de l'Universit   de Montr  al H  tel-Dieu

3850 Saint-Urbain, Montr  al, Qu  bec, Canada, H2W 1T8

Tel: (514) 890-8000 ext.15089 Fax: (514) 412-7204

e-mail: [REDACTED]
[REDACTED]

Keywords: optical system, side-view microscopy, epifluorescence microscopy,
airway surface liquid height

Summary

Lung epithelial cells are covered by a thin layer of airway surface liquid (ASL) whose height is of vital importance for proper lung functioning. The precise measurement of ASL height and its variations is essential to study the mechanisms of its control and regulation. So far, however, no technique was developed which allowed a sufficiently precise resolution of ASL height alterations, neither *in vivo* nor *in vitro*.

In this study, we describe a novel side-view imaging technique which permits recording of ASL height variations on *in vitro* models of airway epithelial cell cultures. The system requires a custom-designed side-view chamber mounted on the microscope stage, equipped with a temperature/humidity control system for maintaining the cell culture at an air/liquid interface (ALI) during the experiment. The set-up is not restricted to any specific type of microscopy and no modification of the microscope itself is necessary. A cell monolayer, grown under ALI condition on the filter membrane of a modified Millicell[®] insert is mounted in a side-view chamber perpendicular to the microscope objective. In this orientation, fluorescently labelled ASL height can be directly recorded by conventional epifluorescence microscopy. Compared to laser scanning confocal microscopy (LSCM), it has the advantage of a shorter image-acquisition time.

INTRODUCTION

The airway epithelium which lines the entire respiratory tract is covered by a thin ASL layer measuring *in vivo* 7 μm to 70 μm in height (Tarran, R., 2004). The ASL defends the lung against infectious and noxious agents, and conditions inhaled air which is associated with the so-called 'insensible water loss' from the ASL (Boucher, R.C., 1999). The height of ASL is a key parameter in airway physiology and is thought to be important in the pathophysiology of cystic fibrosis, asthma, and other diseases of the airways (Verkman, A.S. et al., 2003).

So far, the ASL height of bronchial and trachea cell cultures has been studied by laser scanning confocal microscopy (LSCM) (Boucher, R.C., 1999; Jayaraman, S. et al., 2001; Roomans, G.M. et al., 2004). However, this expensive and complex technique has its downsides, such as low temporal resolution and photobleaching. Accordingly, the acquisition of an image or a sequence of images can take up to 1 min depending on the chosen image resolution. These limitations preclude the possibility to observe fast responses in ASL height alterations upon a cell stimulus, which lie in the range of few seconds. Furthermore, laser scanning causes photobleaching and photodamage to the cells because of the exposure to laser light of high average operating power (Piston, D.W., 1999), an outcome which may alter the cell response to a stimulus.

Side-view imaging of the ASL, which would directly record the profile of the ASL, could obviate these problems. Several approaches for side-view imaging with a routine microscope have already been developed (Boocock, C.A. et al., 1985;

Boudreault, F. & Grygorczyk, R., 2004; Cao, J. et al., 1997; Ingram, V.M., 1969; Sanders, E.J. & Prasad, S., 1979; Tsai, J.W. et al., 2004). All of these techniques were applied to single cell observation with phase contrast illumination, and the cells were cultured on solid substrata under liquid-covered conditions. None of these techniques was, therefore, suitable for ASL height observation.

In response to the described exigencies, we developed a novel approach for side-view ASL observation based on conventional epifluorescence microscopy. The cells were cultured on a filter membrane of a modified Millicell[®] insert under air-liquid interface (ALI) condition and mounted in a chamber which allowed direct side-view imaging of the ASL profile. The ASL height could be measured with accuracy equal to LSCM with the advantage of faster image acquisition (100 ms to 1 s, depending on the NA of the system and the fluorescence intensity of the dye). Furthermore, the short illumination time limits the phototoxic effects on the cell culture.

MATERIALS AND METHODS

Cell Preparation

Filter Preparation

12 mm Millicell[®] inserts with a 0.6 cm² membrane area (PIHA01250; Millipore Corp., Billerica, MA, USA) were modified as shown in Fig. 1A. The rim of the polystyrene cylinder was cut away to obtain an unobstructed side-view of the cells grown on the filter in an up-side down orientation. The modification was accomplished manually with a scalpel, working under sterile conditions. The modified Millicell[®] inserts were then placed into autoclaved biocompatible Tygon[®] tubing pieces (# 54007; United States Plastic Corp., Lima, OH, USA), as shown in Fig. 1B, which enabled seeding and culturing cells on the outer side of the filter membrane. After the modification of the Millicell[®] inserts, the outer side of the filter membrane was coated with 120 µl type I collagen (Vitrogen-100; Collagen Corp., Palo Alto, CA, USA). The collagen was left to dry overnight at 37°C and neutralised by washing with PBS before seeding the cells.

Cell Culture

The human bronchial epithelial cell-line 16HBE14o-, a generous gift from Dr. D. Gruenert (University of California at San Francisco, CA, USA), was cultured under ALI conditions similar to the procedure described by (Forbes, B. et al., 2003): The cells were seeded at a density of 2.5×10^5 cells/cm² and were grown in DMEM:F-12

(Gibco, # 12400-024) supplemented with 2% Ultraser G (Life Technologies, Paisley, UK), $1.2 \text{ g} \times \text{l}^{-1}$ NaHCO_3 , $100 \text{ U} \times \text{ml}^{-1}$ penicillin, $100 \text{ } \mu\text{g} \times \text{ml}^{-1}$ streptomycin, and 2 mM L-glutamine. All constituents of the culture medium were from Gibco-BRL, Burlington, ON, Canada, unless otherwise specified. The medium was removed from the apical side after 2 days in culture (37°C , 5% CO_2) and then maintained at an air-liquid interface. The medium on the basal side was replaced every 24 h. The cells were used for experiments between day 7 and day 12 after seeding.

Cell Treatment

To label the ASL, 50 μl of an Alexa Fluor 488 or 594 Dextran conjugate solution (10 kD; Invitrogen-Molecular Probes, Kingston, ON, Canada) was added on top of the cell monolayer, the excess was aspirated. During the system test runs, the cells were left for 1 h in the incubator (37°C , 5% CO_2) to recover their natural ASL height. For future physiological experiments, the recovering time will have to be established for each cell culture. A concentration of $2 \text{ mg} \times \text{ml}^{-1}$ Alexa Fluor Dextran in PBS was used for confocal microscopy measurements, whereas for epifluorescence microscopy measurements the solution was further diluted to $2 \text{ } \mu\text{g} \times \text{ml}^{-1}$ Alexa Fluor Dextran in PBS to reduce background fluorescence coming from beyond the focus. For cell-profile observations, the cell membrane was stained either with 5-hexadecanoylamino fluorescein (HAF) or dapoxyl sulfonic acid (DSA) by covering the cell culture with 30 μl PBS containing $10 \text{ } \mu\text{g} \times \text{ml}^{-1}$ HAF or 10 μM DSA for 5 min.

The cells were then rinsed with PBS. During all experiments, the cells were perfused from the basal side with physiological saline solution (PS) which contained (in mM): 140 NaCl, 5 KCl, 1 MgCl₂, 1 CaCl₂, 10 glucose and 10 HEPES, pH 7.4 adjusted with NaOH. All PS components were obtained from Sigma-Aldrich Canada, Ltd., Oakville, ON. HAF and DSA were purchased from Invitrogen-Molecular Probes, Kingston, ON, Canada.

Experimental Setup

Side-View Chamber

Fig. 2A depicts the side-view chamber (made of non-fluorescent black delrin) which accommodated the modified Millicell[®] insert with the cell culture for side-view observation. The Millicell[®] insert precisely fitted onto the holder with six inlet and one outlet channels. These channels were coupled, respectively, with an inlet and outlet metal tube connected to an in-line heater (Warner Instrument Corp., Hamden, CT, USA) and a peristaltic pump (Gilson Miniplus 3, Worthington, OH, USA) which continuously provided the cells with warm PS (37°C, 0.5 ml*min⁻¹) from the basal side. The holder was designed to rotate around its axis within the chamber frame. This feature allowed finding the best spot for observation which was then secured with the retaining screw.

Mini-Incubator

On the microscope stage, the side-view chamber was placed into a mini-incubator (made of non-fluorescent black delrin) with a temperature and humidity control system (see Fig. 2B) which provided an air compartment of controlled temperature (37°C) and humidity (45-60%). The temperature and humidity sensors were placed close to the cell monolayer on both sides of the side-view chamber to precisely control its incubation conditions and, therefore, to avoid insensible water loss from the surface of the cells. Warm, humidified air entered the incubator from the bottom, whereas the opening on top of the incubator had two functions: firstly, it served as an outlet for the inflowing warm and humidified air to avoid condensation on the objective, and, secondly, it allowed brightfield illumination on the cell profile which was very valuable during initial locating and focusing of the cell profile.

Temperature and Humidity System

An Air-Therm™ ATX Humidifier (ATX-H) was purchased from World Precision Instruments, Inc., Sarasota, FL, USA. It consisted of an air heater with precise temperature and humidity control connected to an ultrasonic humidifier (see Fig. 2C). The air continuously circulated in a closed circuit and was coupled to the microscope stage incubator. The air pressure within the closed circuit was kept constant by air influx through a small cut in the tubing behind the coupling valve. The warm, humid air was fed into the incubator from underneath the microscope stage. This

arrangement prevented the objective to be in the direct flow path of the humid air and, thus, to fog up. The objective was, furthermore, preheated to 37°C and the whole set-up was flushed with warm (37°C) air for about 1 h before turning on the humidifier. This procedure prevented major condensation on any parts of the system for a relative humidity of up to 60% at a steady room temperature of ~25°C. Since inhaled air is gradually humidified to 100% relative humidity by the ASL of the upper airways (Zuchner, K., 2006), the relative humidity in the mini-incubator should be optimized for every cell culture. It should be kept as low as possible to avoid condensation and as high as necessary to countervail evaporation of the ASL. If a humidity level of more than 60% is necessary, the microscope objective can be potentially equipped with an objective heater system. For the cell line 16HBE14o-, the humidity level was set to 55%.

Optical Arrangement

The side-view chamber with the incubator was placed on the stage of a Nikon TE300 inverted microscope (Nikon Canada Inc., Montréal, Qc) equipped with an extra long working distance (ELWD) system condenser. Fluorescently labelled cells and ASL were observed through an ELWD CFI objective (Nikon, 40x/0.60, WD 3.7-2.7, CR 0-2) using epi-fluorescent illumination. The following excitation filters and emission filter blocks (Chroma Technology Corp., Rockingham, VT, USA) were used: a 495 nm excitation filter with a GFP filter block was used for Alexa 488 and HAF, a 340

nm excitation filter with a Fura-2 filter block was used for DSA, and a Texas Red filter block was used for Alexa 594. The microscope was focused on the lower edge of the vertically-oriented filter with the cell culture, and the image was directly projected on the camera chip via a C-mount 1x (or 4x) coupler (Nikon Canada Inc., Montréal, Qc). The cover-slip correction collar (CR) on the objective was essentially set to 0.

Data Acquisition and Analysis

Image Acquisition

Brightfield and fluorescent images of the cell profile and ASL layer were acquired with a monochromatic T57 Micromax CCD camera (Princeton Instruments, Trenton, NJ, USA) and MetaVue software version 7.0 (Molecular Devices Corp., Sunnyvale, CA, USA). The camera chip had 512×512 imaging pixels with an individual pixel size of 13 μm .

Image Analysis

The acquired images were processed using MetaVue software (Molecular Devices Corp., Sunnyvale, CA, USA). Background flattening has been applied to reduce stray light coming from fluorescence beyond the plane in focus. This procedure subtracts the large gradient of background fluorescence intensity and reveals additional details without losing image data. A line scan perpendicular through the ASL produces a

fluorescence intensity profile and facilitates the estimation of ASL height and to monitor its variations.

Confocal Microscopy

Images of fluorescently labelled ASL were also recorded using a TE300 inverted microscope (Nikon Canada Inc., Mississauga, ON) equipped with a confocal laser-scanning system (BioRad MRC 1024, Hercules, CA, USA) and a monochrome CoolSnap-Fx CCD camera (Photometrics, Tucson, AZ, USA). The camera chip had 1300×1030 imaging pixels with an individual pixel size of $6.7 \mu\text{m}$.

The ASL was scanned in the x-y-plane and the x-z-plane (see Fig. 2 A), respectively. Each scanning plane was separated by $1.2 \mu\text{m}$. The images were analysed using the Confocal Assistant software version 4.02 (© Todd Clark Brelje). While x-z scanning directly displayed side-view images of the ASL, the x-y-scanning planes had to be merged and processed to generate a side-view of the ASL.

RESULTS AND DISCUSSION

Cell Culture

16HBE14o- cell cultures grown at ALI condition do not reflect the *in vivo* situation of the mammalian airways since they consist of only one cell type and form a very thin ASL layer. Nevertheless, 16HBE14o- is a good choice as cell model for the development of a method to measure ASL height since it is a cell culture which is easy to culture under air-liquid conditions. The thin ASL layer may also be seen as an advantage to test the limits of the system in its potential to create an appropriate surrounding of humidity and temperature and to resolve details in the shape of the ASL profile.

The Optical System

Depth of Field

The depth of field is defined as the range of distances within an object that appears in focus. Observing a curved surface with a conventional microscope, as depicted in Fig. 3A, implies that only part the surface will be in focus. To be able to record fluorescently labelled ASL over a representative area, we needed to have a sufficiently broad section in focus. Fig. 3A sketches the depth of field (d) referring to the circular filter membrane of the Millicell[®] insert in observation orientation. The depth of field is given by the following equation (Shillaber, C.P., 1944):

$$d = \frac{\lambda \sqrt{n^2 - NA^2}}{NA^2}.$$

The equation results in $d = 1.1 \mu\text{m}$ for a numerical aperture of $NA_{\text{objective}} = 0.6$, a wavelength of $\lambda_{\text{ex}} = 495 \text{ nm}$, and a refractive index of $n \approx 1$ for air (Lide, D.R.ed., 2007). As a result, a maximum section of $l \approx 220 \mu\text{m}$ of the Millicell[®] insert is theoretically in focus. This section size exceeds the field of view size (FoV) of the camera chip when using 40x TM (FoV = $512 \text{ pixels} \times 13 \mu\text{m} \div 40 = 166.4 \mu\text{m}$). Accordingly, the camera chip can be used to its full capacity.

Evaluation of the fluorescence intensity profile

To facilitate the evaluation of the fluorescence intensity profile of the ASL, an image of yellow-green fluorescent microbeads (505/515) of $4 \mu\text{m}$ diameter (# F8859 Invitrogen-Molecular Probes, Kingston, ON, Canada) was taken and their fluorescence intensity profiles were plotted. As can be seen in Fig. 3B, the precise value of $4 \mu\text{m}$ for the diameter lies on 0.4 of the altitude of the profile curve. According to this observation, the reading position for the evaluation of the ASL heights was set to be 0.4 of the altitude of the fluorescence profile curves.

Resolution and Brightness

Since ALI cultured 16HBE14o- cells are covered by a rather thin layer of ASL ($\sim 3\text{-}6 \mu\text{m}$, see below), we required a high resolution power to observe ASL height

variations. With the ELWD CFI objective ($NA_{objective} = 0.6$), we achieved an optical resolution of $r_{opt} = 0.61 \times \lambda \times NA^{-1} = 0.5 \text{ } \mu\text{m}$ at $\lambda_{ex} = 495 \text{ nm}$. To obtain a final image resolution of r_{opt} , the resolution on the camera chip r_{chip} needed to be equal to or greater than (of lower value than) r_{opt} . If r_{chip} was greater than r_{opt} , the final image resolution was reduced to the value of r_{chip} . According to the Nyquist-Shannon sampling theorem, r_{chip} is of higher value than the two-fold individual pixel size of the camera chip (pix) divided by the total optical magnification (TM) ($r_{chip} > 2 \times pix \times TM^{-1}$). The TM in our optical arrangements was set either at 40x (40x objective magnification and 1x coupler magnification) or at 160x (40x objective magnification and 4x coupler magnification). The camera chip from the epifluorescence microscopy system ($pix = 13 \text{ } \mu\text{m}$) achieved a maximal resolution of $r_{chip} \approx 0.65 \text{ } \mu\text{m} > r_{opt}$ for 40x TM and $r_{chip} \approx 0.16 \text{ } \mu\text{m} < r_{opt}$ for 160x TM, considering an approximation for the pixel size of half the sampling size. An approximation of a smaller sampling pixel size would lead to an inferior resolution with the same parameters. The superior resolution for 160x TM has, however, its drawback to the image brightness (B_{im}) which decreased substantially with the increased TM and the reduced NA of the 4x-coupler ($B_{im} \propto (NA/TM)^2$) (Born, M. & Wolf, E., 1999)). The image acquisition required a ten- to twenty-fold longer illumination time, one of about 1000 ms (see Fig. 2B bottom right) compared to around 100 ms by direct 1x-

coupling in all other images taken by means of the epifluorescence microscope (Fig. 4A-D). Before an experiment, the necessity for a (slight) increase in resolution has to be, therefore, weighed up against the disadvantage of a longer illumination time.

The resolution on the camera chip from the confocal microscopy system ($\text{pix} = 6.7 \mu\text{m}$) was $r_{chip} = 0.34 \mu\text{m} < r_{opt}$ for 40x TM. However, the resolution of an image reconstructed from a stack of sequential images acquired by confocal microscopy is not only defined by r_{opt} or r_{chip} , but also by the distance of the scanning planes. An optimal scanning distance should be chosen considering similar principles as above: the smaller the scanning distance, the better is the resolution. At the same time, the acquisition-, and with it, the illumination-time can increase enormously. On the other hand, the greater the scanning distance, the worse the resolution, though in exchange, the acquisition and illumination times get shorter. Fig. 5A shows a reconstructed image from sequential x-y-scans of the fluorescently labelled ASL on a 16HBE14o- cell monolayer. We chose a scanning distance of $1.2 \mu\text{m}$ to minimize the acquisition time which resulted in rather low image resolution. The fluorescent ASL band appears to be straightened and missing the typical undulating profile of the cell monolayer which was seen on the epifluorescence images of higher resolution (Fig. 4B, D). Nevertheless, the ASL height can still be correctly estimated to be approx. $5 \mu\text{m}$.

Temperature, Humidity and Perfusion

A precise adjustment of surrounding temperature and humidity is essential for accurate and reproducible measurements of the ASL height on living cell cultures. The temperature and humidity system with the ATX-H allowed us to control the temperature inside the stage incubator to $\pm 0.2^{\circ}\text{C}$ and the air humidity to a precision of $\pm 3\%$. The perfusion system of the side-view chamber supplied the cells with warm (37°C) solution to nourish and to bathe them from the basal side. Both, a humidity level of 50-55% and a continuous perfusion of the basal side of the cell monolayer, were necessary to prevent the 16HBE14o- cell monolayer from drying out. During our short-term experiments (up to 30 min), we perfused the cells with PS. They can, however, be also perfused with pH-adjusted cell media (bubbled through with air / 5% CO_2) for experiments of longer duration. For specific cell stimulation, selected drugs can be added to the perfusion medium, and the perfusate temperature as well as the temperature inside the stage incubator can be changed if necessary.

Side-View Imaging

Conventional Microscopy

To verify the evenness and smoothness of the Millicell[®] insert after its modification, we took side-view images of the Millicell[®] insert with and without cell culture. Fig. 4A shows brightfield images of the modified Millicell[®] insert in profile without cell culture (left side) and with a cell monolayer (right side). Fig. 2B (right bottom)

displays identical cell profiles in brightfield and epifluorescence illumination after labelling the cell membrane with HAF. Whereas the profile of the Millicell[®] insert without cell culture is even and flat, the profiles with a cell monolayer appear undulating. All profiles in brightfield illumination clearly display an Airy pattern as a result of light diffraction at the air-cell frontier line. The fluorescence image in Fig. 2B reveals a cell height of 3-5 μm . The TM of all images was 160x with 40x objective magnification and 4x coupler magnifications.

Fig. 4B shows a side-view image of fluorescently labelled ASL which was recorded with 40x TM and an acquisition time of 100 ms. The fluorescence intensity profiles of three different locations are displayed on the right side of the image and facilitate the estimation of the ASL height. The peak of fluorescence intensity corresponds to the ASL height and measures between ~ 4 and 6 μm . On the cell side of the peak, the fluorescence intensity stays slightly elevated compared to the side facing the air compartment. To verify if the elevated fluorescence intensity originates from the cell monolayer, an image of the fluorescent cell monolayer profile was superimposed with an image of the fluorescent ASL. Fig. 4C shows the two-coloured superimposed image in which the ASL layer is displayed in red colour and the cell profile in green. It becomes now apparent that the elevated fluorescence on the cell side in Fig. 4B is indeed caused by the cell monolayer – probably due to the scattering of fluorescence light – and measures around 5 μm .

The ability to measure ASL height alterations was tested by taking pictures of the fluorescent ASL layer in an interval of 15 min. Fig. 4D shows two sequential images of the fluorescent ASL. The left picture was taken directly after labelling the ASL and the right after the cell monolayer with the labelled ASL stayed in the mini-incubator for 15 min. The enlarged fluorescence intensity profile reveals a small decrease in the ASL height of less than 1 μm , and demonstrates that ASL height variations in the range close to the resolution limit are detectable.

Confocal Microscopy

To validate the results obtained with epifluorescence microscopy, the ASL height was measured with confocal microscopy using the same side-viewing chamber system. Fig. 5B was recorded by x-z-scanning confocal microscopy and is displayed unprocessed. It resembles the image in Fig. 4B and shows fluorescent ASL with a height of 4-7 μm and a drift of fluorescent light toward the cell monolayer.

Fig. 5A was generated from x-y-scans of the cell culture. This approach corresponds to the hitherto applied procedure for ASL height measurements (Tarran, R., 2004; Verkman, A.S. et al., 2003). The resolution is confined to the distance of the scanning planes which was chosen to be 1.2 μm to keep the acquisition time in a reasonable range. As mentioned above, although the resolution is evidently lower than in Fig. 5B as well as in Fig. 4B and D, the ASL height can still be estimated to be around 5 μm .

CONCLUSION AND FUTURE DIRECTIONS

The custom-designed side-viewing chamber equipped with the temperature and humidity control system enables fast imaging of ASL height and its variations during cell stimulation with epifluorescence microscopy as well as with confocal microscopy. It will allow a qualitative evaluation (limited by the resolution of the system) of ASL height alterations with respect to time. Epifluorescence microscopy provides similar images to confocal microscopy with the advantage of requiring a considerably lower acquisition time. Images recorded by epifluorescence microscopy and confocal x-z-scanning have a comparably high resolution ($r = 0.65$ and $0.5 \mu\text{m}$, respectively), whereas the resolution of the calculated side-viewing images from x-y-scanning confocal microscopy is noticeably lower ($r = 1.2 \mu\text{m}$) and limited by the distance of the scanning planes. However, x-y-scanning confocal microscopy has the advantage of not being limited to the edge of the filter membrane of the Millicell[®] insert and generates ASL images throughout the filter area.

Further advancement of the system is desirable to make the side-viewing technique more versatile. The installation of a microscope objective heater would allow an increase in the relative humidity level inside the mini-incubator close to saturation. Cell cultures demanding a very high level of air humidity could then be studied. The development of an easy access to the surface of the cell monolayer – through e.g. an opening in the mini-incubator – would enable cell stimulation from the apical side.

Both technical improvements would be very useful to take the full advantage of this new method.

REFERENCE LIST

- Boocock, C.A., Brown, A.F. & Dunn, G.A. (1985) A simple chamber for observing microscopic specimens in both top and side views. *J Microsc.* **137**[Pt 1], 29-34.
- Born, M. & Wolf, E. (1999) *Principles of Optics. 7th expanded.* Cambridge ; New York, Cambridge University Press.
- Boucher, R.C. (1999) Molecular insights into the physiology of the 'thin film' of airway surface liquid. *J. Physiol* **516** (Pt 3), 631-638.
- Boudreault, F. & Grygorczyk, R. (2004) Evaluation of rapid volume changes of substrate-adherent cells by conventional microscopy 3D imaging. *J. Microsc.* **215**[Pt 3], 302-312.
- Cao, J., Usami, S. & Dong, C. (1997) Development of a side-view chamber for studying cell-surface adhesion under flow conditions. *Ann. Biomed. Eng* **25**[3], 573-580.
- Forbes, B., Shah, A., Martin, G.P. & Lansley, A.B. (2003) The human bronchial epithelial cell line 16HBE14o- as a model system of the airways for studying drug transport. *International Journal of Pharmaceutics* **257**[1-2], 161-167.
- Ingram, V.M. (1969) A side view of moving fibroblasts. *Nature* **222**[5194], 641-644.
- Jayaraman, S., Song, Y., Vetrivel, L., Shankar, L. & Verkman, A.S. (2001) Noninvasive in vivo fluorescence measurement of airway-surface liquid depth, salt concentration, and pH. *J Clin Invest* **107**[3], 317-324.
- Lide, D.R.ed. (2007) *CRC Handbook of Chemistry and Physics. Taylor and Francis. Internet Version 2007, <<http://www.hbcnetbase.com>>* [87th Edition]. Boca Raton, FL.

- Piston, D.W. (1999) Imaging living cells and tissues by two-photon excitation microscopy. *Trends Cell Biol.* **9**[2], 66-69.
- Roomans, G.M., Kozlova, I., Nilsson, H., Vanthanouvong, V., Button, B. & Tarran, R. (2004) Measurements of airway surface liquid height and mucus transport by fluorescence microscopy, and of ion composition by X-ray microanalysis. *J. Cyst. Fibros.* **3 Suppl 2**, 135-139.
- Sanders, E.J. & Prasad, S. (1979) Observation of cultured embryonic epithelial cells in side view. *Journal of Cell Science* **38**, 305-314.
- Shillaber, C.P. (1944) Photomicrography In Theory and Practice. New York, John Wiley and Sons.
- Tarran, R. (2004) Regulation of airway surface liquid volume and mucus transport by active ion transport. *Proc. Am Thorac. Soc* **1**[1], 42-46.
- Tsai, J.W., Yi, Y.S. & Lin, C.H. (2004) Cell Observing Method and the System Thereof. [00594011]. Patent of the Republic of China.
- Verkman, A.S., Song, Y. & Thiagarajah, J.R. (2003) Role of airway surface liquid and submucosal glands in cystic fibrosis lung disease. *AJP - Cell Physiology* **284**[1], C2-15.
- Zuchner, K. (2006) Humidification: Measurement and Requirements. *Respiratory Care Clinics of North America* **12**[2], 149-163.

ACKNOWLEDGEMENTS

This study was supported in part by the Canadian Institutes of Health Research and the Canadian Cystic Fibrosis Foundation (CCFF). S.T. was the recipient of a CCFF studentship. The authors acknowledge Jean Soucy (Atelier d'usinage du Groupe technologique de l'Université de Montréal) for manufacturing the set-up components, and Denis Flipo (Département des sciences biologiques at the Université de Québec à Montréal) for assistance with the acquisition of the confocal microscopy images.

FIGURE CAPTIONS

Figure 1. Modification of Millicell[®] inserts for cell culture growth and cell side-view observation from the outer side of the filter membrane.

- A. Manual modification of the Millicell[®] insert: the rim of the polystyrene cylinder is cut away with a scalpel under sterile conditions for obstruction-free cell side-view observation.
- B. Insertion of a modified Millicell[®] insert into a tubing piece: the autoclavable Tygon[®] tubing is cut into 14-mm long pieces and modified in the illustrated way. The Millicell[®] inserts are placed into the tubing pieces to enable cell culture on the outer side of the filter membrane.

Figure 2. Set-up components and arrangement.

- A. Three-dimensional view of the side-view chamber to accommodate the Millicell[®] insert with a cell culture grown on the outer side of the filter membrane. The chamber consists of a chamber frame which fits on a microscope stage and a filter holder with inlet and outlet tubes to supply the basal side of the cell monolayer with physiological solution.
- B. Cross-section of the complete microscope stage assembly. The stage assembly consists of a stage ring with an air-inlet tube, an incubator and the side-view chamber. The microscope condenser illuminates the cell profile through the top

opening of the incubator for brightfield images. Recorded brightfield and fluorescent images of the cell profile are shown at the bottom right.

- C. Temperature and humidity control system connected to the microscope stage assembly. The air circulates in a closed circuit and is coupled to the stage incubator via a coupling valve through the air-inlet tube of the stage ring. A small opening behind the coupling valve regulates the air pressure within the circuit.

Figure 3. Geometrical diagram of the depth of field.

- A. Radius of the Millicell[®] insert at the filter membrane side after its modification: $r \approx 5.5$ mm. Depth of field: $d = 1.1$ μm . Length of the Millicell[®] insert section which is simultaneously in focus: $l = 2\sqrt{r^2 - (r-d)^2} = 220$ μm .
- B. Yellow-green fluorescent microbeads ($\lambda_{\text{ex}}=505$ nm / $\lambda_{\text{em}}=515$ nm) of 4 μm diameter. The fluorescent profiles of three microbeads with 4- μm section marks are represented below the image.

Figure 4. Side-view images recorded by epifluorescence microscopy.

- A. Brightfield image of the modified Millicell[®] insert without cell culture (left) and with cell culture (right).
- B. Fluorescence image of the ASL labelled with Alexa Fluor 488 Dextran recorded with a conventional epifluorescence microscope (illumination time: 100 ms). The

fluorescence intensity profiles at three different locations are displayed separately on the right side and superimposed below the image.

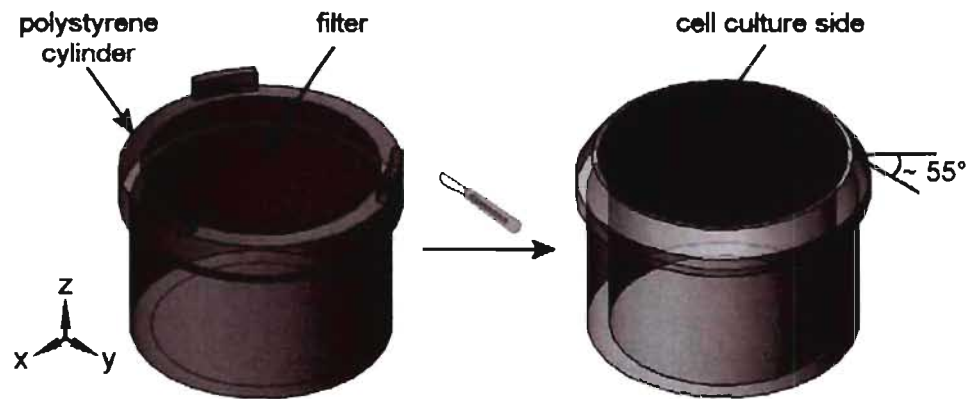
- C. Two-colour image of superimposed fluorescent ASL layer, labelled with Alexa Fluor 594, and fluorescent cell profile, labelled with DSA. The ASL layer is displayed in red and the cell profile in green.
- D. Two sequential images taken at 15 min interval. The left fluorescent image was taken immediately after labelling the ASL layer with Alexa Fluor 488 Dextran. The right fluorescent image of the cell monolayer was taken after 15 min in the mini-incubator (37°C, 55% relative humidity). On the right side of the images, the fluorescence intensity profiles at two locations are displayed, green representing the fluorescence intensities of the first taken image and blue of the next one. An enlargement of the upper panel fluorescence intensity profiles is displayed over the upper panel.

Figure 5. Side-view images by confocal microscopy.

- A. X-Z fluorescence image of the ASL reconstructed from z-y sections recorded by scanning confocal microscopy.
- B. X-Z fluorescence image of the ASL recorded by x-z-scanning confocal microscopy.

Figure 1

A



B

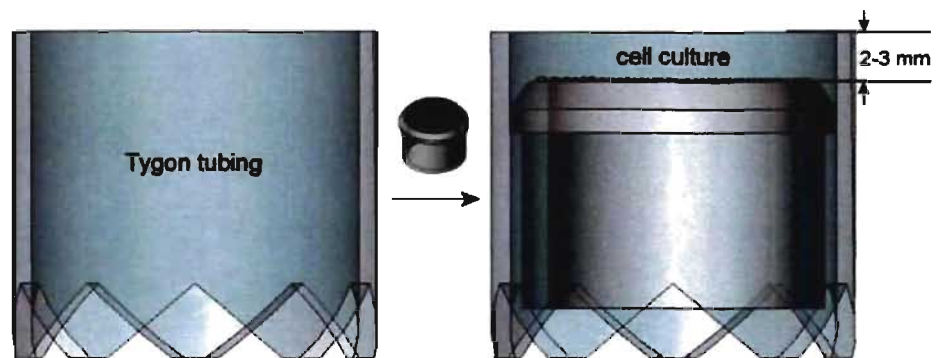
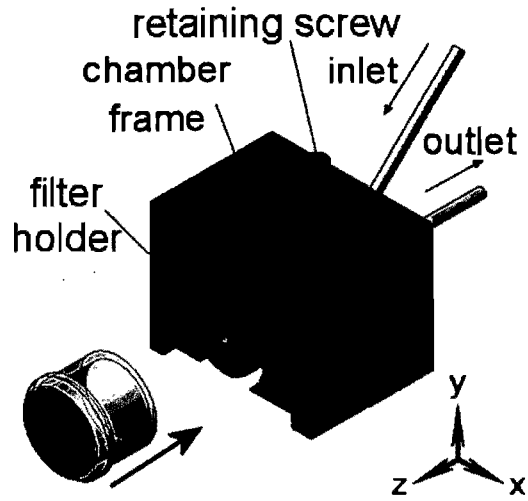
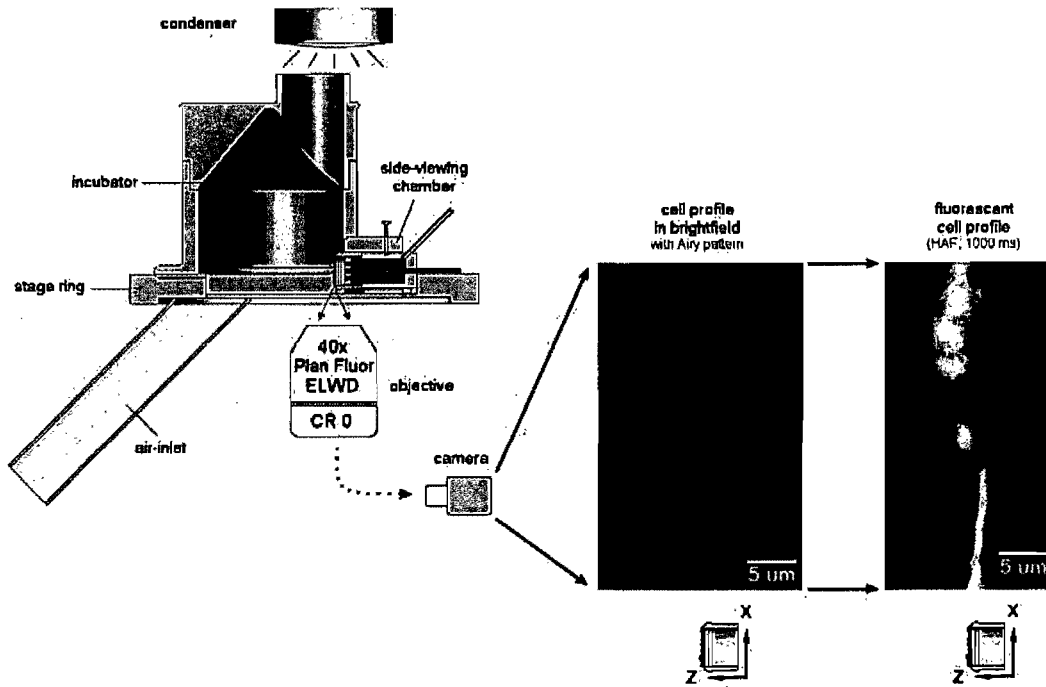


Figure 2

A



B



C

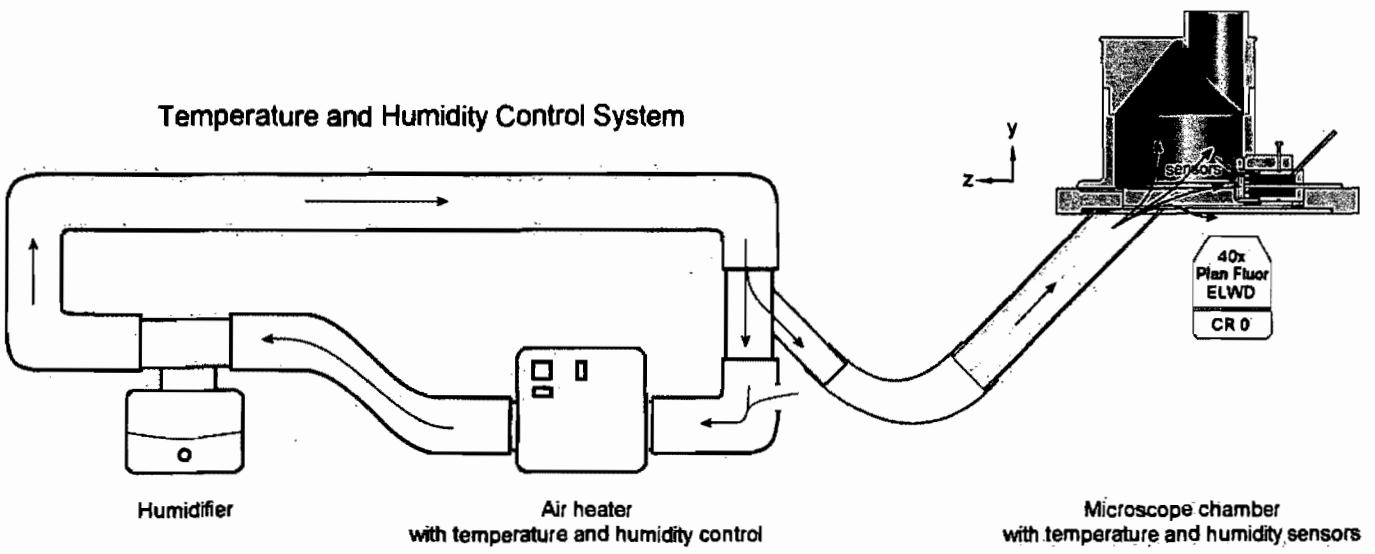
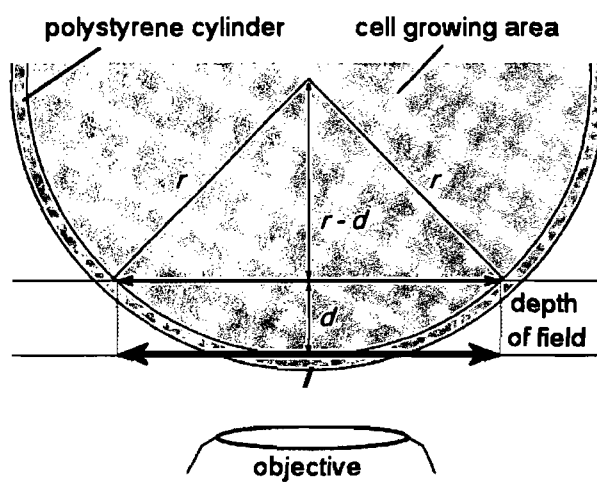


Figure 3

A



B

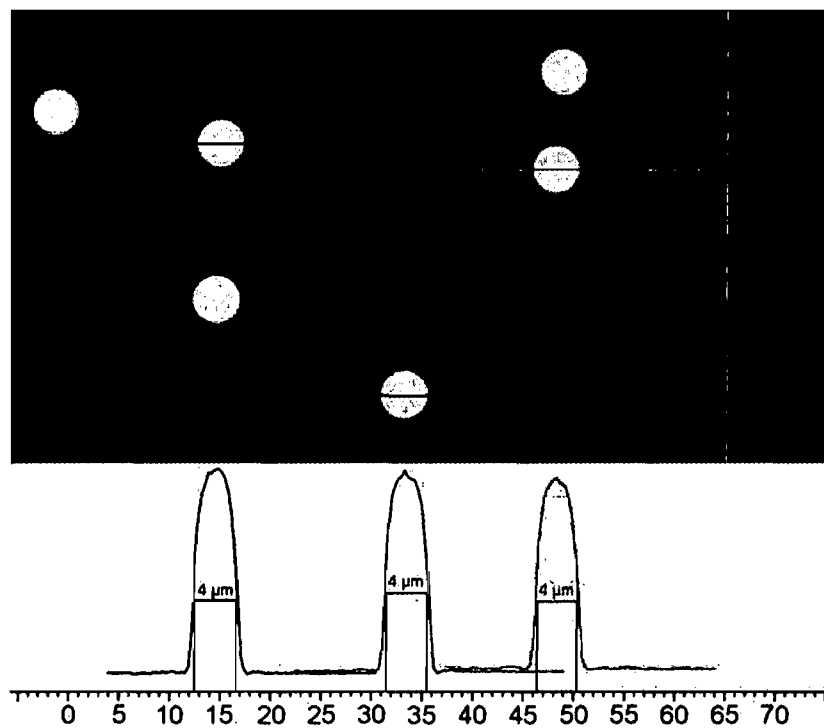
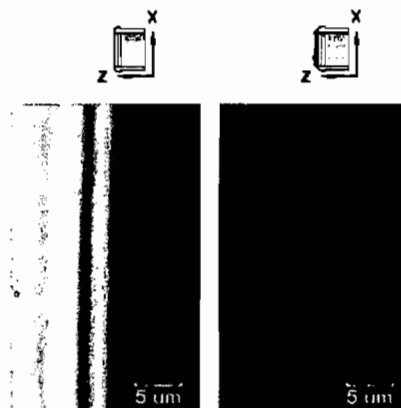
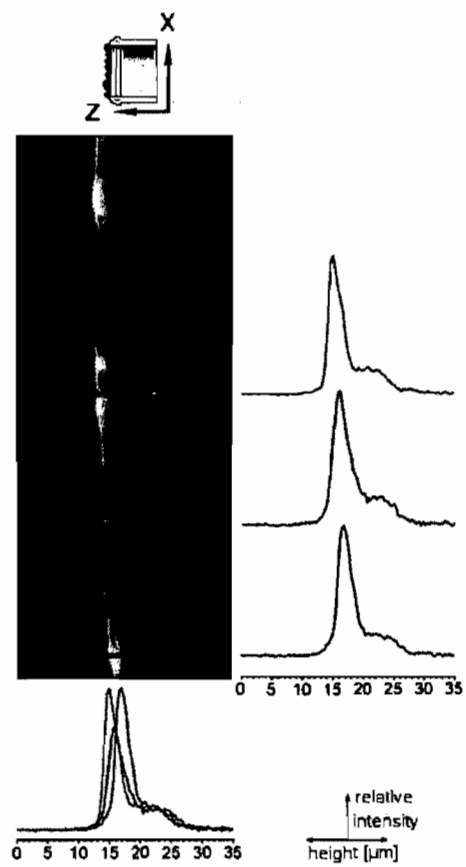


Figure 4

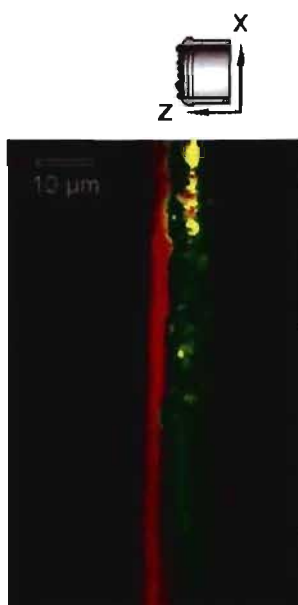
A



B



C



D

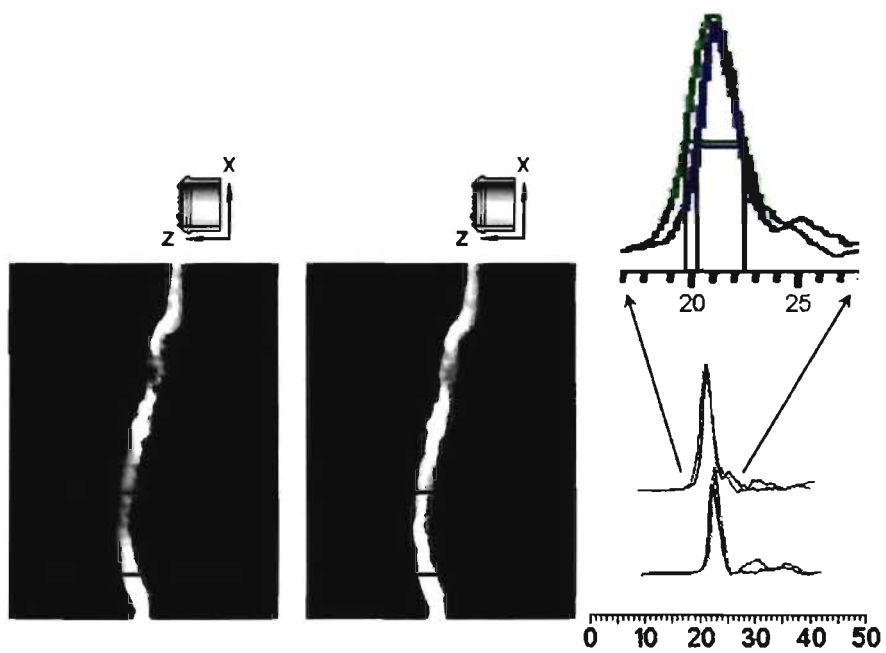


Figure 5

A.



B.



Chapter 7

Conclusions and future directions

Figure 7.1 on page 213 summarizes the mechanism of Ca^{2+} -dependent ATP release discussed in sections 3.1 and 3.2:

A 50% hypotonic shock triggers a gradual rise in intracellular Ca^{2+} (pre-spike) originating from a TG-insensitive Ca^{2+} store, probably via a preceding intracellular acidification. The precise mechanism of cell acidification and the source of the associated Ca^{2+} elevation are not yet identified. The slow rise in intracellular Ca^{2+} may evoke a Ca^{2+} -induced Ca^{2+} release from RyR and IP_3R channels, and initiates a Ca^{2+} -dependent release of nucleotides. The principal nucleotide release mechanism from A549 cells upon hypotonic shock is regarded as being exocytosis for the following reasons:

- Previous results showed tight Ca^{2+} -dependence of ATP release [26, and sections 3.1.2 and 3.2.2].
- The ratio of co-released UTP:UDP was 2:1 which suggests a vesicular rather than a cytosolic source (UTP:UDP \simeq 10:1) of the nucleotides (see section 3.1.2).
- Inhibitors affecting the exocytotic pathway significantly inhibited ATP release (see section 3.1.3).

The released nucleotides stimulate the metabotropic purinergic receptors present on the A549 cell membrane (P2Y_1 , P2Y_2 , P2Y_6). From these receptors, the P2Y_6 receptor, whose most potent agonist is UDP, plays a promi-

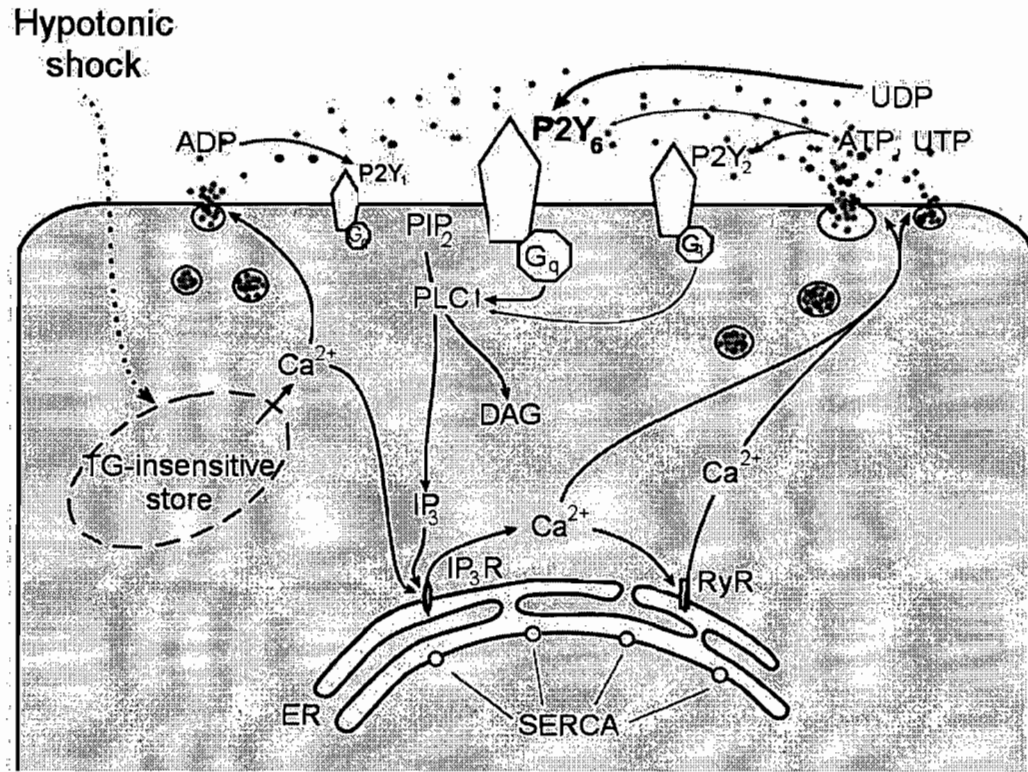


Figure 7.1: Signalling pathway of Ca²⁺-dependent ATP release from A549

ment role in this paracrine/autocrine stimulation that leads to the activation of IP₃R channels and evokes the rapid Ca²⁺ spike. The final result of the intensified Ca²⁺ signal is a regeneratively amplified exocytotic nucleotide release.

The origin of the TG-insensitive Ca²⁺ elevation remains to be further investigated. Although a correlation between hypotonic shock-induced intracellular acidification and intracellular Ca²⁺ increase has been found, the origin of the acidification and the mechanism of pH_i-dependent control of the intracellular Ca²⁺ level are still unknown. After organelles (mitochondria and lysosomes) were proven not to be responsible for the intracellular acidification (see section 3.2.3), it seems that the intracellular pH alteration is generated by a mechanism involving either ion channels, co-transporters or exchang-

ers [217–219]; this question, however, still needs to be addressed in detail. pH-sensitive proteins are probably responsible for the pH-dependent increase in the intracellular Ca^{2+} level (see section 3.2.3); also, these proteins need to be identified.

Chapter 6 describes a novel technique for visualizing ASL height on *in vitro* air-liquid cultured lung epithelial cells in a temperature- and humidity-controlled environment. It enables time-resolved (100 ms) side viewing of a fluorescently marked cell monolayer and/or ASL with a conventional epifluorescence microscope. A further development of the system would include the installation of a microscope objective heater that would prevent condensation on the objective at relative humidity levels above 60%. This improvement would allow to study cell cultures demanding very high levels of air humidity. In addition, the insertion of an opening in the mini-incubator would give easy access to the surface of the cell monolayer and would enable cell stimulation from the apical side.

To further investigate the ATP-dependence of ASL regulation, the choice of an appropriate *in vitro* cell culture system that reproduces an *in vivo* airway epithelial morphology is essential. Several continuous cell lines, such as HBE1 (immortalized human bronchial epithelial cell line [248]), MM-39 (transformed human tracheal gland cell line [249]), NuLi (normal lung, airway epithelial cell line [250]), and CuFi (cystic fibrosis, airway epithelial cell line [250]) are capable of becoming fully polarized at an air-liquid interface and should be tested for their suitability for ATP-dependent ASL height studies. Methods for the development of new, well-differentiated human airway epithelial cell cultures have been described in [251–253].

To find ways to stimulate ATP secretion from these cell cultures and to study the relationship between these stimuli and the ASL height alterations will be another important issue in the investigation of ATP-dependent ASL height control. Knowledge about the ATP release mechanism from lung epithelial cells (see sections 3.1 and 3.2) is crucial in this context and suggests the stimulation of exocytosis.

In conclusion, the understanding of the physiological mechanisms of ATP release from lung epithelial cells and the resulting ATP-dependent ASL control are the basis for developing novel therapies for diseases of impaired ASL regulation, such as cystic fibrosis and asthma.

References

- [1] G. Scheuch, M.J. Kohlhaeufel, P. Brand, and R. Siekmeier. Clinical perspectives on pulmonary systemic and macromolecular delivery. *Adv Drug Deliv Rev*, 58(9-10):996–1008, October 2006.
- [2] J.P.T. Ward, J. Ward, C.M. Wiener, and R.M. Leach. *The Respiratory System at a Glance*. The at Glance Series. Blackwell Science Ltd., Oxford, 2002.
- [3] M.P. Shelly. The humidification and filtration functions of the airways. *Respir Care Clin*, 12(2):139–148, June 2006.
- [4] R.B. Schlesinger. Comparative toxicity of ambient air pollutants: some aspects related to lung defense. *Environ Health Perspect*, 81:123–128, May 1989.
- [5] R.B. Schlesinger. Effects of inhaled acids on respiratory tract defense mechanisms. *Environ Health Perspect*, 63:25–38, November 1985.
- [6] P.J. Delves and I.M. Roitt. The immune system – first of two parts. *N Engl J Med*, 343(1):37–49, July 2000.
- [7] C. Delclaux and E. Azoulay. Inflammatory response to infectious pulmonary injury. *Eur Respir J*, 22(Suppl 42):10s–14s, August 2003.
- [8] M.C. Plotkowski, O. Bajolet-Laudinat, and E. Puchelle. Cellular and molecular mechanisms of bacterial adhesion to respiratory mucosa. *Eur Respir J*, 6(6):903–916, June 1993.
- [9] P. Zhang, W.R. Summer, G.J. Bagby, and S. Nelson. Innate immunity and pulmonary host defense. *Immunol Rev*, 173(1):39–51, 2000.

- [10] H. Fehrenbach. Alveolar epithelial type II cell: defender of the alveolus revisited. *Respir Res*, 2(1):33–46, 2001.
- [11] A. Bogenrieder, K.G. Collatz, H. Kössel, and G. Osche, editors. *Lexikon der Biologie*. Herder Verlag, Freiburg, Basel, Wien, 1988.
- [12] H.P. Haagsman, V. Herias, and M. van Eijk. Surfactant phospholipids and proteins in lung defence. *Acta Pharmacol Sin*, 24(12):1301–1303, December 2003.
- [13] R.J. Mason and D.R. Voelker. Regulatory mechanisms of surfactant secretion. *Biochim Biophys Acta - Mol Basis Dis*, 1408(2-3):226–240, November 1998.
- [14] P. Roger, J.P. Gascard, J. Bara, V.T. de Montpreville, M. Yeadon, and C. Brink. ATP induced MUC5AC release from human airways in vitro. *Mediat Inflamm*, 9(6):277–284, 2000.
- [15] T. Nakahari. Regulation of ciliary beat frequency in airways: shear stress, ATP action, and its modulation. *Am J Physiol - Lung Cell Mol Physiol*, 292(3):L612–L613, March 2007.
- [16] M. Salathe. Regulation of mammalian ciliary beating. *Annu Rev Physiol*, 69(1):401–422, 2007.
- [17] E.R. Lazarowski, R. Tarran, B.R. Grubb, C.A. Van Heusden, S. Okada, and R.C. Boucher. Nucleotide release provides a mechanism for airway surface liquid homeostasis. *J Biol Chem*, 279(35):36855–36864, August 2004.
- [18] H.R. Wirtz and L.G. Dobbs. Calcium mobilization and exocytosis after one mechanical stretch of lung epithelial cells. *Science*, 250(4985):1266–1269, November 1990.
- [19] N.E. Vlahakis and R.D. Hubmayr. Response of alveolar cells to mechanical stress. *Curr Opin Crit Care*, 9(1):2–8, February 2003.

- [20] M. Oike, G. Schwarz, J. Sehrer, M. Jost, V. Gerke, K. Weber, G. Droogmans, and B. Nilius. Cytoskeletal modulation of the response to mechanical stimulation in human vascular endothelial cells. *Pflügers Arch*, 428(5-6):569–576, October 1994.
- [21] H.L. Knudsen and J.A. Frangos. Role of cytoskeleton in shear stress-induced endothelial nitric oxide production. *Am J Physiol*, 273(1 Pt 2):H347–H355, July 1997.
- [22] P. Bodin, D. Bailey, and G. Burnstock. Increased flow-induced ATP release from isolated vascular endothelial cells but not smooth muscle cells. *Br J Pharmacol*, 103(1):1203–1205, May 1991.
- [23] M. Oike, C. Kimura, T. Koyama, M. Yoshikawa, and Y. Ito. Hypotonic stress-induced dual Ca^{2+} responses in bovine aortic endothelial cells. *Am J Physiol – Heart Circul Physiol*, 279(2):H630–H638, August 2000.
- [24] B. Nilius, J. Eggermont, T. Voets, and G. Droogmans. Volume-activated Cl^- channels. *Gen Pharmacol*, 27(7):1131–1140, October 1996.
- [25] A.I. Barakat, E.V. Leaver, P.A. Pappone, and P.F. Davies. A flow-activated chloride-selective membrane current in vascular endothelial cells. *Circ Res*, 85(9):820–828, October 1999.
- [26] F. Boudreault and R. Grygorczyk. Cell swelling-induced ATP release is tightly dependent on intracellular calcium elevations. *J Physiol*, 561(2):499–513, October 2004.
- [27] D.L. Shapiro, L.L. Nardone, S.A. Rooney, E.K. Motoyama, and J.L. Munoz. Phospholipid biosynthesis and secretion by a cell line (A549) which resembles type II alveolar epithelial cells. *Biochim Biophys Acta*, 530(2):197–207, August 1978.
- [28] A.N. Drury and A. Szent-Györgyi. The physiological activity of adenine compounds with especial reference to their action upon the mammalian heart. *J Physiol*, 68(3):213–237, November 1929.

- [29] H.N. Green and H.B. Stoner. *Biological Actions of the Adenine nucleotides*. H.K. Lewis & Company, London, 1950.
- [30] A. Carlsson and N.A. Hillarp. Release of adenosine triphosphate along with adrenaline and noradrenaline following stimulation of the adrenal medulla. *Acta Physiol Scand*, 37(2-3):235–239, September 1956.
- [31] P. Holton. The liberation of adenosine triphosphate on antidromic stimulation of sensory nerves. *J Physiol*, 145(3):494–504, March 1959.
- [32] R.M. Berne. Cardiac nucleotides in hypoxia: possible role in regulation of coronary blood flow. *Am J Physiol*, 204(2):317–322, February 1963.
- [33] A. Sattin and T.W. Rall. The effect of adenosine and adenine nucleotides on the cyclic adenosine 3',5'-phosphate content of guinea pig cerebral cortex slices. *Mol Pharmacol*, 6(1):13–23, January 1970.
- [34] G. Burnstock. Purinergic Nerves. *Pharmacol Rev*, 24(3):509–581, September 1972.
- [35] G. Burnstock. Do some nerve cells release more than one transmitter? *Neuroscience*, 1(4):239–248, August 1976.
- [36] F. Lipmann. Metabolic generation and utilization of phosphate bond energy. *Adv Enzymol*, 1:99–162, 1941.
- [37] G. Burnstock. Purinergic signalling. *Br J Pharmacol*, 147(S1):S172–S181, January 2006.
- [38] G. Burnstock and G.E. Knight. Cellular distribution and functions of P2 receptor subtypes in different systems. In W.Jeon Kwang, editor, *International Review of Cytology*, volume 240, pages 31–304. Academic Press, Philadelphia, 2004.
- [39] G. Burnstock. A basis for distinguishing two types of purinergic receptor. In R.W. Straub and L Bolis, editors, *Cell membrane receptors for drugs and hormones: a multidisciplinary approach*, pages 107–118. Raven Press, New York, 1978.

- [40] V. Ralevic and G. Burnstock. Receptors for purines and pyrimidines. *Pharmacol Rev*, 50(3):413–492, September 1998.
- [41] A. Zsembery, A.T. Boyce, L. Liang, J. Peti-Peterdi, P.D. Bell, and E.M. Schwiebert. Sustained calcium entry through P2X nucleotide receptor channels in human airway epithelial cells. *J Biol Chem*, 278(15):13398–13408, April 2003.
- [42] R. Schäfer, F. Sedehizade, T. Welte, and G. Reiser. ATP- and UTP-activated P2Y receptors differently regulate proliferation of human lung epithelial tumor cells. *Am J Physiol – Lung Cell Mol Physiol*, 285(2):L376–L385, August 2003.
- [43] T. Müller, H. Bayer, D.I Myrtek, D. Ferrari, S. Sorichter, M.W. Ziegenhagen, G. Zissel, Jr. Virchow, J.C., W. Luttmann, J. Norgauer, F. Di Virgilio, and M. Idzko. The P2Y₁₄ receptor of airway epithelial cells: Coupling to intracellular Ca²⁺ and IL-8 secretion. *Am J Respir Cell Mol Biol*, 33(6):601–609, December 2005.
- [44] J.D. Conway, T. Bartolotta, L.H. Abdullah, and C.W. Davis. Regulation of mucin secretion from human bronchial epithelial cells grown in murine hosted xenografts. *Am J Physiol – Lung Cell Mol Physiol*, 284(6):L945–L954, June 2003.
- [45] A.L. Taylor, L.M. Schwiebert, J.J. Smith, C. King, J.R. Jones, E.J. Sorscher, and E.M. Schwiebert. Epithelial P2X purinergic receptor channel expression and function. *J Clin Invest*, 104(7):875–884, October 1999.
- [46] A.M. Gilfillan, M. Hollingsworth, and A.W. Jones. The pharmacological modulation of [³H]-disaturated phosphatidylcholine overflow from perfused lung slices of adult rats: a new method for the study of lung surfactant secretion. *Br J Pharmacol*, 79(2):363–371, June 1983.
- [47] W.R. Rice. Effects of extracellular ATP on surfactant secretion. *Ann NY Acad Sci*, 603:64–74, 1990.

- [48] V. Saano, J. Nuutinen, P. Virta, S. Joki, P. Karttunen, and M. Silvasti. The effect of ATP on the ciliary activity of normal and pathological human respiratory mucosa in vitro. *Acta Oto-Laryngol*, 111(1):130–134, 1991.
- [49] M. Yoshitsugu, M. Rautiainen, S. Matsune, J. Nuutinen, and M. Ohyama. Effect of exogenous ATP on ciliary beat of human ciliated cells studied with differential interference microscope equipped with high speed video. *Acta Oto-Laryngol*, 113(5):655–659, September 1993.
- [50] C.W. Davis, M.L. Dowell, M. Lethem, and M. Van Scott. Goblet cell degranulation in isolated canine tracheal epithelium: response to exogenous ATP, ADP, and adenosine. *Am J Physiol - Cell Physiol*, 262(5):C1313–C1323, May 1992.
- [51] K.C. Kim, Q.X. Zheng, and I. Van Seuning. Involvement of a signal transduction mechanism in ATP-induced mucin release from cultured airway goblet cells. *Am J Respir Cell Mol Biol*, 8(2):121–125, February 1993.
- [52] B.K. Kishore, S.M. Ginns, C.M. Krane, S. Nielsen, and M.A. Knepper. Cellular localization of P2Y₂ purinoceptor in rat renal inner medulla and lung. *Am J Physiol - Renal Physiol*, 278(1):F43–F51, January 2000.
- [53] M.R. Van Scott, T.C. Chinet, A.D. Burnette, and A.M. Paradiso. Purinergic regulation of ion transport across nonciliated bronchiolar epithelial (Clara) cells. *Am J Physiol - Lung Cell Mol Physiol*, 269(1):L30–L37, July 1995.
- [54] A. Guyot and J.W. Hanrahan. ATP release from human airway epithelial cells studied using a capillary cell culture system. *J Physiol*, 545(1):199–206, November 2002.
- [55] S.H. Donaldson, E.R. Lazarowski, M. Picher, M.R. Knowles, M.J. Stutts, and R.C. Boucher. Basal nucleotide levels, release, and

- metabolism in normal and cystic fibrosis airways. *Mol Med*, 6(11):969–982, November 2000.
- [56] A.L. Taylor, B.A. Kudlow, K.L. Marrs, D.C. Gruenert, W.B. Guggino, and E.M. Schwiebert. Bioluminescence detection of ATP release mechanisms in epithelia. *Am J Physiol*, 275(5 Pt 1):C1391–C1406, November 1998.
- [57] H. Zimmermann. Extracellular metabolism of ATP and other nucleotides. *Naunyn-Schmiedebergs Arch Pharmacol*, 362(4-5):299–309, November 2000.
- [58] D.M. Morse, J.L. Smullen, and C.W. Davis. Differential effects of UTP, ATP, and adenosine on ciliary activity of human nasal epithelial cells. *Am J Physiol – Cell Physiol*, 280(6):C1485–C1497, June 2001.
- [59] M. Picher and R.C. Boucher. Human airway ecto-adenylate kinase. A mechanism to propagate ATP signaling on airway surfaces. *J Biol Chem*, 278(13):11256–11264, March 2003.
- [60] B. Sperlágh and S.E. Vizi. Neuronal synthesis, storage and release of ATP. *Semin Neurosci*, 8(4):175–186, August 1996.
- [61] R.J. Thompson, H.C.S.R. Akana, C. Finnigan, K.E. Howell, and J.H. Caldwell. Anion channels transport ATP into the Golgi lumen. *Am J Physiol – Cell Physiol*, 290(2):C499–C514, February 2006.
- [62] S.J. Shin, W.K.g Lee, H.W. Lim, and J.S. Park. Characterization of the ATP transporter in the reconstituted rough endoplasmic reticulum proteoliposomes. *Biochim Biophys Acta – Biomembr*, 1468(1-2):55–62, September 2000.
- [63] N. Ishida and M. Kawakita. Molecular physiology and pathology of the nucleotide sugar transporter family (SLC35). *Pflügers Arch*, 447(5):768–775, February 2004.
- [64] L. Puglielli, E.C. Mandon, and C.B. Hirschberg. Identification, purification, and characterization of the rat liver Golgi membrane ATP transporter. *J Biol Chem*, 274(18):12665–12669, April 1999.

- [65] P. Bodin and G. Burnstock. Purinergic signalling: ATP release. *Neurochem Res*, 26(8-9):959–969, September 2001.
- [66] E.M. Schwiebert and A. Zsembery. Extracellular ATP as a signaling molecule for epithelial cells. *Biochim Biophys Acta*, 1615(1-2):7–32, September 2003.
- [67] J. Nagasawa. Exocytosis: the common release mechanism of secretory granules in glandular cells, neurosecretory cells, neurons and paraneurons. *Arch Histol Jpn*, 40 Suppl:31–47, 1977.
- [68] Y. Pankratov, U. Lalo, A. Verkhratsky, and R.A. North. Vesicular release of ATP at central synapses. *Pflügers Arch*, 452(5):589–597, August 2006.
- [69] P.F. Santos, O.L. Caramelo, A.P. Carvalho, and C.B. Duarte. Characterization of ATP release from cultures enriched in cholinergic amacrine-like neurons. *J Neurobiol*, 41(3):340–348, November 1999.
- [70] E.H. Abraham, A.G. Prat, L. Gerweck, T. Seneveratne, R.J. Arceci, R. Kramer, G. Guidotti, and H.F. Cantiello. The multidrug resistance (mdr1) gene product functions as an ATP channel. *Proc Natl Acad Sci USA*, 90(1):312–316, January 1993.
- [71] I.L. Reisin, A.G. Prat, E.H. Abraham, J.F. Amara, R.J. Gregory, D.A. Ausiello, and H.F. Cantiello. The cystic fibrosis transmembrane conductance regulator is a dual ATP and chloride channel. *J Biol Chem*, 269(32):20584–20591, August 1994.
- [72] E.H. Abraham, P. Okunieff, S. Scala, P. Vos, M.J. Oosterveld, A.Y. Chen, and B. Shrivastav. Cystic fibrosis transmembrane conductance regulator and adenosine triphosphate. *Science*, 275(5304):1324–1326, February 1997.
- [73] M.L. Cotrina, J.H. Lin, A. Alves-Rodrigues, S. Liu, J. Li, H. Azmi-Ghadimi, J. Kang, C.C. Naus, and M. Nedergaard. Connexins regulate calcium signaling by controlling ATP release. *Proc Natl Acad Sci USA*, 95(26):15735–15740, December 1998.

- [74] C.E. Stout, J.L. Costantin, C.C. Naus, and A.C. Charles. Intercellular calcium signaling in astrocytes via ATP release through connexin hemichannels. *J Biol Chem*, 277(12):10482–10488, March 2002.
- [75] Y.J. Huang, Y. Maruyama, G. Dvoryanchikov, E. Pereira, N. Chaudhari, and S.D. Roper. The role of pannexin 1 hemichannels in ATP release and cell-cell communication in mouse taste buds. *Proc Natl Acad Sci USA*, pages 6436–6441, March 2007.
- [76] H.K. Kimelberg, B.A. Macvicar, and H. Sontheimer. Anion channels in astrocytes: biophysics, pharmacology, and function. *Glia*, 54(7):747–757, November 2006.
- [77] C.H. Mitchell, D.A. Carre, A.M. McGlenn, R.A. Stone, and M.M. Civan. A release mechanism for stored ATP in ocular ciliary epithelial cells. *Proc Natl Acad Sci USA*, 95(12):7174–7178, June 1998.
- [78] P. Bodin and G. Burnstock. Evidence that release of adenosine triphosphate from endothelial cells during increased shear stress is vesicular. *J Cardiovasc Pharmacol*, 38(6):900–908, December 2001.
- [79] E.M. Schwiebert. ABC transporter-facilitated ATP conductive transport. *Am J Physiol - Cell Physiol*, 276(1):C1–C8, January 1999.
- [80] R. Grygorczyk, J.A. Tabcharani, and J.W. Hanrahan. CFTR channels expressed in CHO cells do not have detectable ATP conductance. *J Membr Biol*, 151(2):139–148, May 1996.
- [81] C. Li, M. Ramjeesingh, and C.E. Bear. Purified cystic fibrosis transmembrane conductance regulator (CFTR) does not function as an ATP channel. *J Biol Chem*, 271(20):11623–11626, May 1996.
- [82] M.M. Reddy, P.M. Quinton, C. Haws, J.J. Wine, R. Grygorczyk, J.A. Tabcharani, J.W. Hanrahan, K.L. Gunderson, and R.R. Kopito. Failure of the cystic fibrosis transmembrane conductance regulator to conduct ATP. *Science*, 271(5257):1876–1879, March 1996.

- [83] R. Grygorczyk and J.W. Hanrahan. CFTR-independent ATP release from epithelial cells triggered by mechanical stimuli. *Am J Physiol*, 272(3 Pt 1):C1058–C1066, March 1997.
- [84] M. Sugita, Y. Yue, and J.K. Foskett. CFTR Cl⁻ channel and CFTR-associated ATP channel: distinct pores regulated by common gates. *EMBO J*, 17(4):898–908, February 1998.
- [85] W.J. Marshall. *Clinical Chemistry*. Mosby, Edinburgh; New York, 5th edition, 2004.
- [86] J.J.R. Fraústo da Silva and R.J.P. Williams. *The biological chemistry of the elements: the inorganic chemistry of life*. Oxford University Press, New York; Oxford, 2nd edition, 2001.
- [87] M.D. Bootman, T.J. Collins, C.M. Peppiatt, L.S. Prothero, L. MacKenzie, P. de Smet, M. Travers, S.C. Tovey, J.T. Seo, M.J. Berridge, F. Ciccolini, and P. Lipp. Calcium signalling – an overview. *Semin Cell Dev Biol*, 12(1):3–10, February 2001.
- [88] M.J. Berridge, M.D. Bootman, and P. Lipp. Calcium – a life and death signal. *Nature*, 395(6703):645–648, October 1998.
- [89] S. Ringer and H. Sainsbury. The action of potassium, sodium and calcium salts on *Tubifex Rivulorum*. *J Physiol*, 16(1-2):1–9, March 1894.
- [90] S. Ringer. A further contribution regarding the influence of the different constituents of the blood on the contraction of the heart. *J Physiol*, 4(1):29–42, January 1883.
- [91] S. Ringer. Concerning the influence of saline media on fish, etc. *J Physiol*, 5(2):98–115, June 1884.
- [92] S. Ringer. Further experiments regarding the influence of small quantities of lime potassium and other salts on muscular tissue. *J Physiol*, 7(4):291–308, September 1886.

- [93] S. Ringer. Concerning experiments to test the influence of lime, sodium and potassium salts on the development of ova and growth of tadpoles. *J Physiol*, 11(1-2):79–84, January 1890.
- [94] F.S. Locke. Notiz über den einfluss physiologischer Kochsalzlösung auf die elektrische Erregbarkeit von Muskel und Nerv. *Centralbl Physiol*, 8:166–167, 1894.
- [95] E. Overton. Beiträge zur allgemeinen Muskel- und Nervenphysiologie. iii. Mittheilung. Studien über die Wirkung der Alkali- und Erdalkalisalze auf Skelettmuskeln und Nerven. *Pflügers Arch*, 105(3):176–290, November 1904.
- [96] L.V. Heilbrunn. *An outline of general physiology*. W.B. Saunders, Philadelphia, London, 2nd edition, 1943.
- [97] O.H. Petersen, M. Michalak, and A. Verkhratsky. Calcium signalling: Past, present and future. *Cell Calcium*, 38(3-4):161–169, 2005.
- [98] A. Verkhratsky. The endoplasmic reticulum and neuronal calcium signalling. *Cell Calcium*, 32(5-6):393–404, 2002.
- [99] O.H. Petersen. Can Ca^{2+} be released from secretory granules or synaptic vesicles? *Trends Neurosci*, 19(10):411–413, October 1996.
- [100] H.C. Lee. Multiple calcium stores: separate but interacting. *Sci STKE*, 2000(40):E1–E3, July 2000.
- [101] P. Pinton, T. Pozzan, and R. Rizzuto. The Golgi apparatus is an inositol 1,4,5-trisphosphate-sensitive Ca^{2+} store, with functional properties distinct from those of the endoplasmic reticulum. *EMBO J*, 17(18):5298–5308, September 1998.
- [102] M.T. Alonso, C. Villalobos, P. Chamero, J. Alvarez, and J. Garcia-Sancho. Calcium microdomains in mitochondria and nucleus. *Cell Calcium*, 40(5-6):513–525, 2006.
- [103] K. Lange and J. Gartzke. F-actin-based Ca signaling – a critical comparison with the current concept of Ca signaling. *J Cell Physiol*, 209(2):270–287, November 2006.

- [104] M.J. Berridge. The endoplasmic reticulum: a multifunctional signaling organelle. *Cell Calcium*, 32(5-6):235–249, 2002.
- [105] Jr. Putney, J. W. New molecular players in capacitative Ca^{2+} entry. *J Cell Sci*, 120(12):1959–1965, June 2007.
- [106] Jr Putney, J.W. Recent breakthroughs in the molecular mechanism of capacitative calcium entry (with thoughts on how we got here). *Cell Calcium*, 42(2):103–110, August 2007.
- [107] V.Y. Ganitkevich. The role of mitochondria in cytoplasmic Ca^{2+} cycling. *Exp Physiol*, 88(1):91–97, January 2003.
- [108] M. Campanella, P. Pinton, and R. Rizzuto. Mitochondrial Ca^{2+} homeostasis in health and disease. *Biol Res*, 37(4):653–660, 2004.
- [109] M.D. Bootman, D. Thomas, S.C. Tovey, M.J. Berridge, and P. Lipp. Nuclear calcium signalling. *Cell Mol Life Sci*, 57(3):371–378, March 2000.
- [110] N.J. Dolman and A.V. Tepikin. Calcium gradients and the Golgi. *Cell Calcium*, 40(5-6):505–512, 2006.
- [111] F. Michelangeli, O.A. Ogunbayo, and L.L. Wootton. A plethora of interacting organellar Ca^{2+} stores. *Curr Opin in Cell Biol*, 17(2):135–140, April 2005.
- [112] M.J. Berridge. Elementary and global aspects of calcium signalling. *J Physiol*, 499(2):291–306, March 1997.
- [113] M. Zayzafoon. Calcium/calmodulin signaling controls osteoblast growth and differentiation. *J Cell Biochem*, 97(1):56–70, January 2006.
- [114] M.J. Berridge. Calcium microdomains: organization and function. *Cell Calcium*, 40(5-6):405–412, November 2006.
- [115] M.D. Bootman, L. Missiaen, J.B. Parys, H. De Smedt, and R. Castels. Control of inositol 1,4,5-trisphosphate-induced Ca^{2+} release by cytosolic Ca^{2+} . *Biochem J*, 306(2):445–451, March 1995.

- [116] J.K. Foskett, C. White, K.H. Cheung, and D.-O.D. Mak. Inositol trisphosphate receptor Ca^{2+} release channels. *Physiol Rev*, 87(2):593–658, April 2007.
- [117] W.B. Busa and R. Nuccitelli. Metabolic regulation via intracellular pH. *Am J Physiol – Regul Integr Comp Physiol*, 246(4):R409–R438, April 1984.
- [118] I. Wakabayashi, M. Poteser, and K. Groschner. Intracellular pH as a determinant of vascular smooth muscle function. *J Vasc Res*, 43(3):238–250, 2006.
- [119] J. Srivastava, D.L. Barber, and M.P. Jacobson. Intracellular pH sensors: Design principles and functional significance. *Physiology*, 22(1):30–39, February 2007.
- [120] T.J. Shuttleworth. Intracellular Ca^{2+} signalling in secretory cells. *J Exp Biol*, 200(2):303–314, January 1997.
- [121] J. Iqbal and M. Zaidi. Molecular regulation of mechanotransduction. *Biochem Biophys Res Commun*, 328(3):751–755, March 2005.
- [122] G. Martino, F. Grohovaz, E. Brambilla, F. Codazzi, A. Consiglio, E. Clementi, M. Filippi, G. Comi, and L.M. Grimaldi. Proinflammatory cytokines regulate antigen-independent T-cell activation by two separate calcium-signaling pathways in multiple sclerosis patients. *Ann Neurol*, 43(3):340–349, March 1998.
- [123] M. Nishida, Y. Hara, T. Yoshida, R. Inoue, and Y. Mori. TRP channels: Molecular diversity and physiological function. *Microcirculation*, 13(7):535–550, 2006.
- [124] V.K. Gribkoff. The role of voltage-gated calcium channels in pain and nociception. *Semin Cell Dev Biol*, 17(5):555–564, October 2006.
- [125] C.J. Jen, S.Ju Jhiang, and H.I. Chen. Cellular responses to mechanical stress: Invited review: Effects of flow on vascular endothelial intracellular calcium signaling of rat aortas ex vivo. *J Appl Physiol*, 89(4):1657–1662, October 2000.

- [126] J.C. Sánchez, T.A. Danks, and R.J. Wilkins. Mechanisms involved in the increase in intracellular calcium following hypotonic shock in bovine articular chondrocytes. *Gen Physiol Biophys*, 22(4):487–500, December 2003.
- [127] A. Menini. Calcium signalling and regulation in olfactory neurons. *Curr Opin Neurobiol*, 9(4):419–426, August 1999.
- [128] L.J. Janssen and C.Y. Kwan. ROCs and SOCs: What's in a name? *Cell Calcium*, 41(3):245–247, March 2007.
- [129] S.R. Nahorski. Pharmacology of intracellular signalling pathways. *Br J Pharmacol*, 147(S1):S38–S45, 2006.
- [130] J.W. Barclay, A. Morgan, and R.D. Burgoyne. Calcium-dependent regulation of exocytosis. *Cell Calcium*, 38(3-4):343–353, 2005.
- [131] M. Oheim, F. Kirchhoff, and W. Stuhmer. Calcium microdomains in regulated exocytosis. *Cell Calcium*, 40(5-6):423–439, 2006.
- [132] R.D. Burgoyne and A. Morgan. Secretory granule exocytosis. *Physiol Rev*, 83(2):581–632, April 2003.
- [133] R.D. Burgoyne and M.J. Clague. Calcium and calmodulin in membrane fusion. *Biochim Biophys Acta*, 1641(2-3):137–143, August 2003.
- [134] M.B. Jackson. In search of the fusion pore of exocytosis. *Biophys Chem*, 126(1-3):201–208, March 2007.
- [135] R. Jahn. Principles of exocytosis and membrane fusion. *Ann NY Acad Sci*, 1014(1):170–178, April 2004.
- [136] R. Jahn, T. Lang, and T.C. Sudhof. Membrane fusion. *Cell*, 112(4):519–533, February 2003.
- [137] R. Jahn and R.H. Scheller. SNAREs – engines for membrane fusion. *Nat Rev Mol Cell Biol*, 7(9):631–643, September 2006.
- [138] M. Leabu. Membrane fusion in cells: molecular machinery and mechanisms. *J Cell Mol Med*, 10(2):423–427, 2006.

- [139] J. García Solé, L.E. Bausá, and D. Jaque. *An Introduction to the Optical Spectroscopy of Inorganic Solids*. John Wiley and Sons, New York, 2005.
- [140] P.W. Atkins. *Physikalische Chemie*. John Wiley and Sons, Weinheim, zweite auflage edition, 1996.
- [141] M.J. Cormier, J. Lee, and J.E. Wampler. Bioluminescence: Recent advances. *Annu Rev Biochem*, 44(1):255–272, 1975.
- [142] T. Goto and Y. Kishi. Luciferins, bioluminescent substances. *Angew Chem Int Ed Engl*, 7(6):407–414, June 1968.
- [143] Therese Wilson and J.W. Hastings. Bioluminescence. *Annu Rev Cell Dev Biol*, 14(1):197–230, 1998.
- [144] F. Fan and K.V. Wood. Bioluminescent assays for high-throughput screening. *Assay Drug Dev Technol*, 5(1):127–136, February 2007.
- [145] B. Levitt, R.J. Head, and D.P. Westfall. High-pressure liquid chromatographic-fluorometric detection of adenosine and adenine nucleotides: Application to endogenous content and electrically induced release of adenylyl purines in guinea pig vas deferens. *Anal Biochem*, 137(1):93–100, February 1984.
- [146] T.D. White. Role of adenine compounds in autonomic neurotransmission. *Pharmacol Ther*, 38(2):129–168, 1988.
- [147] F. McCapra. Chemical mechanisms in bioluminescence. *Acc Chem Res*, 9(6):201–208, June 1976.
- [148] W.D. McElroy and M.A. DeLuca. Firefly and bacterial luminescence: basic science and applications. *J Appl Biochem*, 5(3):197–209, June 1983.
- [149] M. DeLuca and W.D. McElroy. Kinetics of the firefly luciferase catalyzed reactions. *Biochemistry*, 13(5):921–925, February 1974.

- [150] M. DeLuca, J. Wannlund, and W.D. McElroy. Factors affecting the kinetics of light emission from crude and purified firefly luciferase. *Anal Biochem*, 95(1):194–198, May 1979.
- [151] W.C. Rhodes and W.D. McElroy. The synthesis and function of luciferyl-adenylate and oxyluciferyl-adenylate. *J Biol Chem*, 233(6):1528–1537, December 1958.
- [152] S.R. Ford, M.S. Hall, and F.R. Leach. Enhancement of firefly luciferase activity by cytidine nucleotides. *Anal Biochem*, 204(2):283–291, August 1992.
- [153] D.M. Karl. A rapid sensitive method for the measurement of guanine ribonucleotides in bacterial and environmental extracts. *Anal Biochem*, 89(2):581–595, September 1978.
- [154] F. Boudreault and R. Grygorczyk. Cell swelling-induced ATP release and gadolinium-sensitive channels. *Am J Physiol - Cell Physiol*, 282(1):C219–C226, January 2002.
- [155] N.S. Rodionova and V.N. Petushkov. Effect of different salts and detergents on luciferin-luciferase luminescence of the enchytraeid *Fridericia heliota*. *J Photochem Photobiol B-Biol*, 83(2):123–128, May 2006.
- [156] J.L. Denburg and W.D. McElroy. Anion inhibition of firefly luciferase. *Arch Biochem Biophys*, 141(2):668–675, December 1970.
- [157] H.H. Seliger and W.D. McElroy. Spectral emission and quantum yield of firefly bioluminescence. *Arch Biochem Biophys*, 88(1):136–141, May 1960.
- [158] L.J. Kricka and M. De Luca. Effect of solvents on the catalytic activity of firefly luciferase. *Arch Biochem Biophys*, 217(2):674–681, September 1982.
- [159] A. Takahashi, P. Camacho, J.D. Lechleiter, and B. Herman. Measurement of intracellular calcium. *Physiol Rev*, 79(4):1089–1125, October 1999.

- [160] K.L. Hyrc, J.M. Bownik, and M.P. Goldberg. Ionic selectivity of low-affinity ratiometric calcium indicators: mag-Fura-2, Fura-2FF and BTC. *Cell Calcium*, 27(2):75–86, February 2000.
- [161] R.Y. Tsien. Intracellular measurements of ion activities. *Ann Rev Biophys Bioeng*, 12(1):91–116, 1983.
- [162] M.W. Roe, J.J. Lemasters, and B. Herman. Assessment of Fura-2 for measurements of cytosolic free calcium. *Cell Calcium*, 11(2-3):63–73, February 1990.
- [163] F. Di Virgilio, T.H. Steinberg, and S.C. Silverstein. Inhibition of Fura-2 sequestration and secretion with organic anion transport blockers. *Cell Calcium*, 11(2-3):57–62, February 1990.
- [164] G. Grynkiewicz, M. Poenie, and R.Y. Tsien. A new generation of Ca^{2+} indicators with greatly improved fluorescence properties. *J Biol Chem*, 260(6):3440–3450, March 1985.
- [165] Michael J. Petr and Robert D. Wurster. Determination of in situ dissociation constant for Fura-2 and quantitation of background fluorescence in astrocyte cell line U373-MG. *Cell Calcium*, 21(3):233–240, March 1997.
- [166] J.A. Thomas, R.N. Buchsbaum, A. Zimniak, and E. Racker. Intracellular pH measurements in Ehrlich ascites tumor cells utilizing spectroscopic probes generated in situ. *Biochemistry*, 18(11):2210–2218, May 1979.
- [167] T.J. Rink, R.Y. Tsien, and T. Pozzan. Cytoplasmic pH and free Mg^{2+} in lymphocytes. *J Cell Biol*, 95(1):189–196, October 1982.
- [168] R. Bals. [Cell types of respiratory epithelium: morphology, molecular biology and clinical significance]. *Pneumologie*, 51(2):142–149, February 1997. Article in German.
- [169] H. Fehrenbach. [Development of the pulmonary surfactant system]. *Pneumologie*, 61(7):488–489, July 2007. Article in German.

- [170] Y. Kikkawa and F. Smith. Cellular and biochemical aspects of pulmonary surfactant in health and disease. *Lab Invest*, 49(2):122–139, August 1983.
- [171] S.R. Walker, M.C. Williams, and B. Benson. Immunocytochemical localization of the major surfactant apoproteins in type II cells, Clara cells, and alveolar macrophages of rat lung. *J Histochem Cytochem*, 34(9):1137–1148, September 1986.
- [172] S.A. Rooney. Regulation of surfactant secretion. *Comp Biochem Physiol A – Mol Integr Physiol*, 129(1):233–243, May 2001.
- [173] H. Kleinig and P. Sitte. *Zellbiologie – Ein Lehrbuch*. Gustav Fischer Verlag, Stuttgart; New York, zweite auflage edition, 1986.
- [174] C.B. Hirschberg, P.W. Robbins, and C. Abeijon. Transporters of nucleotide sugars, ATP, and nucleotide sulfate in the endoplasmic reticulum and Golgi apparatus. *Annu Rev Biochem*, 67(1):49–69, 1998.
- [175] K. Osanai, R.J. Mason, and D.R. Voelker. Pulmonary surfactant phosphatidylcholine transport bypasses the brefeldin A sensitive compartment of alveolar type II cells. *Biochim Biophys Acta – Mol Cell Biol Lipids*, 1531(3):222–229, April 2001.
- [176] K. Osanai, C. Tsuchihara, R. Hatta, T. Oikawa, K. Tsuchihara, M. Iguchi, T. Seki, M. Takahashi, J. Huang, and H. Toga. Pulmonary surfactant transport in alveolar type II cells. *Respirology*, 11 Suppl:S70–S73, January 2006.
- [177] J.A. Whitsett, G. Ross, T. Weaver, W. Rice, C. Dion, and W. Hull. Glycosylation and secretion of surfactant-associated glycoprotein A. *J Biol Chem*, 260(28):15273–15279, December 1985.
- [178] M.F. Beers. Inhibition of cellular processing of surfactant protein C by drugs affecting intracellular pH gradients. *J Biol Chem*, 271(24):14361–14370, June 1996.

- [179] A. Chander, R.G. Johnson, J. Reicherter, and A.B. Fisher. Lung lamellar bodies maintain an acidic internal pH. *J Biol Chem*, 261(13):6126–6131, May 1986.
- [180] L.A. Brown, S.M. Pasquale, and W.J. Longmore. Role of microtubules in surfactant secretion. *J Appl Physiol*, 58(6):1866–1873, June 1985.
- [181] F.R.A.N. Rose, C.R.I.S. Kurth-Landwehr, U.L.F. Sibelius, K.A.R.L. Reuner, K.L.A.U. Aktories, W.E.R.N. Seeger, and F.R.I.E. Griminger. Role of actin depolymerization in the surfactant secretory response of alveolar epithelial type II cells. *Am J Respir Crit Care Med*, 159(1):206–212, January 1999.
- [182] W.R. Rice, K.C. Osterhoudt, and J. A. Whitsett. Effect of cytochalasins on surfactant release from alveolar type II cells. *Biochim Biophys Acta - Mol Cell Res*, 805(1):12–18, September 1984.
- [183] B. Zimmermann. Secretion of lamellar bodies in type II pneumocytes in organoid culture: effects of colchicine and cytochalasin B. *Exp Lung Res*, 15(1):31–47, 1989.
- [184] E. Urbanik and B.R. Ware. Actin filament capping and cleaving activity of cytochalasins B, D, E, and H. *Arch Biochem Biophys*, 269(1):181–187, February 1989.
- [185] H. Verschueren, I. van der Taelen, J. Dewit, J. De Braekeleer, P. De Baetselier, K. Aktories, and I. Just. Effects of clostridium botulinum C2 toxin and cytochalasin D on in vitro invasiveness, motility and F-actin content of a murine T-lymphoma cell line. *Eur J Cell Biol*, 66(4):335–341, April 1995.
- [186] U.J. Zimmerman, S.K. Malek, L. Liu, and H.L. Li. Proteolysis of synaptobrevin, syntaxin, and SNAP-25 in alveolar epithelial type II cells. *IUBMB Life*, 48(4):453–458, October 1999.
- [187] B. O. Abonyo, P. Wang, T.A. Narasaraaju, III Rowan, W.H., D.H. McMillan, U.J. Zimmerman, and L. Liu. Characterization of α -soluble N-ethylmaleimide-sensitive fusion attachment protein in alveolar type

- II cells: Implications in lung surfactant secretion. *Am J Respir Cell Mol Biol*, 29(3):273–282, September 2003.
- [188] A.V. Sokoloff, T. Whalley, and J. Zimmerberg. Characterization of *N*-ethylmaleimide-sensitive thiol groups required for the GTP-dependent fusion of endoplasmic reticulum membranes. *Biochem J*, 312(1):23–30, November 1995.
- [189] Y. Goda and S.R. Pfeffer. Identification of a novel, *N*-ethylmaleimide-sensitive cytosolic factor required for vesicular transport from endosomes to the trans-Golgi network in vitro. *J Cell Biol*, 112(5):823–831, March 1991.
- [190] J.H. Song, Y.Y. Jang, Y.K. Shin, C.S. Lee, and S. Chung. *N*-ethylmaleimide modulation of tetrodotoxin-sensitive and tetrodotoxin-resistant sodium channels in rat dorsal root ganglion neurons. *Brain Res*, 855(2):267–273, February 2000.
- [191] C. Wu and C.H. Fry. The effects of extracellular and intracellular pH on intracellular Ca^{2+} regulation in guinea-pig detrusor smooth muscle. *J Physiol*, 508 (Pt 1):131–143, April 1998.
- [192] A. Salvi, J.M. Quillan, and W. Sadee. Monitoring intracellular pH changes in response to osmotic stress and membrane transport activity using 5-chloromethylfluorescein. *AAPS PharmSci*, 4(4):E21, 2002.
- [193] A.J. Meijer, W.H. Lamers, and R.A. Chamuleau. Nitrogen metabolism and ornithine cycle function. *Physiol Rev*, 70(3):701–748, July 1990.
- [194] A.F. Holleman and E. Wiberg. *Lehrbuch der Anorganischen Chemie*. Walter de Gruyter, Berlin, New York, 101nd edition, 1995.
- [195] T.N. Nagaraja and N. Brookes. Intracellular acidification induced by passive and active transport of ammonium ions in astrocytes. *Am J Physiol – Cell Physiol*, 274(4):C883–C891, April 1998.
- [196] N.L. Nakhoul, K.S. Hering-Smith, S.M. Abdunour-Nakhoul, and L.L. Hamm. Ammonium interaction with the epithelial sodium channel. *Am J Physiol – Renal Physiol*, 281(3):F493–F502, September 2001.

- [197] A.E. Frank, C.S. Wingo, P.M. Andrews, S. Ageloff, M.A. Knepper, and I.D. Weiner. Mechanisms through which ammonia regulates cortical collecting duct net proton secretion. *Am J Physiol – Renal Physiol*, 282(6):F1120–F1128, June 2002.
- [198] V. Felipo and R.F. Butterworth. Neurobiology of ammonia. *Prog in Neurobiol*, 67(4):259–279, July 2002.
- [199] C. Rose. Effect of ammonia on astrocytic glutamate uptake/release mechanisms. *J Neurochem*, 97(s1):11–15, April 2006.
- [200] J. Browning and R. Wilkins. The effect of intracellular alkalinisation on intracellular Ca^{2+} homeostasis in a human chondrocyte cell line. *Pflügers Arch*, 444(6):744–751, September 2002.
- [201] C. Rose, W. Kresse, and H. Kettenmann. Acute insult of ammonia leads to calcium-dependent glutamate release from cultured astrocytes, an effect of pH. *J Biol Chem*, 280(22):20937–20944, June 2005.
- [202] W. Eto, K. Hirano, M. Hirano, J. Nishimura, and H. Kanaide. Intracellular alkalinization induces Ca^{2+} influx via non-voltage-operated Ca^{2+} channels in rat aortic smooth muscle cells. *Cell Calcium*, 34(6):477–484, December 2003.
- [203] S.L. Shorte, G.L. Collingridge, A.D. Randall, J.B. Chappell, and J.G. Schofield. Ammonium ions mobilize calcium from an internal pool which is insensitive to TRH and ionomycin in bovine anterior pituitary cells. *Cell Calcium*, 12(4):301–312, April 1991.
- [204] A. Minelli, S. Lyons, C. Nolte, A. Verkhratsky, and H. Kettenmann. Ammonium triggers calcium elevation in cultured mouse microglial cells by initiating Ca^{2+} release from thapsigargin-sensitive intracellular stores. *Pflügers Arch*, 439(3):370–377, January 2000.
- [205] F. Lundquist, N. Tygstrup, K. Winkler, K. Mellempgaard, and S. Munck-Petersen. Ethanol metabolism and production of free acetate in the human liver. *J Clin Invest*, 41:955–961, May 1962.

- [206] C.L. Skutches, C.P. Holroyde, R.N. Myers, P. Paul, and G.A. Reichard. Plasma acetate turnover and oxidation. *J Clin Invest*, 64(3):708–713, September 1979.
- [207] H. Yamashita, T. Kaneyuki, and K. Tagawa. Production of acetate in the liver and its utilization in peripheral tissues. *Biochim Biophys Acta - Mol Cell Biol Lipids*, 1532(1-2):79–87, May 2001.
- [208] F.J. Ballard. Supply and utilization of acetate in mammals. *Am J Clin Nutr*, 25(8):773–779, August 1972.
- [209] S.E. Knowles, I.G. Jarrett, O.H. Filsell, and F.J. Ballard. Production and utilization of acetate in mammals. *Biochem J*, 142(2):401–411, August 1974.
- [210] H.A. Barker. The path from acetylphosphate to acetyl CoA. *FASEB J*, 6(11):3014–3015, August 1992.
- [211] J.T. Daugirdas, V. Swanson, S. Islam, C. Nutting, D.D. Kim, X.A. Wang, and R.R. Fiscus. Acetate causes endothelium-independent increases in cyclic AMP in rat caudal artery. *Am J Physiol - Heart Circul Physiol*, 255(6):H1378–H1383, December 1988.
- [212] C.W. Nutting, S. Islam, M.H. Ye, D.C. Battle, and J.T. Daugirdas. The vasorelaxant effects of acetate: role of adenosine, glycolysis, lyotropism, and pH_i and Ca_i^{2+} . *Kidney Int*, 41(1):166–174, January 1992.
- [213] C. Aalkjaer, F.V. Mortensen, P.E. Jensen, and H. Nielsen. The role of $[\text{Ca}^{2+}]_i$, membrane potential and pH_i in the relaxation of rat mesenteric arteries to hyperosmolar acetate. *Pflügers Arch*, 436(5):705–711, August 1998.
- [214] K. Burvall, L. Palmberg, and K. Larsson. Metabolic activation of A549 human airway epithelial cells by organic dust: A study based on microphysiometry. *Life Sci*, 71(3):299–309, June 2002.
- [215] K.J. Buckler and R.D. Vaughan-Jones. Effects of mitochondrial uncouplers on intracellular calcium, pH and membrane potential in rat carotid body type I cells. *J Physiol*, 513(3):819–833, December 1998.

- [216] L.K. Putney, S.P. Denker, and D.L. Barber. The changing face of the Na^+/H^+ exchanger, NHE1: Structure, regulation, and cellular actions. *Annu Rev Pharmacol Toxicol*, 42(1):527–552, 2002.
- [217] H. Barriere, C. Poujeol, M. Tauc, J.M. Blasi, L. Counillon, and P. Poujeol. CFTR modulates programmed cell death by decreasing intracellular pH in Chinese hamster lung fibroblasts. *Am J Physiol - Cell Physiol*, 281(3):C810–C824, September 2001.
- [218] H. Izumi, T. Torigoe, H. Ishiguchi, H. Uramoto, Y. Yoshida, M. Tanabe, T. Ise, T. Murakami, T. Yoshida, M. Nomoto, and K. Kohno. Cellular pH regulators: potentially promising molecular targets for cancer chemotherapy. *Cancer Treat Rev*, 29(6):541–549, December 2003.
- [219] A.L. Tararthuch, R. Fernandez, and G. Malnic. Cl^- and regulation of pH by MDCK-C11 cells. *Brazilian J Med Biol Res*, 40(5):687–696, May 2007.
- [220] D.A. Scott, S.N. Moreno, and R. Docampo. Ca^{2+} storage in *Trypanosoma brucei*: the influence of cytoplasmic pH and importance of vacuolar acidity. *Biochem J*, 310(3):789–794, September 1995.
- [221] T. Speake, S. Yodozawa, and A.C. Elliott. Modulation of calcium signalling by intracellular pH in exocrine acinar cells. *Eur J Morphol*, 36 Suppl:165–169, August 1998.
- [222] T.A. Heming, N.N. Bulayeva, and A. Bidani. Cell alkalosis elevates cytosolic Ca^{2+} in rabbit resident alveolar macrophages. *Clin Sci*, 105(1):21–28, July 2003.
- [223] M. Poteser, I. Wakabayashi, C. Rosker, M. Teubl, R. Schindl, N.M. Soldatov, C. Romanin, and K. Groschner. Crosstalk between voltage-independent Ca^{2+} channels and L-type Ca^{2+} channels in A7r5 vascular smooth muscle cells at elevated intracellular pH: Evidence for functional coupling between L-type Ca^{2+} channels and a 2-APB-sensitive cation channel. *Circ Res*, 92(8):888–896, May 2003.

- [224] T. Kesvatera, B. Jonsson, A. Telling, V. Tougu, H. Vija, E. Thulin, and S. Linse. Calbindin D(9k): a protein optimized for calcium binding at neutral pH. *Biochemistry*, 40(50):15334–15340, December 2001.
- [225] R.M. Donlan and J.W. Costerton. Biofilms: survival mechanisms of clinically relevant microorganisms. *Clin Microbiol Rev*, 15(2):167–193, April 2002.
- [226] B.K. Rubin. Mucolytics, expectorants, and mucokinetic medications. *Respir Care*, 52(7):859–865, July 2007.
- [227] S.H. Randell and R.C. Boucher. Effective mucus clearance is essential for respiratory health. *Am J Respir Cell Mol Biol*, 35(1):20–28, July 2006.
- [228] U. Raviv, S. Giasson, N. Kampf, J.F. Gohy, R. Jerome, and J. Klein. Lubrication by charged polymers. *Nature*, 425(6954):163–165, September 2003.
- [229] R.C. Boucher. Evidence for airway surface dehydration as the initiating event in CF airway disease. *J Intern Med*, 261(1):5–16, 2007.
- [230] R. Tarran, L. Trout, S.H. Donaldson, and R.C. Boucher. Soluble mediators, not cilia, determine airway surface liquid volume in normal and cystic fibrosis superficial airway epithelia. *J Gen Physiol*, 127(5):591–604, April 2006.
- [231] C. Jacker. *Window on the unknown: a history of the microscope*. Scribner, New York, 1966.
- [232] R. Hooke. *Micrographia: or Some physiological descriptions of minute bodies made by magnifying glasses with observations and inquiries thereupon*. <<http://www.gutenberg.org/etext/15491>>, 2003–2006. Project Gutenberg.
- [233] The Nobel Foundation. Nobel Prize. <<http://nobelprize.org/>>, 2007.
- [234] M. Pluta. *Advanced light microscopy*, volume 1–3. Elsevier, New York, 1988.

- [235] M. Born and E. Wolf. *Principles of Optics*, volume 7th expanded. Cambridge University Press, Cambridge; New York, 1999.
- [236] H. Hartridge. Visual acuity and the resolving power of the eye. *J Physiol*, 57(1-2):52–67, December 1922.
- [237] C.P. Shillaber. *Photomicrography In Theory and Practice*. John Wiley and Sons, New York, 1944.
- [238] M. Laikin. *Lens design*. Boca Raton, FL: CRC Press, 4th edition, 2007.
- [239] M.W. Davidson. Exploring the World of Optics and Microscopy. <<http://micro.magnet.fsu.edu/>>, 1995-2007.
- [240] SCHOTT AG. SCHOTT glass made of ideas. <<http://www.schott.com/>>, 2007.
- [241] NIKON CORPORATION. Nikon CFI₆₀ Objectives. <<http://www.nikon-Instruments.com/>>, 2005.
- [242] C. Hammond. A symmetrical representation of the geometrical optics of the light microscope. *J Microsc*, 192(1):63–68, 1998.
- [243] J. A. Kiernan. *Histological and histochemical methods: theory and practice*. Butterworth Heinemann, Oxford; Boston, 1999.
- [244] F. Zernike. How I discovered phase contrast. *Science*, 121(3141):345–349, March 1955.
- [245] R.A. Cardullo. Fundamentals of image processing in light microscopy. *Method Cell Biol*, 72:217–242, 2003.
- [246] T. Inoue and N. Gliksmann. Techniques for optimizing microscopy and analysis through digital image processing. *Method Cell Biol*, 72:243–270, 2003.
- [247] K.R. Spring. Cameras for digital microscopy. *Method Cell Biol*, 72:87–102, 2003.

- [248] Ken Yoneda, Mary Mann-Jong Chang, Ken Chmiel, Yin Chen, and Reen Wu. Application of high-density DNA microarray to study smoke- and hydrogen peroxide-induced injury and repair in human bronchial epithelial cells. *J Am Soc Nephrol*, 14(8 Suppl 3):S284–S289, August 2003.
- [249] J.M. Lo-Guidice, M.D. Merten, G. Lamblin, N. Porchet, M.C. Houvenaghel, C. Figarella, P. Roussel, and J.M. Perini. Mucins secreted by a transformed cell line derived from human tracheal gland cells. *Biochem J*, 326(2):431–437, September 1997.
- [250] J. Zabner, P. Karp, M. Seiler, S.L. Phillips, C.J. Mitchell, M. Saavedra, M. Welsh, and A.J. Klingelutz. Development of cystic fibrosis and noncystic fibrosis airway cell lines. *Am J Physiol – Lung Cell Mol Physiol*, 284(5):L844–L854, May 2003.
- [251] P.H. Karp, T.O. Moninger, S.P. Weber, T.S. Nesselhauf, J.L. Launspach, J. Zabner, and M.J. Welsh. An in vitro model of differentiated human airway epithelia. Methods for establishing primary cultures. *Method Mol Biol*, 188:115–137, 2002.
- [252] M.L. Fulcher, S. Gabriel, K.A. Burns, J.R. Yankaskas, and S.H. Randell. Well-differentiated human airway epithelial cell cultures. *Method Mol Med*, 107:183–206, 2005.
- [253] L. Wiszniewski, L. Jornot, T. Dudev, A. Pagano, T. Rochat, J.S. Lacroix, S. Suter, and M. Chanson. Long-term cultures of polarized airway epithelial cells from patients with cystic fibrosis. *Am J Respir Cell Mol Biol*, 34(1):39–48, January 2006.
- [254] D.C. Gruenert, C.B. Basbaum, M.J. Welsh, M. Li, W.E. Finkbeiner, and J.A. Nadel. Characterization of human tracheal epithelial cells transformed by an origin-defective simian virus 40. *P Natl Acad Sci USA*, 85(16):5951–5955, August 1988.
- [255] A.L. Cozens, M.J. Yezzi, K. Kunzelmann, T. Ohrui, L. Chin, K. Eng, W.E. Finkbeiner, J.H. Widdicombe, and D.C. Gruenert. CFTR ex-

- pression and chloride secretion in polarized immortal human bronchial epithelial cells. *Am J Respir Cell Mol Biol*, 10(1):38–47, January 1994.
- [256] C. Ehrhardt, C. Kneuer, J. Fiegel, J. Hanes, U.F. Schaefer, K.-J. Kim, and C.-M. Lehr. Influence of apical fluid volume on the development of functional intercellular junctions in the human epithelial cell line 16HBE14o-: implications for the use of this cell line as an in vitro model for bronchial drug absorption studies. *Cell Tissue Res*, V308(3):391–400, June 2002.
- [257] M. Yamaya, W.E. Finkbeiner, S.Y. Chun, and J.H. Widdicombe. Differentiated structure and function of cultures from human tracheal epithelium. *Am J Physiol – Lung Cell Mol Physiol*, 262(6):L713–L724, June 1992.
- [258] B. Forbes, A. Shah, G.P. Martin, and A.B. Lansley. The human bronchial epithelial cell line 16HBE14o- as a model system of the airways for studying drug transport. *Int J Pharm*, 257(1-2):161–167, May 2003.
- [259] D.J. Giard, S.A. Aaronson, G.J. Todaro, P. Arnstein, J.H. Kersey, H. Dosik, and W.P. Parks. *In vitro* cultivation of human tumors: establishment of cell lines derived from a series of solid tumors. *J Natl Cancer Inst*, 51(5):1417–1423, November 1973.
- [260] M. Lieber, B. Smith, A. Szakal, W. Nelson-Rees, and G. Todaro. A continuous tumor-cell line from a human lung carcinoma with properties of type II alveolar epithelial cells. *Int J Cancer*, 17(1):62–70, January 1976.
- [261] H. Vais, G.P. Gao, M. Yang, P. Tran, J.P. Louboutin, S. Somanathan, J.M. Wilson, and W.W. Reenstra. Novel adenoviral vectors coding for GFP-tagged wtCFTR and Δ F508-CFTR: characterization of expression and electrophysiological properties in A549 cells. *Pflügers Arch*, 449(3):278–287, December 2004.
- [262] C. Dahout-Gonzalez, H. Nury, V. Trézéguet, G.J.-M. Lauquin, E. Pebay-Peyroula, and G. Brandolin. Molecular, functional, and

- pathological aspects of the mitochondrial ADP/ATP carrier. *Physiology*, 21(4):242–249, August 2006.
- [263] B.N. Kahner, H. Shankar, S. Murugappan, G.L. Prasad, and S.P. Kunapuli. Nucleotide receptor signaling in platelets. *J Thromb Haemost*, 4(11):2317–2326, 2006.
- [264] S. Murugappa and S.P. Kunapuli. The role of ADP receptors in platelet function. *Front Biosci*, 11:1977–1986, 2006.
- [265] A.J. Marcus, L.B. Saifer, M.J. Broekman, N. Islam, J.H. Fliessbach, K.A. Hajjar, W.E. Kaminski, E. Jendraschak, R.L. Silverstein, and C. von Schacky. Thrombosis and inflammation as multicellular processes: significance of cell-cell interactions. *Thromb Haemost*, 74(1):213–217, July 1995.
- [266] J.L. Boyer, T. Romero-Avila, J.B. Schachter, and T.K. Harden. Identification of competitive antagonists of the P2Y₁ receptor. *Mol Pharmacol*, 50(5):1323–1329, November 1996.
- [267] N. Panchuk-Voloshina, R.P. Haugland, J.I. Bishop-Stewart, M.K. Bhalgat, P.J. Millard, F. Mao, W.Y. Leung, and R.P. Haugland. Alexa dyes, a series of new fluorescent dyes that yield exceptionally bright, photostable conjugates. *J Histochem Cytochem*, 47(9):1179–1188, September 1999.
- [268] G.M. Roomans, I. Kozlova, H. Nilsson, V. Vanthanoouvong, B. Button, and R. Tarran. Measurements of airway surface liquid height and mucus transport by fluorescence microscopy, and of ion composition by X-ray microanalysis. *J Cyst Fibros*, 3 Suppl 2:135–139, August 2004.
- [269] M.D. Bootman, T.J. Collins, L.A.U.R. Mackenzie, H.L. Roderick, M.J. Berridge, and C.M. Peppiatt. 2-Aminoethoxydiphenyl borate (2-APB) is a reliable blocker of store-operated Ca²⁺ entry but an inconsistent inhibitor of InsP₃-induced Ca²⁺ release. *FASEB J*, 16:1145–1150, 2002.
- [270] S. Padar, D.D. Bose, J.C. Livesey, and D.W. Thomas. 2-aminoethoxydiphenyl borate perturbs hormone-sensitive calcium stores

- and blocks store-operated calcium influx pathways independent of cytoskeletal disruption in human A549 lung cancer cells. *Biochem Pharmacol*, 69(8):1177–1186, April 2005.
- [271] M. Komoszyński and A. Wojtczak. Apyrases (ATP diphosphohydrolases, EC 3.6.1.5): function and relationship to ATPases. *Biochim Biophys Acta*, 1310(2):233–241, February 1996.
- [272] MERCK & CO. The Merck Index Online, 14th Edition. <<https://themerckindex.cambridgesoft.com/>>, 2006.
- [273] S. Gagliardi, P.A. Gatti, P. Belfiore, A. Zocchetti, G.D. Clarke, and C. Farina. Synthesis and structure-activity relationships of bafilomycin A1 derivatives as inhibitors of vacuolar H⁺-ATPase. *J Med Chem*, 41(11):1883–1893, May 1998.
- [274] M. Tymianski, M.P. Charlton, P.L. Carlen, and C.H. Tator. Properties of neuroprotective cell-permeant Ca²⁺ chelators: effects on [Ca²⁺]_i and glutamate neurotoxicity in vitro. *J Neurophysiol*, 72(4):1973–1992, October 1994.
- [275] S.L. Dargan and I. Parker. Buffer kinetics shape the spatiotemporal patterns of InsP₃-evoked Ca²⁺ signals. *J Physiol-London*, 553(3):775–788, December 2003.
- [276] T. Fujiwara, K. Oda, S. Yokota, A. Takatsuki, and Y. Ikehara. Brefeldin A causes disassembly of the Golgi complex and accumulation of secretory proteins in the endoplasmic reticulum. *J Biol Chem*, 263(34):18545–18552, December 1988.
- [277] J.G. Donaldson, D. Finazzi, and R.D. Klausner. Brefeldin A inhibits Golgi membrane-catalysed exchange of guanine nucleotide onto ARF protein. *Nature*, 360(6402):350–352, November 1992.
- [278] G.A. Spiller. *Caffeine*. CRC Press LCC, 2000 Corporate Blvd., N.W., Boca Raton, Florida 33431, USA, 1998.

- [279] G. Fisone, A. Borgkvist, and A. Usiello. Caffeine as a psychomotor stimulant: mechanism of action. *Cell Mol Life Sci*, V61(7):857–872, April 2004.
- [280] B.E. Ehrlich, E. Kaftan, S. Bezprozvannaya, and I. Bezprozvanny. The pharmacology of intracellular Ca^{2+} -release channels. *Trends Pharmacol Sci*, 15(5):145–149, May 1994.
- [281] J.A. Cooper. Effects of cytochalasin and phalloidin on actin. *J Cell Biol*, 105(4):1473–1478, October 1987.
- [282] Z. Diwu, Y.X. Lu, C.L. Zhang, D.H. Klaubert, and R.P. Haugland. Fluorescent molecular probes .2. The synthesis, spectral properties and use of fluorescent solvatochromic Dapoxyl(TM) dyes. *Photochem Photobiol*, 66(4):424–431, October 1997.
- [283] M.W. Pantoliano, E.C. Petrella, J.D. Kwasnoski, V.S. Lobanov, J. Myslik, E. Graf, T. Carver, E. Asel, B.A. Springer, P. Lane, and F.R. Salemme. High-density miniaturized thermal shift assays as a general strategy for drug discovery. *J Biomol Screen*, 6(6):429–440, December 2001.
- [284] W.W. Epstein and F.W. Sweat. Dimethyl sulfoxide oxidations. *Chem Rev*, 67(3):247–260, June 1967.
- [285] S.W. Jacob. Dimethyl Sulfoxide (DMSO). <<http://www.dmsso.org/>>, 2001-2007.
- [286] T.J. Collins, P. Lipp, M.J. Berridge, W. Li, and M.D. Bootman. Inositol 1,4,5-trisphosphate-induced Ca^{2+} release is inhibited by mitochondrial depolarization. *Biochem J*, 347(2):593–600, April 2000.
- [287] I. Gautier, V. Geeraert, J. Coppey, M. Coppey-Moisan, and C. Durieux. A moderate but not total decrease of mitochondrial membrane potential triggers apoptosis in neuron-like cells. *Neuroreport*, 11(13):2953–2956, September 2000.
- [288] T.O. Berg, E. Stromhaug, T. Lovdal, O. Seglen, and T. Berg. Use of glycyl-L-phenylalanine 2-naphthylamide, a lysosome-disrupting

- cathepsin C substrate, to distinguish between lysosomes and prelysosomal endocytic vacuoles. *Biochem J*, 300(1):229–236, May 1994.
- [289] K. Kachel, E. Asuncion-Punzalan, and E. London. The location of fluorescence probes with charged groups in model membranes. *Biochim Biophys Acta – Biomembr*, 1374(1-2):63–76, September 1998.
- [290] L. Jacob, V. Beecken, L.J. Bartunik, M. Rose, and H.D. Bartunik. Purification and crystallization of yeast hexokinase isoenzymes. Characterization of different forms by chromatofocusing. *J Chromatogr*, 587(1):85–92, November 1991.
- [291] E. Claeysen and J. Rivoal. Isozymes of plant hexokinase: Occurrence, properties and functions. *Phytochemistry*, 68(6):709–731, March 2007.
- [292] A. Kaji, K.A. Trayser, and S.P. Colowick. Multiple forms of yeast hexokinase. *Ann NY Acad Sci*, 94:798–811, November 1961.
- [293] M.R. Bubb, A.M. Senderowicz, E.A. Sausville, K.L. Duncan, and E.D. Korn. Jasplakinolide, a cytotoxic natural product, induces actin polymerization and competitively inhibits the binding of phalloidin to F-actin. *J Biol Chem*, 269(21):14869–14871, May 1994.
- [294] M.R. Bubb, I. Spector, B.B. Beyer, and K.M. Fosen. Effects of jasplakinolide on the kinetics of actin polymerization. An explanation for certain *in vivo* observations. *J Biol Chem*, 275(7):5163–5170, February 2000.
- [295] D. Blasberger, S. Carmely, M. Cojocaru, I. Spector, N.R. Shochet, and Y. Kashman. On the Chemistry of Latrunculins A and B. *Liebigs Ann der Chem*, 1989(12):1171–1188, 1989.
- [296] I. Spector, N.R. Shochet, D. Blasberger, and Y. Kashman. Latrunculins – novel marine macrolides that disrupt microfilament organization and affect cell growth: I. comparison with cytochalasin D. *Cell Motil Cytoskeleton*, 13(3):127–144, 1989.
- [297] I. von Kügelgen. Pharmacological profiles of cloned mammalian P2Y-receptor subtypes. *Pharmacol Ther*, 110(3):415–432, June 2006.

- [298] G.F. Zhang, A. Driouich, and L.A. Staehelin. Effect of monensin on plant Golgi: re-examination of the monensin-induced changes in cisternal architecture and functional activities of the Golgi apparatus of sycamore suspension-cultured cells. *J Cell Sci*, 104(3):819–831, March 1993.
- [299] R.F. Luduena and M.C. Roach. Tubulin sulfhydryl groups as probes and targets for antimitotic and antimicrotubule agents. *Pharmacol Therapeut*, 49(1-2):133–152, 1991.
- [300] G.L. Lukacs, A. Nanda, O.D. Rotstein, and S. Grinstein. The chloride channel blocker 5-nitro-2-(3-phenylpropyl-amino) benzoic acid (NPPB) uncouples mitochondria and increases the proton permeability of the plasma membrane in phagocytic cells. *FEBS Lett*, 288(1-2):17–20, August 1991.
- [301] J.L. England. Stabilization and release effects of Pluronic f127 in protein drug delivery. *JUS Biochem*, 5(2):17–24, August 1998.
- [302] W.S. Liu and C.A. Heckman. The sevenfold way of PKC regulation. *Cell Signal*, 10(8):529–542, September 1998.
- [303] G. Lambrecht, K. Braun, S. Damer, M. Ganso, C. Hildebrandt, H. Ullmann, M.U. U.Kassack, and P. Nickel. Structure-activity relationships of suramin and pyridoxal-5'-phosphate derivatives as P2 receptor antagonists. *Curr Pharm Design*, 8(26):2371–2399, December 2002.
- [304] L.X.A. Tripathy, D.A. Pasek, and G.E.R.H. Meissner. Potential for pharmacology of ryanadine receptor/calcium release channels. *Ann NY Acad Sci*, 853(1):130–148, September 1998.
- [305] G.G. Du, X. Guo, V.K. Khanna, and D.H. MacLennan. Ryanodine sensitizes the cardiac Ca^{2+} release channel (ryanodine receptor isoform 2) to Ca^{2+} activation and dissociates as the channel is closed by Ca^{2+} depletion. *P Natl Acad Sci USA*, 98(24):13625–13630, November 2001.
- [306] G. Meissner. Ryanodine activation and inhibition of the Ca^{2+} release

- channel of sarcoplasmic reticulum. *J Biol Chem*, 261(14):6300–6306, May 1986.
- [307] J.T. Emmick, S. Kwon, K.R. Bidasee, K.T. Besch, and HR Jr Besch. Dual effect of suramin on calcium fluxes across sarcoplasmic reticulum vesicle membranes. *J Pharmacol Exp Ther*, 269(2):717–724, May 1994.
- [308] O. Thastrup, P.J. Cullen, B.K. Drobak, M.R. Hanley, and A.P. Dawson. Thapsigargin, a tumor promoter, discharges intracellular Ca^{2+} stores by specific inhibition of the endoplasmic reticulum Ca^{2+} -ATPase. *Proc Natl Acad Sci USA*, 87(7):2466–2470, April 1990.
- [309] M.P. Abbracchio, J.M. Boeynaems, E.A. Barnard, J.L. Boyer, C. Kennedy, M.T. Miras-Portugal, B.F. King, C. Gachet, K.A. Jacobson, G.A. Weisman, and G. Burnstock. Characterization of the UDP-glucose receptor (re-named here the P2Y_{14} receptor) adds diversity to the P2Y receptor family. *Trends Pharmacol Sci*, 24(2):52–55, February 2003.
- [310] T.A. Ta, W. Feng, T.F. Molinski, and I.N. Pessah. Hydroxylated xestospongins block inositol-1,4,5-trisphosphate-induced Ca^{2+} release and sensitize Ca^{2+} -induced Ca^{2+} release mediated by ryanodine receptors. *Mol Pharmacol*, 69(2):532–538, February 2006.

APPENDICES

Appendix A

Materials

A.1 Cell lines

A.1.1 16HBE14o-

Nomenclature

Clone number **16** of a **H**uman **B**ronchial **E**pithelial cell line; **14th** sample of human bronchial epithelial cells received in the laboratory; transformed by an origin-defective simian virus 40 (pSVori⁻) [254].

Description

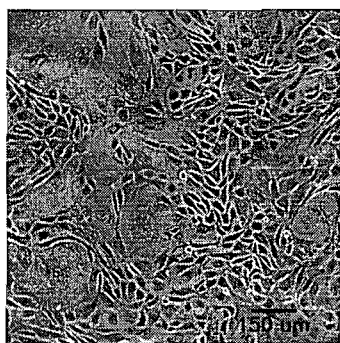


Figure
16HBE14o-

A.1:

Epithelial cells of mainstream, second-generation bronchi from a 1-year-old, male heart-lung transplant patient were transformed by calcium phosphate transfection with the pSVori⁻ plasmid [255]. The established cell line, 16HBE14o-, shows the presence of tight junctions and retains vectorial ion transport *in vitro*. When cells are grown at an air/liquid-interface, they develop cilia [255]. Both the mRNA for CFTR and the protein itself are present in the cell [256].

The choice of culture conditions is highly relevant for the proliferation and

differentiation of the cells. In addition to the choice of culture medium, substratum coating and cell-seeding density, the volumes of media on each side of the epithelial barrier is crucial for the differentiated phenotype of the cells [257].

Cultured under liquid-covered conditions, 16HBE14o- cells form layers with a height of 1-5 cells, comparable with bronchial epithelium *in vivo*. These cell layers form well-defined, tight adherens and gap junctions, as well as highly organized actin filaments which lead to high transepithelial electrical resistance (TEER) values (up to $\sim 800 \Omega \cdot \text{cm}^2$) [256]. In contrast, 16HBE14o-cells, cultured at an air/liquid interface, display no clear polar organization and form cell layers of 10-16 cells in thickness. Cellular contacts are weak, and the actin filaments show characteristics similar to cells growing separated from each other. The TEER values are not greater than $130 - 250 \Omega \cdot \text{cm}^2$ [256, 258].

Subculturing

1) *Liquid-covered culture condition:*

1. Check the confluence of the cells in a Petri dish (\varnothing 100 mm) under the microscope.
2. Warm up MEM (see section A.2.1), PBS (see section A.2.2) and trypsin (0.05 %) to 37°C .
3. Wash the cells twice with 10 ml of PBS.
4. Cover the cells with 4 ml of trypsin and incubate at 37°C for 5 min.
5. Shake the Petri dish until all cells are detached.
6. Add 10 ml of MEM, to neutralize the trypsin.
7. Transfer the cell suspension into a sterile 50 ml tube.
8. Pellet the cells by centrifugation at 1400 rpm for 5 min.
9. Resuspend the cells in 10 ml of MEM.

10. Add 3 ml of cell suspension to each Petri dish containing 7 ml of MEM.
11. Rock the Petri dishes gently to evenly distribute the cells.
12. Leave them in the incubator at 37 ° C and 5 % CO₂.
13. Replace the growth medium every 2-3 days.

Time to obtain confluent monolayer: ~ 1 week.

2) Air/liquid culture condition:

1. Coat the inverted, modified Millicell[®] Culture Plate Inserts (MCPI) (Ø 6 mm²; see section C.4) with 120µl of PureCol (Type I collagen, 3 mg/ml, pH 2; INAMED Corporation).
2. Leave the filters to dry overnight under laminar air flow.
3. Wash the filters with PBS and distribute them into 6-well plates.
4. Proceed with the cells as described above until number 9.
5. Warm up DMEM:F-12 (see section A.2.1) to 37 ° C.
6. Count the cells using a hemocytometer.
7. Pellet the cells by centrifugation at 1400 rpm for 5 min.
8. Resuspend the cells in an adequate volume of DMEM:F-12 to receive a final concentration of $1.25 \cdot 10^6$ cells/ml.
9. Fill the basal chamber of the coated MCPI with DMEM:F-12 (~ 9 ml).
10. Add 200 µl of cell suspension on the apical side of the MCPI.
11. Leave them in the incubator at 37 ° C and 5 % CO₂.
12. Replace the growth medium on the basal side every day.

13. Remove the growth medium from the apical side after 2 days in culture. Keep removing the growth medium from the apical side until the cells are confluent.

Culture time: 6-12 days.

A.1.2 A549

Nomenclature

Epithelial Adherent Cells growing in monolayers; colony number 549 [259].

Description

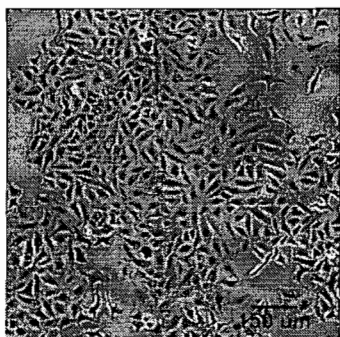


Figure A.2: A549

The A549 cell line was established from an explanted alveolar adenocarcinoma which was removed from a 58-year-old Caucasian man in 1972 [259].

A549 cells synthesize lecithin with a high percentage of disaturated fatty acids and contain multilamellar cytoplasmic inclusion bodies typical of those found in type II alveolar epithelial cells (AT II) which are responsible for pulmonary surfactant secretion [260]. They are cultured under

liquid-covered conditions and grow adherently as monolayers.

In contrast to 16HBE14o-, A549 does not contain endogenous CFTR channels [261].

Subculturing

Liquid-covered culture condition:

1. Check the confluence of the cells in a Petri dish (\varnothing 100 mm) under the microscope.

2. Warm up DMEM (see section A.2.1), PBS (see section A.2.2) and trypsin (0.05 %) to 37 ° C.
3. Wash the cells twice with 10 ml of PBS.
4. Cover the cells with 4 ml of trypsin and incubate at 37 ° C for 3 min.
5. Shake the Petri dish until all cells are detached.
6. Add 10 ml of DMEM, to neutralize the trypsin.
7. Transfer the cell suspension into a steril 50 ml tube.
8. Pellet the cells by centrifugation at 1400 rpm for 5 min.
9. Resuspend the cells in 10 ml of DMEM.
10. Add:
 - ◊ 1 ml of cell suspension to a Petri dish containing 9 ml of DMEM to receive a confluent monolayer after 5 days of culture.
 - ◊ 2 ml of cell suspension to a Petri dish containing 8 ml of DMEM to receive a confluent monolayer after 4 days of culture.
11. Rock the Petri dishes gently to evenly distribute the cells.
12. Leave them in the incubator at 37 ° C and 5 % CO₂.
13. Replace the growth medium every 2-3 days.

Doubling time: 22 h.

A.2 Solutions

A.2.1 Growth media

Recipes for growth media can vary in pH, glucose concentration, growth factors, and the presence of other nutrient components. The growth factors used to supplement media are often derived from animal blood, such as calf serum.

The medium in which cells are cultured has to be changed regularly to replenish nutrients and avoid the build up of potentially harmful metabolic biproducts and dead cells.

Dulbecco's Modified Eagle's Medium (DMEM) was used for the culture of A549, and the Minimum Essential Medium (MEM) for the culture of 16HBE14o- cells under liquid-covered conditions on culture petri-dishes or glass coverslips.

A 1:1-mixture of DMEM and Ham's Nutrient Mixture F-12 (F-12) was taken for culture of 16HBE14o- cells at an air/liquid-interface on filters.

DMEM

Preparation of 1 l:

1. Dissolve a bag of DMEM (Gibco-BRL #12100-046) in 500 ml Millipore water²⁷. Rinse the bag well!
2. Add 3.7 g of NaHCO₃.
3. Adjust the pH to 7.0 with 1 M HCl.
4. Fill up to 900 ml with Millipore water.
5. Filter through a 0.22 μ m filter under the sterile hood.
6. Store at 4 °C.
7. Before utilization add to each 500 ml:

²⁷purest water (deionized water additionally purified of organic impurities; resistance: 18.2 MW · cm @ 25 °C)

- ◇ 50 ml of FBS to reach 10% final concentration.
- ◇ 2.8 ml of penicillin-streptomycin (10 000 U/ml and 10 000 g/ml, respectively).
- ◇ 5 ml of glutamine (200 mM).

The DMEM must be pink. It turns red as soon as it is too old. penicillin-streptomycin and glutamine have to be added every 3-4 weeks.

MEM

Preparation of 1 l:

1. Dissolve a bag of MEM (Gibco-BRL #61100-061) in 500 ml Millipore water. Rinse the bag well!
2. Add 2.2 g of NaHCO₃.
3. Adjust the pH to 7.0 with 1 M HCl.
4. Fill up to 900 ml with Millipore water.
5. Filter through a 0.22 μ m filter under the sterile hood.
6. Store at 4 °C.
7. Before utilization add to each 500 ml:
 - ◇ 50 ml of FBS to reach 10% final concentration.
 - ◇ 5 ml of penicillin-streptomycin (10 000 U/ml and 10 000 g/ml, respectively).
 - ◇ 5 ml of glutamine (200 mM).

DMEM:F-12 (1:1 mixture)

Preparation of 1 l:

1. Dissolve a bag of DMEM / F-12 (Gibco-BRL #12400-024) in 500 ml Millipore water. Rinse the bag well!

2. Add 1.2 g of NaHCO_3 .
3. Adjust the pH to 7.0 with 1 M NaOH.
4. Fill up to 960 ml with Millipore water.
5. Complete to 1 l with 20 ml Ultrosor G (light sensitive) to reach 2% final concentration.
6. Filter through a 0.22 μm filter under the sterile hood.
7. Store at 4 ° C.
8. Before utilization add to each 500 ml:
 - ◇ 5 ml of penicillin-streptomycin (10 000 U/ml and 10 000 g/ml, respectively).
 - ◇ 5 ml glutamine (200 mM).

A.2.2 Balanced salt solutions (BSS)

BSSs are aqueous solutions of inorganic salts with the following principle functions:

- They serve as irrigating, transporting and diluting fluids while maintaining intra- and extra-cellular osmotic balance.
- They provide cells with water and certain bulk inorganic ions essential for normal cell metabolism.
- Combined with a carbohydrate, such as glucose, they provide the principle energy source for cell metabolism.
- They provide a buffering system to maintain the medium within the physiological pH range (7.2-7.6).

Different BSSs have been developed since the discovery that cells basically require five ions: Ca^{2+} , Mg^{2+} , K^+ , Na^+ , and Cl^- .

Physiological solution (PS)

PS is an isotonic BSS (also physiologic isotonic solution (IS)) containing a synthetic buffer, e.g. HEPES, and is used for short-time experiments (up to 2 h for A549).

Preparation of 1 l:

<i>Concentrations</i> [mM]	<i>F. W.</i> [g/mol]	<i>Amount</i> [g]
140 NaCl	58.443	8.18
5 KCl	74.561	0.37 (5 ml of 1 M stock)
10 HEPES	238.301	2.38
1 MgCl ₂ · 6H ₂ O	203.302	0.20 (10 ml of 100 mM stock)
1 CaCl ₂ · 2H ₂ O	147.016	0.15 (10 ml of 100 mM stock)
10 glucose	180.157	1.80

- ◇ Adjust the pH to 7.4 with NaOH.
- ◇ Filter the solution under the sterile hood.
- ◇ Store at 4 ° C.

Ringer solution (RS)

RS is an isotonic BSS comparable with PS. It contains, however, inorganic phosphate and carbonate salts as a buffer. It is used in case synthetic organic buffers interfere with the experiments.

Preparation of 1 l:

<i>Concentrations</i> [mM]	<i>F. W.</i> [g/mol]	<i>Amount</i> [g]
110.5 NaCl	58.443	6.46
24 NaHCO ₃	84.007	2.02
1.3 KCl	74.561	0.0969 (1.3 ml of 1 M stock)

1	MgCl ₂ · 6H ₂ O	203.302	0.20 (10 ml of 100 mM stock)
1	CaCl ₂ · 2H ₂ O	147.016	0.15 (10 ml of 100 mM stock)
2.5	Na ₂ HPO ₄	141.947	0.355
or 2.5	Na ₂ HPO ₄ · 7H ₂ O	268.053	0.67
2.5	KH ₂ PO ₄	136.085	0.34
1.2	K ₂ HPO ₄	174.175	0.21
10	glucose	180.157	1.80

- ◇ Filter the solution under the sterile hood.
- ◇ Store at 4 ° C.
- ◇ Before use, adjust the pH to 7.4 bubbling through 5% CO₂.

Phosphate buffered saline (PBS)

PBS is an isotonic BSS mainly used to wash cells. It also can be used to dilute substances.

Preparation of 1 l:

<i>Concentrations</i> [mM]	<i>F.W.</i> [g/mol]	<i>Amount</i> [g]
137.0 NaCl	58.443	8.01
2.7 KCl	74.561	0.22 (3 ml of 1 M stock)
7.7 Na ₂ HPO ₄	141.959	1.09
2.3 KH ₂ PO ₄	136.085	0.31

- ◇ Adjust the pH to 7.4 with HCl.
- ◇ Filter the solution under the sterile hood.
- ◇ Store at 4 ° C.

A.2.3 Hypotonic solution (HS)

A hypotonic solution contains a lower concentration of solutes relative to an isotonic BSSs. When a cell is placed in a hypotonic solution, the water diffuses into the cell, causing the cell to swell.

Preparation:

Hypotonic solutions were prepared starting from isotonic solutions (e.g. physiological solution, Ringer solution). The isotonic solutions were diluted to the desired concentration with Millipore water containing 1mM of CaCl_2 and 1mM of MgCl_2 to keep the concentration of the divalent cations constant. The osmolarity was controlled with a freezing point osmometer (Micro Osmometer 3300, Advanced Instruments Inc., Norwood, MA, USA).

A.3 Chemicals and active agents

Adenosine 5'-diphosphate (ADP)

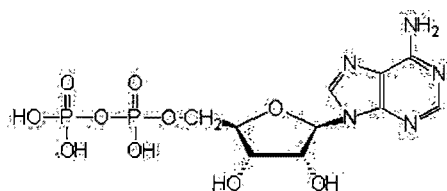


Figure A.3: ADP

Molecular formula: $C_{10}H_{15}N_5O_{10}P_2$

Molecular weight: 427.2

Description

ADP, such as ATP (see page 264), consists of an adenine ring and a ribose sugar (together called adenosine). It is the product of ATP dephosphorylation by ATPases and possesses two phosphate groups compared to three in ATP. ADP is converted back to ATP through an oxidative phosphorylation process in the mitochondrial matrix [262]. ADP also acts as an important signalling molecule. Especially in platelets, it is involved in the regulation of thrombosis and hemostasis [263]. Extracellular ADP interacts with the purinergic receptors $P2Y_1$, $P2Y_{12}$ and $P2X_1$, leading to further platelet activation [264]. In the blood, ADP is, eventually, converted to adenosine by the action of ecto-ADPases [265].

Adenosine-3'-phosphate-5'-phosphosulfate (A3P5PS)

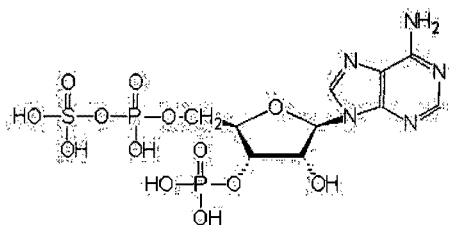


Figure A.4: A3P5PS

Molecular formula: $C_{10}H_{15}N_5O_{13}P_2S$

Molecular weight: 507.26

Stock solution: 1 mM in H_2O

Active concentration: 1 μM

Description

A3P5PS is a competitive $P2Y_1$ receptor antagonist. The presence of a phosphate in the 2'- or 3'-position appears to be crucial for antagonist activity, because adenosine-3'-phosphate-5'-phosphate and adenosine-2'-phosphate-5'-phosphate also exhibit antagonist/partial agonist activities, whereas other

3'-substituted analogues, such as 3'-amino-ATP, are full agonists with no antagonist activity [266].

Alexa Fluor[®] 488 dextran

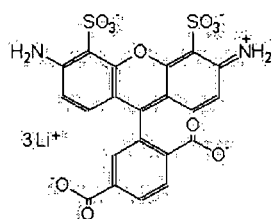


Figure A.5:
Alexa Fluor[®]
488

Molecular weight: 10 000

Stock solution: 2 mg/ml

Description

Alexa Fluor[®] 488 is a green-fluorescent dye that exhibits the following unique features: the fluorescence spectra are almost identical to those of fluorescein, with excitation/emission maxima of 495/519 nm; the absorption is strong with an extinction coefficient greater than $65\,000\text{ cm}^{-1}\text{M}^{-1}$; the photostability is much greater than that of fluorescein, allowing more time for observation and image capture; the fluorescence is pH-insensitive between pH 4 and 10 [267].

In Alexa Fluor[®] 488 dextran, the Alexa Fluor[®] 488 dye is conjugated to 10 kDa dextran (1-2 dyes per dextran). Dextrans are hydrophilic polysaccharides synthesized by *Leuconostoc bacteria*. They are characterized by their high molecular weight, good water solubility, low toxicity and relative inertness. They easily dissolve in the ASL, without penetrating across the epithelium [268].

2-Aminoethoxy-diphenylborate (2-APB)

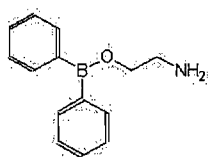


Figure A.6:
2-APB

Molecular formula: $(\text{C}_6\text{H}_5)_2\text{BOCH}_2\text{CH}_2\text{NH}_2$

Molecular weight: 225.09

Stock solution: 75 mM in DMSO

Active concentration: 75 μM

Description

2-APB is a low-cost, cell-permeable inositol-1,4,5-triphosphate receptor (InP_3R) antagonist. In addition to attenuating the release

of internal Ca^{2+} stores, 2-APB can also inhibit the store-operated channels (SOCs) that replenish the Ca^{2+} pool, and affect phospholipase C activity as well as IP_3 production [269, 270]. 2-APB can, therefore, be very useful in analyzing certain aspects of Ca^{2+} -signalling. It should, however, be used with care.

Apyrase

Activity: ~ 200 units/mg Protein

Stock solution: 1 mg/ml in H_2O

Active concentration: 2 units/ml

Description

ATP diphosphohydrolases, commonly called apyrases, are made up of a single polypeptide chain. The molecular weight of known plant apyrases varies from 40 – 51 kDa. Some apyrases from animal sources are known to be glycopeptide with a molecular weight between 50 and 189 kDa.

Apyrases are nucleotide hydrolyzing enzymes. In contrast to ATPases, which use the energy stored in ATP for metabolite and ion transport processes, apyrases reveal low substrate specificity, hydrolyzing different di- and triphosphonucleotides to their monophosphates. Their physiological role is to control the concentration of nucleotides destined for information transmission.

The optimal range of pH and temperature for apyrase activity varies from 6.5 – 7 and from 30 – 37 °C, respectively, depending on the origin (plant or animal) of the enzyme [271].

6-*N,N*-diethyl- β , γ -dibromomethylene-D-adenosine-5'-triphosphate (ARL 67156)

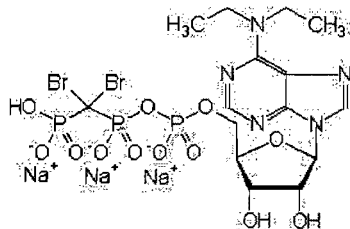


Figure A.7: ARL

Molecular formula: $C_{15}H_{21}Br_2N_5Na_3O_{12}P_3$

Formula weight: 785.05

Stock solution: 10 mM in H_2O Active concentration: 100 μM

Description

ARL 67156 is a non-hydrolyzable structural analogue of ATP and inhibits non-specifically ecto-triphosphate nucleotidases. It prevents hydrolysis of ATP without significantly acting on purinergic receptors [57].

Adenosine 5'-triphosphate (ATP)

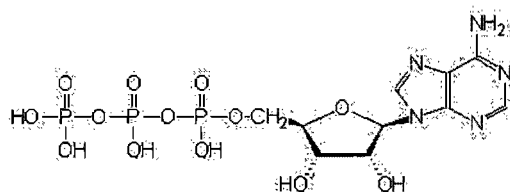


Figure A.8: ATP

Molecular formula: $C_{10}H_{16}N_5O_{13}P_3$

Molecular weight: 507.18

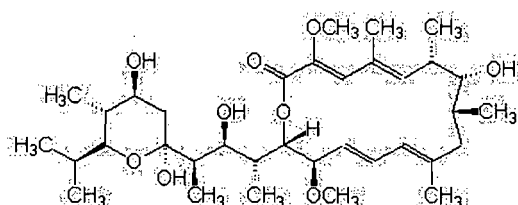
Stock solution: 10 mM in H_2O

Description

ATP consists of an adenine ring and a ribose sugar (together called adenosine) and three phosphate groups. The phosphoryl groups, starting with the group closest to the ribose ring, are referred to as the α , β , and γ phosphates. ATP is highly soluble in water and is quite stable in solutions between pH 6.8 – 7.4. However, it is rapidly hydrolyzed at extreme pH and should be best stored as an anhydrous salt [272].

ATP is the main energy source for the majority of cellular functions. This includes the synthesis of macromolecules and their transportation within the cytoplasm and across membranes. Beyond this, ATP – and its hydrolysis products ADP (see page 261), AMP and adenosine – functions as a signalling molecule in the extracellular space of almost all cells of the body [38].

Bafilomycin A1



Molecular formula: $C_{35}H_{58}O_9$

Molecular weight: 622.83

Stock solution: 100 μM in DMSO

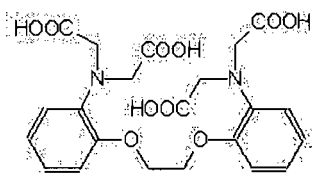
Active concentration: 1 μM

Description

Figure A.9: Bafilomycin A1

Bafilomycin A1 is a macrolide antibiotic produced by *Streptomyces griseus*. It is a highly specific inhibitor of vacuolar type H^+ -ATPase (V-ATPase). However, it is not selective for any particular subclass, but, instead generally inhibits all essential V-ATPases [273].

1,2-Bis(2-aminophenoxy)ethane-*N,N,N',N'*-tetraacetic acid (BAPTA)



Molecular formula: $C_{22}H_{24}N_2O_{10}$

Molecular weight: 476.43

Stock solution: 5 mM in H_2O

Active concentration: 25 μM

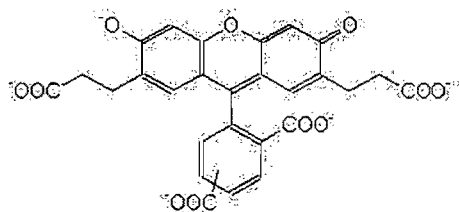
Figure A.10:
BAPTA

Description

BAPTA is a Ca^{2+} -specific chelator. The presence of four carboxylic acid functional groups makes the binding of two Ca^{2+} ions possible. The flexibility of the functional groups is crucial for the coordination geometry of the divalent Ca^{2+} ions.

BAPTA has a high affinity to Ca^{2+} with a dissociation constant $K_d \approx 100$ nM [274]. It has fast buffer kinetics and is used in the AM-form for noninvasive cell loading as intracellular Ca^{2+} -buffer [275].

2',7'-bis-(2-carboxyethyl)-5,6-carboxyfluorescein (BCECF)



Molecular formula: $C_{27}H_{15}O_{11}$

Molecular weight: 515.41

Stock solution: 1 mM in DMSO

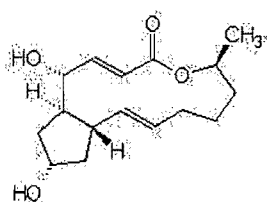
Active concentration: 2.5 μ M

Description

Figure A.11: BCECF, free acid

BCECF is the most widely used fluorescent indicator for intracellular pH with a pK_a of 7.0, which matches the normal range of cytoplasmic pH (~6.8 - 7.4). It belongs – such as Fura-2 (see page 270) – to the group of ratiometric indicators with excitation wavelengths of 440 and 495 nm. The acetoxymethyl ester derivative (BCECF-AM) is membrane-permeable and allows non-invasive bulk loading of cells [167].

Brefeldin A (BFA)



Molecular formula: $C_{16}H_{24}O_4$

Molecular weight: 280.36

Stock solution: 5 mg/ml in DMSO

Active concentration: 10 μ g/ml

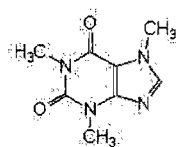
Figure A.12:

Brefeldin A

Description

Brefeldin A is a macrolide antibiotic produced by fungal organisms such as *Eupenicillium brefeldianum*. It strongly inhibits protein transport from the ER to the Golgi complex [276]. The main target of Brefeldin A appears to be a GTP-exchange factor responsible for activating the GTP-binding protein ADP-ribosylation factor (ARF1). ARF1 is involved in the formation of transport vesicles by recruiting coat proteins to intracellular membranes [277].

Caffeine



Molecular formula: $C_8H_{10}N_4O_2$

Molecular weight: 194.19

Active concentration: 10 mM

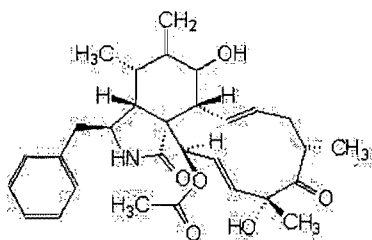
Figure A.13: *Description*

Caffeine Caffeine is a xanthine alkaloid compound which can be found in the leaves and beans of the coffee plant, in tea, as well as in the beans, leaves and fruits of more than 60 plants [278].

Caffeine is a central nervous system stimulant believed to act through adenosine receptors. It is an adenosine receptor antagonist and adenosine 3',5'-cyclic monophosphate (cAMP) phosphodiesterase inhibitor [279].

It also affects intracellular calcium levels, acting as an agonist for the ryanodine receptor and as an inhibitor of the InP_3R on the ER [280].

Cytochalasin D



Molecular formula: $C_{30}H_{37}NO_6$

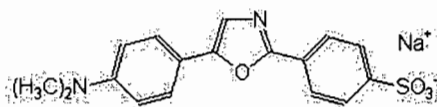
Molecular weight: 507.62

Stock solution: 10 mM in H_2O

Active concentration: 2 μM

Description

Cytochalasin D Cytochalasins are a group of fungal metabolites which permeate the cell membrane, bind to one end of actin filaments and inhibit the association and dissociation of subunits [281]. Cytochalasin D was found to be very effective in binding to the barbed end of actin filaments [281].

Dapoxyl[®] sulfonic acid, sodium saltFigure A.15: Dapoxyl[®]Molecular formula: C₁₇H₁₅N₂NaO₄S

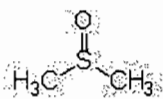
Molecular weight: 366.37

Stock solution: 10 mM in H₂O

Active concentration: 10 μM

Description

5-(4''-Dimethylaminophenyl)-2-(4'-phenyl)oxazoles are fluorescent solvatochromic dyes whose fluorescence strongly depends on solvent polarity. The fluorescence-environment dependence, large extinction coefficients, high fluorescence quantum yields, and large Stokes shift of the fluorophores are used for the development of fluorescent molecular probes to study a variety of biological events and processes [282]. Dapoxyl sulfonic acid is an amphiphilic dapoxyl derivative with an absorption maxima near 370 nm, and an emission maximum close to 520 nm when bound to phospholipid bilayer membranes [283].

Dimethylsulfoxide (DMSO)Molecular formula: (CH₃)₂SO

Molecular weight: 78.13

Solubility: miscible in water, ethanol, chloroform, benzene

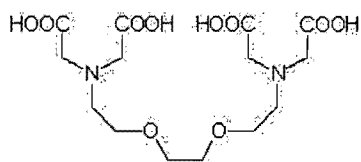
Figure A.16: Melting point: 18.5 °C

DMSO Boiling point: 189 °C

Description

DMSO is a colourless polar aprotic solvent. It readily dissolves a variety of organic substances as well as many inorganic salts and gases. Pure DMSO is not considered toxic. However, DMSO increases the rate of absorption of some compounds through organic tissues including skin, which makes it potentially dangerous [284]. On the other hand, DMSO can be used as a drug delivery system, when properly administered, on account of this property [285].

Ethylene glycol-bis(β -aminoethylether)-*N,N,N',N'*-tetraacetic acid (EGTA)



Molecular formula: $C_{14}H_{24}O_{10}N_2$

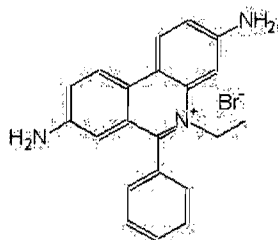
Molecular weight: 380.35

Active concentration: 100 μ M

Description

Figure A.17: EGTA
EGTA is a chelating agent that is related to the better known ethylenediaminetetraacetic acid (EDTA), but with a much higher affinity for Ca^{2+} than for Mg^{2+} ions. It has a similar affinity to Ca^{2+} as BAPTA (see page 265), but its buffer kinetics is slow [274, 275]. It is usually used for making BSSs with a low content of Ca^{2+} .

Ethidium bromide



Molecular formula: $C_{21}H_{20}BrN_3$

Formula weight: 394.31

Stock solution: 10 mg/ml in H_2O

Active concentration: 10 μ g/ml

Description

Figure A.18:
Ethidium bromide
Ethidium bromide (systematic nomenclature: 2,7-Diamino-10-ethyl-6-phenylphenanthridinium bromide) is a fluorescent, intercalating agent for nucleic acid. It is commonly used to detect nucleic acids from PCRs, restriction digests, etc. It can also be used to differentiate between viable and necrotic cells.

Ethidium bromide is a very strong mutagen, carcinogen and teratogen [272].

FCCP (Carbonylcyanide-4-(trifluoromethoxy)phenyl-hydrazine)

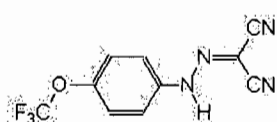


Figure A.19:
FCCP

Molecular formula: $C_{10}H_5F_3N_4O$

Molecular weight: 254.17

Stock solution: 0.5 mM in DMSO

Active concentration: 10 μ M

Description

FCCP is a protonophore (H^+ ionophore) and an uncoupler of mitochondrial phosphorylation. It reduces intracellular pH and is capable of depolarizing the mitochondrial membranes and the plasma membrane [286]. Treatment of cells with FCCP at varying concentrations leads to partial (100 nM) or complete (10 μ M) depolarization and apoptosis [287].

Fura-2-AM (Fura-2 pentakis(acetoxymethyl)ester)

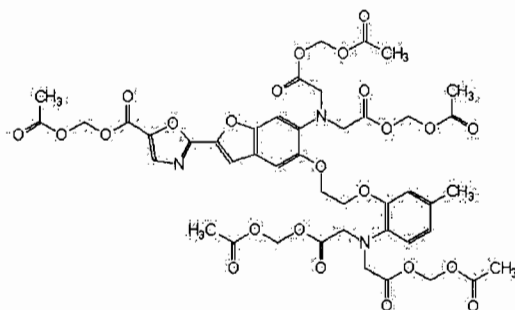


Figure A.20: Fura 2-AM

Molecular formula: $C_{44}H_{47}N_3O_{24}$

Molecular weight: 1001.85

Stock solution: 0.5 mM in DMSO

Active concentration: 2.5 μ M

Description

Fura-2 is an intracellular fluorescent indicator with a high selectivity and low affinity for Ca^{2+} ($K_d \approx 224$ nM) [164]. It belongs to the group of ra-

tiometric indicators (see also BCECF page 266) with excitation wavelengths of 340 and 380 nm. The intensity of fluorescent emission depends on the concentration of the dye, the thickness of the cell, an optical constant of the set-up, and a non-linear function of the Ca^{2+} -concentration. Ratioing has, therefore, the advantage of reducing the effects of uneven dye-loading, dye-leakage, and photo-bleaching [164]. The AM form is used for noninvasive intracellular loading [164].

Glycyl-L-Phenylalanin- β -Naphthylamide (GPN)

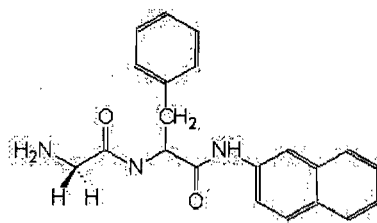


Figure A.21: GPN

Molecular formula: $C_{21}H_{21}N_3O_2$

Molecular weight: 347.41

Stock solution: 100 mM in DMSO

Active concentration: 100 μ M

Description

GPN is a substrate for cathepsin C, a protease located exclusively in lysosomes. GPN diffuses to the lysosomes after permeabilization of the cell membrane. It is hydrolyzed by cathepsin C and the hydrolysis products are trapped inside the lysosomes due to their increased polarity. The accumulation of these substrates causes an osmotic lysis of the lysosomes [288]. GPN appears to be an excellent tool for the specific disruption of lysosomes.

5-Hexadecanoylamino fluorescein (HAF)

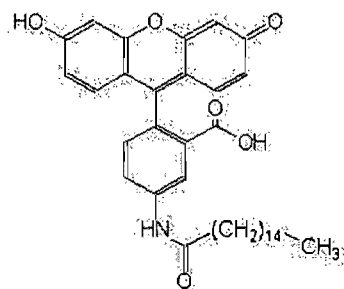


Figure A.22: 5-Hexadecanoylamino fluorescein

Molecular formula: $C_{36}H_{43}NO_6$

Molecular weight: 585.74

Stock solution: 10 mg/ml DMSO

Active concentration: 10 μ g/ml

Description

Fluorescein is a hydrophilic fluorophore with a pH-dependent absorption maximum at 494 nm and emission maximum at 521 nm in water [272]. 5-Hexadecanoylamino fluorescein is an amphiphilic isocyanate-derivative of fluorescein with an alkyl tail. It is a fluorescent membrane probe that localizes at the aqueous interface of cell membranes. The lipophilic alkyl tail anchors in the outer lipid layer, and the polar fluorescein-group resides on the outer surface of the cell membrane [289]. To minimize dye internalization, experiments should be carried out between 21 – 23 °C.

Hexokinase

Activity: ≥ 135 units/mg Protein

Stock solution: 1 mg/ml in H₂O

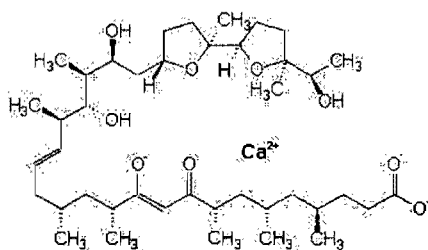
Active concentration: 10 units/ml

Description

Hexokinase is a dimeric protein made of two equal ~ 54 kDa monomers [290]. It catalyzes the phosphorylation of D-hexose sugars at the C6 position utilizing ATP as a phosphate source, which is the first step of intracellular metabolic processes such as glycolysis and glycogen synthesis [291].

The rate of phosphorylation varies with different hexoses and Nucleotides triphosphates, and is highest with D-glucose and ATP. The optimal range of pH and temperature for hexokinase activity lies between 7.5 – 9 and from 25 – 33 °C depending on its isoform [292].

Ionomycin



Molecular formula: C₄₁H₇₀CaO₉

Formula weight: 747.07

Stock solution: 1 mM in DMSO

Active concentration: 1-5 μ M

Description

Ionomycin is a nonfluorescent Ca²⁺-ionophore used to transport Ca²⁺ across biological membranes [272]. In the presence of high extracellular Ca²⁺-concentrations it can induce apoptotic degeneration of the cell due to the sudden increase of intracellular Ca²⁺ [272].

Jasplakinolide

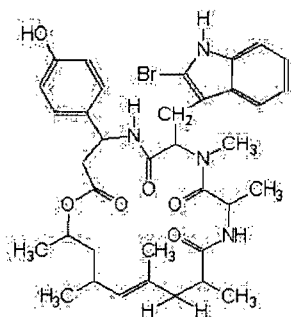


Figure A.24: Jasplakinolide

Molecular formula: $C_{36}H_{45}BrN_4O_6$

Molecular weight: 709.68

Stock solution: 1 mM in DMSO

Active concentration: 1 μ M

Description

Jasplakinolide is a membrane-permeable cyclic peptide produced by the marine sponge *Jaspis johnstoni*.

It is composed of three amino acids, D-alanine as well as the rare D- β -tyrosine and D-2-bromoabrine [293].

It induces actin polymerization and stabilizes actin filaments. The peptide has a much greater effect on Mg^{2+} -actin than on Ca^{2+} -actin [294].

Latrunculin A

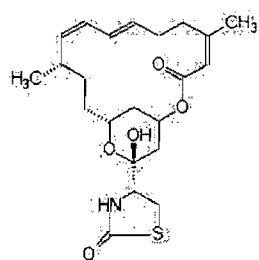


Figure A.25: Latrunculin A

Molecular formula: $C_{22}H_{31}NO_5S$

Molecular weight: 421.55

Stock solution: 1 mM in DMSO

Active concentration: 1 μ M

Description

Latrunculin A is a membrane-permeable macrolide toxin produced by the Red Sea sponge *Latrunculia magnifica*.

Besides the macrolide ring, it is composed of a rare 2-thiazolidinone ring as well as a tetrahydropyran-lactol ring [295]. Latrunculin A is an actin-disrupting agent, which prevents microfilament polymerization due to one-to-one binding with monomeric G-actin. Latrunculin does not, however, alter the microtubular structure [296].

2-(Methylthio)adenosine 5'-diphosphate (2-MeSADP)

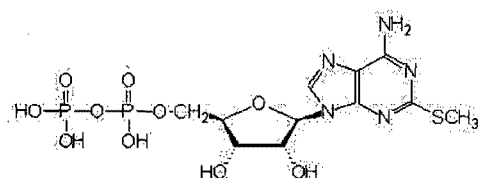


Figure A.26: 2-MeSADP

Molecular formula: $C_{11}H_{17}N_5O_{10}P_2S$

Molecular weight: 539.24

Description

2-MeSADP is an ADP analogue with a 10-times higher affinity to the human P2Y₁-receptor than ADP [297].

Monensin

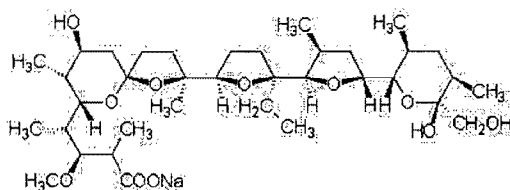


Figure A.27: Monensin

Molecular formula: $C_{36}H_{61}NaO_{11}$

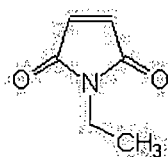
Formula weight: 692.85

Stock solution: 10 mM in DMSO

Active concentration: 10 μ M

Description

Monensin, a polyether antibiotic, is a monovalent ionophore that exchanges Na^+ , K^+ ions and protons across membranes. It affects the acidification of acidic compartments and has been shown to influence the function of the Golgi apparatus. It causes swelling of Golgi cisternae and secretory vesicles; slows or arrests intra-Golgi transport of newly synthesized secretory proteins; interferes with the late Golgi functions, such as proteolytic processing and attaching of terminal sugars to N-linked glycoproteins; and leads to the accumulation of membrane and secretory protein precursors in medial or trans-Golgi cisternae [298].

N-Ethylmaleimide (NEM)Molecular formula: $C_6H_7NO_2$

Molecular weight: 125.13

Stock solution: 1 M in Methanol

Active concentration: 1 mM

Figure A.28:

NEM

Description

NEM is a chemical derivative of maleic acid imide. It alkylates sulfhydryl groups, thereby irreversibly inhibiting the formation of cysteine linkages in proteins. As a result of the alkylation of the *N*-ethylmaleimide sensitive fusion protein (NSF), NEM blocks vesicular transport [272].

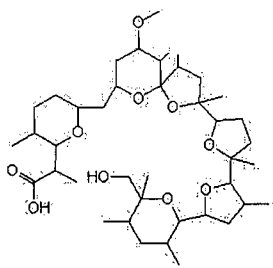
Nigericin

Figure A.29:

Nigericin

Molecular formula: $C_{40}H_{68}O_{11}$

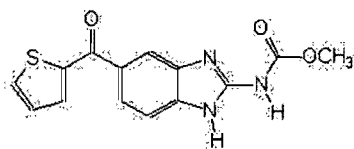
Molecular weight: 724.97

Stock solution: 10 mM in DMSO

Active concentration: 10-50 μ M*Description*

Nigericin is a polyether antibiotic produced by *Streptomyces hygroscopicus*. It acts as an ionophore for monovalent cations with an ion selectivity such as K^+ , H^+ , Rb^+ and Na^+ . It most commonly functions as an antiporter of H^+ and K^+ [272].

Nocodazole



Molecular formula: C₁₄H₁₁N₃O₃S

Molecular weight: 301.32

Stock solution: 20 mM in DMSO

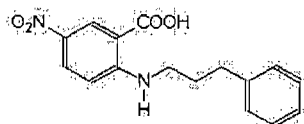
Active concentration: 20 μM

Figure A.30: Nocodazole

Description

Nocodazole is a synthetic antimitotic agent that disrupts microtubules by binding to β-tubulin. It prevents the formation of interchain disulfide linkage, thus inhibiting microtubule dynamics, disrupting the mitotic spindle function, and fragmenting the Golgi complex [299].

5-Nitro-2-(3-phenylpropylamino)benzoic acid (NPPB)



Molecular formula: C₁₆H₁₆N₂O₄

Molecular weight: 300.31

Stock solution: 125 mM in DMSO

Active concentration: 125 μM

Figure A.31: NPPB

Description

NPPB is a chloride channel blocker, which is highly membrane permeable. It blocks unselectively all kinds of chloride channels in a reversible manner. In addition, it has been shown to have protonophoric activity, potentially disturbing cytosolic pH and mitochondrial ATP synthesis [300].

Oligomycins

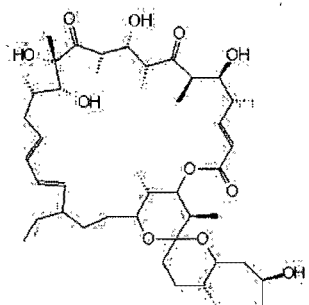


Figure A.32:
Oligomycin A

Oligomycin A

Molecular formula: $C_{45}H_{74}O_{11}$

Molecular weight: 791.06

Stock solution: 10 mM in DMSO

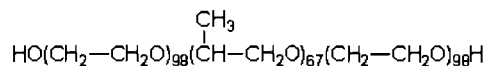
Active concentration: 10 μ M

Description

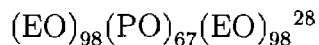
Oligomycin A, B, C and D are a complex of several closely related compounds of macrolide antibiotics produced by *Streptomyces diastatochromogenes*.

They inhibit oxidative phosphorylation in the mitochondria [272].

Pluronic[®] F-127



Average molecular formula:



Average molecular weight: 12 600

Figure A.33: Pluronic[®] F-127

Description

Pluronic[®] F-127 is a polyoxypropylenepolyoxyethylene block copolymer with a low absorbance in UV. It is a non-ionic detergent which can be dissolved in DMSO up to a final concentration of 0.2% (w/v). It is non-toxic and often used to facilitate cell loading with AM-compounds. The 0.2% (w/v) solution can be used to prepare the compound stock solution [301].

²⁸(EO) = ethylene oxide; (PO) = propylene oxide.

Phorbol 12-myristate 13-acetate (PMA)

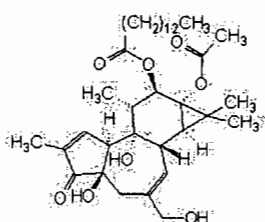


Figure A.34:
PMA

Molecular formula: $C_{36}H_{56}O_8$

Molecular weight: 616.83

Stock solution: 1 mM in DMSO

Active concentration: 1 μ M

Description

PMA is an activator of the signal transduction enzyme protein kinase C (PKC). The effects of PMA on PKC result from its similarity to diacylglycerol (DAG), which is one of the natural activators of some PKC isoforms [302]. It has also been shown to be a highly potent tumor promoter and mitogen [272].

Pyridoxal phosphate-6-azo(benzene-2,4-disulfonic acid) tetrasodium salt (PPADS)

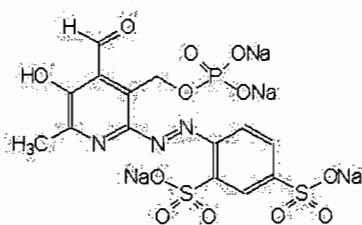


Figure A.35: PPADS

Molecular formula: $C_{14}H_{10}N_3Na_4O_{12}PS_2$

Molecular weight: 599.31

Stock solution: 100 mM in H_2O

Active concentration: 100 μ M

Description

PPADS is a highly specific, non-selective (but non-universal) P2 antagonist with a small preference for P2X₁ receptors. It also blocks P2X₂, P2X₃, P2X₅ and P2Y₁ receptors with similar potencies. It is weaker as an antagonist for homomeric P2X₄, P2X₆ and P2X₇, P2Y₄, P2Y₆, P2Y₁₁ and P2Y₁₂ receptors [303].

Probenecid

Molecular formula: $C_{13}H_{19}NO_4S$

Molecular weight: 285.36

Active concentration: 2.5 mM

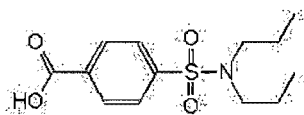


Figure A.36: Probenecid

Description

Probenecid is commonly used to inhibit organic-anion transporters located in the cell membrane. Such transporters can extrude dyes and indicators and thus contribute to poor loading or a high background signal in assays based on retention of the dyes or indicators inside cells [163].

Ruthenium Red

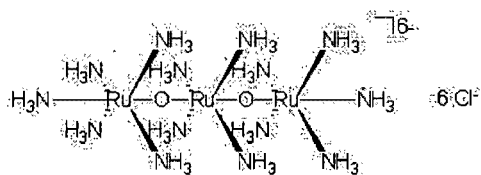


Figure A.37: Ruthenium Red

Molecular formula: $N_{14}H_{42}O_2Cl_6Ru_3$

Formula weight: 786.35

Stock solution: 100 mM in H_2O

Active concentration: 100 μM

Description

Ruthenium red is a polycationic reagent that is effective in inhibiting ER Ca^{2+} release channels. In contrast to heparin and caffeine, it inhibits only the ryanodine receptor without affecting the InP_3R [280, 304].

Ryanodine

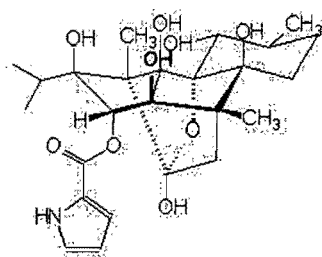


Figure A.38: Ryanodine

Molecular formula: $C_{25}H_{35}NO_9$

Molecular weight: 493.63

Stock solution: 100 mM in H_2O

Active concentration: 100 μM

Description

Ryanodine is a naturally occurring alkaloid which binds specifically to a Ca^{2+} release channel on the ER with high affinity. It also accounts for the name of this Ca^{2+} release channel, the ryanodine receptor channel (RyR).

Stimulation or inhibition of Ca^{2+} efflux by ryanodine is influenced by divalent cation concentration, temperature and time of incubation, as well as by the concentration of ryanodine itself. At low concentrations ($< 10 \mu\text{M}$), ryanodine sensitizes the channel to activation and dissociates along with the closure of the channel [305]. At high concentrations ($> 10 \mu\text{M}$), ryanodine blocks the release of Ca^{2+} through the RyR Ca^{2+} channels [306].

Suramin

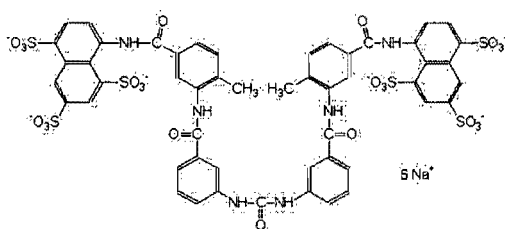


Figure A.39: Suramin

Mol. formula: $\text{C}_{51}\text{H}_{34}\text{N}_6\text{Na}_6\text{O}_{23}\text{S}_6$

Molecular weight: 1429.17

Stock solution: 100 mM in H_2O

Active concentration: 100 μM

Description

Suramin is a symmetric polysulfonated naphthylurea. It releases Ca^{2+} from skeletal muscle sarcoplasmic reticulum vesicles in a concentration-dependent manner and is also a ligand for P2 receptors [307]. However, its interaction with a large range of other proteins, in addition to P2 receptors, limits the application of this agent as a tool for the characterization of P2 receptors. These proteins include interleukin, glutamate, nicotinic, 5-hydroxytryptamine and GABA receptors, various proteases, Na^+/K^+ - and Ca^{2+} -ATPases, ecto-nucleotidases, G protein-coupled receptor kinases, as well as G protein subunits, basic fibroblast growth factor and reverse transcriptase [303].

Thapsigargin

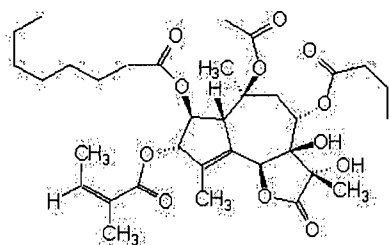


Figure A.40: Thapsigargin

Thapsigargin is a plant-derived sesquiterpene lactone, and functions as a membrane-permeable, tight-binding inhibitor of the sarco/endoplasmic reticulum Ca^{2+} -ATPase (SERCA). It increases the concentration of cytosolic free Ca^{2+} in sensitive cells by an acute and highly specific arrest of the sarco/endoplasmic reticulum Ca^{2+} pump, followed by a rapid Ca^{2+} leak from the IP_3R and RyR Ca^{2+} channels [308].

Molecular formula: $\text{C}_{34}\text{H}_{50}\text{O}_{12}$

Molecular weight: 650.75

Stock solution: 1 mM in DMSO

Active concentration: 1 μM

Description

Uridine 5'-diphosphate (UDP)

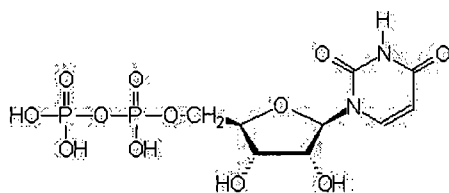


Figure A.41: UDP

UDP serves as a carrier for hexoses, hexosamines and hexuronic acids in the synthesis of glycogen, glycoproteins and glycosaminoglycans. It is also an agonist of P2Y_6 receptors [272].

Molecular formula: $\text{C}_9\text{H}_{14}\text{N}_2\text{O}_{12}\text{P}_2$

Molecular weight: 404.16

Stock solution: 10 mM in H_2O

Description

Uridine 5'-diphosphoglucose (UDP-glc)

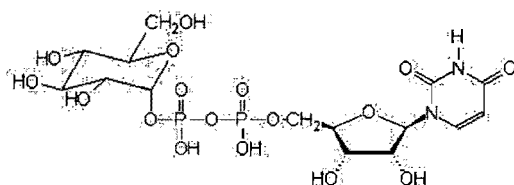


Figure A.42: UDP-glucose

Molecular formula: $C_{15}H_{22}N_2O_{17}P_2$

Molecular weight: 564.29

Stock solution: 10 mM in H_2O

Description

UDP-glucose is used in cells as an activated form of glucose, as a substrate for glycosyltransferases as well as for glycogen and glycoprotein metabolism. In the extracellular space, it functions as a specific agonist for the $P2Y_{14}$ receptor [309].

Uridine 5'-triphosphate (UTP)

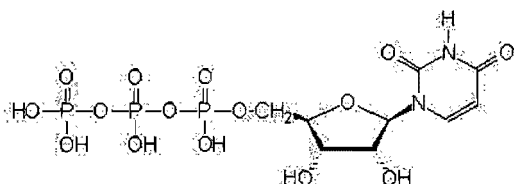


Figure A.43: UTP

Molecular formula: $C_9H_{15}N_2O_{15}P_3$

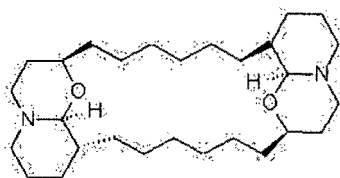
Molecular weight: 484.14

Stock solution: 10 mM in H_2O

Description

UTP is a pyrimidine analog of ATP. It is an activated precursor in the synthesis of RNA, and in glycogen and glycoprotein metabolism. It is also an agonist of $P2Y_2$ and $P2Y_4$ receptors that activate chloride channels in epithelial cells, increasing ciliary beat frequency and inducing degranulation of goblet cells in airway epithelia [272].

Xestospongine C



Molecular formula: $C_{23}H_{50}N_2O_2$

Molecular weight: 446.71

Stock solution: 1 mM in DMSO

Active concentration: 3-10 μM

Figure A.44:

Xestospongine C

Description

Xestospongine C is a marine alkaloid isolated from the Okinawan sponge *Xestospongia Sp.*. It is a potent, cell-permeable inhibitor of IP₃R-mediated Ca²⁺-release. It also sensitizes RyR-mediated CICR [310].

Appendix B

Microscope components

The components of a Nikon Inverted Microscope ECLIPSE TE300, which was used in the course of this Ph.D. project, are depicted on the following two pages.

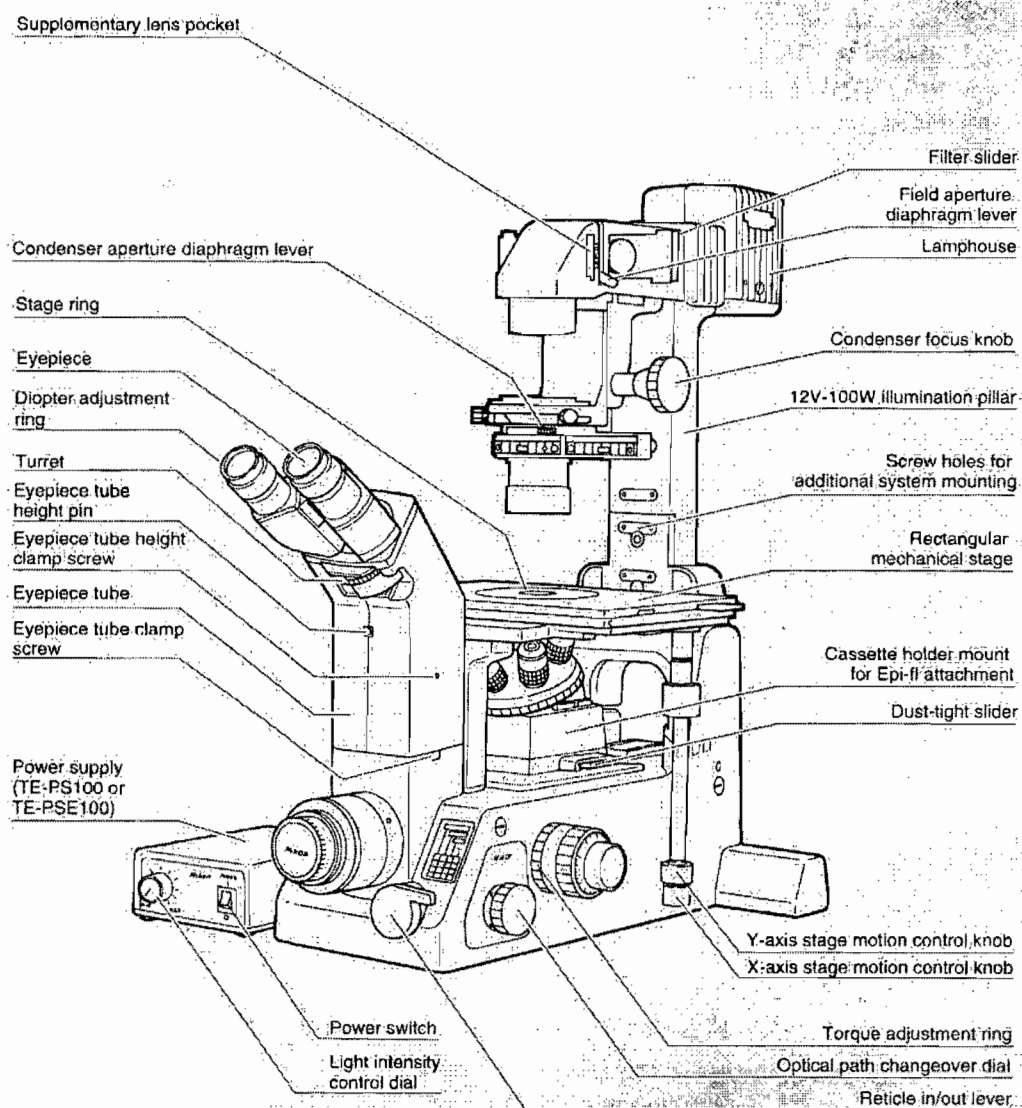


Figure B.1: Right-hand view of the Nikon inverted microscope TE300; taken from the microscope operation manual

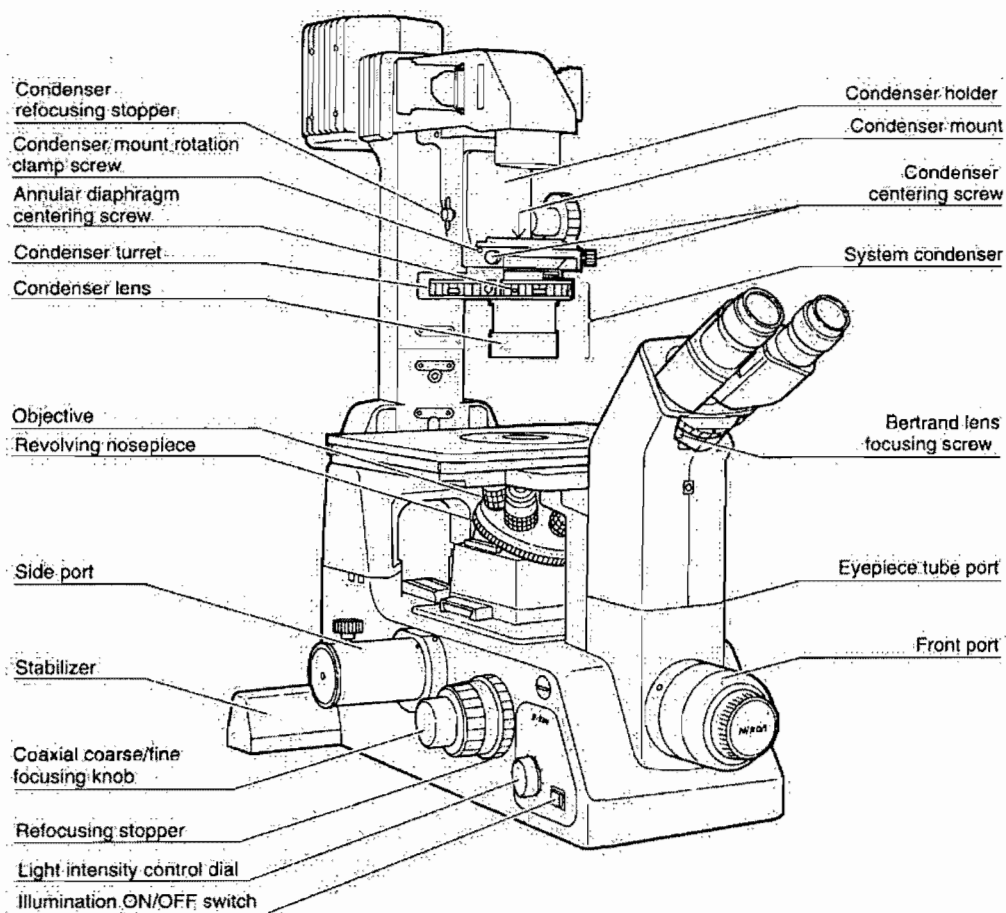


Figure B.2: Left-hand view of the Nikon inverted microscope TE300; taken from the microscope operation manual

Appendix C

Technical drawings

C.1 Side-view microscopy set-up – Essential elements

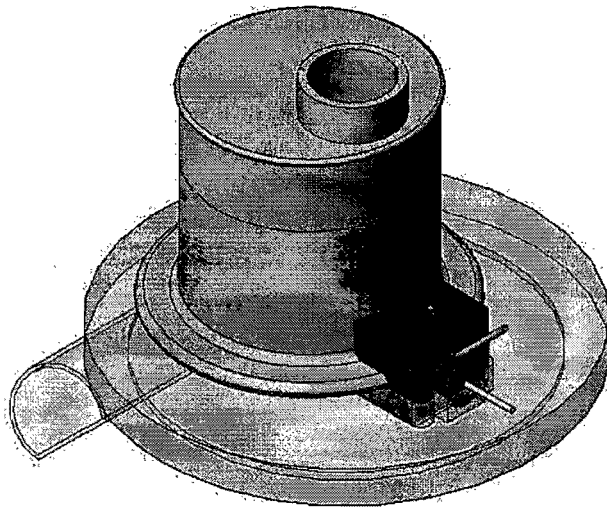


Figure C.1: Assembled view of the entire stage set-up

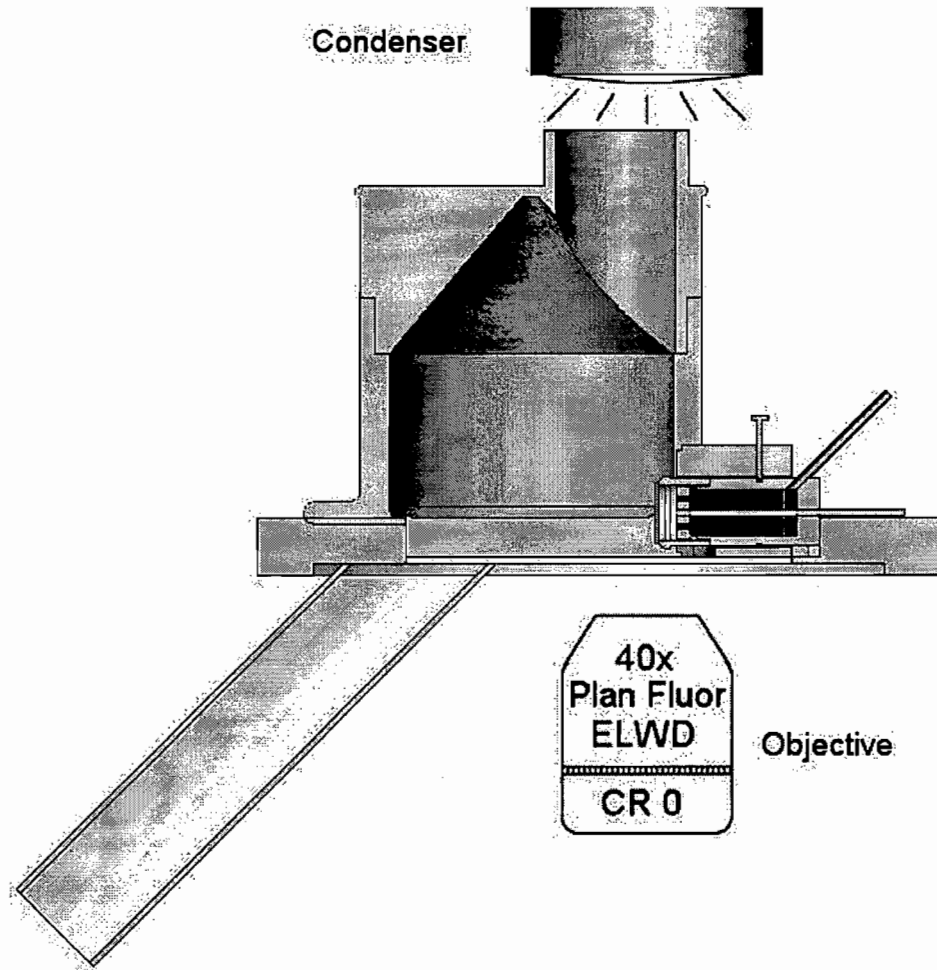


Figure C.2: Cross-section of the entire stage set-up

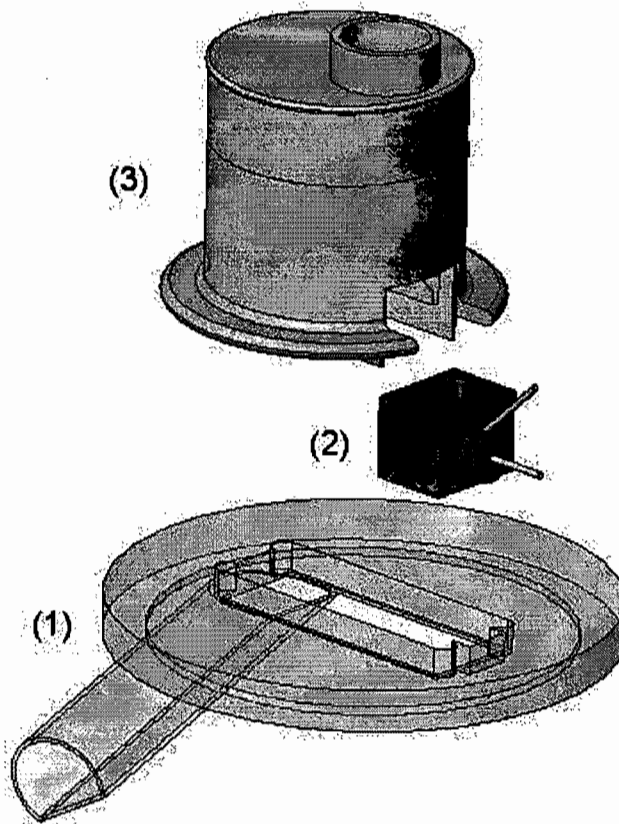


Figure C.3: Exploded view of the entire stage set-up:

- (1) Stage ring with air-inlet (see section C.2)
- (2) Side-view chamber (see section C.3)
- (3) Incubator (see section C.5)

C.2 Stage ring

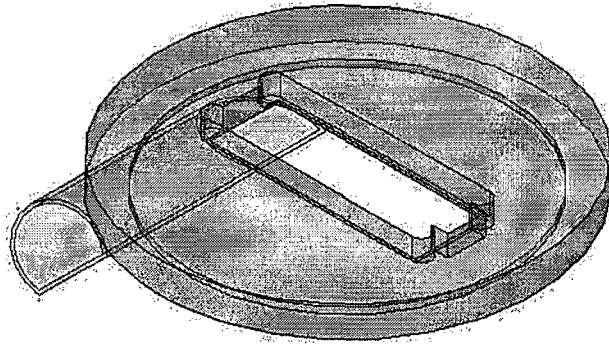


Figure C.4: 3D view of the stage ring with air inlet

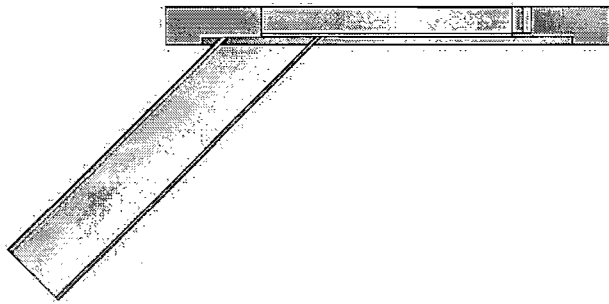


Figure C.5: Cross-section of the stage ring with air inlet

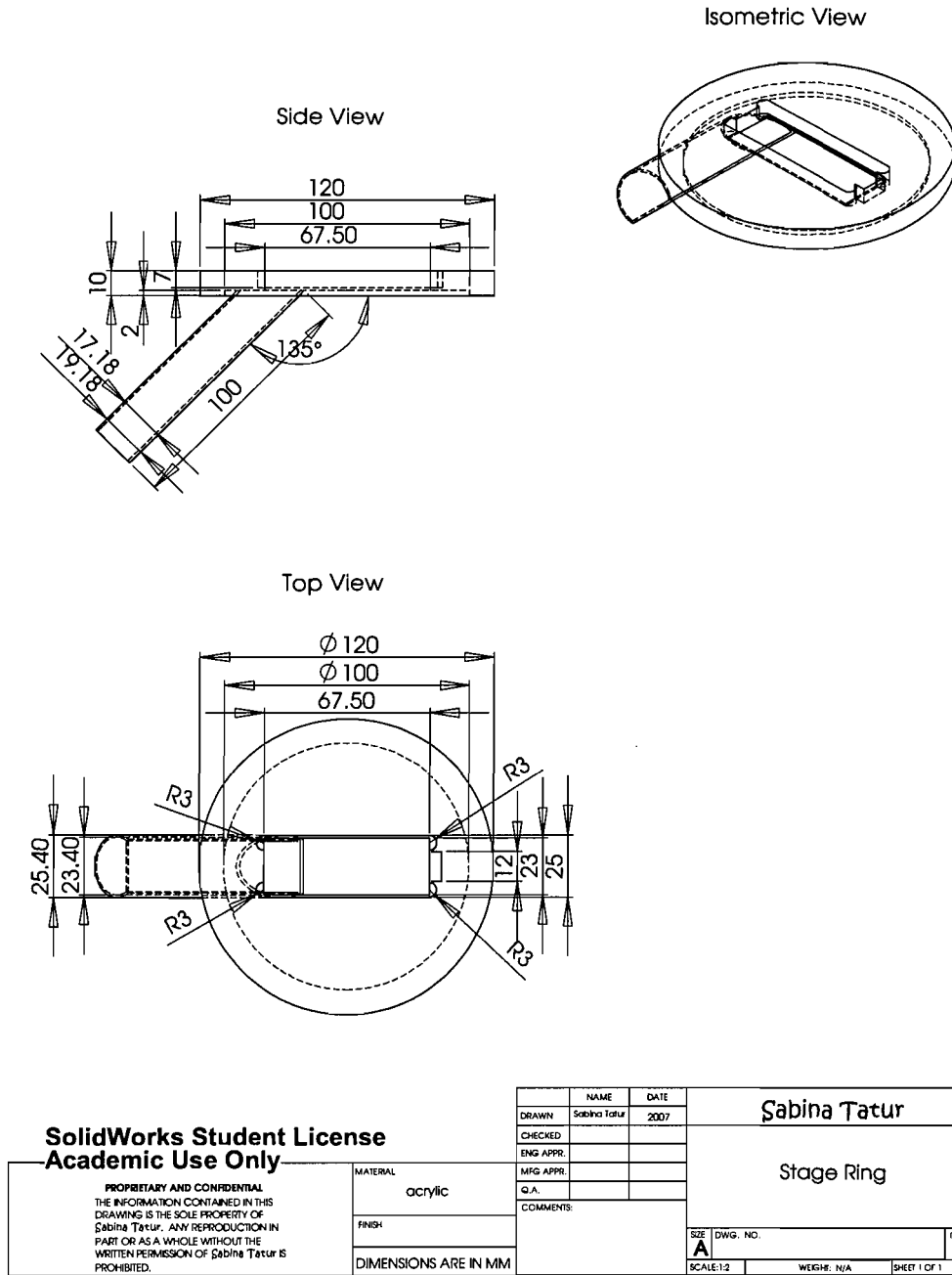


Figure C.6: Detailed 2D engineering drawing of the stage ring with air inlet

C.3 Side-view chamber

C.3.1 Assembly

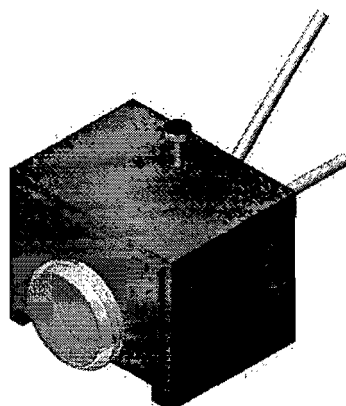


Figure C.7: Assembled view of the side-view chamber

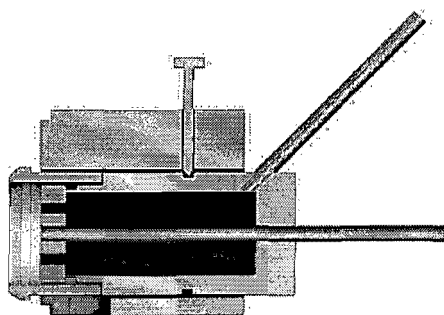


Figure C.8: Cross-section of the side-view chamber

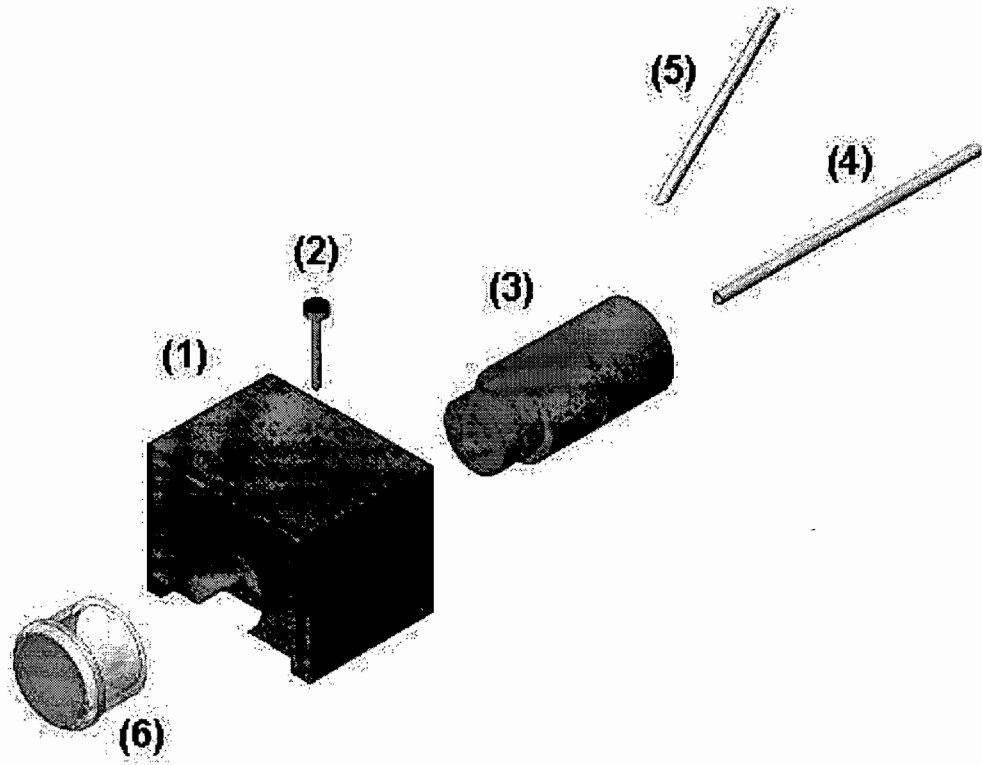


Figure C.9: Exploded view of the side-view chamber:

- (1) Chamber frame (see section C.3.2)
- (2) Retaining screw
- (3) Filter holder (see section C.3.3)
- (4) Inlet tube
- (5) Outlet tube
- (6) Modified Millicell[®] Culture Plate Insert (see section C.4)

C.3.2 Chamber frame

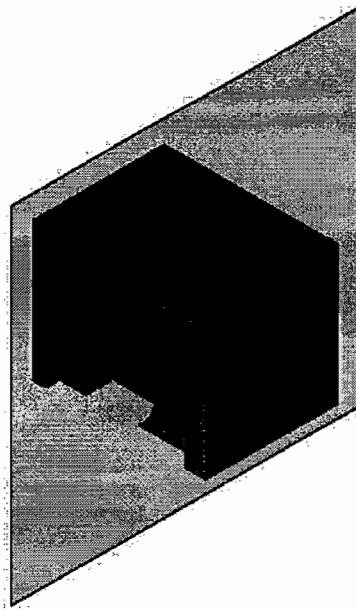


Figure C.10: 3D view of the chamber frame including the section plane for Fig. C.11

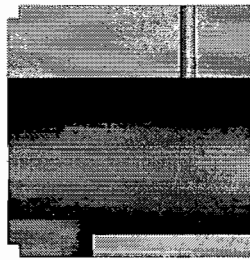
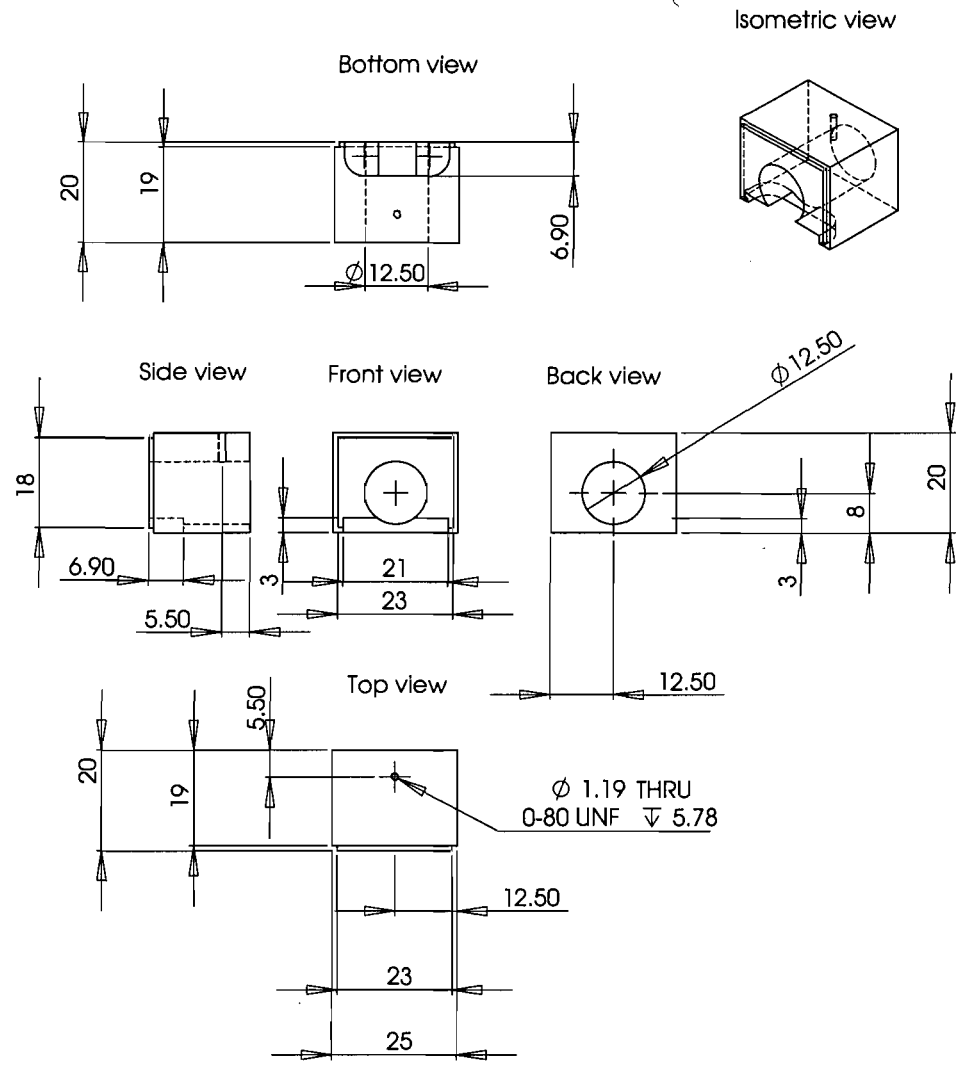


Figure C.11: Cross-section of the chamber frame



SolidWorks Student License		NAME		DATE	
Academic Use Only		DRAWN		Sabina Tatur	
<p><small>PROPRIETARY AND CONFIDENTIAL</small> THE INFORMATION CONTAINED IN THIS DRAWING IS THE SOLE PROPERTY OF Sabina Tatur. ANY REPRODUCTION IN PART OR AS A WHOLE WITHOUT THE WRITTEN PERMISSION OF Sabina Tatur IS PROHIBITED.</p>		CHECKED			
		ENG APPR.			
		MFG APPR.			
		Q.A.			
		COMMENTS:			
MATERIAL		black delrin			
FINISH					
DIMENSIONS ARE IN MM		SIZE		DWG. NO.	
		SCALE: 1:1		WEIGHT: N/A	
				SHEET 1 OF 1	
		Sabina Tatur			
		Chamber frame			
				REV.	

Figure C.12: Detailed 2D engineering drawing of the chamber frame

C.3.3 Filter holder

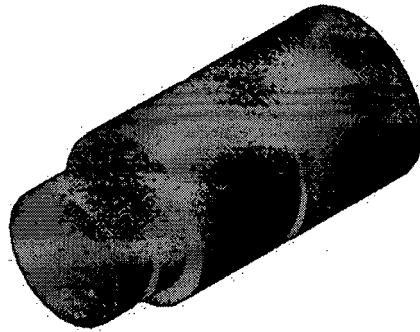


Figure C.13: 3D view of the filter holder

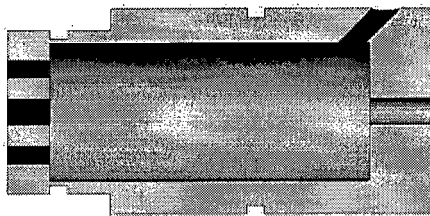
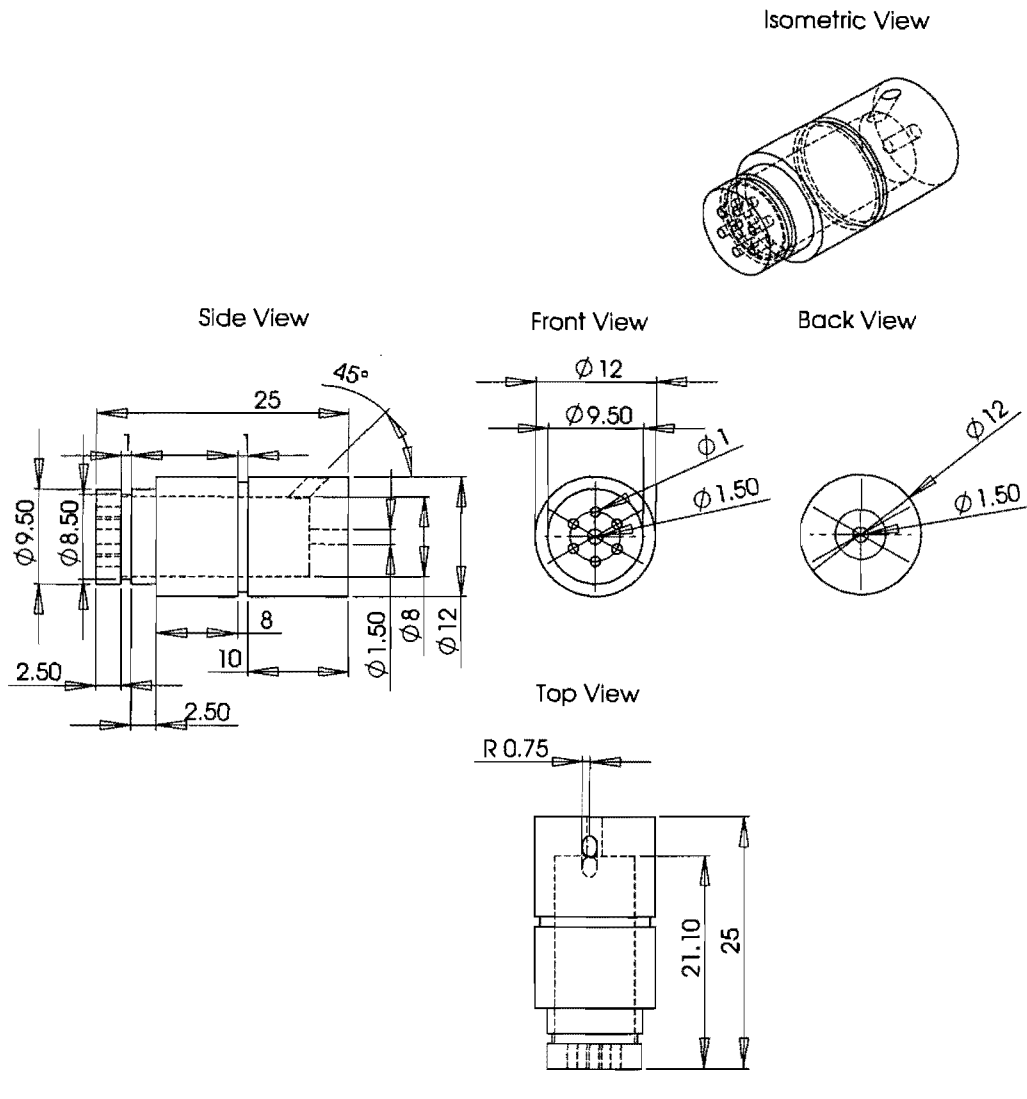


Figure C.14: Cross-section of the filter holder



SolidWorks Student License		NAME		DATE	
Academic Use Only		DRAWN		Sabina Tatur	
<p>PROPRIETARY AND CONFIDENTIAL THE INFORMATION CONTAINED IN THIS DRAWING IS THE SOLE PROPERTY OF Sabina Tatur. ANY REPRODUCTION IN PART OR AS A WHOLE WITHOUT THE WRITTEN PERMISSION OF Sabina Tatur IS PROHIBITED.</p>		MATERIAL		2007	
		black delrin		CHECKED	
		FINISH		ENG APPR	
		DIMENSIONS ARE IN MM		MFG APPR	
				Q.A.	
		COMMENTS:			
		SCALE		DWG. NO.	
		A		REV.	
		1		WEIGHT: N/A	
				SHEET 1 OF 1	

Figure C.15: Detailed 2D engineering drawing of the filter holder

C.4 Cell culture filter inserts

C.4.1 Modification of the Millicell[®] culture plate inserts (MCPI)

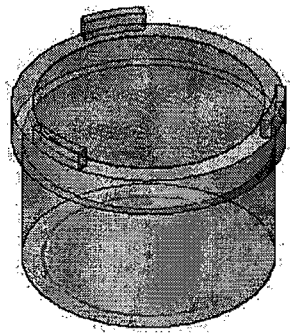


Figure C.16: Original MCPI

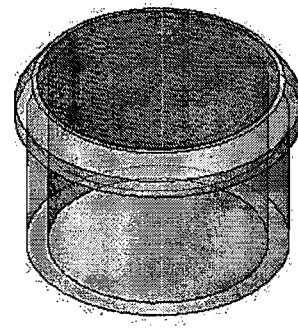


Figure C.17: Modified MCPI

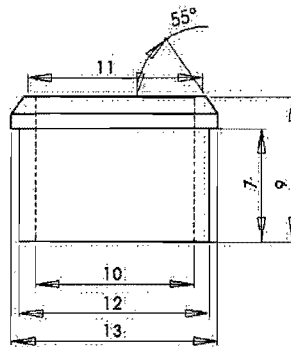


Figure C.18: Dimensions of the modified MCPI

C.4.2 Preparation of the MCPI for cell culture

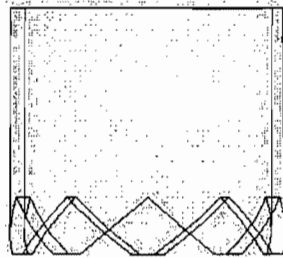


Figure C.19: Design of the MCPI holding tube

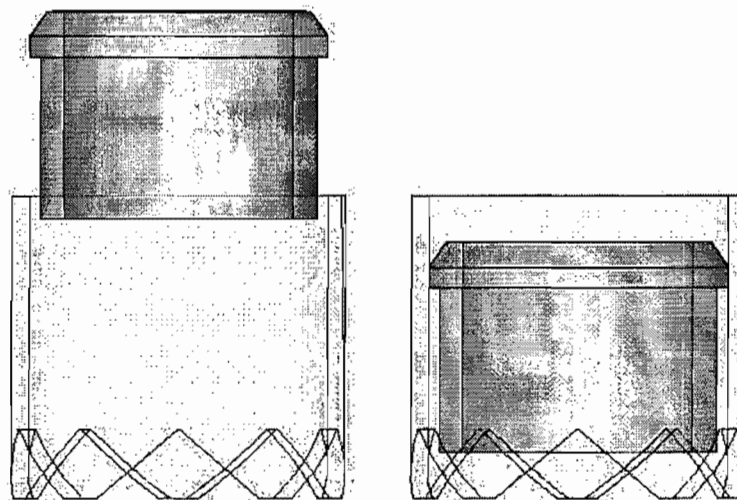


Figure C.20: Inserting the modified MCPI into the tube

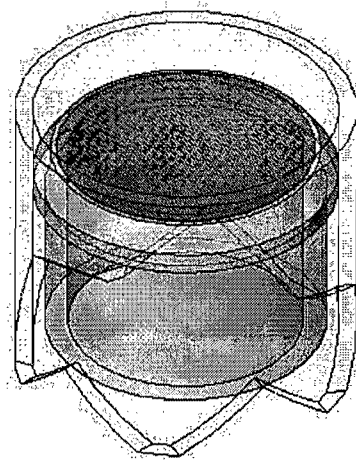


Figure C.21: 3D view of modified MCPI in the tube

C.5 Incubator

C.5.1 Assembly

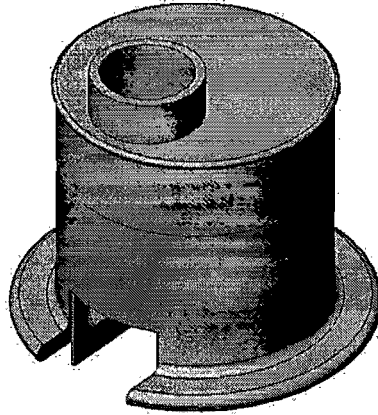


Figure C.22: Assembled view of the incubator

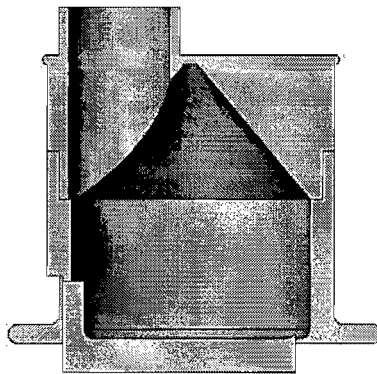


Figure C.23: Cross-section of the incubator

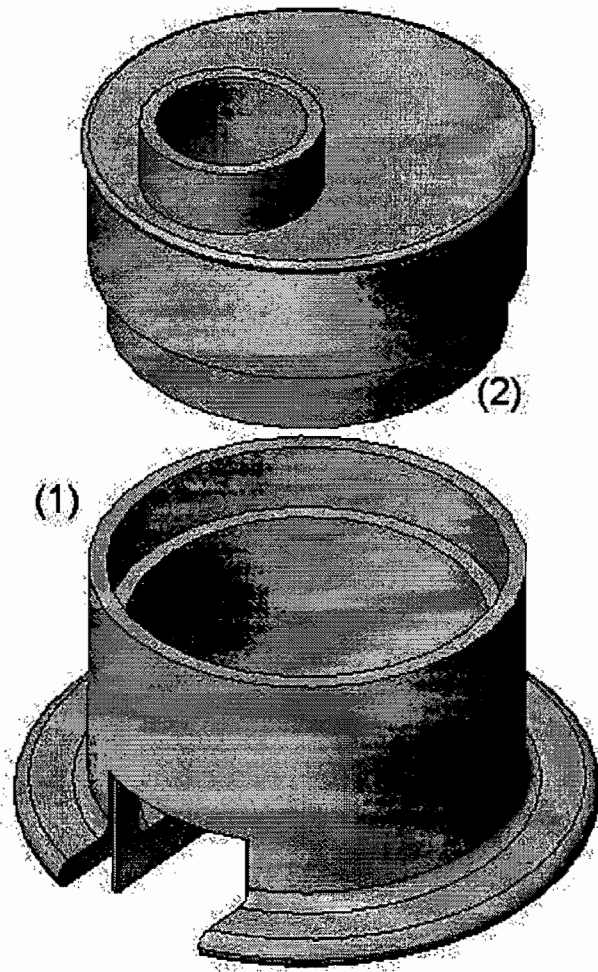


Figure C.24: Exploded view of the incubator:

- (1) Main chamber (see section C.5.2)
- (2) Cover (see section C.5.3)

C.5.2 Main chamber

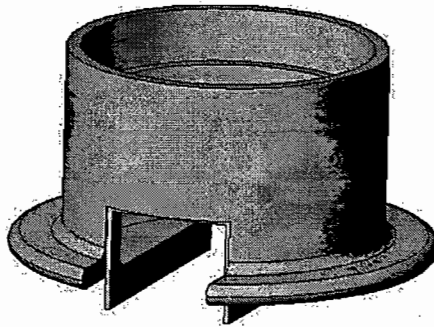


Figure C.25: 3D view of the main incubator chamber

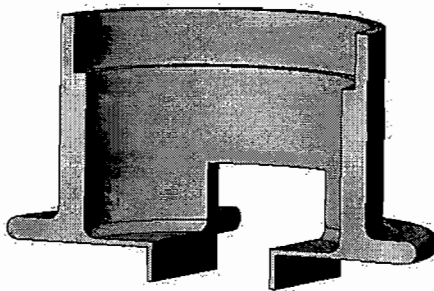
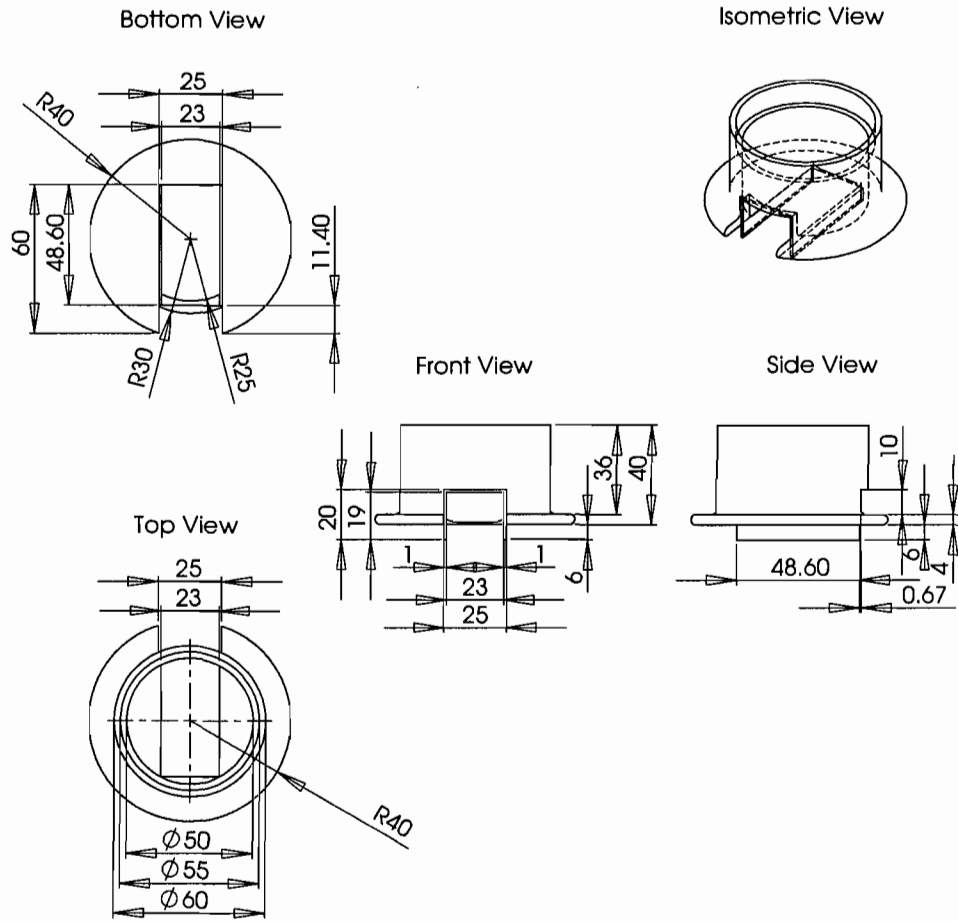


Figure C.26: Cross-section of the main incubator chamber



SolidWorks Student License Academic Use Only									
<small>PROPRIETARY AND CONFIDENTIAL THE INFORMATION CONTAINED IN THIS DRAWING IS THE SOLE PROPERTY OF Şabina Tatur. ANY REPRODUCTION IN PART OR AS A WHOLE WITHOUT THE WRITTEN PERMISSION OF Şabina Tatur IS PROHIBITED.</small>		MATERIAL: black delrin		<table border="1"> <tr> <th>NAME</th> <th>DATE</th> </tr> <tr> <td>Şabina Tatur</td> <td>2007</td> </tr> </table>		NAME	DATE	Şabina Tatur	2007
NAME	DATE								
Şabina Tatur	2007								
FINISH:		DIMENSIONS ARE IN MM		COMMENTS:					
				Şabina Tatur					
				Main Incubator Chamber					
				SIZE: A DWG. NO. REV.					
				SCALE: 1:2 WEIGHT: N/A SHEET 1 OF 1					

Figure C.27: Detailed 2D engineering drawing of the main incubator chamber

C.5.3 Cover

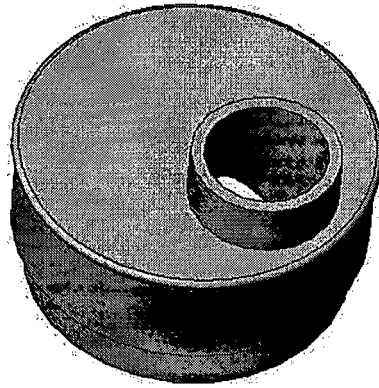


Figure C.28: 3D view of the chamber cover

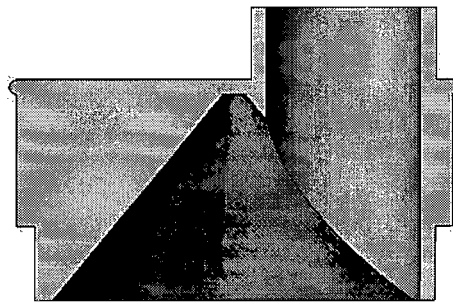


Figure C.29: Cross-section of the chamber cover

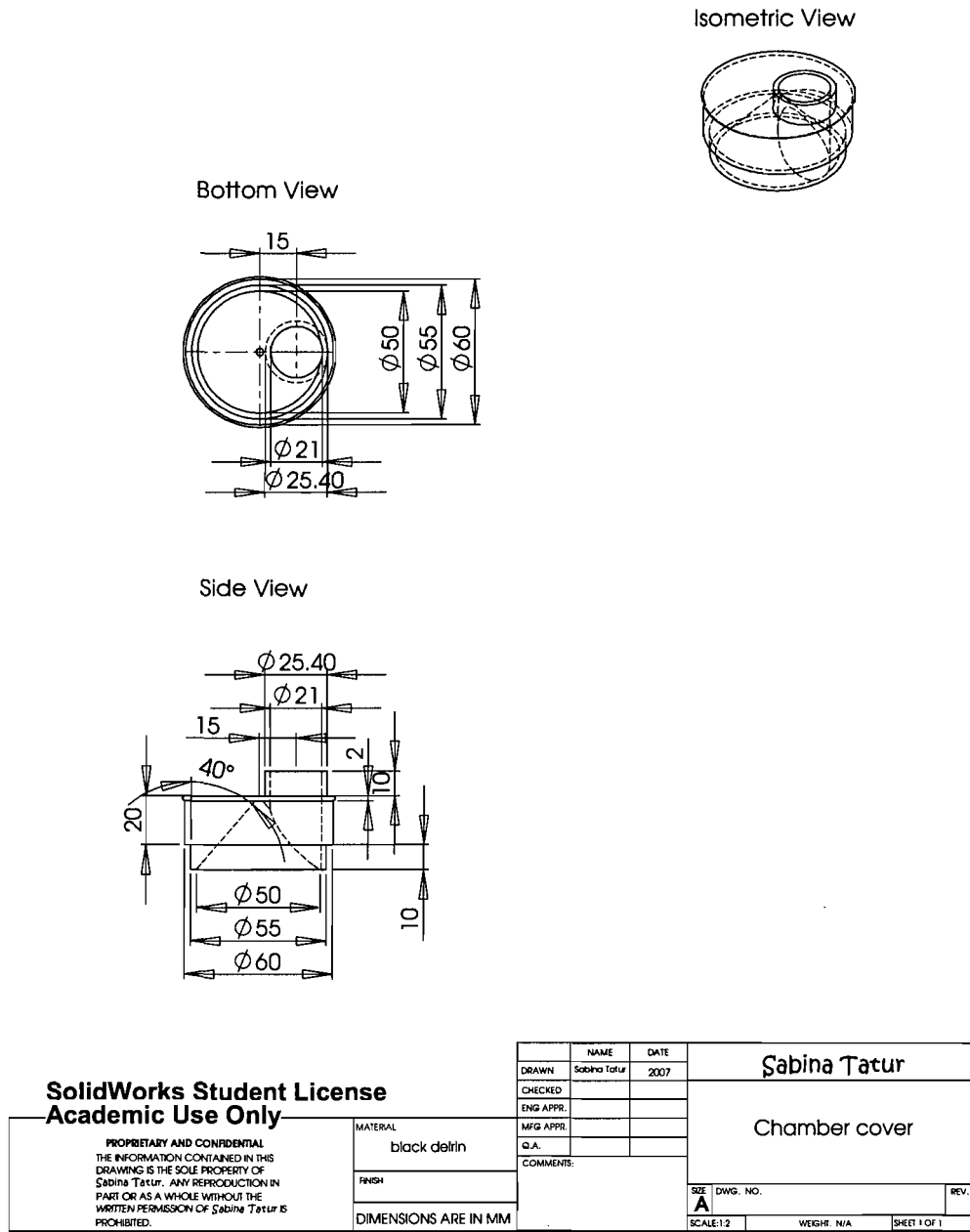


Figure C.30: Detailed 2D engineering drawing of the chamber cover

C.6 Valve

C.6.1 Assembly

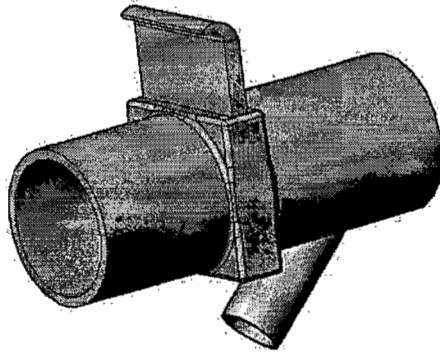


Figure C.31: Assembled view of the valve

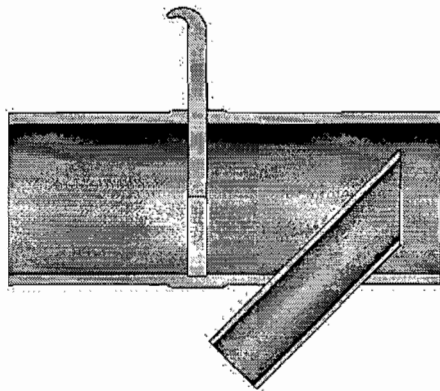


Figure C.32: Cross-section of the valve

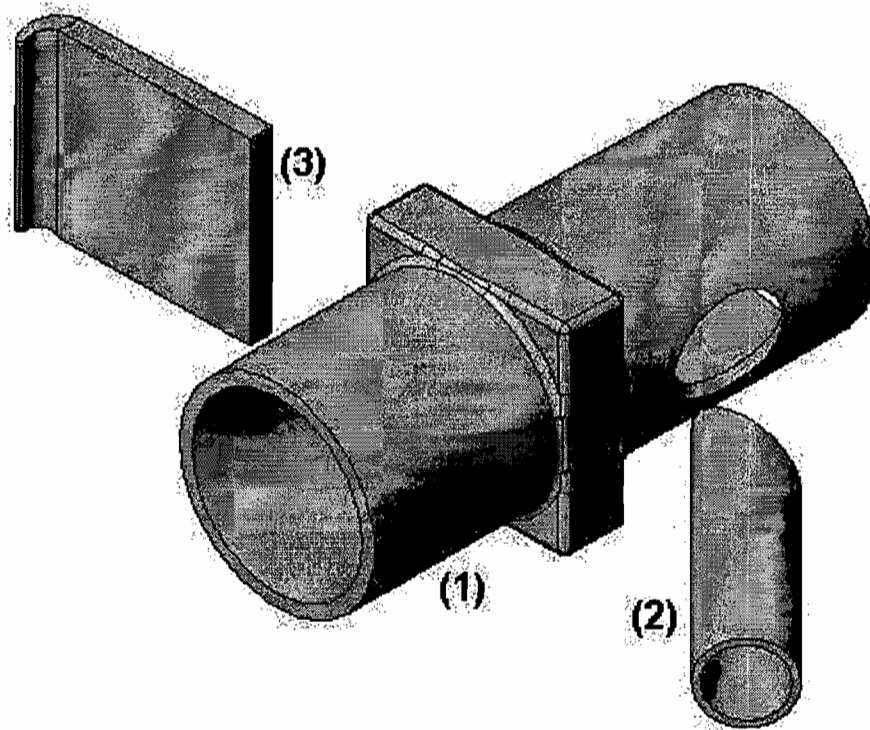


Figure C.33: Exploded view of the valve:

- (1) Main valve tube (see section C.6.2)
- (2) Reducing tube (see section C.6.3)
- (3) Shutter (see section C.6.3)

C.6.2 Main valve tube

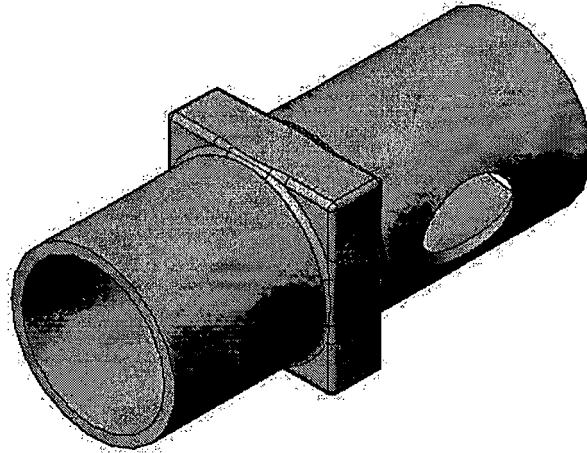


Figure C.34: 3D view of the main valve tube

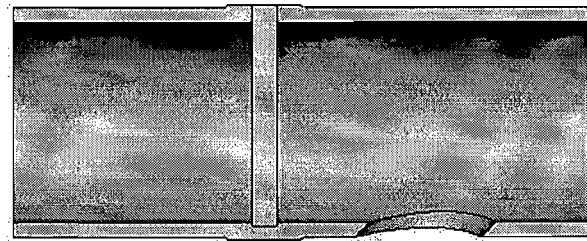


Figure C.35: Cross-section of the main valve tube

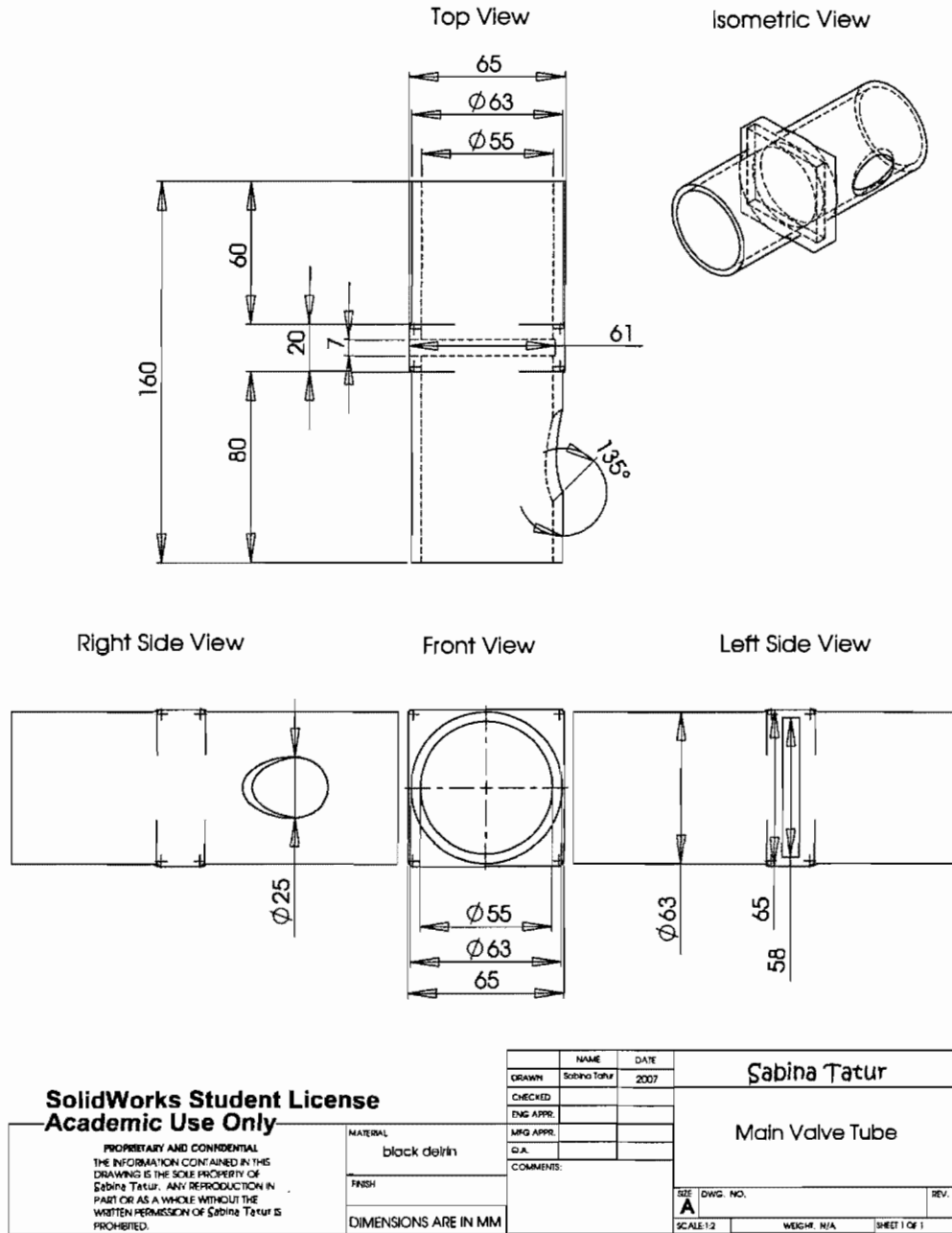


Figure C.36: Detailed 2D engineering drawing of the main valve tube

C.6.3 Valve tube accessories

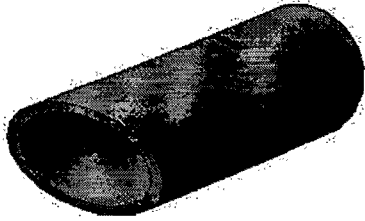


Figure C.37: 3D view of the reducing tube

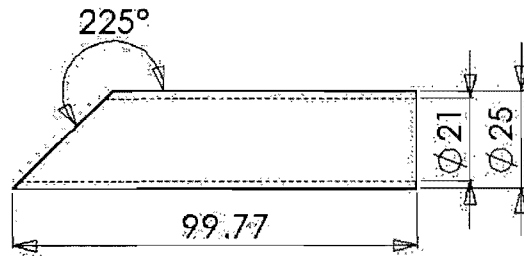


Figure C.38: Dimensions of the reducing tube

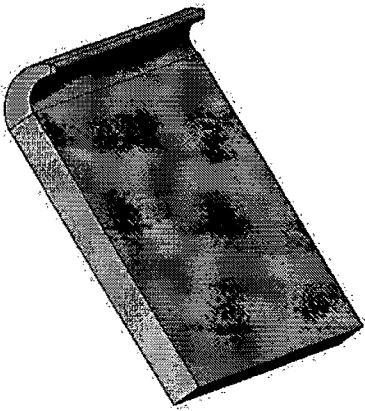


Figure C.39: 3D view of the valve shutter

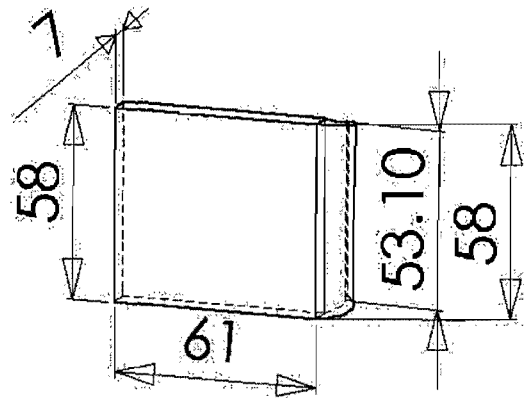


Figure C.40: Dimensions of the valve shutter